Assessment of the role of cannabinoid receptor 2 in innate immune cell trafficking during acute inflammation

A thesis submitted for the degree of Doctor of Philosophy in Cardiovascular Science

University of Oxford

Michaelmas Term 2016

Lewis Taylor

New College

Sir William Dunn School of Pathology

Abstract

Activation of the cannabinoid receptor CB_2 has been shown to induce directed leukocyte migration and inhibit leukocyte chemotaxis towards CC chemokines. However, the role that CB_2 plays in regulating macrophage chemotaxis remains understudied. Using a real-time chemotaxis assay and a panel of chemically diverse CB_2 agonists, I set out to examine whether CB_2 modulates primary macrophage chemotaxis. Of 14 agonists tested, only a subset acted as *bona fide* macrophage chemoattractants. Surprisingly, despite being pertussis toxin-sensitive, neither pharmacological inhibition nor genetic ablation of CB_2 had any effect on CB_2 agonist-induced macrophage chemotaxis. Furthermore, the activation of CB_2 had no effect on CCL2 or CCL5-induced macrophage chemotaxis. Therefore, the activation of CB_2 does not inhibit CC chemokine-induced macrophage migration and a non-CB_1/CB_2, $G_{i/o}$-coupled GPCR must transduce CB_2 agonist-induced macrophage chemotaxis. To identify the GPCR responsible, I examined primary murine macrophage GPCR expression and found that they express 124 non-sensory GPCRs. Functional screening of candidate receptors demonstrated that the putative cannabinoid receptors GPR18 and GPR55 and the lipid binding GPCRs LPAR1&5, CYSLTR1&2 and GPER1, were not responsible for CB_2 agonist-induced macrophage chemotaxis. Alongside, a ligand-directed virtual screen, combined with functional testing, uncovered a novel chemotaxis positive chemical scaffold. Importantly, compounds in this series containing a photoaffinity label retained activity and will aid in the identification of the target(s) responsible for CB_2 agonist-induced macrophage chemotaxis in future photocrosslinking experiments. Finally, I assessed whether CB_2 controls innate immune cell recruitment *in vivo* using the zymosan-induced dorsal air pouch inflammation model and animals genetically deleted for CB_2. I found that $CB_2^{-/-}$ mice had increased air pouch neutrophil and monocyte numbers, as well as pro-inflammatory mediators, during the acute inflammatory phase. Interestingly, mixed bone marrow chimera experiments demonstrated that lack of CB_2 specifically in the myeloid population is responsible for increased neutrophil trafficking. Therefore these data demonstrate that CB_2 acts to regulate neutrophil recruitment during the acute inflammatory response.

Acknowledgements

I would like to begin by thanking my supervisor Professor David Greaves. Thank you for awarding me my studentship in the first place and allowing me to join your group. I have learnt so much throughout my time in the lab, both scientifically and about myself, and have had an absolutely amazing 4 years.

Next I want to thank the entire Greaves lab for all of their input, time, effort, support and most importantly, their friendship. I really couldn't have wished for a better group to have worked alongside. Max, the summer you were in the lab is one of the fondest I can remember, particularly when we were working together as the croquet dream team. Thank you for your friendship ever since. Gemma, you always put up with my terrible jokes (and occasionally even laughed at them) and you inspired my love of the bake off. Sophia, I always knew I could count on you to come for a tea no matter the time and to talk with me when I clearly wanted to procrastinate. Carlota, thank you for tolerating the constant question of: "How do you say this in Spanish?" and then telling me all over again when I inevitably forgot. Danny, thank you for your great sense of humour (I swear I will publish my memoirs and stories someday), constant jokes and for the greatest of football commentary. Asif, you have not only been an immensely patient and supportive mentor, but someone I respect scientifically and consider a true friend. Thank you for all of the help and advice you have given me throughout my DPhil. Lastly Theo, my CB_2 partner in crime. I will miss our gym sessions and project discussions and all of the important questions you were always asking (many not scientific in nature). Thank you for all of the help you have given me and all of the good and bad times we have shared along our DPhil journey, I have had an awesome time. You truly are a life-long friend.

Carmen. Thank you for all of the patience, love and friendship you have given me in our time together. I know I am not always the easiest person to deal with and I would have gone crazy at multiple points throughout my DPhil if you had not been there to listen to my ramblings and always make me feel better. I can't wait to see what the future holds for us.

Next I would like to thank my entire family. Without them I would not be where I am today. Connie, Connor, Reece and Rebecca, thank you for always being there for me, for making me laugh and for being my best friends. I am very proud of you all. Finally, Mum and Dad. Words cannot really express how grateful I am for the constant love and support you have given me throughout my life and for your unwavering belief that (perhaps sometimes with a little push) I can achieve anything I want. I love you both very much. This thesis is for you.

Abbreviations

2-AG	2-arachidonolyglycerol
5-HT	5-hydroxytryptamine
Δ9-THC	Δ9-tetrahydrocannabinol
Δ-9THCV	Δ9-tetrahydrocannabivarin
AA	Arachidonic acid
Abn-CBD	Abnormal cannabidiol
ADR	Adverse drug reaction
AEA	*N*-arachidonoylethanolamine
ApoE	Apolipoprotein E
C5aR1	C5a receptor 1
CB_1	Cannabinoid receptor 1
CB_2	Cannabinoid receptor 2
CBD	Cannabidiol
CD	Crohn's disease
CG	Cathepsin G
CGD	Chronic granulomatous disease
CHO	Chinese hamster ovary
CI	Cell index
CIA	Collagen-induced arthritis
CLP	Cecal ligation and puncture
CLR	C-type lectin receptor
cMoP	Common myeloid progenitor
CNS	Central nervous system
COX	Cyclooxygenase
Ct	Cycle threshold
cysLT	Cysteinyl leukotriene
CYSLTR	Cysteinyl leukotriene receptor
DAG	Diacylglycerol
DAGL	Diacylglycerol lipase
DAMP	Danger-associated molecular pattern

DMEM	Dulbecco's modified Eagle's medium
DMSO	Dimethylsulphoxide
DSS	Dextran sulphate sodium
EAE	Experimental autoimmune encephalomyelitis
FAAH	Fatty acid amine hydrolase
FADD	fas-associated death domain
FCS	Fetal calf serum
FLS	Fibroblast-like synoviocytes
G-CSF	Granulocyte colony-stimulating factor
GEF	Guanine nucleotide exchange factor
GFP	Green fluorescent protein
GM-CSF	Granulocyte macrophage colony-stimulating factor
GPCR	G Protein-coupled receptor
GPER1	G protein-coupled estrogen receptor 1
HA	Hemagglutinin
HSC	Haematopoetic stem cell
IBD	Inflammatory bowel disease
IL	Interleukin
IR	Ischaemia reperfusion
Ldlr	Low density lipoprotein receptor
LHS	Left hand side
LPA	Lysophosphatidic acid
LPAR	Lysophosphatidic acid receptor
LPS	Lipopolysaccharide
LT	Leukotriene
LTB4R1	Leukotriene B4 receptor 1
M-CSF	Macrophage colony-stimulating factor
MAC	Membrane attack complex
MAGL	Monoacylglycerol lipase
MCps	Mast cell precursor
MMP-9	Matrix metalloproteinase 9
MPO	Myeloperoxidase
MS	Multiple sclerosis
MSU	Monosodium urate
NAAA	*N*-acylethanolamine acid amide hydrolase
NAGly	*N*-arachidonoylglycine
NAPE	*N*-arachidonoyl-phosphatidyl-ethanolamine
NAPE-PLD	NAPE-phospholipase D
NE	Neutrophil elastase

NET	Neutrophil extracellular trap
NLR	Nod-like receptor
NPF	Nucleation promoting factor
PAMP	Pathogen-associated molecular pattern
PBS	Phosphate buffered saline
PCR	Polymerase chain reaction
PDE	Phosphodiesterase
PEC	Peritoneal exudate cell
PG	Prostaglandin
PH	Pleckstrin homology
PI3K	Phosphoinositide 3-kinase
PIP_2	Phosphatidylinositol 4,5-bisphosphate
PIP_3	Phosphatidylinositol 3,4,5-triphosphate
PLC	Phospholipase C
PMN	Polymorphonuclear cell
PPAR	Peroxisome proliferator-activated receptor
PRR	Pattern recognition receptor
PSGL1	P-selectin glycoprotein ligand 1
PTX	Pertussis toxin
RA	Rheumatoid arthritis
RHS	Right hand side
RLR	RIG-I-like receptor
ROS	Reactive oxygen species
RPMI	Roswell Park Memorial Institute medium
S1PR	Sphingosine-1-phosphate receptor
SAR	Structure-activity relationship
SCF	Stem cell factor
SPM	Specialised pro-resolving mediator
TBS-T	Tris-buffered saline supplemented with 0.1% tween
TEM	Transendothelial migration
TIR	Toll/interleukin-1 receptor
TLR	Toll-like receptor
TNBS	2,4,6-Trinitrobenzene sulphonic acid
TNFR	TNF receptor
TRADD	TNF receptor-associated death domain
TRAF2	TNF receptor-associated factor 2
TRP	Transient receptor potential
UC	Ulcerative colitis
WT	Wild type

Contents

Abstract **I**

Ackowledgements **II**

Abbreviations **III**

Contents **VI**

List of Figures **XI**

List of Tables **XIV**

1 Chapter 1: Introduction **1**

1.1 Inflammation and the acute inflammatory response 1

1.2 Cells of the innate immune system 2

1.2.1 Neutrophils 2

1.2.2 Monocytes 4

1.2.3 Macrophages 5

1.2.4 Eosinophils 7

1.2.5 Mast cells 8

1.3 Sensing of infection or tissue damage by innate immune cells 9

1.3.1 Extracellular pathogen recognition 10

1.3.2 Intracellular pathogen recognition 10

1.3.3 Recognition of endogenous danger-associated molecules 11

1.4 Mediators of the acute inflammatory response 11

1.4.1 Cytokines 11

1.4.2 Chemokines - chemoattractant cytokines 13

1.4.3 The complement system 14

1.4.4 pro-inflammatory eicosanoids 15

1.5 Neutrophil recruitment to sites of inflammation 16

1.6 Monocyte recruitment to sites of inflammation 19

1.7 The resolution of inflammation 20

1.8 The endocannabinoid system 22
1.8.1 The cannabinoid receptors 22
1.8.2 Expression pattern of CB_1 23
1.8.3 Expression pattern of CB_2 24
1.8.4 The endocannabinoids - synthesis and degradation 25
1.8.5 Phytocannabinoids 29
1.8.6 Synthetic cannabinoid receptor agonists 31
1.8.7 Cannabinoid receptor inverse agonists 35
1.8.8 CB_2 knockout mice 36
1.9 The role of CB_2 in inflammatory disease 37
1.9.1 The role of CB_2 in intestinal inflammation and inflammatory bowel disease 37
1.9.2 The role of CB_2 in sepsis and endotoxic shock 39
1.9.3 The role of CB_2 in multiple sclerosis 41
1.9.4 The role of CB_2 in rheumatoid arthritis 43
1.9.5 The role of CB_2 in ischaemia reperfusion injury 44
1.9.6 The role of CB_2 in the development of atherosclerosis 46
1.10 Original hypothesis for this thesis 49
1.11 Experimental aims 49

2 Chapter 2: Materials and Methods 50
2.1 Reagents 50
2.2 Animals 51
2.3 Bio-gel and thioglycollate elicitation of peritoneal exudate cells 51
2.4 Bio-gel macrophage enrichment 52
2.5 ACEA xCELLigence real-time chemotaxis assay 52
2.6 ACEA 96 well ECIS cell spreading assay 53
2.7 Flow cytometry 54
2.8 Cell counting using flow cytometry 57
2.9 Discoverx intracellular cAMP assay 57
2.10 Discoverx β-arrestin recruitment assay 58
2.11 Discoverx β-arrestin GPCR screen 58
2.12 Cannabinoid stimulation of bio-gel elicited murine macrophages . . . 59
2.13 Western blotting 60
2.14 ELISA 60
2.15 Luminex® inflammatory mediator screening 61
2.16 Generation of N-terminal tagged GPCR constructs 62
2.17 CHO cell GPCR transfections 63
2.18 Bone marrow neutrophil isolation 64

2.19 RNA extraction and cDNA synthesis . . . 65
2.20 Real-time PCR . . . 65
2.21 Murine Taqman GPCR expression array . . . 66
2.22 Ligand-directed virtual screening . . . 66
2.23 Zymosan-induced peritonitis . . . 67
2.24 Dorsal air pouch inflammation model . . . 67
2.25 Generation of mixed bone marrow chimeric animals . . . 68
2.26 Culture and stimulation of air pouch fibroblasts . . . 69
2.27 Data and statistical analysis . . . 69

3 Chapter 3: Cannabinoid receptor 2 and macrophage chemotaxis 71
3.1 Introduction . . . 71
3.1.1 Chemotaxis - Directional cellular migration towards a chemoattractant . . . 71
3.1.2 Chemotactic receptor signalling . . . 72
3.1.3 PI3K signalling and leading edge formation . . . 73
3.1.4 Control of actin dynamics at the leading edge . . . 73
3.1.5 Signalling and actin-myosin dynamics at the rear of the cell . 75
3.1.6 The role of CB_2 within immune cell chemotaxis . . . 75
3.1.7 Cannabinoids inhibiting chemotaxis elicited by other chemoattractants . . . 77
3.2 Rationale for the experiments presented in this chapter . . . 79
3.3 Results . . . 80
3.3.1 The CB_2 selective agonists JWH133 and HU308 are chemoattractants for bio-gel elicited PECs . . . 80
3.3.2 Macrophages are the dominant population in bio-gel elicited PECs that are being measured in real-time chemotaxis . . . 82
3.3.3 Only a subset of CB_2 agonists act as chemoattractants for murine macrophages . . . 86
3.3.4 PI3K signalling is essential for CB_2 agonist-induced macrophage chemotaxis . . . 88
3.3.5 Screening for activity of the CB_2 ligand panel reveals functional selectivity at CB_2 . . . 91
3.3.6 CB_2 selective agonists induce primary macrophage chemotaxis independently of CB_2 . . . 94
3.3.7 JWH133 and HU308 enhance chemokine-induced macrophage chemotaxis in a CB_2 independent manner . . . 98
3.3.8 JWH133 and HU308 enhance C5a-induced macrophage chemotaxis . . . 101

3.3.9 The CB_2 inverse agonist SR144528 acts as a macrophage chemoattractant . . . 101
3.3.10 CP55,940 and DIAS2 do not negatively regulate chemokine-induced macrophage chemotaxis . . . 104
3.4 Discussion . . . 106
3.4.1 Limitations of this study . . . 113

4 Chapter 4: Identification of the off-target GPCR(s) responsible for CB_2 agonist-induced macrophage chemotaxis 115
4.1 Introduction . . . 115
4.1.1 Drug promiscuity - Off-target effects of small molecules . . . 115
4.1.2 Adverse drug reactions - The negative side of drug off-target effects . . . 116
4.1.3 Drug repurposing - The positive side of drug off-target effects 117
4.1.4 Off-target effects of cannabinoids . . . 118
4.1.5 Off-target effects at GPCRs . . . 119
4.1.6 Off-target effects at non-GPCR targets . . . 122
4.2 Rationale for the experiments presented in this chapter . . . 126
4.3 Results . . . 127
4.3.1 Bio-gel elicited macrophages express 124 GPCRs . . . 127
4.3.2 GPR18 and GPR55 are not responsible for the off-target effects of JWH133 and HU308 . . . 129
4.3.3 Functional screening of JWH133 at 241 human GPCRs . . . 133
4.3.4 Functional testing of lipid binding GPCRs expressed in bio-gel elicited macrophages . . . 133
4.3.5 Ligand based virtual screening discovers a novel chemoattractant chemical scaffold . . . 137
4.3.6 SAR studies on the 2-thioxo-2,3-dihydroquinazolin-4(1H)-one series . . . 140
4.3.7 SAR studies on the right hand side phenyl group . . . 142
4.3.8 Compounds containing the photoactive benzophenone group retain functional activity . . . 146
4.4 Discussion . . . 146
4.4.1 Limitations of this study . . . 151

5 Chapter 5: Innate immune mobilisation in $CB_2^{-/-}$ animals 154
5.1 Introduction . . . 154
5.1.1 Animal models for studying the inflammatory response . . . 154
5.1.2 The dorsal air pouch inflammation model . . . 155

5.1.3 Peritonitis models of inflammation . . . 156
5.1.4 Carrageenan-induced paw oedema . . . 157
5.1.5 Mouse ear oedema models . . . 158
5.1.6 LPS-induced endotoxemia . . . 158
5.1.7 Chemically-induced intestinal inflammation models . . . 159
5.2 Rationale for the experiments presented in this chapter . . . 160
5.3 Results . . . 161
5.3.1 WT and $CB_2^{-/-}$ mice have no difference in their baseline air pouch cellular composition . . . 161
5.3.2 $CB_2^{-/-}$ animals with dorsal air pouches have increased B cell numbers in their blood under basal conditions . . . 165
5.3.3 $CB_2^{-/-}$ animals have an exaggerated acute inflammatory response in the zymosan-induced dorsal air pouch inflammation model . . . 165
5.3.4 There is no difference in the inflammatory response between WT and $CB_2^{-/-}$ animals 2 hours after zymosan challenge . . . 175
5.3.5 $CB_2^{-/-}$ animals have elevated myeloid cell numbers in the dorsal air pouch 48 hours after zymosan challenge . . . 179
5.3.6 Time course of the zymosan-induced inflammatory response in the dorsal air pouch of WT and $CB_2^{-/-}$ animals . . . 182
5.3.7 Male $CB_2^{-/-}$ animals also have an exaggerated acute inflammatory response . . . 186
5.3.8 Genetic deletion of CB_2 has no effect on the acute inflammatory response in the zymosan-induced peritonitis model . . . 188
5.3.9 Lack of CB_2 in the myeloid population is responsible for increased neutrophil recruitment to the dorsal air pouch in $CB_2^{-/-}$ animals . . . 190
5.3.10 Genetic deletion of CB_2 has no effect on inflammatory mediator production by air pouch-derived fibroblasts . . . 194
5.4 Discussion . . . 198
5.4.1 Limitations of this study . . . 203

6 Chapter 6: Thesis summary and final discussion 206
6.1 Key findings . . . 206
6.2 How can CB_2 regulate neutrophil, but not macrophage, migration? . . . 209
6.3 Future work . . . 210

References 211

List of Figures

1.1 The major routes of anandamide synthesis and degradation 26
1.2 The major routes of 2-arachidonoylglycerol synthesis and degradation 28
1.3 Cannabinoid receptor ligands used throughout my thesis 32

3.1 The CB_2 selective agonists JWH133, HU308 and DIAS2 differ in their ability to induce the directed migration of murine PECs. 81
3.2 The bio-gel batch or the animal housing facility used have no effect on the cellular composition of bio-gel elicited murine PECs. 83
3.3 Macrophages are the dominant cell population in bio-gel elicited PECs that migrate toward CB_2 agonists. 85
3.4 Only a subset of CB_2 agonists are macrophage chemoattractants. . . 87
3.5 Chemotaxis positive CB_2 agonists induce concentration-dependent cytoskeletal rearrangements in primary murine macrophages. 89
3.6 PI3K signalling is essential for JWH133 and HU308-induced murine macrophage chemotaxis. 90
3.7 Measurement of intracellular cAMP levels demonstrates activity of the cannabinoid ligands at CB_2. 92
3.8 CB_2 ligands display marked variation in their ability to recruit β-arrestin to CB_2. 93
3.9 Macrophage chemotaxis towards CB_2 selective agonists is blocked by pertussis toxin, but not by CB_2 or CB_1 inverse agonists. 95
3.10 JWH133, HU308 and L-759,656 are chemoattractants for $CB_2^{-/-}$ primary macrophages. 97
3.11 JWH133 and HU308 enhance chemokine-induced murine macrophage chemotaxis. 99
3.12 JWH133 and HU308 enhance chemokine-induced chemotaxis of $CB_2^{-/-}$ macrophages 100
3.13 JWH133 and HU308 enhance C5a-induced chemotaxis. 102
3.14 The CB_2 inverse agonist SR144528 acts as a macrophage chemoattractant. 103

3.15 CP55,940 and DIAS2 do not negatively regulate chemokine-induced murine macrophage chemotaxis. 105

4.1 Representative real-time PCR traces of selected GPCRs from the bio-gel macrophage GPCR expression array. 128
4.2 JWH133 and HU308 do not elicit cytoskeletal rearrangements in CHO cells expressing murine GPR18 or GPR55. 130
4.3 JWH133 and HU308 do not elicit cytoskeletal rearrangements in CHO cells co-expressing murine GPR18 or GPR55. 131
4.4 Out of 241 GPCRs, JWH133 only elicits β-arrestin recruitment at CB_1 and CB_2. 134
4.5 LPAR1, LPAR5, GPER1, CYSLTR1 and CYSLTR2 agonists do not elicit cytoskeletal responses similar to JWH133 or HU308 in bio-gel elicited macrophages. 135
4.6 Virtual screening identifies a novel chemical scaffold that retains chemoattractant properties. 138
4.7 Structure activity relationship studies surrounding the 2-thioxo-2,3-dihydroquinazolin-4(1H)-one scaffold. 141
4.8 SAR studies on the right hand side of the 2-thioxo-2,3-dihydroquinazolin-4(1H)-one scaffold identify positions suitable for the addition of a photoaffinity group. 143
4.9 Compounds with a photoreactive benzophenone group at the 3' or 4' position in the right hand phenyl ring retain the ability to elicit macrophage cytoskeletal rearrangement. 145

5.1 Baseline analysis of cells present in day 6 dorsal air pouches in WT and $CB_2^{-/-}$ mice by flow cytometry. 163
5.2 There is no difference in the baseline leukocyte composition of day 6 dorsal air pouches between WT and $CB_2^{-/-}$ mice. 164
5.3 There are no differences in the myeloid cell populations present in the blood of WT and $CB_2^{-/-}$ mice with day 6 dorsal air pouches under baseline conditions. 166
5.4 $CB_2^{-/-}$ mice have increased B cell, but not T cell, numbers in their blood under baseline conditions compared to WT animals. 167
5.5 $CB_2^{-/-}$ mice have increased air pouch neutrophil recruitment 6 hours after zymosan injection. 169
5.6 There are no differences in blood leukocyte numbers between WT and $CB_2^{-/-}$ mice 6 hours after pouch zymosan injection. 170

5.7 $CB_2^{-/-}$ mice have significantly higher levels of pro-inflammatory mediators in the dorsal air pouch 6 hours after zymosan injection compared to WT animals. 171
5.8 $CB_2^{-/-}$ mice have significantly more myeloid cells recruited to the dorsal air pouch 16 hours after zymosan injection compared to WT animals. 173
5.9 There are no differences in blood leukocyte numbers between WT and $CB_2^{-/-}$ mice 16 hours after pouch zymosan injection. 174
5.10 There is no difference in pouch myeloid cell recruitment between WT and $CB_2^{-/-}$ animals 2 hours after zymosan injection. 176
5.11 There are no differences in blood leukocyte numbers between WT and $CB_2^{-/-}$ mice 2 hours after pouch zymosan injection. 177
5.12 There are no differences in the levels of pro-inflammatory mediators in the dorsal air pouch 2 hours after zymosan injection between WT and $CB_2^{-/-}$ animals. 178
5.13 $CB_2^{-/-}$ mice have significantly more myeloid cells in the dorsal air pouch 48 hours after zymosan injection compared to WT animals. . . 180
5.14 $CB_2^{-/-}$ mice have elevated B cell numbers in the blood 48 hours after zymosan injection into the dorsal air pouch. 181
5.15 Time course of the zymosan air pouch inflammation model in female WT and $CB_2^{-/-}$ animals. 183
5.16 Time course of blood leukocyte dynamics in the zymosan air pouch inflammation model in female WT and $CB_2^{-/-}$ animals. 185
5.17 Male $CB_2^{-/-}$ animals have an exaggerated acute inflammatory response 6 hours after pouch zymosan injection. 187
5.18 Genetic deletion of CB_2 has no effect on the acute inflammatory response in the zymosan-induced peritonitis model. 189
5.19 Generation of mixed bone marrow chimeric animals. 191
5.20 Lack of CB_2 in myeloid cells is responsible for increased neutrophil air pouch recruitment in $CB_2^{-/-}$ animals. 193
5.21 There is no difference in the proportion of CD45.1 to CD45.2 neutrophils in the blood of WT or $CB_2^{-/-}$ bone marrow chimera recipient animals 6 hours after zymosan challenge. 195
5.22 Genetic deletion of $CB_2^{-/-}$ in air pouch fibroblasts has no effect on inflammatory mediator production in response to zymosan. 197

6.1 Summary of the main findings of my thesis. 208

List of Tables

2.1 Antibodies used throughout this thesis. 56
2.2 Surface markers used for cell identification. 56

4.1 Bio-gel macrophage GPCR expression summary. 129

5.1 Surface markers used for leukocyte identification. 162

Chapter 1

Introduction

1.1 Inflammation and the acute inflammatory response

Acute inflammation is a complex and co-ordinated response mounted by the host as a result of tissue injury or infection. The acute inflammatory response is established minutes to hours after local sensing of infectious or inflammatory stimuli and is mediated by the various cells of the innate immune system. The aim of the inflammatory process is to quickly isolate and remove the dangerous causative agent, repair any local damage and restore tissue homeostasis [1].

This is achieved by the sensing of pathogens or endogenous danger molecules by tissue resident macrophages and mast cells, which causes them to produce a range of pro-inflammatory mediators [2, 3]. This induces the local accumulation of fluid and blood-borne proteins and the recruitment of neutrophils and other leukocytes to the site of inflammation. Once here these innate immune cells attempt to eliminate any pathogens present. If successful the process of inflammation resolution begins, with the removal of dead and dying neutrophils and the start of tissue repair orchestrated by tissue resident and monocyte-derived macrophages [4]. Far from being a passive process, inflammation resolution relies on multiple mediators to induce the return to tissue homeostasis [5, 6]. However, if the acute inflammatory response fails and the

pathogen is not killed or contained, then the inflammatory response can turn chronic. This involves a switch in the immune cells found at sites of inflammation, with activated macrophages and T and B lymphocytes becoming the most prevalent [7]. Chronic inflammation generally leads to unwanted and excessive tissue damage and is a predominant feature of many inflammatory diseases [7].

Clearly the immune system and the inflammatory response is complex and multifaceted and a complete description is outside the remit of this thesis. Instead, I will focus on the acute inflammatory response, detailing the innate immune cells and inflammatory mediators involved, how tissue damage and infection is detected, how innate immune cells are recruited to sites of inflammation and the mediators, cells and processes involved in the resolution of an inflammatory response.

1.2 Cells of the innate immune system

1.2.1 Neutrophils

Neutrophils are the first cells recruited to areas of inflammation, appearing only hours after the initiation of the acute response, and their primary function is to eliminate any pathogens present at the inflammatory site [8]. These innate immune cells are also known as polymorphonuclear cells (PMNs), due to their multi-lobed nuclei. Like all myeloid cells, they are generated in the bone marrow from haematopoetic stem cells (HSCs), with the cytokines, granulocyte colony-stimulating factor (G-CSF) and granulocyte macrophage colony-stimulating factor (GM-CSF) and the transcription factors PU.1, C/EBPα, C/EBPϵ and GFI-1 predominantly required for neutrophil specification [9, 10]. Almost 60% of the haematopoetic capacity in the bone marrow is dedicated to generating neutrophils, and therefore as many as 10^{11} are made per day, with this number increasing during times of infection [11]. One reason why production levels are so high is that neutrophils are relatively short lived cells, with half life estimates ranging from a few hours to a few days, depending on the labelling

technique used and species studied [12].

After exiting the bone marrow and homing to an inflamed tissue (see section 1.5), neutrophils are fully activated by exposure to pathogen-derived products and/or host-derived damage molecules (see section 1.3), which causes them to up-regulate and engage a variety of microbial killing mechanisms [13]. To begin, neutrophils engulf and internalise opsonised pathogens, those marked by antibodies or complement proteins, in a receptor-dependent manner termed phagocytosis [14,15]. The pathogen is contained intracellularly in a membrane-derived vesicle, known as the phagosome. This then fuses with various other endocytic compartments, especially neutrophil intracellular granules, to facilitate microbe destruction [14, 16].

Neutrophils contain three main types of granules differentiated by their main contents: primary - mainly myeloperoxidase (MPO), secondary - mainly lactoferrin and tertiary - mainly gelatinase [17]. Alongside, these granules contain a range of anti-microbial peptides, such as α-defensins and cathelicidins and serine proteases, such as neutrophil elastase (NE) and cathepsin G (CG), that all contribute to microbial killing [18]. However, components that generate reactive oxygen species (ROS) are among the most important for killing in the phagosome. The NADPH oxidase complex is contained in secondary granules and generates the oxygen free radical, superoxide (O_2^-) [19, 20]. This can cause pathogen damage directly, but normally is rapidly converted into hydrogen peroxide, which is then converted by MPO into hypochlorus acid, and it is this compound that plays a critical role in bacterial killing [21]. The importance of ROS generation *in vivo* is demonstrated in chronic granulomatous disease (CGD) patients who lack a functional NADPH oxidase complex and therefore often suffer from chronic infections [22]. Additionally, these anti-microbial peptides and serine proteases can be secreted and ROS generated extracellularly for microbial killing without phagocytosis [11, 13].

As a last ditch attempt at bacterial killing, neutrophils can purposefully exude their DNA into an extracellular structure known as a neutrophil extracellular trap

(NET), to catch and kill pathogens [23]. This process of chromatin extrusion is now seen as a specialised form of cell death, known at NETosis, and the chromatin mesh expelled from the neutrophil is coated with many anti-microbial peptides, NE and MPO for bacterial killing, and also contains histones that themselves have high levels of anti-microbial activity [24].

1.2.2 Monocytes

Following from neutrophils, monocytes are the next cells to arrive at a site of inflammation. Monocytes are mononuclear cells formed in the bone marrow [25], and are ultimately derived from the recently discovered common monocyte progenitor (cMoP) population, which is the terminal precursor in their development cascade [26]. Monocyte specification is absolutely dependent on the cytokine macrophage colony-stimulating factor (M-CSF) and the transcription factor PU.1 [27–29]. In mice, two subsets of monocytes exist: the classical/inflammatory monocytes and the non-classical/patrolling monocytes [30]. These are commonly delineated by their differential expression of the Ly6C surface protein, with classical monocytes having high expression of Ly6C and non-classical monocytes having low surface levels of Ly6C.

The Ly6C^{hi} inflammatory monocytes are further characterised by their expression of a range of surface markers, being fully defined as: Ly6C^{hi}, CCR2^{+}, CX$_3$CR1^{mid}, CD62L^{+} and CD43^{lo} [30]. These Ly6C^{hi} monocytes are termed inflammatory as their high surface expression of the chemokine receptor CCR2 causes their mobilisation from the bone marrow and subsquent recruitment to sites of inflammation [31, 32]. They have a short half life ($\sim$ 8-20 hours [33]), high phagocytic and bacterial killing capacity and, once inside the tissue, differentiate into macrophages to aid with pathogen and cell debris clearance [34].

Ly6C^{lo} monocytes are fully defined as: Ly6C^{lo}, CCR2^{-}, CX$_3$CR1^{hi}, CD62L^{-} and CD43^{hi} [30]. They have been conclusively demonstrated to derive entirely

from the Ly6C^{hi} population, but curiously have a much longer half life of around 5-7 days [33]. Due to their low expression of CCR2, they do not rapidly traffic to sites of inflammation and instead seem to act as sentinel cells, watching for endothelial damage. Intravital microscopy has found that these Ly6C^{lo} monocytes slowly crawl on the luminal endothelial layer (hence their patrolling moniker) where they check for damaged endothelium and orchestrate its repair [35, 36]. They can be recruited to sites of inflammation due to their high expression of the fractalkine receptor CX_3CR1 [25], however they normally arrive much later than inflammatory monocytes. Once inside the tissue, they can differentiate into macrophages and contribute to tissue repair and the return to homeostasis [34].

1.2.3 Macrophages

Macrophages (literally 'big eaters' derived from the Greek *makros*, meaning large and *phagein*, meaning eat) are professional phagocytes found in almost all tissues throughout the body [25]. As mentioned above, they can be derived from blood monocytes that have entered into the tissue during an inflammatory response, and these monocyte-derived macrophages contribute to bacterial killing and clearance of dead leukocytes by phagocytosis. Indeed it was long thought that tissue resident macrophages were constantly replenished and maintained from blood monocytes [37]. However, recent and elegant fate mapping studies have demonstrated that this is not the case. In fact, almost all tissue resident macrophage populations are seeded before birth, derived from the yolk sac and/or the foetal liver, and are then maintained throughout life by local macrophage proliferation [30, 33, 38]. The only exception to this is the intestine, as the CX_3CR1^{hi} macrophages of the lamina propria are constantly renewed from Ly6C^{hi} monocytes [39]. Importantly, recent work has demonstrated that resident macrophages from different tissues have distinct transcriptional and epigenetic profiles, programmed by their local tissue environment, that allow them to perform niche specific functions [40–42].

Macrophages play many vital roles *in vivo*, with tissue resident macrophages shaping the architecture of developing tissues alongside helping maintain tissue homeostasis [43]. However, perhaps their most important role is as sentinel cells, patrolling the tissue and raising the alarm if signs of infection or tissue damage are detected. Macrophages can sense pathogens via the recognition of conserved microbial motifs, known as pathogen-associated molecular patterns (PAMPs), by specialised pattern recognition receptors (PRRs) and endogenous danger-associated molecules, known as danger-assocaited molecular patterns (DAMPs) or Alarmins, by a variety of mechanisms [44, 45] (see section 1.3). This polarises them towards the pro-inflammatory 'M1' phenotype and these activated macrophages secrete a range of pro-inflammatory molecules, that serve to initiate the inflammatory response and recruit neutrophils and monocytes to the tissue [46]. Additionally, bacterial products such as fMLF, complement components such as C3a and C5a, and a variety of CC chemokines, signalling via specific surface expressed GPCRs, act as macrophage chemoattractant factors to further aid macrophage tissue recruitment and to direct these cells towards pathogens [47]. As with neutrophils, macrophages kill infectious agents by phagocytosis and the generation of ROS, but also heavily rely on the generation of nitric oxide and reactive nitrogen species, by nitric oxide synthase, for bacterial killing [48, 49].

After pathogen clearance, the inflammatory response needs to be terminated to inhibit unwanted tissue damage and to return the local environment to homeostasis. This is known as inflammation resolution and macrophages play a core role in orchestrating this vital process [43]. If the containment and elimination of any infectious agents present at a site of inflammation has been successful, then there is a switch towards the local production of anti-inflammatory/pro-resoultion mediators, such as the cytokines IL-4, IL-13, IL-10 and TGF-β and the lipid-derived lipoxins, resolvins, maresins and protectins [5, 50] (see section 1.7). Together, these serve to skew macrophages towards the pro-resolution/tissue repair 'M2' phenotype [46]. These alternatively activated macrophages then phagocytose dead and dying leukocytes

as well as tissue debris and also guide angiogenesis [51–53]. Furthermore, specific deletion of macrophages during an *in vivo* skin wound model blocked correct healing of the damaged area, demonstrating that M2 macrophages also play a crucial role in tissue repair and remodelling [54].

1.2.4 Eosinophils

First identified in 1879, these cells received their name from the finding that they are strongly stained by the acidic dye eosin [55]. They are part of the granulocyte family, along with neutrophils and basophils, and develop in the bone marrow from HSCs with the transcription factors PU.1, C/EBP and GATA-1 and the cytokines GM-CSF, IL-3 and IL-5 essential for esoinophil specification [56]. Following their maturation they exit briefly into the blood, where they have a half-life of around 18 hours, before marginating into peripheral tissues such as the thymus and intestines [57]. They are characterised by the presence of large specific granules enriched for eosinophil peroxidase, major basic protein, eosinophil-derived neurotoxin and eosinophil cationic protein [58]. However, they also have granules containing various cytokines and enzymes, as well as leukotrienes, thromboxanes and prostaglandins [59, 60]. Mature eosinophils contain a large range of innate immune cell-associated surface proteins, such as lipid and chemoattractant binding GPCRs, cytokine receptors, Fc receptors, adhesion molecules and PRRs that act to activate and recruit these cells to sites of infection [55]. However the most important surface receptors expressed by eosinophils are arguably the IL-5 receptor, as IL-5 is a cytokine essential for differentiation, proliferation and survival of mature eosinophils [61] and the chemokine receptor CCR3, which binds eotaxin (also known as CCL11), and is central for eosinophil tissue recruitment [62].

During times of inflammation, eosinophils leave the bone marrow and traffic to inflammatory sites mainly via the actions of IL-5 and the eotaxins. These, as well as various cytokines, stimulate eosinphil de-granulation, providing the main

mechanism of eosinophil-mediated pathogen killing [63]. Although evidence exists that eosinophils contribute to viral and bacterial defence [64] (recent work has even demonstrated that eosinophils can make NETs in a fashion similar to neutrophils to trap and kill bacteria [65]), historically they are considered to defend against helminth infection [66]. Indeed eosinophil granule proteins have potent anti-parasitic activity *in vitro* and eosinophil depleted mice fail to efficiently clear helminth infections [66]. However, it has also been discovered that eosinophil depletion has no effect on *Schistosoma mansoni* containment [67] and some studies have even found that in certain situations, eosinophils can actually promote helminth survival *in vivo* [68], thereby demonstrating that the role of the eosinophil within helminth infection may be more complex that currently thought.

Eosinophilia contributes to many different inflammatory pathologies, but is most commonly associated with asthma; a chronic inflammatory disease of the airway. Excessive eosinophil recruitment to the lungs and airways is commonly seen in patients with asthma and a central role for these granulocytes in disease progression is supported by a range of animal models of airway inflammation [55]. Importantly, therapies that target eosinophils specifically, such as anti-IL-5 monoclonal antibodies, are currently in clinical development for the treatment of eosinophil-associated diseases [62].

1.2.5 Mast cells

Mast cells begin their life in the bone marrow, but are released into the circulation and seeded into almost all tissues in an immature form (known simply as mast cell precursors - MCps) characterised by the high expression of the stem cell factor receptor (SCF) c-kit and the high-affinity IgE receptor FcϵRI [69]. Here they complete their differentiation in response to locally produced SCF and various cytokines, of which IL-3 is especially important [69]. Fully mature mast cells are characterised by an abundance of cytoplasmic electron-dense vesicles that contain many pre-formed

inflammatory mediators, such as histamines, prostaglandins, serotonin, TNF-α and proteases, including chymase and tryptase [70].

Due to their predominant localisation in tissues that are exposed to the external environment, such as the lungs, skin and GI tract, these cells are ideally placed to act as sentinel cells, monitoring for signs of tissue damage and infection [71]. Mast cells express a wide range of PRRs that allow their activation in response to pathogens and damage molecules [72]. The main consequence of mast cell activation is the rapid release of their granule contents into the extracellular environment, to quickly initiate the acute inflammatory response. However, activation also stimulates their *de novo* production of leukotrienes, prostaglandins, platelet-activating factor, cytokines and chemokines that act to further strengthen the inflammatory response and recruit innate immune cells to the site of infection or tissue damage [70, 71].

Clearly mast cells play a critical role in host pathogen defence, but they have also been implicated in many inflammatory diseases [72]. However, their major pathological function is within allergic inflammation [73]. During an allergic reaction, IgE produced by activated B cells binds to FcϵRI that is present at high levels on the mast cell surface [74]. Subsequent antigen binding to the IgE Fab region results in Fc receptor clustering and downstream signalling, ultimately leading to mast cell degranulation and the initiation of an inflammatory response [73, 74].

1.3 Sensing of infection or tissue damage by innate immune cells

As briefly mentioned above, cells of the innate immune system can recognise and respond to a wide range of PAMPs (the molecular signatures of pathogens) via PRRs. These receptors can be grouped by their cellular location, with Toll-like receptors (TLRs) and C-type lectin-receptors (CLRs) present on the cell surface for extracellular pathogen detection [75], and Nod-like receptors (NLRs) and RIG-I-like

receptors (RLRs) present throughout the cytoplasm to monitor for intracellular PAMPs [45].

1.3.1 Extracellular pathogen recognition

The TLRs were discovered in 1998 by Bruce Beutler with the identification of the lipopolysaccharide (LPS) sensor TLR4 [76]. TLRs receive their name due to their homology with the *Drosophila melanogaster* Toll protein and are transmembrane glycoproteins containing extracellular leucine-rich repeat regions, central for ligand binding, and an intracellular toll/interleukin-1 receptor (TIR) homology domain [75]. To date, 10 TLR family members have been discovered in humans and each recognises a specific type or class of ligand, allowing specific immune responses to be mounted against different stimuli. For example, TLR2 recognises β-glycans and zymosan, TLR3 recognises dsRNA, TLR5 recognises bacterial flagellin and TLR9 recognises unmethylated CpG DNA present in bacterial DNA [45]. Ligand binding causes TLR oligomerisation via their intracellular TIR domains and the recruitment of adaptor proteins such as MyD88 and/or TRIF [2]. These adaptor proteins mediate the activation of various transcription factors, with NF-κB being the canonical example, which results in the transcription of pro-inflammatory cytokines, interferons, chemokines and the initiation of an inflammatory response [2].

1.3.2 Intracellular pathogen recognition

There are three intracelluar RLRs, RIG-I, MDA5 and LGP2, and all are central for cytoplasmic RNA detection; a signature of viral infection [77]. The NLRs can sense a wide range of intracellular PAMPs, mostly of a bacterial nature, and of the 23 and 34 members in humans and mice respectively, NOD-1 and NOD-2 are the most widely studied [45]. For both RLRs and NLRs, PAMP binding to their C-terminal domains leads to their cytoplasmic oligomerisation via interactions between their N-terminal CARD domains. As with the TLRs, this ultimately leads to the

activation of the NF-κB and MAPK pathways and the transcription of cytokines and type I interferons [45, 75, 77]. However, the NLRs are also capable of forming a large intracellular complex, known as the inflammasome, consisting of an NLR family member (which defines the type and ligand specificity or the inflammasome), AIM-2, ASC and pro-caspase 1 [78]. NLR-PAMP binding leads to the formation of the inflammasome complex and the proteolytic activation of caspase-1. Active caspase-1 then cleaves pro-IL-1β to yield the active IL-1β, which is then secreted from the cell to induce an inflammatory response [78].

1.3.3 Recognition of endogenous danger-associated molecules

However the immune system also responds during sterile injuries, such as tissue cuts, wounds and ischaemia, via endogenous molecules known as DAMPs or Alarmins [44]. Importantly, these are host-derived components normally absent from the extracellular environment under homeostatic conditions. However during times of cell stress or after necrosis, these are released from the cell and activate tissue resident leukocytes, initiating an inflammatory response [3]. To date a large range of DAMPs have been discovered, such as the heat shock and S100 proteins, uric acid crystals and ATP [3, 44], but the canonical alarmin is high mobility group box-1. This DNA chaperone is released during necrosis, but not apoptosis [79], and binds to multiple surface receptors, such as TLRs and RAGE, resulting in innate immune cell activation and pro-inflammatory mediator production, predominantly via the NF-κB pathway [3].

1.4 Mediators of the acute inflammatory response

1.4.1 Cytokines

Cytokines are small secreted proteins that are central for coordinating an inflammatory response. There are over 100 genes encoding for cytokine members, and this fam-

ily comprises of monokines (monocyte-derived cytokines) lymphokines (lymphocyte-derived cytokines), chemokines (chemoattractant cytokines - see section 1.4.2), and interleukins (ILs - cytokines made by, and acting on, leukocytes) [80, 81]. In response to infection or tissue damage, cytokines can be made by a range of cell types, including mast cells, eosinophils and endothelial cells, but macrophages and T helper cells are the main producers *in vivo* [82]. By binding to their specific cell surface receptors, cytokines can act both locally and systemically, in an autocrine and paracrine manner, to elicit changes in cell behaviour.

The cytokine tumor necrosis factor-α (TNF-α) plays a central role in regulating many aspects of an inflammatory response, such as programmed cell death, the generation of other pro-inflammatory mediators, inflammatory pain, the activation of endothelial cells, and the recruitment of immune cells to sites of inflammation [83]. TNF-α has both a membrane tethered and a soluble form (with soluble TNF-α generated from the transmembrane version via the activity of TNF-α-converting enzyme [84]) and binds and activates to two structurally distinct cell surface receptors known as TNF receptor 1 (TNFR1) and TNFR2 [81]. TNFR1 is expressed by all cell types (the only exception being erythrocytes) and ligation by both membrane bound and soluble TNF-α results in the association of the TNF receptor-associated death domain (TRADD) protein with the intracellular death domain of TNFR1. TRADD can then cause apoptosis by activating fas-associated death domain (FADD) protein and pro-inflammatory gene expression by stimulating TNF receptor-associated factor 2 (TRAF2), which results in the activation both AP-1 and NF-κB-mediated gene transcription [83, 85]. In contrast, the expression of TNFR2 is restricted to neurones, microglia, endothelial cells and innate and adaptive immune cells, and this receptor is thought to be primarily activated by membrane tethered TNF-α [86]. Furthermore, TNFR2 signals exclusively via the TRAF2 pathway, due to the lack of an intracellular death domain, and results in sustained NF-κB activation that can occur independently of TNFR1 [85, 86]. Clinically, inhibition of TNF-α signalling with anti-TNF-α blocking antibodies is now used to successfully treat a wide range

of inflammatory autoimmune diseases, such as rheumatoid arthritis (RA), ankylosing spondylitis and inflammatory bowel disease (IBD) [83]. The impact of the discovery and development of anti-TNF-α biologicals is underscored by the fact that the top selling drug of 2015 was Adalimumab (trade name: Humira), a TNF-α blocking, fully humanised, monoclonal antibody that generated sales in excess of 14 billion US dollars [87].

Alonside TNFα, the cytokines IL-1α and β, IL-6, IL-8 and IFN-γ also have a wide range of potent pro-inflammatory actions, including activating innate immune and endothelial cells to promote a local inflammatory response [80–82]. However, cytokines can also have anti-inflammatory properties, with IL-4, IL-10, IL-13 and TGF-β acting to inhibit pro-inflammatory mediator production, promote Th2 and regulatory T cell generation and function, and polarise macrophages towards the anti-inflammatory M2 phenotype [46, 88].

1.4.2 Chemokines - chemoattractant cytokines

Chemokines are a sub-family of cytokines that play a central role in regulating leukocyte migration and tissue recruitment [89]. Some are homeostatic, regulating immune cell tissue localisation and retention under basal conditions, whereas others are pro-inflammatory, synthesised after the induction of an immune response to recruit leukocytes to areas of tissue damage or infection [90]. In humans and mice there are approximately 50 chemokines split into 4 classes: C, CC, CXC and CX_3C, based on the location and spacing of their conserved cysteine residues. Unlike the other cytokines, chemokines act via $G_{i/o}$-coupled GPCRs, of which approximately 20 are currently known, and these receptors are named for the class of chemokine they bind, i.e CCRs or CXCRs [89]. As a general rule, CC chemokines are potent inflammatory monocyte recruitment factors (with CCL2 being the classic example), but also stimulate the chemotaxis of T cells, NK cells and eosinophils [91], whereas CXC chemokines, especially CXCL1 and 2, act to mobilise and recruit

neutrophils [89, 90]. Fractalkine (also known as CX_3CL1) is the only member of the CX_3C family and is unique among the cytokines as it exists in a soluble and plasma membrane tethered form, which allows it to act as a chemoattractant and an adhesion molecule respectively [92]. CX_3CL1 acts as a chemoattractant for NK and T cells, but is particularly important in recruiting the patrolling $Ly6C^{lo}$ monocytes to inflamed tissues as these cells have high surface levels of CX_3CR1 [92].

1.4.3 The complement system

Complement is an ancient and evolutionarily conserved system of more than 30 proteins present in high concentrations in the blood that provides a rapid first line defence against infection [93]. At its core, the complement system is proteolytic protein cleavage cascade, initiated following pathogen recognition, that activates innate immune cells, coats pathogens with complement-derived opsonins and attemps target cell lysis via the formation of a multi-protein, pore forming structure known as the membrane attack complex (MAC) [94]. Complement is activated by one of three pathways: classical, lectin and alternative. Initiation of the classical pathway occurs via the recognition of antibody coated cells by the C1 complex, whereas the lectin pathway is activated in an antibody-independent manner, instead relying on pathogen recognition mainly via the mannose-binding lectin PRR [95]. The alternative pathway utilises the spontaneous hydrolysis of the C3 complement protein, which is amplified by the presence of an infectious agent [95]. All three pathways converge on the generation of the C3 convertase complex that cleaves C3 into C3a and C3b. C3b then drives the formation of the C5 convertase, which cleaves the C5 complement protein into C5a and C5b. C5b then drives the formation of the MAC, comprised of C5b and C6-9, which then forms a membrane pore, leading to target cell lysis [94–96]. Importantly, C3b acts as a potent opsonin, facilitating pathogen phagocytosis, whereas C3a and C5a act as potent pro-inflammatory molecules and leukocyte chemoattractants, stimulating the inflammatory response and recruiting innate immune cells to sites of infection [93].

1.4.4 pro-inflammatory eicosanoids

The eicosanoids are a group of lipid signalling molecules that act locally to regulate both homeostatic and inflammatory processes. The two main classes that act as pro-inflammatory mediators are the leukotrienes (LTs) and the prostaglandins (PGs) [97]. Both are derived from arachidonic acid (AA), which is itself generated after being liberated from plasma membrane lipids by the actions of cytosolic phospholipase A2 [98].

LT synthesis begins with the oxygenation of AA by 5-lipoxygenase, which generates the LTA4 intermediate [99]. This is then either hydrolysed to LTA4 hydrolase to form LTB4, or acted on by LTC4 synthase to generate LTC4. LTC4 is the parent compound for the cysteinyl LT (cysLT) sub-class, from which the other members LTD4 and LTE4 can be made [99]. Interestingly, LTs are synthesised in a cell type specific manner during an inflammatory response, with neutrophils and dendritic cells primarily producing LTB4, eosinophils and mast cells producing mainly cysLTs and macrophages capable of producing both [100]. They mediate their effects via GPCR ligation, and to date 4 LT receptors have been discovered; LTB4R1 and LTB4R2, which bind LTB4, and CYSLTR1 and CYSLTR2, which bind the cysLTs [101]. LTB4 acts as a potent innate immune cell chemoattractant, helping recruit leukocytes to sites of inflammation, and also facilitates neutrophil activation and de-granulation and well as monocyte inflammatory mediator production [99, 100]. The cysLTs act to cause the contraction of airway smooth muscle cells and aid the inflammatory response by increasing vascular permeability [99, 100]. The importance of LTs for host defence is highlighted in mice that lack 5-lipoxygenase, as these animals have impaired survival and bacterial clearance in a pulmonary infection model [102].

Alongside their homeostatic roles, the PGs are critical for the generation of an inflammatory response and are largely responsible for the cardinal signs of inflammation: pain, swelling, heat and redness [103]. They are produced at low levels under basal conditions, but their tissue production is rapidly and strongly

up-regulated during an acute inflammatory response [101]. PGs can be made by almost any cell type, but are predominantly produced by tissue resident mast cells and macrophages [103]. There are 4 main PGs *in vivo*, PGE_2, PGD_2, PGI_2 and $PGF_{2\alpha}$ [103] and their synthesis is dependent on the action of cyclooxygenase (COX) 1 and 2, with COX-1 being constitutively expressed in most cell types, and COX-2 strongly up-regulated during an inflammatory response [104]. COX-1/2 generates the PGH_2 intermediate from AA, which is used as the substrate for the production of the specific PGs via the activity of PGE, PGI or PGF synthase [104]. Like the LTs, PGs act via GPCRs, of which 7 have been discovered. During inflammation, the PGs regulate inflammatory pain alongside promoting blood vessel dilatation and permeability, and regulate immune cell function, vascular adhesion and inflammatory mediator production [103]. The importance of PGs within an inflammatory response is highlighted by the fact that both COX-1 and 2 are the targets for a wide range of non-steroidal anti-inflammatory drugs, commonly used to manage the clinical symptoms of inflammation [101].

1.5 Neutrophil recruitment to sites of inflammation

Under homeostatic conditions the vast majority of mature neutrophils are retained in the bone marrow, with only 2% existing in the circulation [105], by the CXCR4-CXCL12 signalling axis. Mature neutrophils express low levels of the chemokine receptor CXCR4, bone marrow stromal cells constitutively produce the ligand for this GPCR, known as CXCL12, and this signalling system acts to keep neutrophils in the bone marrow [106]. Indeed genetic deletion of CXCR4, specifically in the myeloid compartment, results in increased blood neutrophil numbers, and treatment of both mice and humans with CXCR4 antagonists results in swift bone marrow neutrophil mobilisation [106–108]. Additionally, patients with wart, hypogammaglobulinaemia, infection and myelokathexis syndrome exhibit profound blood neutropenia, but increased bone marrow neutrophil content, as they have a mutation in CXCR4 that

makes the receptor more sensitive to CXCL12, therefore increasing the strength of the retention signalling axis [109].

During an inflammatory response, neutrophils are mobilised from the bone marrow and recruited to sites of infection or damage. Chemoattractants such as LTB4 and C5a contribute to neutrophil moibilisation and tissue recruitment, as their intravenous injection leads to blood neutrophilia [110], however the cytokine G-CSF and the chemokines CXCL1 and CXCL2 are central for bone marrow neutrophil release [106,110]. G-CSF production is up-regulated during an inflammatory response, and its *in vivo* administration leads to increased bone marrow neutrophil mobilisation. G-CSF achieves this by decreasing both neutrophil CXCR4 expression and bone marrow stromal cell production of CXCL12, thereby disrupting the neutrophil bone marrow retention signalling pathway [105, 111]. Large amounts of CXCL1 and 2 are produced during the acute inflammatory response and mice lacking CXCR1 or CXCR2, the cognate receptors for these chemokines, have impaired neutrophil recruitment to sites of inflammation [112]. Their central role in neutrophil bone marrow mobilisation was demonstrated by Wengner *et al* who found that i.p injection of CXCL1 or 2 led to increased blood neutrophil numbers and that pre-treatment with CXCL1 or 2 blocking antibodies ablated bone marrow neutrophil mobilisation in response to i.p thioglycollate injection [111]. Therefore it is currently believed that G-CSF and CXCL1 and 2 work in concert to inhibit bone marrow retention signals and stimulate neutrophil chemotaxis to cause their release from the bone marrow [110].

Once the neutrophil has entered into the blood, it next has to exit the circulation and enter into the inflamed tissue. To do this the neutrophil has to interact with, and arrest on, the vessel wall and then move through the endothelial cell layer and the basement membrane. This is commonly referred to as the neutrophil recruitment cascade and comprises of 5 steps: tethering, rolling, adhesion, crawling and finally transmigration. Importantly, the whole process relies on components expressed on both neutrophils and endothelial cells.

Due to the laminar flow of blood, neutrophils and other leukocytes are passively transported in the centre of the major vessels [113]. However the blood flow in postcapillary venules (the vessels closest to sites of inflammation) is greatly reduced and this increases the chance that a neutrophil will come into contact with the endothelial cells that line the vessel wall [113]. Concomitantly, and in response to the local inflammatory mediators produced by activated tissue resident mast cells and macrophages such as TNF-α, cytokines and histamine, endothelial cells up-regulate their surface expression of selectin adhesion molecules. This begins with P-selectin, as this is stored pre-formed inside intracellular Weibel-Palade bodies, and is followed by E-selectin, which takes longer to peak as it is synthesised *de novo* [114]. Together these adhesion molecules interact with their glycoprotein ligands expressed on the neutrophil surface, of which the best characterised is P-selectin glycoprotein ligand 1 (PSGL1), and this beings the tethering process [115]. As the selectins have fast on and off rates, this causes the neutrophil to roll along the vessel wall due to rapid selectin-ligand binding and unbinding [115].

The purpose of rolling is to slow the neutrophil down and bring it into close proximity with the vessel wall to allow further neutrophil activation by locally produced pro-inflammatory mediators and chemokines [113]. In fact, chemokines are transported across the endothelial layer and are displayed on the luminal cell wall via their interaction with heparin sulphate [116]. For neutrophils, the chemokines CXCL1, CXCL2 and CXCL5 are crucially important, activating both CXCR1 and CXCR2, to facilitate neutrophil-endothelial cell adhesion [8]. The combined action of local inflammatory mediators and chemokines serves to activate the neutrophil surface integrins LFA-1 and MAC-1, allowing them to bind the endothelial-localised adhesion molecules ICAM-1 and ICAM-2 [8]. This interaction is high affinity, essential for firm adhesion, and serves to arrest the neutrophil on the vessel wall [115].

Next, the neutrophil migrates through the endothelial cell layer (2-5 minutes) and then the basement membrane (5-15 minutes) to enter into the tissue, in a process known as transendothelial migration (TEM) [115]. Interstingly, TEM does not have

to occur at the point where the neutrophil arrests on the vessel wall. Instead the neutrophil can crawl along the vessel, in a process dependent on MAC-1/ICAM-1 interactions, to find a point of entry [8]. The preferred route for neutrophils is at an endothelial cell-cell junction (paracellular - 90% of all TEM [113]), but they can also move through an endothelial cell (transcellular). However, this route is less efficient, taking 20-30 minutes *in vivo* [117]. TEM relies on the homophilic interactions between neutrophil and endothelial cell junctional adhesion molecules, importantly PECAM-1, CD99 and JAM-A, that allow the neutrophil to squeeze between or through the endothelial cell layer [118,119]. Once inside the tissue, local chemoattractant gradients then guide the neutrophil towards the area of infection or tissue damage.

1.6 Monocyte recruitment to sites of inflammation

As briefly mentioned in section 1.2.2, monocytes develop in the bone marrow and can be mobilised to sites of tissue damage or infection. Inflammatory Ly6C^{hi} monocytes express high levels of CCR2, and this chemokine receptor is essential for their bone marrow mobilisation, as in animals lacking CCR2, Ly6C^{hi} monocytes accumulate in the bone marrow due to their impaired entry into the blood upon infection with *Listeria monocytogenes* [31,32]. This CCR2-dependent mobilisation is predominantly triggered by CCL2 and CCL7 as genetic deletion of either chemokine results in impaired Ly6C^{hi} monocyte release from the bone marrow under basal and inflammatory conditions [31,120]. Interestingly however, CCR2 does not seem to be required for Ly6C^{hi} monocyte tissue recruitment as Ccr2$^{-/-}$ Ly6C^{hi} monocytes are still able to efficiently enter sites of inflammation [32]. Instead, the chemokine receptors CCR1 and CCR5 (responding to a range of CC chemokines including CCL3 and CCL5) are essential for tissue recruitment of Ly6C^{hi} monocytes, as animals lacking either receptor have impaired Ly6C^{hi} monocyte recruitment to sites of inflammation *in vivo* [121]. For the non-classical Ly6C^{lo} monocyte population,

CX_3CL1 is important for their tissue recruitment, as this population expresses high surface levels of CX_3CR1 [36].

In a classic inflammatory response, $Ly6C^{hi}$ monocytes arrive at a site of inflammation after neutrophils, and it is now well established that the neutrophils themselves are central for the subsequent tissue recruitment of monocytes. Several studies, using different inflammatory animal models, have demonstrated that neutrophil depletion results in impaired monocyte tissue recruitment [122]. Indeed, the neutrophil granule-derived components azurocidin and proteinase-3 cause the increased endothelial expression of adhesion molecules, which facilitates firm monocyte adhesion [123, 124], and multiple granule proteins, including LL-37, azurocidin and CG all act as monocyte chemoattractants [125]. Furthermore, neutrophil-derived proteinase-3 promotes endothelial cell expression of CC chemokines, and neutrophils themselves can generate a range of CC chemokines once activated [122]. Together these findings demonstrate that neutrophils are essential for monocyte tissue recruitment and this provides and elegant method for the step-wise recruitment of different leukocyte populations, that perform distinct functions, during an inflammatory response.

The process of monocyte capture and TEM is largely the same as for neutrophils (described in section 1.5), however there are a few subtle differences. During the endothelial cell adhesion phase, monocyte expressed VLA-4 engages with VCAM-1, localised on the endothelium, and this integrin-ligand interaction is essential for monocyte firm adhesion to the vessel wall [113, 115]. Additionally, rather than CXC chemokines, monocytes heavily rely on CC chemokines for their recruitment to sites of inflammation, with the chemokine receptors CCR1 and CCR5 aiding in monocyte endothelial recruitment and TEM [121].

1.7 The resolution of inflammation

The outcome of a successful inflammatory response is the return of the tissue to homeostatic conditions. This process, known as the resolution of inflammation,

is characterised by the removal of dead cells and tissue debris, the restoration of normal vascular permeability and blood flow, tissue repair and recovery from fever and pain [6]. For a long time it was considered that this return to normality was a passive process, with local pro-inflammatory mediators naturally reducing over time [5]. However, it has now been firmly established that, far from happening passively, an active and co-ordinated system of anti-inflammatory and pro-resolution mediators are responsible for restoring tissue homeostasis.

Perhaps the most well studied pro-resolution compounds are the specialised pro-resolving mediators (SPMs); lipids consisting of the lipoxins (AA-derived), resolvins, maresins and protectins (eicosapentaenoic and docosahexaenoic acid-derived) [126]. These share many common elements with the pro-inflammatory leukotrienes, with all being synthesised by lipoxygenase family members and the lipoxins deriving from AA [6], however towards the end of the acute inflammatory response there is a switch in lipoxygenase expression that shifts away from leukotriene synthesis and towards the production of the SPM family members [5, 127]. Together these lipid mediators promote the resolution of inflammation by blocking neutrophil migration, adhesion and TEM, inhibiting local pro-inflammatory mediator production, neutrophil degranulation and ROS production, as well as promoting macrophage phagocytosis of dead neutrophils and tissue debris [4–6, 126–128]. The SPMs exert these effects by activating leukocyte surface GPCRs, with lipoxin A_4 binding FPR2 (also known as ALX), resolvin E1 binding ChemR23, resovin D1 binding GPR32 and resolvin D2 binding GPR18.

However these lipid mediators only form part of a greater resolution signalling network [6]. For example, the anti-inflammatory cytokines TGF-β and IL-10 promote the polarisation of monocyte-derived and tissue resident macrophages towards the M2 phenotype to promote tissue debris clearance and repair [129]. Additionally, the glucocorticoid regulated protein annexin A1 has been demonstrated to potently direct the resolution of an inflammatory response by limiting tissue neutrophil influx and local pro-inflammatory mediator production, as well as inducing neutrophil

apoptosis and macrophage phagocytosis [130]. It is only by working in tandem that these pathways result in the return to tissue homeostasis. Indeed there is a high degree of overlap between these pathways, as annexin A1 binds and activates FPR2, thereby explaining why the function of annexin A1 strongly resembles that of the lipoxins, resolvin E1 stimulates the production of lipoxin A_4 and the lipoxins and the resolvins promote macrophage IL-10 production to further increase their M2 polarisation [127].

1.8 The endocannabinoid system

Alongside the eicosanoids and the SPMs, the endocannabinoid system is also an endogenous AA-dependent lipid signalling network that controls many fundamental processes in the body, including the inflammatory response [131]. After more than six decades of work, it is now established that the endocannabinoid system is comprised of two GPCRs, cannabinoid receptor 1 (CB_1) and cannabinoid receptor 2 (CB_2), the cognate ligands for these receptors, known as the endocannabinoids, and the enzymes that synthesise and degrade these endogenous lipids [132, 133]. I will now introduce these components in more detail below, but will concentrate mainly on CB_2 and the role this plays in health and disease, as this receptor forms the main focus of my thesis.

1.8.1 The cannabinoid receptors

As its name suggests, CB_1 was the first of the cannabinoid receptors to be discovered. Pioneering work throughout the late 80's demonstrated that the pharmacological actions of the cannabis-derived compound Δ9-tetrahydrocannabinol (Δ9-THC) and its synthetic analogues were in fact mediated by a PTX-senstive GPCR found in neuronal cell lines and brain tissue. [134–139]. Then in 1990, Matsuda *et al* cloned an orphan GPCR, known as SKR6, from a rat cerebral cortex cDNA library and

demonstrated that this receptor binds and is activated by Δ9-THC [140]. As this GPCR binds cannabis-derived compounds, it was christened cannabinoid receptor 1.

The second cannabinoid receptor, CB_2, was discovered three years later in 1993 by Munro *et al* [141]. The authors of this study were attempting to uncover novel GPCRs expressed in myeloid cells and found that a clone they isolated named CX5 shared a high degree of sequence homology with the newly discovered CB_1. They then demonstrated that this receptor binds and is activated by cannabinoid compounds in cells transfected with the CX5 clone, conclusively demonstrating that this was a *bona fide* cannabinoid receptor and suggested it be called CB_2 [141].

CB_1 and CB_2 have an overall sequence homology of 44%, however this rises to around 70% homology when only considering residues important for ligand binding [141, 142]. The cannabinoid receptors are highly conserved across species as sequence homology between human, mouse and rat receptors is between 97 to 99% for CB_1 [140, 143–146] and around 80% for CB_2 [141, 146–148]. Both CB_1 and CB_2 are class A rhodopsin-like GPCRs, and are $G_{i/o}$-coupled, as their activation results in the inhibition of adenylyl cyclase and the lowering of intracellular cAMP levels [131, 146]. Additionally, signalling via the $G_{\beta/\gamma}$ subunits downstream of CB_1 and CB_2 activation also leads to intracellular Ca^{2+} release and activation of ligand gated ion channels, PI3K and the MAP kinase pathway [149]. Furthermore, like most GPCRs, their activation causes the recruitment of β-arrestin to the intracellular face of the receptor, which then mediates cannabinoid receptor internalisation and removal from the cell surface [150–153].

1.8.2 Expression pattern of CB_1

CB_1 is the most abundant GPCR expressed in the brain and is highly enriched in the cortex, cerebellum, ventral striatum, hippocampus and the substantia nigra [154, 155]. At the cellular level, CB_1 is primarily localised on presynaptic axon terminals [149], where it functions to negatively regulate neurotransmitter release, acting as a signal

gate to limit unwanted presynaptic activity. CB_1 activation has been demonstrated to block the release of GABA, glutamate, dopamine, cholecytokinin and noradrenaline due to its expression on the corresponding neuronal populations [156]. This expression pattern and function means that CB_1 regulates a large range of brain functions, such as mood, behaviour, memory, cognition, motor coordination, food intake and pain [155,157–160], and also explains the effects of recreational inhalation of Δ9-THC. Additionally it is now being discovered that, rather than being restricted to the brain, CB_1 is expressed in a range of peripheral tissues including, the liver, heart, adipose tissue, skeletal muscle, reproductive system and the intestinal tract [161], showing that CB_1 likely regulates a vast range of processes throughout the body.

1.8.3 Expression pattern of CB_2

CB_2 is most abundantly expressed in cells of the immune system, with B cells, NK cells and monocytes exhibiting the highest expression [162]. At the tissue level, CB_2 is found at high levels in the spleen, tonsils, thymus and bone marrow [146,163], all organs intimately involved with the immune system. The primary localisation of CB_2 on cells of the immune system means that this receptor regulates many aspects of immune cell function, such as B cell retention in the spleen and leukocyte migration, and plays an important role in the control of an inflammatory response [163,164]. However, in a manner similar to CB_1, others have found that CB_2 is expressed in a wide range of tissues and cell types throughout the body. These include: the gastrointestinal tract, the liver, the eye, skeletal muscle and the male and female reproductive system as well as endothelial cells, keratinocytes, osteocytes, osteoclasts and osteoblasts. Here, CB_2 acts to regulate many physiological and pathological processes [161,165,166].

Initially it was considered that CB_2 was entirely absent from the brain, as a large number of studies failed to find any expression of CB_2 throughout the central nervous system [165]. However, recent work has demonstrated that CB_2 is expressed

in a wide range of brain areas including the brainstem, hippocampus and the amygdala, but in contrast to CB_1, seems to be localised postsynaptically [155, 165]. Additionally, multiple reports exist detailing the presence of CB_2 in peripheral neuronal populations [165]. However, these findings are not without controversy as some have suggested that CB_2 expressed by microglia and the techniques used to examine CB_2 expression provide confounding factors, potentially leading to false positive results [165]. Nevertheless, the current weight of evidence supports the conclusion that CB_2 is expressed throughout the brain.

1.8.4 The endocannabinoids - synthesis and degradation

The endocannabinoids are the endogenous ligands for CB_1 and CB_2 and are synthesised on-demand in a Ca^{2+}-sensitive manner from plasma membrane lipids [167]. Currently there are 12 members of the endocannabinoid family that have been shown to bind and activate either or both of the cannabinoid receptors; however the most well characterised are *N*-arachidonoylethanolamine (AEA) and 2-arachidonoylglycerol (2-AG) [168]. Both of these endocannabinoids are AA-containing lipids, but despite this similarity the routes of synthesis and degradation for AEA and 2-AG are completely distinct from one another.

AEA synthesis and degradation

AEA was the first endocannabinoid discovered, isolated from pig brain in 1992 and shown to bind and activate CB_1 [169]. Since then it has been demonstrated that AEA binds to both CB_1 and CB_2 and acts as a partial agonist at both receptors, being slightly more efficacious at CB_1 [168]. Depending on the assay, the EC_{50} value for this ligand varies, but is commonly in the low nanomolar region for CB_1 and the high nanomolar to micromolar region for CB_2 [131].

The most common route of AEA synthesis occurs in a two-step process. Firstly an acyl chain, taken from any member of the membrane glycerophopholipid family, is

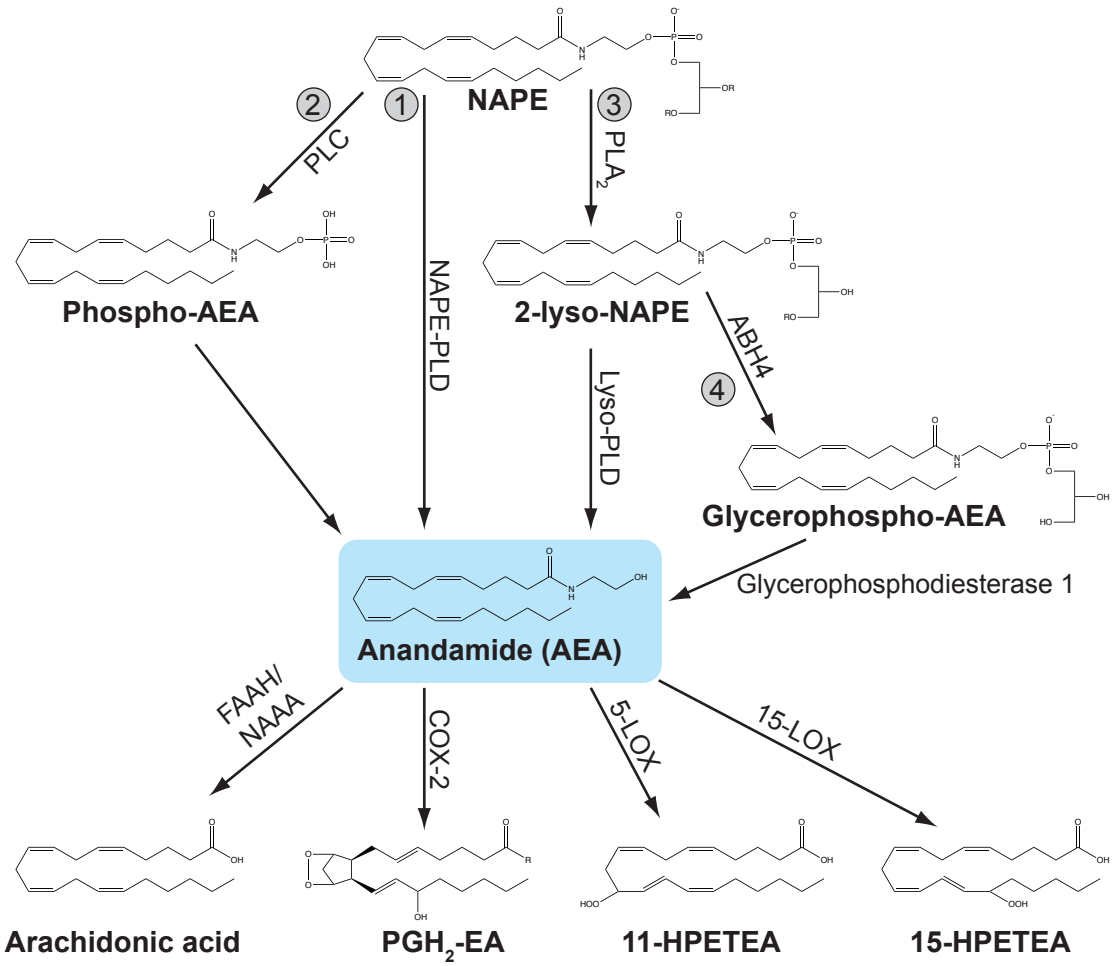

Figure 1.1 The major routes of anandamide synthesis and degradation. Chemical representation of the 4 main synthetic pathways for anandamide (each pathway is denoted by the number in the gray circle) and the main routes of anandamide degradation. *NAPE* *N*-arachidonoyl-phosphatidyl-ethanolamine, *PLA_2* phospholipase A2, *PLC* phospholipase C, *PLD* phospholipase D, *ABH4* α/β-hydrolase domain-containing protein 4, *COX* cyclooxygenase, *LOX* lipoxygenase, *FAAH* fatty acid amine hydrolase, *NAAA* *N*-acylethanolamine acid amide hydrolase, *PG* prostaglandin, *HPETEA* hydroxyperoxyeicosatetraenoylethanolamide.

transferred onto phosphatidylethanolamine to generate *N*-arachidonoyl-phosphatidyl-ethanolamine (NAPE). Subsequently, the enzyme NAPE-phospholipase D (NAPE-PLD) catalyses the formation of AEA [170]. Surprisingly however, it was found that NAPE-PLD$^{-/-}$ mice had little to no difference in brain levels of AEA, strongly suggesting that other AEA synthetic pathways exist [171]. To date alongside the canonical pathway, three other synthetic routes have been demonstrated to exist: 1) NAPE can be firstly hydrolysed by phospholipase C, to generate phospho-AEA, and secondly dephosphorylated by various phosphatases to form AEA [172]. 2) Phospholipase A2 can act on NAPE to generate 2-lyso-NAPE, which is then converted to AEA by lysophospholipase-PLD [173]. 3) NAPE or lyso-NAPE can be hydrolysed by α/β-hydrolase domain-containing protein 4 to glycerophospho-AEA which is then converted to AEA by the action of glycerophosphodiesterase 1 [174].

The degradation of AEA is primarily mediated by the serine hydrolase, fatty acid amine hydrolase (FAAH) [170, 175]. The importance of this enzyme *in vivo* for AEA degradation has been conclusively demonstrated, as pharmacological inhibition or genetic deletion of FAAH leads to the build up of AEA in tissues throughout the body [176–178]. FAAH breaks AEA down into AA, providing a link between endocannabinoid metabolism and the eicosanoid pathway, and is expressed in the same brain regions as CB_1 [170]. However, recent work has demonstrated that alongside FAAH, AEA can be degraded into various other breakdown products by *N*-acylethanolamine acid amide hydrolase (NAAA) [179], COX-2 [180] and by 5 and 15-lipoxygenases [170]. A schematic diagram depicting the major routes of both AEA synthesis and degradation is shown in Figure 1.1.

2-AG synthesis and degradation

Three years after AEA, 2-AG was discovered as a second endocannabinoid. It was found that 2-AG, purified from canine gut, could bind to CB_1 and CB_2 in receptor transfected cells and brain membrane preparations and mimic the *in vivo* actions of

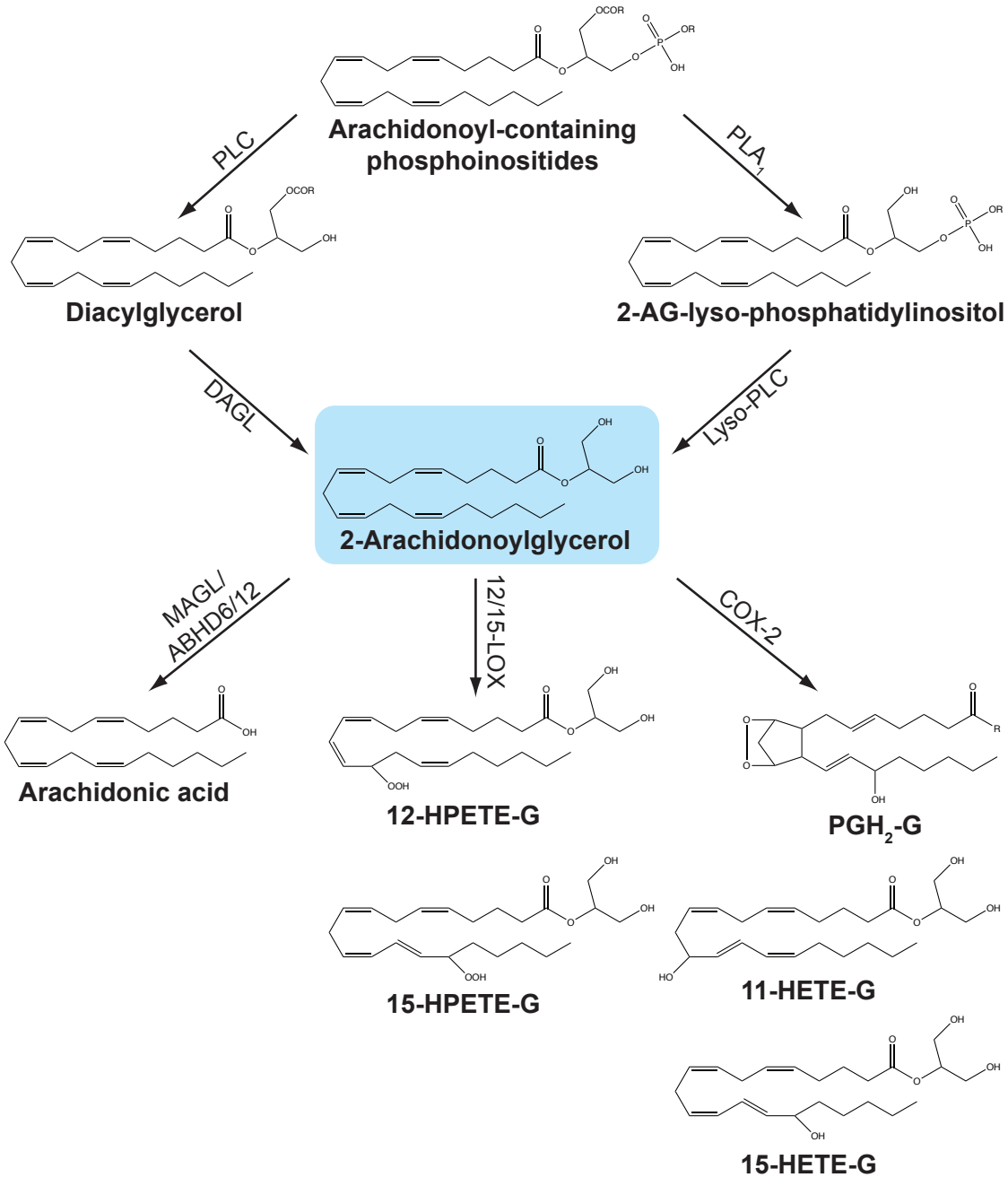

Figure 1.2 The major routes of 2-arachidonoylglycerol synthesis and degradation. Chemical representation of the main pathways responsible for the synthesis and degradation of 2-arachidonoylglycerol (2-AG). *PLA$_1$* phospholipase A1, *PLC* phospholipase C, *DAGL* diacylglycerol lipase, *MAGL* monoacylglycerol lipase, *ABHD* α/β-hydrolase domain, *COX* cyclooxygenase, *LOX* lipoxygenase, *PG* prostaglandin, *HPETE-G* hydroxyperoxyeicosatetraenoyl-glycerol, *HETE-G* hydroxyeicosatetraenoyl-glycerol.

Δ9-THC [181, 182]. To date, multiple studies have demonstrated that 2-AG binds and activates CB_1 and CB_2 with a similar potency but a higher degree of efficacy than AEA [168].

The major synthetic route of 2-AG is the sequential hydrolysis of arachidonoyl-containing membrane phosphoinositides, firstly by phospholipase C (PLC)β to generate diacylglycerol (DAG) and secondly by DAG lipase (DAGL) to generate 2-AG [170, 179]. There are two DAGL isoforms currently known, DAGLα and DAGLβ [183], however studies using knockout animals have demonstrated that DAGLα is the most important for 2-AG synthesis *in vivo* [183–185]. Similarly to AEA, 2-AG can also be synthesised by alternative pathways. It has been shown that cleavage of arachidonoyl-containing membrane phosphoinositides by phospholipase A1 generates 2-AG-lyso-phosphatidylinositol that can be further hydrolysed by lyso-PLC to produce 2-AG [186, 187]. Finally, 2-AG can be generated directly from 2-AG-lysophosphatidic acid [188].

The degradation of 2-AG is almost entirely mediated by monoacylglycerol lipase (MAGL), with it estimated that MAGL is responsible for 85% of 2-AG degradation *in vivo* as $MAGL^{-/-}$ animals have significantly increased tissue levels of 2-AG [189–191]. Mirroring AEA, this primary degredation pathway converts 2-AG into AA [170, 179]. The remaining 15% of 2-AG is mostly removed by ABHD6 and ABHD12, however FAAH, COX-2 and 5-/15-lipoxygenases also have been found to catalyse the degradation of 2-AG into various other breakdown products [180, 191, 192]. A schematic diagram depicting the major routes of both 2-AG synthesis and degradation is shown in Figure 1.2.

1.8.5 Phytocannabinoids

It is currently estimated that there are over 100 compounds present in the cannabis plant that have cannabinoid-like properties [193, 194]. These compounds, now termed phytocannabinoids, receive their cannabinoid status not because they share a common

mechanism of action, but because they are all structurally related. Unfortunately due to the vast number present, the pharmacology of most of these phytocannabinoids remains unknown, however the three best studied to date are Δ9-THC, cannabidiol (CBD) and Δ9-tetrahydrocannabivarin (Δ9-THCV) [195].

The most abundant, and undoubtedly the most (in)famous, phytocannabinoid present in cannabis is Δ9-THC; discovered in 1964 and almost entirely responsible for the psychoactive effects seen when using marijuana [133, 196]. *In vivo* administration of Δ9-THC causes feelings of euphoria, impairment of memory and motor co-ordination, hypothermia, increased appetite, reduced pain sensation as well as a wide range of other physical effects [197]. Since its discovery, Δ9-THC has been extensively studied and has been found to bind both CB_1 and CB_2 with high affinity and act as a partial agonist at both receptors [131, 146]. Clinically, Δ9-THC (marketed as dronabinol and nabilone) is currently used as an anti-emetic for patients undergoing chemotherapy [198] and as an appetite stimulant for HIV/AIDs patients [199].

Discovered in the 1960s, CBD is the second most abundant cannabis-derived cannabinoid and is synthesised from the same precursor as Δ9-THC [200, 201]. Despite this similarity however, it does not have any psychotropic effects *in vivo* making it of great clinical interest [202]. Furthermore, it displays markedly different pharmacological properties, having weak affinity for both CB_1 and CB_2 and little to no activity at either receptor in various functional assays [202, 203]. Nevertheless, recent work has demonstrated that CBD can potently inhibit the binding of other cannabinoid receptor agonists [204] and has also been found to inhibit the cellular uptake of AEA and its degradation by FAAH [200, 205]. Additionally, CBD has been found to have multiple effects at various other targets *in vitro* and *in vivo* (discussed in more detail in section 4.1.4). Currently, CBD in a 1:1 mixture with Δ9-THC (marketed as Sativex) is used to treat pain for patients suffering with multiple sclerosis [206]. It is believed that CBD acts to limit unwanted side effects of Δ9-THC by inhibiting its metabolism into a more active form and also by limiting its activity at CB_1 [207].

Δ9-THCV is structurally similar to Δ9-THC, being its n-propyl analogue, and binds to both CB_1 and CB_2 with high affinity [202]. However, in contrast to Δ9-THC, Δ9-THCV acts as an antagonist at both receptors, blocking the binding of other cannabinoid receptor ligands [208]. Additionally, Δ9-THCV has been demonstrated to block the activity of Δ9-THC and endocannabinoids *in vivo*, as administration of Δ9-THCV inhibits Δ9-THC-induced anti-nociception and hypothermia [209] and causes decreased food intake and body weight in both normal and obese mice [202]. Importantly, Δ9-THCV acts as a neutral CB_1 antagonist rather than an inverse agonist [202]. As the unwanted side effects that led to the withdrawal of rimonabant (a CB_1 inverse agonist formerly licensed to treat obesity - see section 1.8.7) may be due to its inverse agonism of CB_1 [210], Δ9-THCV has received clinical interest as a potential cannabinoid-based therapy for obesity that may have reduced adverse effects.

1.8.6 Synthetic cannabinoid receptor agonists

The discovery and structural elucidation of Δ9-THC prompted many efforts to generate small molecule ligands active at the cannabinoid receptors. This was further bolstered by the discovery of CB_1 and CB_2 in the early 90s, and as a consequence a vast array of synthetic cannabinoid receptor ligands now exist. These vary from being mixed cannabinoid receptor agonists to being extremely receptor selective and have undoubtedly proved vital to our current understanding of the pharmacology and *in vivo* role of the cannabinoid receptors.

The synthetic cannabinoid agonists are split into four separate groups based on their core structures and these are: 1) The classical cannabinoids 2) The non-classical cannabinoids 3) The aminoalkyindoles and 4) Other chemical classes. I will now briefly introduce the synthetic cannabinoids from each class that I have used throughout my thesis, with their chemical structures displayed in figure 1.3.

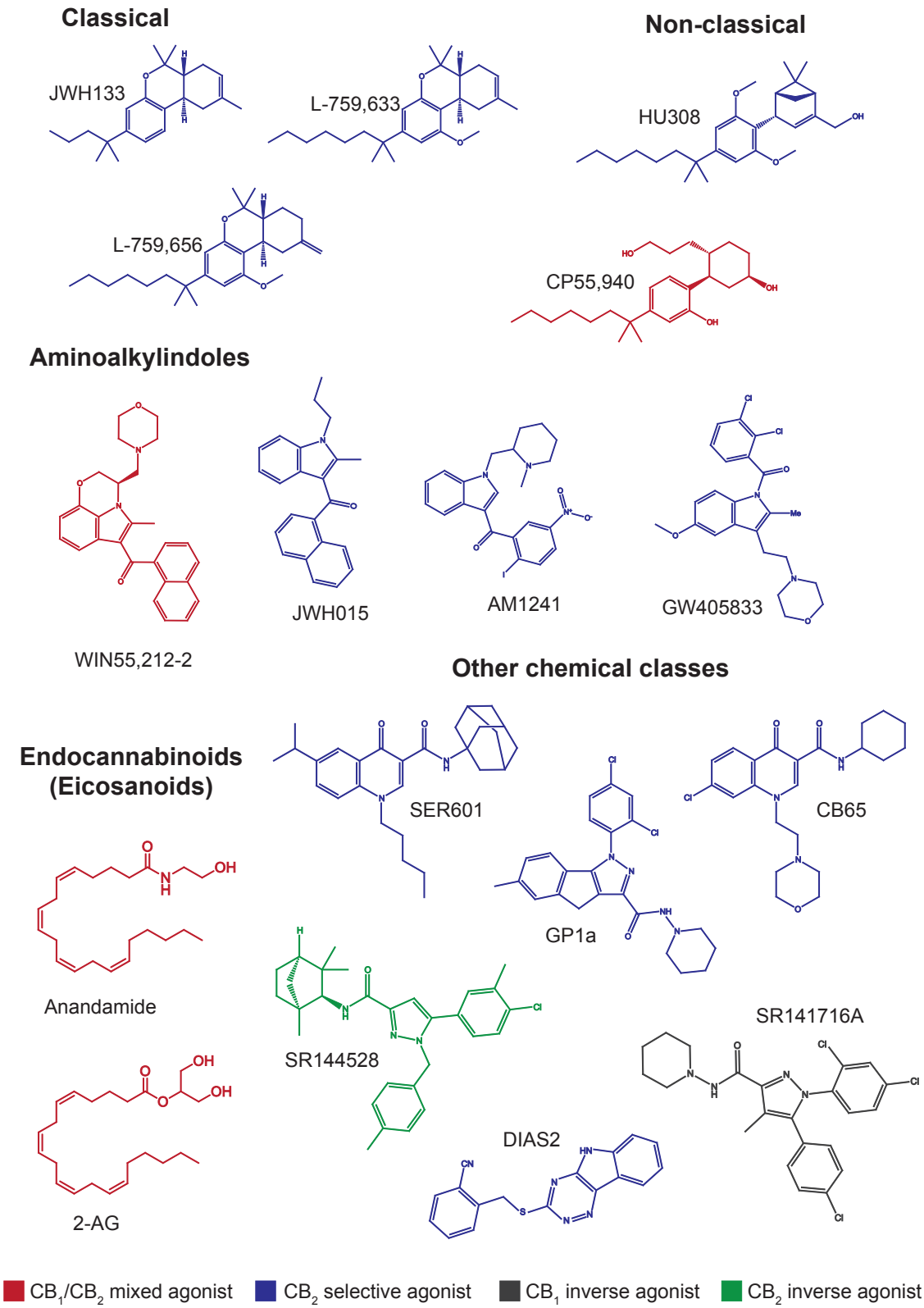

Figure 1.3 Cannabinoid receptor ligands used throughout my thesis.

The classical cannabinoids

The classical cannabinoids are structurally related to the phytocannabinoid Δ9-THC, with all members belonging to the tricyclic dibenzopyran chemical class. Interestingly however, it was found that by making minor chemical modifications to Δ9-THC that the selectivity for CB_2 over CB_1 could be greatly enhanced [146]. Perhaps the prototypical synthetic classical cannabinoid is JWH133. First synthesised in 1999 and named after its discoverer John W Huffmann, this compound displays 200-fold selectivity for CB_2 over CB_1 with K_i values of 3.4 and 667 nM respectively, and is now one of the ligands most widely used to examine the effects of CB_2 activation *in vitro* and *in vivo* [131]. Around the same time L-759,633 and L-759,656, two sister compounds, were discovered by the pharmaceutical company Merck Frosst [146]. Both have identical pharmacology, being highly selective for CB_2, with K_i values of 20 nM for CB_2 and $>10\mu$M for CB_1 [211]. Furthermore, both compounds potently inhibit forskolin-induced cAMP production in CHO cells transfected with CB_2, displaying EC_{50} values of 8.1 and 3.1 nM for L-759,633 and L-759,656 respectively [211].

The non-classical cannabinoids

The non-classical cannabinoids are so named because, despite being based on its structure, they lack the dihydropyran ring found in Δ9-THC. This class of synthetic cannabinoid was originally discovered by Pzifer in 1984 and is typified by the compound designated CP55,940 [212]. This compound was synthesised before the identification of the cannabinoid receptors and played a crucial role in the discovery of CB_1 [140]. CP55,940 binds to CB_1 and CB_2 with equal affinity ($K_i = 2$ nM) and acts as a full agonist at both receptors in a range of functional assays [152, 213, 214]. Additionally, it is 10-50 times more potent than Δ9-THC *in vivo* when examining the classical signs of cannabinoid administration in mice [146]. However, non-classical compounds can also show cannabinoid receptor selectivity as HU308, discovered in 1999, binds to CB_2 with a K_i of 23 nM but does not bind to CB_1, making it

one of the most CB_2 selective agonists currently available [215, 216]. Furthermore, HU308 potently inhibits forskolin-induced cAMP accumulation in CB_2, but not CB_1, expressing CHO cells [215].

The aminoalkylindoles

Until the mid-90s, all of the synthetic cannabinoids identified were based on Δ9-THC. However, the discovery of WIN55,212-2 by the pharmaceutical company Sterling Winthrop provided the first cannabinoid receptor ligand with a different chemical class; the aminoalklyindole [146, 217, 218]. WIN55,212-2 binds to both cannabinoid receptors with nanomolar affinity, but has a slight preference for CB_2. It is thought to be a full agonist at both receptors [146], however recent work has found that in contrast to CP55,950, WIN55,212-2 does not cause β-arrestin recruitment at CB_2 [152], thereby highlighting that the term agonist needs to be carefully used when discussing the actions of cannabinoids, and indeed small molecules in general. Nevertheless, when used *in vivo* WIN55,212-2 mimics the physical effects of Δ9-THC [219, 220]. Since the discovery of WIN55,212-2, multiple members of the aminoalkylindole family have been found, including JWH015, GW405833 and AM1241. These three compounds all show selectivity towards CB_2, with K_i values in the low nanomolar range and 28, 82 and 1200 fold selectivity for CB_2 over CB_1 for JWH015, AM1241 and GW405833 respectively [221–224].

Other chemical classes

There are currently many cannabinoid receptor ligands belonging to chemical classes other than those mentioned above. In the interests of brevity however, I will only introduce the ligands that I have used in this study. GP1a is a tricyclic pyrazole and was discovered in 2006. With a K_i value of 3.7 pM at CB_2, it is the highest affinity CB_2 ligand discovered to date [225]. Furthermore, it is highly selective for CB_2 over CB_1. CB65 and SER601 both belong to the quinolone-3-carboxamide class

and are high affinity, highly selective CB_2 agonists with K_i values of 3.3 and 6.3 nM at CB_2 respectively, and no appreciable binding at CB_1 [226–228].

Finally, the CB_2 agonist DIAS2 is a member of the triazinoindole class and was discovered in our laboratory by ligand-directed virtual screening, using HU308 as the bait compound [229]. Functional testing of highly ranked compounds uncovered DIAS2 as a highly selective CB_2 agonist with a K_i value of 355 nM at CB_2 and an EC_{50} of 112 nM for inhibition of forskolin-induced cAMP production in CB_2 transfected CHO cells [229]. DIAS2 has no appreicable binding or functional activity at CB_1 [229].

1.8.7 Cannabinoid receptor inverse agonists

Alongside cannabinoid receptor agonists, compounds that antagonise CB_1 and CB_2 have been of vital importance for understanding the endocannabinoid system. To date there are multiple cannabinoid receptor antagonists/inverse agonists available [131], but perhaps the most widely used are the diarylpyrazoles discovered by Sanofi-Aventis; SR144528 and SR141716A [230, 231]. SR144528 targets only CB_2 [231], whereas SR141716A targets only CB_1 [230], with both compounds binding to their respective cannabinoid receptor with high affinity, displaying K_i values in the low nanomolar range. Alongside antagonising the binding of receptor agonists, both compounds also inhibit the constitutive activity of their respective cannabinoid receptor, and are therefore classed as inverse agonists [146].

Due to the role of CB_1 in stimulating appetite, early animal experiments found that SR141716A acted as an appetite suppressant and facilitated weight loss [232]. Therefore, under the name rimonabant, SR141716A went into the phase 3 Rimonabant in Obesity trial to evaluate the efficacy of SR141716A as a weight loss therapy. The result of the trial was positive and found that SR141716A caused significant weight loss in comparison to placebo control and subsequently led to SR141716A being approved for weight loss in 2006 [233–235]. Currently, SR141716A is the only synthetic cannabinoid receptor ligand that has been clinically licensed. However,

SR141716A also caused multiple adverse psychiatric events, including anxiety, despression, suicidal thoughts and even suicide itself [236,237]. Due to these side effects, SR141716A was withdrawn from sale by both the FDA and the EMA by 2008 [237].

1.8.8 CB_2 knockout mice

Alongside the synthetic cannabinoids detailed above, animals genetically deleted for CB_2 have proved instrumental in understanding the role that CB_2 plays during health and disease. Currently, there are two different strains available where the CB_2 gene has been disrupted, with the first reported by Buckley *et al* in 2000 [238]. This knockout line was generated using homologous recombination, whereby the last 341 bp of the CB_2 coding exon was replaced with a neomycin resistance cassette. This translates into the deletion of most of intracellular loop three, transmembrane regions 6 and 7, extracellular loop 3 and the remaining C terminus of CB_2. The authors demonstrated that macrophages derived from these $CB_2^{-/-}$ animals are not responsive to Δ9-THC, proving functional deletion of CB_2 [238]. To date this is the most commonly used $CB_2^{-/-}$ strain and it has been used to elucidate the role that CB_2 plays in a range of physiological and pathological settings (reviewed in [239]).

The second $CB_2^{-/-}$ strain available was generated by Deltagen (designated B6.129P2-Cnr2^{tm1Dgen}/J), also using homologous recombination to disrupt CB_2, and this is the line that I have used for my studies. Insertion of the Neo555T construct into the CB_2 coding exon resulted in a 334 bp deletion that translates into the removal of transmembrane regions 1, 2 and 3, as well as extracellular loop 1, intracellular loop 1 and part of intracellular loop 2 [240,241]. Overall $CB_2^{-/-}$ animals have no overt phenotype, except from a reduction in the number of splenic marginal zone B cells [238,242,243].

1.9 The role of CB_2 in inflammatory disease

Due to its wide ranging expression pattern, CB_2 has been demonstrated to play a role in a very large number of physiological and pathological settings, and it is generally considered that CB_2 activation and signalling results in protective/positive outcomes [244]. For example, CB_2 has been found to regulate bone development and turnover, fertility in males and females and skeletal muscle formation and function [161]. Furthermore, it acts to limit pain, modulates behaviour and has been implicated in psychiatric disorders such as schizophrenia, anxiety and depression as well as in neurodegenerative disorders such as Alzheimer's, Parkinson's and Huntington's disease [245–248]. A detailed introduction of the role of CB_2 in these processes is outside the scope of my thesis and has already been covered in detail in a variety of excellent reviews [161, 244, 249], however this summary serves to demonstrate the vast array of settings impacted upon by CB_2.

Instead I will focus on the role of CB_2 in inflammation and inflammatory disease. Due to its predominant expression on cells of the immune system, it is perhaps not surprising that CB_2 acts as an immunomodulatory receptor. Indeed its major *in vivo* role seems to be the regulation of immune cell function and inflammation and for this reason CB_2 has been demonstrated to play a crucial role in multiple inflammatory diseases (reviwewed in [163]).

1.9.1 The role of CB_2 in intestinal inflammation and inflammatory bowel disease

The intestinal inflammatory conditions Crohn's disease (CD) and ulcerative colitis (UC) together comprise the dominant forms of IBD [250]. They are both chronic inflammatory pathologies of the gastrointestinal tract, but differ in their localisation (UC: restricted to the colon - CD: any area of the GI tract) and extent of inflammation (UC: inflammation in the mucosa only - CD: inflammation present throughout the

intestinal wall) [251].

Currently, multiple studies have been published demonstrating that activation of CB_2 has beneficial outcomes in murine models of intestinal inflammation [251]. In 2006, Kimball *et al* found that treatment of mice with JWH133 significantly reduced overall weight loss, colon shrinkage, inflammatory damage score and other histological makers of disease, as well as colonic inflammatory cell infiltration, in the oil of mustard and the dextran sulphate sodium (DSS) models of colitis [252]. This protective effect of JWH133 has been confirmed in subsequent studies as Singh *et al* also found that treatment of mice with JWH133 reverses signs of intestinal inflammatory disease in the DSS colitis model and in IL-$10^{-/-}$ animals that spontaneously develop colitis [253]. Importantly, the protective effect of JWH133 in the DSS colitis model could be reversed by co-administration of a CB_2 antagonist.

Alongside these results, JWH133 and AM1241 have been shown to reverse colon shrinkage, ulcer formation and other inflammatory and histological disease markers in the 2,4,6-Trinitrobenzene sulfonic acid (TNBS)-induced colitis model [254]. Treatment with these CB_2 agonists also caused a reduction in inflammatory cell recruitment and MPO activity in the colon, strongly indicating that activation of CB_2 blocks colonic neutrophil recruitment during colitis. The authors detailed that administration of a CB_2 antagonist blocked the beneficial effect of both JWH133 and AM1241, even resulting in worse disease pathology, but interestingly found that $CB_2^{-/-}$ animals did not exhibit exacerbated colonic inflammation [254].

This result contradicts that reported by Engel *et al*, who showed that animals genetically deleted for CB_2 have increased colon weight, decreased colon length, increased histopathological disease scores and increased inflammatory cell infiltration into the colon in comparison to WT animals [255]. Furthermore, $CB_2^{-/-}$ animals also had increased colonic mRNA levels of TNF-α and IL-1β. The reason for this discrepancy is currently unclear. Both studies used the same $CB_2^{-/-}$ strain and the same method for inducing colitis. One potential explanation could be differences in

the microbiotia of the experimental animals used as this has been shown to impact the results seen in colitis models [256, 257].

Alongside using synthetic CB_2 agonists, other studies have shown that small molecule inhibition of the enzymes that degrade the endocannabinoids results in beneficial outcomes in colitis models of intestinal inflammation. Inhibition of MAGL by JZL184 or FAAH by URB597 or PF-3845 causes increased endogenous levels of 2-AG or AEA respectively and results in better disease outcomes in the TNBS-induced colitis model [258–260]. Furthermore, $FAAH^{-/-}$ mice have increased resistance towards developing colitis [261]. Interestingly, it is likely that CB_1 and CB_2 are both mechanistically involved, as co-administration of a CB_1 or CB_2 antagonist or the usage of mice genetically null for either receptor reverses the beneficial effect of MAGL or FAAH inhibition [254, 259].

Taken together these data demonstrate that activation of CB_2 by small molecule drugs or by increasing the levels of endogenous cannabinoids may provide a therapeutic avenue for the treatment of IBD. Indeed, it has been shown that in humans CB_2 and other members of the endocannabinoid system are present throughout the GI tract [251] and that the intestinal levels of CB_2 are increased in patients with IBD [262]. Furthermore, multiple reports examining the cannabis usage of patients with IBD have found that a significant number self-medicate as a way to control the symptoms associated with both CD and UC [263, 264].

1.9.2 The role of CB_2 in sepsis and endotoxic shock

Sepsis comprises a complex series of inflammatory events that occur when a bacterial infection is not successfully contained by the host. The failure to contain the infection leads to an overwhelming systemic inflammatory response, culminating in tissue damage, organ failure and eventually death, with mortality rates reaching 47% [265]. Despite being an inflammatory disease, therapeutic intervention with anti-inflammatory compounds has to date been largely unsuccessful, leaving a currently

unmet clinical need [266]. Therefore, as CB_2 regulates the immune system, it has received attention as a target within sepsis.

However, its role within this complex inflammatory pathology remains unclear, as the first reports examining CB_2 in sepsis, both published in 2009, presented opposite results. Both studies used the cecal ligation and puncture (CLP) model of sepsis, which involves the ligation and puncture of the caecum to allow the leakage of faeces into the peritoneal cavity and the generation of a polymicrobial immune response [267]. Tschöp *et al* found that after CLP, $CB_2^{-/-}$ animals had a higher mortality rate, which correlated with elevated serum levels of IL-6 and increased bacterial load in the blood in comparison to WT animals [268]. Furthermore, $CB_2^{-/-}$ mice had increased numbers of neutophils in the lung and increased lung tissue damage, alongside higher lung bacterial load. Finally, they found that treatment of WT mice with the CB_2 agonist GP1a improved sepsis outcome, with treated mice displaying a reduction in mortality, serum IL-6 levels, blood bacterial load and lung neutrophil recruitment and tissue damage [268]. Therefore this would suggest that CB_2 acts to limit bacterial infection by enhancing bacterial killing. Nonetheless, data published by Csóka *et al* provide entirely contradictory results. They found that after CLP, $CB_2^{-/-}$ animals had a lower mortality rate, lower levels of IL-6 and CXCL2 in the serum and lower bacterial load in the blood and the peritoneum, compared to WT mice [269]. Additionally, $CB_2^{-/-}$ animals had lower levels of LDH, a general marker of tissue damage, and muscle and kidney damage markers in the blood [269].

To date these are the only two studies that have used the CLP model to study the role of CB_2 in sepsis and it is unclear why the results are contradictory. In comparison to Tschöp *et al* who only made one puncture, Csóka *et al* punctured the caecum twice. This would have resulted in a more robust inflammatory response, as higher amounts of faecal material would have been exposed to the peritoneum, potentially underlying the difference between the two models. Furthermore as the CLP model relies on the bacterial flora of the gut, differences in animal microbiota

could also impact on the results obtained.

The only other studies examining CB_2 in sepsis have used injection of LPS to induce a rapid and systemic immune response, known as endotoxic shock [270, 271], and imply that CB_2 plays a protective role. $CB_2^{-/-}$ animals have an increased mortality rate, which correlates with higher serum levels of IL-6 and TNF-α, in comparison to WT animals, after intraperitoneal injection of LPS. Furthermore, pre-treatment of mice with the CB_2 agonist GW405833 results in a reduction in mortality and serum levels of pro-inflammatory mediators after high dose injection of LPS into WT animals [272]. Additionally, LPS-induced leukocyte-endothelial interactions are blunted in mice by HU308 and in rats by WIN55,212-2 in a CB_2-dependent manner [273, 274].

1.9.3 The role of CB_2 in multiple sclerosis

Multiple sclerosis (MS) is a chronic inflammatory disease of the central nervous system (CNS), characterised by immune cell infiltration into the CNS, neuronal demyelination and axonal damage and loss, which causes multiple neurological defects [275]. In animals, MS can be modelled using experimental autoimmune encephalomyelitis (EAE), which is induced by the immunisation of experimental animals with homogenates of CNS tissue or specific myelin-derived antigens, such as proteolipid protein, myelin basic protein or myelin oligodendrocyte protein, in combination with complete Freund's adjuvant. This leads to a rapid onset of disease, typically within 9-15 days, that is reproducible and recapitulates many of the pathological features of human MS [276].

Indication that the cannabinoid receptors might be an interesting target within the EAE model came from the findings that rats treated with WIN55,212-2, Δ9-THC, or its more stable and less psychoactive analogue Δ8-THC, had reduced clinical symptoms and CNS inflammation after EAE induction [277–279]. Initial evidence suggesting that CB_2 was responsible for this beneficial effect was provided by Baker *et*

al, who found that, alongside WIN55,212-2 and CP55,940, the CB_2 selective agonist JWH133 decreased both hind leg tremor and spasticity in a mouse EAE model [280]. Since then, others have also shown that specific activation of CB_2 has beneficial outcomes in the EAE model, as treatment of mice with WIN55,212-2 decreases EAE-induced leukocyte-endothelial interactions in the cerebral microvasculature and improves clinical outcome in a CB_2 antagonist-sensitive manner [281]. Furthermore, HU308 has been shown to improve EAE clinical score and inhibit T cell and myeloid cell infiltration into the CNS and reduce axonal loss [282, 283]. Importantly, these benefical outcomes were absent in $CB_2^{-/-}$ animals [283]. Conversely, treatment of mice with SR144528 increases EAE disease severity and body weight loss [284].

Alongside small molecule modulation, multiple studies have demonstrated that when used in EAE models, $CB_2^{-/-}$ animals have increased disease severity, increased T cell and mononuclear cell CNS infiltration, as well as increased demyelination and axonal loss [283, 285, 286]. This therefore strengthens the hypothesis that CB_2 has a protective role within EAE. However, the mechanism behind this beneficial effect remains unclear. Currently, decreased leukocyte-endothelial interactions [281] and increased T cell apoptosis [279] following CB_2 activation and decreased T cell apoptosis, increased T cell proliferation (specifically Th17 cells) and inflammatory mediator production [284, 286], increased CNS levels of CX_3CL1 [284] as well as increased myeloid cell expression of chemokines and chemokine receptors [283] in $CB_2^{-/-}$ animals have all been proposed to explain the positive action of CB_2 in EAE.

Additional complexity surrounding the role of CB_2 in EAE has recently been provided by Sisay *et al* who found that the genetic background of experimental mice used determines whether deletion of CB_2 results in increased EAE disease severity. They show that when performing the EAE model using C57BL/6J animals, $CB_2^{-/-}$ mice have worse disease manifestation, but when crossed onto the ABH strain, $CB_2^{-/-}$ animals display no difference in EAE disease severity in comparison to WT mice [285]. Instead they found that in the ABH background, it is CB_1 and not CB_2 that is responsible for the beneficial effects seen when animals are treated with

Δ9-THC [285]. Interestingly, this mirrors the previous findings that it is CB_1, and not CB_2, that is responsible for decreased EAE clinical score, CNS inflammatory cell infiltration and axonal damage following treatment of mice with non-selective cannabinoid receptor agonists [287, 288]. This therefore demonstrates that the role CB_2 plays within EAE is complex and dependent on multiple parameters, and in some situations it may not impact on disease progression at all. Clearly future work is needed to address these discrepancies and determine whether CB_2 may be a viable therapeutic target within MS.

1.9.4 The role of CB_2 in rheumatoid arthritis

RA is caused by the chronic inflammation of a synovial joint and is clinically characterised by joint swelling, pain, stiffness and bone and cartilage destruction [289]. Cells lining the joint, as well as macrophages and T cells are important for disease initiation and progression, as they contribute to inflammatory mediator production and joint damage. There are multiple animal models available to study RA, such as collagen-induced arthritis (CIA), collagen-antibody-induced arthritis and the K/BxN serum transfer model (reviewed in [290]). One of the most important inflammatory mediators present in RA is TNF-α and great success have been achieved by treating RA patients with TNF-α blocking antibodies [291]. However around 30% of RA patients do not respond well to anti-TNF-α treatment [292] and therefore there is still a clinical need to uncover novel therapeutic avenues for the treatment of RA.

It has only recently become apparent that the endocannabinoid system may play a role in RA. The first indication came from Richardson *et al* who found that the endocannabinoids AEA and 2-AG were present in the synovial fluid from RA patients, but entirely absent in fluid from healthy donors, and that CB_2 was highly expressed on RA-derived synovial tissue [293]. However since then only a handful of studies have examined the role of CB_2 within RA. The first report was provided by Kinsey *et al* who found that $FAAH^{-/-}$ animals are protected from RA,

displaying a lower arthritis score, less joint inflammation as well as reduced joint catrilage and bone damage in comparison to WT animals in the CIA model [294]. Importantly, the beneficial phenotype seen in $FAAH^{-/-}$ animals was reversed by a CB_2 antagonist. Alongside, two studies also using the CIA model, found that treatment of mice with either JWH133 or HU308 results in decreased arthritis score, paw thickness, neutrophil and mononuclear cell infiltration and joint cartilage and bone damage [295, 296]. However, for both of these studies, the absolute reliance on CB_2 was not demonstrated.

The mechanism behind this beneficial effect is currently unclear. Multiple studies have isolated fibroblast-like synoviocytes (FLS) from RA patients and found that treatment with WIN55,212-2, CP55,940, JWH133 or HU308 inhibits the production of pro-inflammatory cytokines and chemokines by inflammed FLS [295, 297–299]. However, it was also found that CB_1 or CB_2 antagonists were unable to block these anti-inflammatory actions, strongly implying that they occur via a CB_1/CB_2-independent mechanism [297, 298]. Indeed, Lowin *et al* found that, in contrast to cannabinoid receptor antagonists, transient receptor potential (TRP) V1 and TRPA1 (membrane ion channels responsible for many off-target effects of cannabinoid ligands - see section 4.1.6) antagonists were able to reverse the anti-inflammatory action of WIN55,212-2 on inflammatory mediator production by inflamed FLS [297]. To date no study has used $CB_2^{-/-}$ animals in a model of RA to examine its role in this inflammatory disease. This leaves an obvious area of study to fully elucidate the role that CB_2 plays, if any, in RA.

1.9.5 The role of CB_2 in ischaemia reperfusion injury

As its name suggests, ischaemia reperfusion (IR) injury refers to the damage caused to tissues when blood flow is re-established following a period of ischaemia, resulting from a disrupted or absent blood supply [300]. Upon restoration of blood flow, local generation of reactive free radical species causes immediate tissue damage and

elicits an inflammatory response resulting in a large tissue influx of neutrophils and monocytes that contribute to further tissue damage. Ultimately, IR injury can lead to organ failure and even death, and is the predominant mechanism underlying organ damage in both heart attack and stroke [301, 302]. In experimental animals, IR injury can be induced in multiple organs by the ligation of the vessel(s) supplying the tissue, followed by removal of the ligature to restore blood flow. In the heart the left descending coronary artery is ligated [303], in the brain the middle cerebral artery [304], in the kidney the main arterial supply [305] and in the liver the hepatic portal vein and artery [306].

There are now a vast array of studies demonstrating that CB_2 has a protective role during IR injury in multiple tissues [307]. Activation of CB_2 by a range of synthetic agonists has been shown to reduce infarct size and tissue damage/function following IR in the kidney [308], liver [309–312], brain [313–316] and heart [317–323]. Importantly, for the majority of these above studies, the reliance on CB_2 for this beneficial effect has been confirmed by using either a CB_2 antagonist [309–312, 317, 320, 321, 323] or $CB_2^{-/-}$ animals [310, 316, 319]. Conversely, animals lacking CB_2 have been shown to have increased infarct areas and tissue damage following IR in the liver [310], heart [319, 324, 325] and brain [315].

The predominant mechanism responsible for this protective role seems to be the negative regulation of tissue neutrophil recruitment by CB_2, as neutrophils are a major contributor to tissue damage following IR [326]. Specific activation of CB_2 by multiple agonists has been demonstrated to inhibit neutrophil infiltration, whereas $CB_2^{-/-}$ animals have higher tissue neutrophil recruitment after IR injury, in the liver [309–312], brain [313, 315, 316] and heart [317–319]. Exactly how CB_2 inhibits neutrophil tissue infiltration remains understudied, however it has been proposed that activation of CB_2 specifically on the neutrophils themselves inhibits their chemotaxis and endothelial cell adhesion.

In a detailed study by Murikinati *et al*, it was found that JWH133 treatment

resulted in decreased brain infarct area following IR in $CB_2^{-/-}$ animals reconstituted with WT bone marrow, whereas JWH133 had no effect in WT animals reconstituted with $CB_2^{-/-}$ bone marrow, demonstrating that CB_2 in the bone marrow derived cells themselves is responsible for the beneficial actions of CB_2 activation in IR-induced brain injury [316]. Furthermore, the ability of JWH133 to inhibit neutrophil chemotaxis towards CXCL2 and neutrophil-endothelial cell interaction was lost when using $CB_2^{-/-}$ neutrophils [316]. This therefore implies that activation of CB_2 specifically on neutrophils results in their reduced tissue migration and infiltration following IR, resulting in decreased tissue damage and improved outcomes following IR injury.

1.9.6 The role of CB_2 in the development of atherosclerosis

Atherosclerosis is a chronic inflammatory disorder characterised by progressive accumulation of immune cells and lipids within the arterial intima [327]. Atherosclerotic lesions predominantly occur at sites of turbulent blood flow, where retention of modified lipids within the arterial intima results in endothelial dysfunction and the recruitment of blood-borne monocytes [328, 329]. These monocytes then differentiate into macrophages and ingest modified lipoproteins eventually becoming lipid-engorged foam cells, which leads to the formation of an atherosclerotic plaque [330]. Eventual rupture of these fatty lesions results in pathological thrombus formation, making atherosclerosis the primary cause of both myocardial infarction and stroke [331]. Current therapeutic intervention with lipid-lowering statin treatment has helped reduce disease incidence [332]; however atherosclerosis remains the primary cause of mortality worldwide, clearly highlighting a currently unmet clinical need for new classes of anti-atherogenic drugs [333].

A breakthrough study published in 2005 by Steffens *et al* provided the first indication that activation of CB_2 has beneficial effects within atherosclerosis. Low dose (1mg/kg/day) administration of Δ9-THC decreased both the size and macrophage content of atherosclerotic lesions in $ApoE^{-/-}$ mice in a CB_2-dependent manner [334].

Two studies published in 2010 confirmed this finding, demonstrating that the synthetic cannabinoid WIN55,212-2 reduced lesion size, macrophage content and expression of the pro-inflammatory markers TNF-α, IL-6 and CCL2 within these atherosclerotic plaques in ApoE$^{-/-}$ animals [335, 336]. Importantly, pharmacological inhibition of CB_2 reversed these anti-inflammatory and atheroprotective effects [335, 336]. A joint limitation of these initial studies is that they only implicate CB_2 using non-selective agonists combined with pharmacological blockade.

Direct evidence of the protective effects of CB_2 in atherosclerosis came in 2010 where LDL receptor/CB_2 receptor double knockout mice (Ldlr$^{-/-}$ $CB_2^{-/-}$ displayed decreased lesional collagen content and significantly higher levels of matrix metalloproteinase 9 (MMP-9) levels, compared to Ldlr$^{-/-}$ mice, indicating an unstable plaque phenotype. Furthermore, Ldlr$^{-/-}$ $CB_2^{-/-}$ mice were found to have increased lesional macrophage content [337, 338]. Interestingly, a more recent study found irradiated Ldlr$^{-/-}$ mice reconstituted with $CB_2^{-/-}$ bone marrow developed significantly larger aortic valve plaques compared to Ldlr$^{-/-}$ mice receiving WT bone marrow, implying that it is CB_2 expression in bone marrow derived cells that is important for the atheroprotective effects of CB_2. These findings have been replicated using ApoE$^{-/-}$ $CB_2^{-/-}$ mice, as these animals display significantly increased lesional macrophage content compared to ApoE$^{-/-}$ animals and irradiated ApoE$^{-/-}$ mice reconstituted with $CB_2^{-/-}$ bone marrow have increased plaque macrophages compared to ApoE$^{-/-}$ mice receiving WT transplantation [339]. Furthermore, this study also found that atherosclerotic lesion size and macrophage content of ApoE$^{-/-}$, but not ApoE$^{-/-}$ $CB_2^{-/-}$, was significantly decreased after treatment with JWH133 [339].

However, Willecke *et al* found that JWH133 did not have any effect on macrophage content or plaque area in Ldlr$^{-/-}$ animals [338]. The source of this conflict is currently unknown, but could due to differences in compound dosing regimes, experimental model used (Ldlr$^{-/-}$ vs ApoE$^{-/-}$ in this case) and also time point chosen for atherosclerosis quantification. Further controversy about the role of CB_2 in atherosclerosis was recently provided by Netherland-Van Dyke *et al* who found that although

WIN55,212-2 reduced plaque macrophage content in $Ldlr^{-/-}$ mice, mirroring previous results, it also had the same effect in $Ldlr^{-/-}$ $CB_2^{-/-}$ animals implying that this occurs independently of CB_2 [340].

Nevertheless, when taken together these pharmacological and genetic studies demonstrate that CB_2 endogenously inhibits macrophage infiltration and inflammation in murine atherosclerotic lesions. However, the mechanism underlying this beneficial effect still remains unclear. In the seminal paper by Steffens *et al* it was demonstrated that treatment of macrophages with Δ9-THC reduced their migration towards CC chemokines and this was suggested as a potential mechanism for reduced plaque macrophage content [334]. Further support of this hypothesis comes from a number of studies that demonstrate activation of CB_2 blocks macrophage chemotaxis towards CC chemokines (see chapter 3 for a more detailed discussion) and the findings of Delsing and Hoyer that lack of CB_2 in bone marrow derived cells leads to increased lesional macrophages [339, 341].

Additionally, CB_2 expression in the vasculature itself has also been proposed to mediate the beneficial effects of CB_2 activation, as treatment of $ApoE^{-/-}$ mice with WIN55,212-2 causes reduced aortic expression of the adhesion molecules ICAM-1, VCAM-1 and P-selectin. Furthermore, the treatment of HUVECs with WIN55,212-2 blocks monocyte endothelial cell adhesion by downregulating these same adhesion molecules [335]. Additionally, JWH133 and HU308 have been demonstrated to inhibit monocyte ICAM-1, VCAM-1 and CCL2 expression and arterial endothelial cell adhesion both *in vitro* and *in vivo* [342]. Importantly both studies found that this could be blocked by treatment with a CB_2 antagonist [335, 342]. Clearly further work is needed to clarify the exact mechanistic basis behind the anti-atherogenic function of CB_2. Nevertheless, these above studies demonstrate that pharmacological activation of CB_2 may provide a potential therapeutic avenue to inhibit atherosclerosis progression.

1.10 Original hypothesis for this thesis

Clearly the current literature demonstrates that the activation of CB_2 has a beneficial and/or protective outcome in a range of inflammatory diseases. However the mechanistic basis underlying this effect remains poorly defined, although some preliminary experiments suggests that the inhibition of leukocyte chemotaxis and tissue recruitment by CB_2 may be responsible. With this in mind the original hypothesis for this thesis is as follows:

H_0 = Activation of CB_2 does not regulate immune cell chemotaxis or recruitment during an inflammatory response.

H_1 = Activation of CB_2 blocks innate immune cell recruitment to sites of inflammation *in vivo* by inhibiting their chemotaxis towards classical innate immune cell chemoattractants.

1.11 Experimental aims

At the start of my graduate studies in 2012, I set myself the following experimental aims:

- To use real-time chemotaxis analysis to assess whether CB_2 acts as a chemoattractant receptor in primary macrophages.
- To use real-time chemotaxis analysis to discover whether CB_2 activation blocks primary macrophage chemotaxis towards CC chemokines.
- To use the dorsal air pouch acute inflammation model, combined with animals lacking CB_2, to investigate whether CB_2 regulates innate immune cell recruitment to sites on inflammation *in vivo*.

Chapter 2

Materials and Methods

2.1 Reagents

Cannabinoids and cannabinoid receptor inverse agonists, as well as lipid GPCR ligands, were purchased from Tocris (Bristol, UK). Murine CCL5 was purchased from Peprotech (London, UK). Murine chemerin and murine CCL2 were obtained from R & D systems (Abingdon, UK). Pertussis toxin (PTX) was purchased from Merck Millipore (Feltham, UK). Bio-gel polyacrylamide beads (P-100 fine 45-90 μm) were purchased from Biorad (Hertfordshire, UK). cOmplete, EDTA free protease inhibitor cocktail tablets were purchased from Roche (Burgess Hill, UK). Rabbit anti-phospho-ERK1/2, rabbit anti-phospho-Akt and total ERK1/2 were purchased from Cell Signalling Technologies (Danvers, MA, USA). HRP-conjugated Goat anti-rabbit secondary was purchased from Biorad. CIM-16 and 96 well E-plates plates were purchased from Cambridge bioscience (Cambridge, UK). All cell culture media were obtained from PAA systems (Yeovil, UK). Phosphatase inhibitor cocktail 2, Zymosan-A (Z4250) and all other laboratory chemicals were purchased from Sigma Aldrich (Dorset, UK). DIAS2 (3-((2'-cyanobenzyl)thio)-5H-[1,2,4]triazino[5,6b]indole) [229] was synthesized by Dr. Angela Russell (University of Oxford, UK).

2.2 Animals

C57BL/6J mice were obtained from Harlan Laboratories (Oxfordshire, UK) or directly from the in-house colony maintained in our animal facility (also referred to as wild type (WT) animals). B6.SJL animals were obtained from our in-house colony. Cannabinoid receptor 2 knockout mice (officially designated B6.129P2-Cnr2^{tm1Dgen}/J and herein referred to as $CB_2^{-/-}$ mice) were purchased from the Jackson Laboratories (Bar harbour, ME, USA). These mice were originally produced by Deltagen (San Mateo, CA, USA) and have been backcrossed at least 5 generations onto the C57BL/6J background. All animal studies were conducted with ethical approval from the Dunn School of Pathology Local Ethical Review Committee and in accordance with the UK Home Office regulations (Guidance on the Operation of Animals (Scientific Procedures Act) 1986). When designing experiments using animals, the principles of the 3Rs were taken into consideration at every stage. This involved trying to replace animal experimentation with *in vitro* alternatives, to reduce the number of animals used to complete any study and to refine the experimental method(s) to improve animal welfare and minimise suffering.

2.3 Bio-gel and thioglycollate elicitation of peritoneal exudate cells

Male C57BL/6J mice or male and female $CB_2^{-/-}$ mice were injected intraperitoneally with either 1 ml of sterile 2% bio-gel polyacrylamide beads (P100 fine, 45-90 μM; either from our lab stock or from a separate batch obtained from a collaborator) suspended in phosphate buffered saline (PBS) or 1 ml of 4% thioglycollate (brewer thioglycollate media, Sigma-Aldrich). After four days, mice were sacrificed and the elicited cells collected by peritoneal lavage with 10 ml ice cold PBS containing 2 mM EDTA. The cellular composition of both populations was determined by flow cytometry as described in section 2.7.

2.4 Bio-gel macrophage enrichment

Following peritoneal lavage bio-gel elicited PECs were pelleted by centrifugation at 200 xg for 5 min at 4°C and then re-suspended in 10 ml chemotaxis buffer (RPMI 1640 supplemented with 0.5% BSA and 25 mM HEPES) before being transferred into 10 cm petri dishes (one per mouse; non-tissue culture treated) and left for 2 hours at 37°C, 5% CO_2. After three washes with 10 ml PBS to remove any non-adherent cells, the medium was replaced with 10 ml chemotaxis buffer and dishes left overnight at 37°C, 5% CO_2. Adherent macrophages were collected by the addition of PBS, containing 10 mM EDTA, and gentle agitation. Macrophages were then pelleted by centrifugation at 200 xg for 5 min at 4°C, resuspended in chemotaxis buffer, counted and then adjusted to the desired cell concentration. Macrophage purity was determined by flow cytometry as described in section 2.7.

2.5 ACEA xCELLigence real-time chemotaxis assay

Real-time chemotaxis analysis was conducted as previously described [343]. Vehicle (0.3% DMSO in chemotaxis buffer) cannabinoid, chemerin or chemokine (160 μl) at the desired final concentration was added to the lower chamber of a CIM-16 plate. The upper chamber was subsequently attached and 50 μl of pre-warmed chemotaxis buffer added to each of the upper chambers. Following equilibration at RT for 30 min, the plate was transferred into the RTCA-DP system for background analysis. Bio-gel elicited PECs (50 μl - 4 x 10^5 cells/well), enriched macrophages, thioglycollate elicited macrophages or bone marrow neutrophils (50 μl - 2 x 10^5 cells/well) in chemotaxis buffer were then added to all upper wells and plate replaced into the RTCA-DP system. Cell Index (CI) measurements were then taken every 5 seconds over the 3-4 hour assay period. CI is a dimensionless unit that represents the background corrected electrical resistance at a given time point for each well. It

is derived using the following equation:

$$\text{Cell Index} = \frac{(\Omega_{tn} - \Omega_{t0})}{15\ \Omega}$$

Where: Ω_{tn} = Resistance at time point being measured

and Ω_{t0} = Resistance at time point zero

For inhibitor studies, bio-gel elicited PECs were incubated at 37°C, 5% CO_2 with wortmannin (200 nM for 60 min), PTX (200 ng/ml for 90 min), SR144528 or SR141716A (1 μM for 30 min) prior to being placed into the upper chamber of the CIM-16 chemotaxis plate. For the experiments using SR144528 and SR141716A, these inverse agonists were also present in the lower chamber alongside the indicated cannabinoid. For receptor cross-talk experiments, ligands were either added alone or in combination into the lower chamber of a CIM-16 chemotaxis plate. Gradient formation and chemotaxis was then conducted as described above. Chemotaxis traces are either displayed as the raw CI values. Data were analysed by calculating the maximum CI reached minus the minimum CI signal and pooled data are displayed as a fold change relative to cells migrating towards vehicle alone (referred to as Δ Cell Index (Fold change)).

2.6 ACEA 96 well ECIS cell spreading assay

Following peritoneal lavage, bio-gel elicited PECs were pelleted by centrifugation at 200 xg for 5 min at 4°C and then re-suspended at a cell density of 1 x 10^6 cells/ml in chemotaxis buffer pre-warmed to 37°C. Chemotaxis buffer (50 μl) was then added into all wells of a 96 well E-plate and a background measurement taken. Afterwards, 50 μl of cell suspension was added to all wells (50,000 cells/well) and cells were then left at 37°C, 5% CO_2 for 2-3 hours to adhere until the CI had reached a stable plateau. Cells were then stimulated with either vehicle (0.3% DMSO) or cannabinoid at the

indicated concentration and CI measurements taken every 5 s for 1-2 hours after agonist addition. Data are displayed as the raw CI values. The response observed was then calculated as maximum CI minus CI at point of agonist addition (referred to as ΔCell Index). For experiments using LY294002, after the plateau phase was reached, cells were incubated with vehicle, 10, 3 or 1 μM LY294002 (10 μl/well) for 1 hour at 37 °C, 5% CO_2. Following treatment, 10 μM JWH133 or HU308 was added (10 μl/well) and CI measurements taken every 5 s for 1-2 hours after agonist addition. For the receptor transfection studies, 50 μl of Ham's F12 with 2% FCS was added to each well of a 96 well E-plate and a background reading taken. Afterwards, GPCR transfected CHO cells were added to their corresponding wells (50 μl; 25,000 cells/well) in Ham's F12 with 2% FCS and left overnight at 37°C, 5% CO_2 to reach a stable baseline and allow tagged GPCR expression. After stimulation with vehicle (0.3% DMSO) or ligand (Cannabinoid 10 μM or C5a 10 nM), CI measurements were taken every 5 s for 1-2 hours after agonist addition. Response was calculated as: CI immediately before agonist addition minus CI at the time point corresponding to C5a peak in C5aR1 transfected cells.

2.7 Flow cytometry

Cells (5 x 10^5) or 300 μl of pouch or peritoneal lavage fluid was placed into polypropylene tubes and pelleted by centrifugation at 200 xg for 5 mins at 4°C. These were then resuspended in 50 μl of FACS buffer (PBS containing 2% FCS, 25 mM HEPES and 5 mM EDTA) supplemented with mouse IgG (116 μg/ml) and mouse SeroBlock FcR® (6.6 μg/ml AbD Serotec, Oxford, UK) and left on ice for 30 min to allow Fc receptor blocking. For studies using CHO cells, the cell pellet was resuspended in FACS buffer alone. Specific staining was conducted by the addition of 50 μl antibody cocktail in FACS buffer for 1 hour on ice. The antibodies used throughout this thesis are listed in table 2.1, and positive staining was determined using the appropriate isotype controls. Cells were then washed with 1 ml FACS buffer before

being resuspended in 1% PFA and analysed using a Dako Cyan ADP flow cytometer (Beckman Coulter Ltd, High Wycombe, UK) and FlowJo software (V10, Tree Star, Ashland, USA). For whole blood staining, 50 μl of blood was placed into polypropylene tubes containing 50 μl blocking solution as detailed above, and left on ice for 30 min. Antibody staining was then conducted by the addition of 50 μl antibody cocktail and incubation for 1 hour on ice. Next 3 ml BD FACS™ lysing solution was added to each sample and tubes left for 15 min at RT to allow red blood cell lysis. Cells were then pelleted by centrifugation at 200 xg for 5 min, washed twice with 1 ml FACS buffer and then resuspended in 1% PFA for analysis. The antibody staining definitions I have used to identify all of the different cell populations that appear in my thesis can be found in table 2.2.

Antigen	**Isotype**	**Clone**	**Fluorophore**
B220	RA3-6B2	Rat IgG2a	APC
c-myc	SH1-26E7.1.3	Mouse IgG1	FITC
CD11b	M1/70	Rat IgG2b	PerCP
CD19	6D5	Rat IgG2a	Brilliant violet 421
CD115	AFS98	Rat IgG2a	PE
CD3	17A2	Rat IgG2b	PE
CD45	30-F11	Rat IgG2b	APC/Cy7
CD45.1	A20	Mouse IgG2a	APC/Cy7
CD45.2	104	Mouse IgG2a	PE
F4/80	CI:A3-1	Rat IgG2b	FITC
F4/80	CI:A3-1	Rat IgG2b	Alexa Fluor 647
FcϵRIα	MAR-1	Armenian hamster IgG	PE
FLAG	L5	Rat IgG2a	PE
HA	GG8-1F3.3.1	Mouse IgG1	APC

Continued on next page

Table 2.1 – continued from previous page

Antigen	Isotype	Clone	Fluorophore
Ly6C	HK1.4	Rat IgG2c	APC
Ly6C	HK1.4	Rat IgG2c	FITC
Ly6B.2	7/4	Rat IgG2a	Alexa Fluor 647
Ly6G	1A8	Rat IgG2a	PE
Ly6G	1A8	Rat IgG2a	Pacific blue
Siglec-F	E50-2440	Rat IgG2a	Alexa Fluor 647

Table 2.1 Antibodies used throughout this thesis.

Cell Type	Surface Markers Used
Neutrophils	CD45, CD11b, Ly6G, Ly6C, 7/4
$Ly6C^{lo}$ monocytes	CD45, CD11b, CD115, $Ly6C^{lo}$
$Ly6C^{hi}$ monocytes	CD45, CD11b, CD115, $Ly6C^{hi}$
Macrophages	CD45, CD11b, F4/80, 7/4 negative
Eosinophils	CD45, CD11b, $F4/80^{mid}$, Siglec-F
Mast cells	CD45, CD11b, Siglec-F, FcϵRIα
T cells	CD45, CD3
B cells	CD45, CD19, B220
B-1 cells	CD45, CD19, B220 negative
CHO CB_2 cells	FLAG positive
CHO GPR55 cells	c-myc positive
CHO GPR18 cells	HA positive
CHO C5aR1 cells	HA positive

Table 2.2 Surface markers used for cell identification.

2.8 Cell counting using flow cytometry

For elicited cells (peritoneal for the zymosan peritonitis model, pouch for the dorsal air pouch model), 50 μl of CountBright™ Absolute Counting Beads (ThermoFisher Scientific, Paisley, UK) were added to 300 μl of lavage fluid and samples analysed by flow cytometry gating separately on beads (which have high side scatter) and cells, and then calculating the number of events in each gate. For the blood, 50 μl of whole blood was subjected to red blood cell lysis using 3 ml of BD FACS™ lysing solution for 15 min at RT. Cells were then washed twice using 3 ml FACS buffer, resuspended in 300 μl of FACS buffer and supplemented with 50 μl of counting beads before being analysed by flow cytometry. The number of cells per ml of sample was then calculated using the following equation: $\text{Cells/ml} = \left(\left(\frac{\text{Cell events}}{\text{Bead events}} \right) * \left(\frac{\text{Bead concentration}}{\text{Volume in sample}} \right) \right) * 1000$. For cells recruited in the peritonitis and dorsal air pouch models, the resulting number was multiplied by 5 and 3 respectively to calculate the absolute number of cells recruited to each cavity, as this factor represents the lavage volume in ml used in either model.

2.9 Discoverx intracellular cAMP assay

Intracellular cAMP levels were measured using Discoverx cAMP Hunter™ eXpress kits (Discoverx, Birmingham, UK) following the manufacturer's protocol. Briefly, CHO-K1 cells overexpressing the human CB_2 receptor were plated into a 1/2 area 96 well plate (15,000 cells/well) and incubated at 37°C, 5% CO_2 for 24 hours. The media was then removed and replaced with 22.5 μl of assay buffer containing a cAMP capture antibody. Cells were then stimulated for 30 min at 37°C, 5% CO_2 with either vehicle (4.8% DMSO with 80 μM forskolin) or cannabinoid at 4x the final desired concentration (Final concentrations were 1.2% DMSO and 20 μM forskolin). Following stimulation, cell lysis and cAMP detection were performed as per the manufacturer's protocol. Luminescence measurements were taken using a

PHERAstar microplate reader (BMG Labtech, Aylesbury, UK).

2.10 Discoverx β-arrestin recruitment assay

Recruitment of β-Arrestin to murine CB_2 was measured using the Discoverx PathHunter® eXpress β-Arrestin GPCR Assay following the manufacturer's protocol. Briefly, CHO-K1 cells stably expressing murine CB_2 were seeded into 1/2 area 96 well plates (15,000 cells/well) and incubated at 37°C, 5% CO_2 for 48 hours. Cells were then stimulated with vehicle (0.3% DMSO in Cell assay reagent) or cannabinoid at the indicated concentration for 90 min at 37°C, 5% CO_2. Cell lysis and detection of total recruited β-arrestin was determined following the manufacturer's protocol. Luminescence measurements were taken using a PHERAstar microplate reader.

2.11 Discoverx β-arrestin GPCR screen

Recruitment of β-Arrestin to 241 human GPCRs after stimulation with 10 μM JWH133 was measured using the Discoverx PathHunter® eXpress β-Arrestin GPCR Assay. Briefly, cells were seeded into white walled, 384 well microplates and incubated at 37°C for the appropriate time period prior to testing. JWH133 or vehicle (1% DMSO) was then added to the corresponding wells and the plate incubated at either RT or 37°C for 90 or 180 min, depending on the GPCRs being tested. Cell lysis and detection reagents were subsequently added and one hour later, luminescence measurement taken using a PerkinElmer Envision microplate reader. For the GPCRMax panel, % Agonist activity is calculated as 100% x (mean of test sample − mean of vehicle control) / (mean of control ligand − mean of vehicle control). For the OrphanMax panel, % Agonist activity is calculated as 100% x (mean of test sample − mean of vehicle control) / (mean of vehicle control).

2.12 Cannabinoid stimulation of bio-gel elicited murine macrophages

Following peritoneal lavage, bio-gel elicited PECs were pelleted by centrifugation at 200 xg for 5 min at 4°C and then re-suspended at a cell density of 1 x 10^6 cells/ml in chemotaxis buffer pre-warmed to 37°C. PECs (2 x 10^6 cells/well) were then seeded in 6 well plates and allowed to adhere for 2 hours at 37°C, 5% CO_2. After three washes with pre-warmed PBS to remove non-adherent cells and enrich for macrophages, 2 ml of chemotaxis buffer was added to each well and the plates left for 1 hour at 37°C, 5% CO_2. The media was then replaced with 1 ml warmed chemotaxis buffer and left for a further hour at 37°C, 5% CO_2, after which 200 μl of vehicle or cannabinoid was added to the corresponding wells (yielding a final concentration of 10 μM at 0.3% DMSO). Plates were then incubated for 30 min at 37°C, 5% CO_2. For experiments using SR144528, 100 μl of either vehicle or SR144528 was added to the corresponding wells and plates incubated for 30 min at 37°C, 5% CO_2 (yielding a final concentration of 1 μM SR144528 at 0.3% DMSO). Following inverse agonist pre-treatment, wells received 100 μl of either vehicle or cannabinoid (yielding final concentrations of 10 μM cannabinoid and 0.6% DMSO) and plates incubated for 30 min at 37°C, 5% CO_2. After stimulation, the media was rapidly removed and the plates placed at −80°C. Cell lysates were prepared by the addition to each well of 180 μl cell lysis buffer (150 mM NaCl, 0.8 mM $MgCl_2$, 5 mM EGTA, 50 mM HEPES, 1% IGEPAL CA-630) supplemented with protease and phosphatase inhibitors. Cells were then manually disrupted and supernatant centrifuged at 16,000 xg for 10 min at 4°C. Protein concentration of debris free supernatant was determined using a BCA protein assay kit (Thermo Fisher scientific, Loughborough, UK) following the manufacturer's protocol. Samples were then diluted 3:1 with 4x laemmli buffer (250 mM Tris-HCl, pH 6.8, 8% SDS, 40% glycerol, 0.004% bromophenol blue, 20% β-mercaptoethanol), heated at 95°C for 5 min and either loaded directly onto an SDS-PAGE gel or placed at −80°C.

2.13 Western blotting

Samples (30 μg total protein) were separated using a 10% SDS-PAGE gel (120 V for 90 minutes) and transferred (200 mA for 110 minutes) onto Hybond ECL nitrocellulose (GE healthcare, Buckinghamshire, UK). Membranes were blocked with 5% BSA in Tris-buffered saline supplemented with 0.1% tween (TBS-T) for 2 hours at RT or overnight at 4°C. After blocking, membranes were incubated with rabbit anti-phospho-ERK1/2 or rabbit anti-phospho-Akt (both 1:1000) diluted in 5% BSA/TBS-T for 2 hours at RT or overnight at 4°C. Membranes were then incubated with a HRP-conjugated anti-rabbit secondary antibody (1:20,000) for 1 hour at RT. Protein bands were visualised by incubating the membranes for 5 min with Amersham™ ECL prime and subsequent exposure to x-ray film over a range of exposure times. To confirm equal protein loading between samples, bound antibodies were removed by incubating the nitrocellulose membranes in stripping buffer (60 mM Tris-HCl pH 6.8, 2% SDS, 0.8% β-mercaptoethanol) for 30 min at 50°C. Membranes were then blocked with 5% BSA in TBS-T for 2 hours at RT and then incubated with rabbit anti-ERK1/2 (1:1000) diluted in 5% BSA/TBS-T for 2 hours. Protein detection was then conducted as detailed above. Densitometric analysis was conducted using Image Studio Lite (LI-COR Biosciences, Cambridge, UK) with data displayed as fold change compared to vehicle of the phosphorylated protein band density divided by the density of the loading control.

2.14 ELISA

The concentration of murine IL-6, TNF-α, CCL2, CCL3, CXCL1, CXCL2 and CXCL5 in fibroblast cell culture supernatants, air pouch explant culture supernatant and air pouch and peritoneal lavage supernantants was determined using DuoSet® sandwich ELISA assays (R & D systems). To begin, a 96 well MAXISORP plate (Thermo Scientific) was coated with capture antibody by the addition of 100 μl

per well of the corresponding capture antibody, diluted to the desired working concentration in PBS, and incubation overnight at RT. The plate was then washed by completely filling each well with wash buffer (PBS containing 0.05% tween), followed by aspiration, four times. Plates were then blocked by the addition of 300 μl of reagent diluent (PBS containing 1% BSA) per well and incubation for 1 hour at RT. The plates were then washed four times with wash buffer and 100 μl of sample or protein standard diluted in reagent diluent was added per well and the plate incubated for 2 hours at RT. Following another wash step, 100 μl of detection antibody diluted in reagent diluent was added to each well and the plate incubated for 2 hours at RT. The plates were subjected to another wash step and then 100 μl of streptavidin-HRP was added to each well and the plate incubated for 20 min at RT. The plates then had one final round of washing after which 55 μl of 1-Step™ Ultra TMB-ELISA solution was added to each well and the plates incubated for 20 min at RT in the dark. Finally, 55 μl of 2N H_2SO_4 was added to each well to stop the HRP reaction and the absorbance at 450 nm for each well was determined using a PHERAstar plate reader. The obtained values were corrected for optical imperfections in the plate plastic by subtracting absorbance at 570 nm from absorbance at 450 nm for each well. The amount of each analyte was then determined by interpolation from the protein standard curve, taking into account the dilution factor of each sample. If no analyte was detectable in a sample, then a value equal to the lower limit of detection for the kit, multiplied by the dilution factor was used for that sample, as this will at least slightly overestimate the amount of analyte present but means that samples which had detectable levels of analyte will not inappropriately skew the mean of the pooled results.

2.15 Luminex® inflammatory mediator screening

The concentration of murine IL-6, TNF-α, CCL2, CCL3, CCL4, CXCL1, CXCL2, CXCL5, CXCL10, IL-1β and matrix metalloproteinase 9 (MMP-9) in air pouch

lavage supernatants was determined using the bead based Luminex® Screening Assay ELISA. To begin, the air pouch lavage supernatants were diluted 2-fold using calibrator diluent RD6-52 and the 96 well microplate was washed by adding and then removing 100 μl per well of the provided wash buffer. Next 50 μl of the bead cocktail and 50 μl of protein standard or diluted lavage supernatant was added into the corresponding wells and the plate incubated for 2 hours at RT with orbital shaking (500 rpm). Each well was then washed three times with 100 μl of wash buffer, after which all liquid was removed and 50 μl of biotin antibody cocktail was added to each well. The plate was then incubated for 1 hour at RT with orbital shaking. The plate was then washed three times using 100 μl per well of wash buffer, all liquid removed and 50 μl of streptavidin-PE added to all wells. After incubation for 30 min at RT with orbital shaking, the plate was washed three times using 100 μl per well of wash buffer. The beads were then resuspended in 100 μl of wash buffer and samples analysed using a Bio-Rad analyser. The amount of each analyte was determined from the protein standard curve, taking into account the original 2-fold dilution.

2.16 Generation of N-terminal tagged GPCR constructs

All tagged GPCR constructs were purchased from Life Technologies, using their GeneArt® Gene Synthesis service. Briefly, the protein coding regions for murine C5aR1 (Transcript variant 1, NM_007577.4), CB_2 (NM_009924.3), GPR55 (NM_0010-33290.2), GPR18 (NM_182806.1), Lysophosphatidic acid receptor 1 (LPAR1 − Transcript variant 1, NM_010336.2), Lysophosphatidic acid receptor 5 (LPAR5 - Transcript variant 1, NM_001163268.1), Cysteinyl leukotriene receptor 1 (CYSLTR1 - transcript variant 1, NM_021476.5), Cysteinyl leukotriene receptor 2 (CYSLTR2 - transcript variant 1, NM_133720.3) and G protein-coupled estrogen receptor 1 (GPER1 - NM_029771.3) were modified by the removal of the endogenous start codon and the addition of an N-terminal EcoRI restriction site, a Kozak consensus sequence,

an epitope tag (C5aR1, GPR18, LPAR1&5, CYSLTR1&2, LTB4R1, S1PR1 and GPER - hemagglutinin (HA); CB_2 - FLAG; GPR55 - c-myc) and a C-terminal NotI restriction site. The sequences were cloned into pcDNA3.1(+) and all constructs 100% sequence verified. Vectors were propagated by transformation into DH5α chemically competent cells (Life Technologies) following the manufacturer's protocol. After being spread on LB agar plates containing 50 μg/ml ampicillin and incubated overnight at 37°C, single colonies were placed into 7 ml of LB medium containing 50 μg/ml ampicillin and incubated for 10 hours at 37°C with constant shaking (300 rpm). Next 150 μl of this culture was added to 150 ml LB medium containing 50 μg/ml ampicillin and incubated for 20 hours at 37°C with constant shaking (300 rpm). The cells were then pelleted and plasmid DNA extracted using the Qiagen HiSpeed plasmid midi kit following the manufacturer's instructions. DNA concentration and purity was determined using a NanoDrop™ ND-1000 spectrophotometer (Thermo Scientific). All vectors were then sent for Sanger sequencing to confirm sequence identity.

2.17 CHO cell GPCR transfections

CHO cells were cultured in Ham's F12 medium containing 2% FCS until 80-90% confluent. After washing twice with 15 ml PBS, cells were detached by incubation with TrypLE™ Express (5 ml - T75 flask, 10 ml - T175 flask, Life technologies, Paisley, UK) for 3 min at 37°C, 5% CO_2. After being collected into 25 ml Ham's F12 with 2% FCS and pelleted by centrifugation at 200 xg at 4°C, cells were resuspended in Ham's F12 with 2% FCS, counted and cell density adjusted to 1 x 10^6 cells/ml. For receptor transfections, the Amaxa® cell line nucleofector® kit T was used following the manufacturer's recommended protocol for CHO cells. Briefly, 1 x 10^6 cells were pelleted by centrifugation at 200 xg for 10 min at RT and then resuspended in 100 μl nucleofector® solution T. After addition of Plasmid DNA (2 μg - either tagged GPCR or empty vector) the suspension was transferred into a provided cuvette,

placed into the nucleofector® device and transfected using program U-023. Cells were then diluted to a final volume of 2 ml using Ham's F12 with 2% FCS and plated into a 96 well E-plate (see section 2.6 for details). The remaining cells were added into a 6 well dish containing 2 ml Ham's F12 with 2% FCS and left overnight at 37°C, 5% CO_2. The cells were detached by incubation with 500 μl TrypLE™ Express per well for 3 min at 37°C, 5% CO_2 and collected into 5 ml Ham's F12 with 2% FCS. The cells were then pelleted, counted and used for flow cytometric analysis of transfection efficiency as detailed in section 2.7.

2.18 Bone marrow neutrophil isolation

Isolation of murine bone marrow neutrophils was conducted as previously described [344]. Briefly, the femur and tibia were isolated from male C57BL/6J mice with the surrounding tissue carefully removed. The bones were then flushed through with RPMI containing 10% FCS and 2 mM EDTA. The bone marrow cells were then gently resuspended using a pasteur pipette, passed through a 70 μm cell strainer to remove any remaining tissue or cell clumps and pelleted by centrifugation at 250 xg for 5 min at 4°C. Red blood cells were then lysed by hypotonic lysis (20 ml 0.2% NaCl followed by 20 ml 1.6% NaCl) and the remaining cells pelleted by centrifugation at 250 xg for 5 min at 4°C. After washing with RPMI containing 10% FCS and 2 mM EDTA, cells were resuspended in 1 ml PBS and layered onto a Histopaque® gradient consisting of Histopaque® 1077 (3ml) on top of Histopaque® 1119 (3 ml) and centrifuged at 400 xg for 30 min at RT. Neutrophils were then collected from the interface of the Histopaque® layers using a pasteur pipette, pelleted by centrifugation at 250 xg for 5 min at 4°C and then resuspended in 1 ml chemotaxis buffer and counted. Cell density was then adjusted to 4 x 10^6 cells/ml with chemotaxis buffer and 50 μl added to the upper chamber of the CIM-16 chemotaxis plate (2 x 10^5 cells/well). Neutrophil purity was determined by flow cytometry as described in section 2.7.

2.19 RNA extraction and cDNA synthesis

RNA extraction of enriched bio-gel macrophages, cultured air pouch fibroblasts and air pouch tissue explants was conducted using the RNeasy® Mini Kit (Qiagen, Manchester, UK). Briefly, cells and tissue were lysed by addition of 500 μl of buffer RLT and manual disruption, and then total RNA extracted following the manufacturer's instructions. RNA concentration and quality was determined using a NanoDrop™ ND-1000 spectrophotometer. cDNA was produced from the purified RNA using the QuantiTect® Reverse Transcription kit (Qiagen) following the manufacturer's protocol.

2.20 Real-time PCR

Expression of actin, CB_2, vimentin, TLR-2 and/or Dectin-1 in enriched bio-gel macrophages or cultured air pouch fibroblasts was determined using the following primers (5'>3'): Actin Fwd CCAACAGCAGACTTCCAGGATT, Actin Rev CTGGCAAGAAGGAGTGGTAACTG, CB_2 Fwd GGTCCTCTCAGCATTGATTTC, CB_2 Rev GCCCAGTAGGTAGTCGTTAG, Vimentin Fwd TGAAGGAAGAGATGGCTCGT, Vimentin Rev GGAAGAAAAGGTTGGCAGAG, TLR2 Fwd CTCCCACTTCAGGCTCTTTG, TLR2 Rev GCCACTCCAGGTAGGTCTTG, Dectin-1 Fwd CAGGGAGAAATCCAGAGGAG, Dectin-1 Rev TAGGAAGGCAAGGCTGAGAA and SYBR Select PCR master mix (Life Technologies). 500 ng of cDNA was used per reaction with the following thermal profile: 95°C for 5 min, 40 cycles of 95°C for 30 s, 60°C for 20 s, 72°C for 30 s and a final step of 72°C for 5 min using a StepOnePlus™ thermal cycler (Applied biosystems). The StepOne™ software was used for data analysis, with the cycle threshold (Ct) set in the linear phase of the amplification plot.

2.21 Murine Taqman GPCR expression array

cDNA synthesis from bio-gel enriched macrophage RNA was conducted as described above. cDNA was mixed with an equal volume of 2X qPCR mastermix plus (Eurogentec: containing dNTP/dUTP, HotGoldStar Taq DNA polymerase, UNG, $MgCl_2$ and the ROX passive reference dye) and 1000 μg of cDNA was loaded per lane into a 384 well TaqMan Mouse GPCR array (Applied Biosystems) by centrifugation of the plate at 331 xg for 2 consecutive runs of 1 min. The plate was then sealed and the PCR reaction conducted using an Applied Biosystems 7900HT Fast Real-Time PCR System with the following thermal profile: 50°for 2 min (UNG activation), 95°for 10 min (polymerase activation) and 40 cycles of 95°for 15 s and 60°for 1 min. Data analysis was conducted using SDS software version 2.1 (Applied Biosystems) with the cycle threshold (Ct) value set in the linear phase of the amplification plot. A Ct value of 32 was set as a cutoff, above which genes were deemed not expressed.

2.22 Ligand-directed virtual screening

The ligand-directed virtual screen was conducted by Rebecca Hancock from the Department of Chemistry. A virtual representation of the chemistry in-house compound library, containing approximately 25,000 members, was created using OMEGA (OpenEye Scientific, Santa Fe, NM) and used as the screening library. JWH133, HU308, L-759,656 and SER601 were drawn using ChemBioDraw (Perkin Elmer, Massachusetts), converted to an energy minimised three dimensional structure using the MM2 function and used as the reference ligands in four separate virtual screens. The virtual screening was performed using ROCS (OpenEye Scientific) using the simple screen settings, comparing each reference ligand to each compound library member. Compounds were than ranked from high to low based on their combo score (A composite measure of how similar the test compound is to the reference ligand in both three dimensional shape and overall charge distribution.

The higher the combo score, the more similar the test compound is to the reference). From each of the four screens, the top 20 were considered for screening plus any compounds that were present in the top 100 of at least 2 screens. Compounds were then grouped into classes (compounds with a common backbone or substructure) and classes with three or more members were prioritised for biological testing. Finally, any compounds found at this stage that resembled the DIAS scaffold [343] were excluded from biological testing.

2.23 Zymosan-induced peritonitis

Female WT C57BL/6J or $CB_2^{-/-}$ mice were injected intraperitoneally with 100 μg of zymosan A from *Saccharomyces cerevisiae* (Sigma Aldrich). Four hours later, mice were sacrificed and elicited cells collected by peritoneal lavage with 5 ml PBS containing 2 mM EDTA. The total number of cells recruited to the peritoneal cavity was calculated using CountBright™ Absolute Counting Beads (Life technologies) as detailed in section 2.8. Cell populations present in the peritoneum were identified using flow cytometry as described in section 2.7.

2.24 Dorsal air pouch inflammation model

Male or Female WT C57BL/6J or $CB_2^{-/-}$ mice were anaesthetised using isoflurane and then air pouches created by the dorsal subcutaneous injection of 2.5 ml sterile air on day 0 and day 3 to fully establish the dorsal air pouch. On day 6 the mice were again anaesthetised using isoflurane and each pouch injected with 100 μg of zymosan A (500 μl per pouch). The mice were then culled 2, 6, 16 or 48 hours after zymosan injection and the pouches lavaged with 3 ml PBS containing 2 mM EDTA. For baseline analysis, on day 6 mice were culled directly and pouches lavaged with 3 ml PBS containing 2 mM EDTA. After pouch lavage, blood was collected from the hepatic portal vein using a 21 G needle and placed into EDTA containing blood

tubes. Cell counts and populations present were determined by flow cytometry as described in sections 2.7 and 2.8. To collect cells lining the pouch, day 6 pouches were injected with 3 ml TrypLE™ Express pre-warmed to 37°C and left for 15 min before collection into 6 ml DMEM containing 10% FCS. Cell culture and *in vitro* zymosan stimulation was then conducted as described in section 2.26. For pouch explant studies, mice were culled on day 6 after pouch establishment and the pouch exposed by carefully removing the overlying skin. The pouch was then removed and cut into equal pieces before being placed into 6 well dishes containing 500 μl vehicle (DMEM containing 10% FCS) or zymosan (10 μg/ml). The tissue explants were then left for 3 hours before culture supernatants were collected and then stored at −80°C. Inflammatory mediator production was then measured by ELISA as detailed in section 2.14. The remaining pouch tissue was placed into RLT buffer, homogenised and RNA extraction and cDNA synthesis conducted as described in section 2.19.

2.25 Generation of mixed bone marrow chimeric animals

Bone marrow cells were isolated from 8-10 week old female WT B6.SJL animals that have the CD45.1 surface antigen and $CB_2^{-/-}$ animals that have the CD45.2 surface antigen. Red blood cell lysis was conducted by the addition of 10 ml of ACK lysis buffer (155 mM ammonium chloride, 10 mM potassium bicarbonate and 100 μM EDTA) for 5 min. Cells were then pelleted by centrifugation at 250 xg for 5 min. The remaining cells were resuspended in PBS, counted, and then CD45.1 and CD45.2 cells mixed equally to give a final concentration of 2.5 x 10^7 cells/ml. Alongside, 8-10 week old female WT C57BL/6J or $CB_2^{-/-}$ animals were lethally irradiated with two doses of 5 Gy separated by a three hour gap. Afterwards, the animals were injected intravenously with 200 μl of the bone marrow cell suspension (5 x 10^6 cells/mouse) and monitored closely for he next week to ensure bone marrow transplantation was successful. Eight to ten weeks after bone marrow reconstitution, blood was taken from the tail vein of each animal and the proportion of CD45.1 to CD45.2 cells in

the blood was determined by flow cytometry. One week later dorsal air pouches were established, and then each pouch subsequently injected with 100 μg of zymosan. The mice were then culled 6 hours later and pouch and blood leukocyte analysis was conducted as detailed in sections 2.24 and 2.7.

2.26 Culture and stimulation of air pouch fibroblasts

After collection of the cells lining the dorsal air pouch (see section 2.24 for details), the cells were passed through a 0.45 μm cell strainer and then pelleted by centrifugation at 200 xg for 5 min. The cells were then resuspended in 3 ml DMEM containing 10% FCS and seeded into one well of a 6 well dish (one well per mouse). The medium was then replaced every 2 days until the cells were approximately 90% confluent. The cells were then lifted by incubation with 500 μl TrypLE™ Express for 5 min at 37°C and then placed into 5 ml DMEM containing 10% FCS. Fibroblasts were then pelleted by centrifugation, resuspended in 1 ml of DMEM containing 10% FCS and counted using trypan blue exclusion. The cells were then adjusted to a concentration of 2 x 10^6 cells/ml, 1 ml added to each well of a 12 well plate and then left overnight at 37°C, 5% CO_2. The cells were then stimulated with vehicle or zymosan (10 μg/ml) for 6 hours before cell culture supernatants were collected for ELISA analysis (see section 2.14) and cells lysed by the addition of 300 μl RLT buffer in preparation for RNA extraction and cDNA synthesis (see section 2.19).

2.27 Data and statistical analysis

All data presented in this thesis were analysed using GraphPad Prism (Version 7, La Jolla, CA). All data are expressed as mean + or ± SEM, as detailed in each figure legend. For comparisons between two groups only, a Student's t-test was applied. For multiple comparisons with only a single variable, a one-way ANOVA with Dunnett's multiple comparisons correction was applied. For comparisons with

two variables, a two-way ANOVA with Sidak's multiple comparisons correction was applied. The test used for each individual data set is specified in the corresponding figure legend. A P value of <0.05 was taken to be statistically significant.

Chapter 3

Cannabinoid receptor 2 and macrophage chemotaxis

3.1 Introduction

3.1.1 Chemotaxis - Directional cellular migration towards a chemoattractant

Chemotaxis, defined as the directional movement of cells towards a chemoattractant source, is a cellular phenomenon that is fundamental for many physiological processes in the body. It plays crucial a role in the development of the brain, reproduction, wound healing, angio- and vasculogensis and importantly in immune cell mobilisation and recruitment to sites of tissue damage or infection. The process of chemotaxis follows a defined series of events, beginning with the sensing of an external chemoattractant gradient by cell surface receptors. This external gradient is then reproduced and amplified internally resulting in the polarisation of the cell into a front (known as the leading edge) and a back (known as the uropod). Finally, F-actin and actin-myosin polymerisation and contraction allow extension of the cell front and movement of the cell body respectively, resulting in the net movement of the cell towards the chemoattractant.

A large amount of the knowledge gathered surrounding the process of chemotaxis has come from studying the amoeba *Dictyostelium discoideum*. These normally single celled organisms will migrate towards cAMP released by others during periods of starvation to aggregate into a single bodied colony [345]. Whilst it cannot be argued that the discoveries made studying these single celled amoebas are not of merit, there are large differences between the pathways and signalling mechanisms employed by *Dictyostelium discoideum* and mammalian leukocytes [346, 347]. Therefore for the rest of this introduction I will purposefully focus on studies that specifically examine the process of leukocyte chemotaxis.

3.1.2 Chemotactic receptor signalling

In leukocytes, the receptors responsible for sensing of chemoattractants are $G_{i/o}$-coupled GPCRs. Their absolute requirement for the initiation of chemotaxis is demonstrated by the finding that treating cells with pertussis toxin (which irreversibly locks the $G\alpha_i$ protein in the inactive GDP bound state) completely blocks leukocyte chemotaxis [347]. It has long been thought that the $G\alpha$ subunit itself is not required for initiating chemotaxis [348], however recent work has demonstrated that members of the G_α family play a role in the regulation of leukocyte chemotaxis. $G\alpha_{i2}$ has been demonstrated to recruit effector proteins to the leading edge of the cell that help to regulate cell polarisation, actin polymerisation and chemotaxis [349, 350] and genetic deletion of $G\alpha_{i2}$ in neutrophils inhibits their recruitment in a thioglycollate-induced peritonitis model [351]. Furthermore, it is well established that the $G\alpha_{12/13}$ proteins are key for establishing the 'backness' signalling pathway [352] (See section 3.1.5). Nonetheless, the $G\beta\gamma$ subunit plays the dominant role in the initiation of downstream chemotaxis signalling pathways [353, 354]. GPCR activation causes the release of the $G\beta\gamma$ subunit from the inhibitory effects of the $G\alpha$ subunit, allowing it to activate a multitude of downstream effectors, such as cytosolic phospholipase A2 and protein kinase Cζ [347, 355]. However, the most important downstream effector activated after GPCR stimulation is phosphoinositide 3-kinase (PI3K) [356].

3.1.3 PI3K signalling and leading edge formation

As chemoattractant GPCRs remain uniformly distributed throughout the plasma membrane during chemotaxis [357], this cannot account for the front/back polarisation seen in migrating cells. Instead the external chemoattractant gradient is translated into an internal gradient by the activity of PI3K. This is responsible for the formation of the leading edge. PI3K accumulates at the front of the cell, where it is directly activated by the G$\beta\gamma$ subunit [357, 358], and catalyses the conversion of phosphatidylinositol 4,5-bisphosphate (PIP_2) into phosphatidylinositol 3,4,5-triphosphate (PIP_3), causing the asymmetric enrichment of PIP_3 at the leading edge. In leukocytes, the PI3Kγ isoform is the most critical for directed migration, as neutrophils isolated from mice lacking PI3Kγ do not chemotax or produce PIP_3 when stimulated with the chemoattractants C5a, IL-8 or fMLF [359–361]. However the PI3Kβ and δ isoforms also help to regulate leukocyte migration [362, 363]. The asymmetric distribution of PIP_3 is further reinforced by the actions of two PIP_3 phosphatases, PTEN and SHIP-1, which catalyse the breakdown of PIP_3 into PIP_2 [364]. These proteins are believed to localise towards the rear of the cell and act to keep levels of PIP_3 low, thereby inhibiting frontness behaviour at this cellular location. In leukocytes, SHIP-1 appears to be the dominant phosphatase responsible for controlling PIP_3 levels, as neutrophils genetically deleted for SHIP-1 cannot correctly polarise and have severe migratory defects [365]. Taken together, this demonstrates the critical importance of the asymmetric generation of PIP_3 at the leading edge for directional migration.

3.1.4 Control of actin dynamics at the leading edge

The purpose of generating PIP_3 at the front of the cell is to recruit proteins to the leading edge, via their PIP_3 binding pleckstrin homology (PH) domains, that regulate F-actin polymerisation. Using a construct containing the PH domain from Akt tagged with GFP, multiple studies have shown enrichment of this PH domain

at the leading edge of migrating neutrophils [365, 366]. Indeed Akt is a classical downstream target of PI3K [367] and acts to regulate chemotaxis [368], but many other PH domain containing proteins are also recruited to the cell front during migration (see [355]). Perhaps the most important PH domain containing proteins recruited to the leading edge are the Rac guanine nucleotide exchange factors (GEFs), such as the DOCK and Asef families, PIXα and Tiam1 [369]. Once localised, these activate the small GTPases, Rac and Cdc42, which are crucial for regulating actin dynamics at the leading edge. The importance of these GEFs is highlighted in mice which are deficient for the exchange factor DOCK2, as neutrophils isolated from these animals have impaired Rac1/2 activation and fail to polarise when stimulated with a chemoattractant [370].

Active Rac and Cdc42 localise to the leading edge of migrating cells [371,372], due to the distribution of their GEFs as detailed above, and provide the link between the chemotaxis signalling machinery and F-actin polymerisation. Rac initiates F-actin polymerisation by localising and activating the actin nucleation promoting factors (NPFs) WAVE, Spire and formins, causing the formation of F-actin filaments that result in membrane protrusion [373, 374]. Furthermore Rac, acting in a positive feedback loop, is absolutely required to strengthen and maintain PI3K activation, as inhibition or genetic deletion of Rac ablates PIP_3 accumulation at the leading edge and blocks cell migration in response to chemoattratant stimulation [375, 376].

Cdc42 is crucial for maintaining the stability of the leading edge in migrating leukocytes and is seen as a primary regulator of F-actin polymerisation at the cell front [377]. It is activated by the GEF PIXα and p21-activated kinase 1, which in turn allows Cdc42 to bind and activate the NPF WASP at the leading edge. WASP then recruits and activates the Arp2/3 protein complex that catalyses the formation of branched F-actin structures, resulting in plasma membrane protrusion [355]. Genetic deletion of either Cdc42 or WASP leads to impaired leukocyte migration *in vitro* and *in vivo* [378, 379].

3.1.5 Signalling and actin-myosin dynamics at the rear of the cell

Alongside the events at the front of the cell that allow membrane movement toward the chemoattractant, an orchestrated set of events happen at the rear of the cell to allow translocation of the main cell body. As briefly mentioned above, the $G\alpha_{12/13}$ proteins regulate what has been termed the 'backness' signalling pathway [352]. These regulate the activity of the Rho GEFs, including PDZRhoGEF and p115RhoGEF [369,380], which result in the accumulation of activated RhoA towards the rear of the cell [352,381]. RhoA itself then activates Rho-kinase which in turn activates myosin II by phosphorylating Ser19 on the regulatory light chain [382]. This then results in co-ordinated actin-myosin contraction, generating movement of the rear of the cell towards the front [347]. Furthermore, the front signalling pathway also enforces organisation of the cell rear. Cdc42 helps to promote RhoA activity at the back of the cell, therefore ensuring that the polarity of the cell is maintained and 'frontness' bahaviour is restricted to the leading edge [383]. This acto-myosin contraction at the rear of the cell, together with the forward membrane protrusions and anchoring at the leading edge, allows the cell to move towards a chemoattractant source in a controlled manner.

3.1.6 The role of CB_2 within immune cell chemotaxis

As CB_1 is not expressed on cells of the immune system, it cannot regulate their migration. However, this does not mean that it plays no role in regulating the migration of other cell types. Indeed a body of literature exisis demonstrating that CB_1 helps to orchestrate neuronal migration in the developing brain [384], and that HEK293 cells transfected with human CB_1 will migrate towards cannbinoids in a PTX sensitive manner [385]. However, as CB_2 is predominantly expressed on cells of the immune system, this led to the hypothesis that CB_2 acts as an immunomodulatory receptor. Indeed, CB_2 has been demonstrated to modulate multiple multiple inflammatory diseases and immune cell functions [164,386,387],

including directed migration or chemotaxis [388]. Activation of CB_2 has been demonstrated to elicit leukocyte chemotaxis *in vitro* as the synthetic and highly potent CB_2 agonists JWH015 and JWH133 cause human monocyte migration [389] and the endocannabinoid 2-AG induces the directed migration of B lymphocytes [390], natural killer cells [391], eosinophils [392], the myeloid HL-60 cell line [393], the BV-2 microglial cell line [394, 395] and human monocytes [393]. In all cases SR144528 (a CB_2 inverse agonist) inhibited 2-AG-induced chemotaxis, demonstrating dependence on CB_2 signalling. Activation of CB_2 has also been demonstrated to elicit leukocyte recruitment *in vivo*, as intraperitoneal dosing of the synthetic CB_2 agonist HU210 caused significant cell recruitment into the peritoneal cavity of female B6D2/F1 mice [396]. However, to date, no study has directly examined whether CB_2 agonists can elicit the directed migration of primary macrophages.

Nonetheless, it is becoming increasingly apparent that CB_2 plays a complex role in the modulation of leukocyte chemotaxis, as above studies demonstrating that 2-AG acts as a chemoattractant also detailed that other cannabinoids did not elicit directed migration. Jorda *et al* found that, in contrast to 2-AG, the mixed CB_1/CB_2 agonists WIN,55212-2, CP55,940 and the phytocannabinoid Δ9-THC failed to cause the chemotaxis of a myeloid cell line expressing CB_2 [390, 397]. Furthermore, Kishimoto *et al* also found that WIN55,212-2 and CP55,940 did not elicit the chemotaxis of the myeloid HL-60 cell line [393]. Taken together, this data demonstrates that simple activation of CB_2 may not always cause the directed migration of immune cells. Furthermore, it hints that functional selectivity may impact CB_2-mediated chemotaxis. This phenomenon, also known as biased agonism, is defined as the ability of different ligands at the same receptor to activate distinct downstream signalling pathways [398], and has already been documented for ligands acting at CB_2 [152, 399]. Therefore, a situation may exist where only a subset of CB_2 agonists are able to activate the downstream pathway(s) needed to cause chemotaxis. However as previous chemotaxis studies only use and compare a limited range of CB_2 agonists, and rarely examine the signalling pathways activated, the

extent and importance of functional selectivity within CB_2-mediated chemotaxis remains unknown. Additionally, cell type specific differences in CB_2 expression and downstream coupling/signalling may also impact on the role CB_2 plays within cell migration as a recent report by Tanikawa *et al* found that WIN55,212-2 was able to induce the directed migration of murine splenic lymphocytes [400]. This therefore adds even further complexity to the role that CB_2 plays in regulating immune cell chemotaxis and demonstrates that caution should be used when attempting to extrapolate results from one cell type onto another.

3.1.7 Cannabinoids inhibiting chemotaxis elicited by other chemoattractants

Alongside CB_2 acting as a chemoattractant receptor in its own right, a significant body of literature exists showing that activation of CB_2 negatively regulates chemotaxis induced by other chemoattractants. 2-AG, JWH015 and CP55,940 inhibit human neutrophil migration towards the chemoattractant peptide fMLF [401, 402] and CP55,940, alongside the phytocannabinoid cannabidiol, inhibit fMLF-induced chemotaxis of rat macrophages [403, 404]. Furthermore, CP55,940 and Δ9-THC have been demonstrated to blunt microglial and macrophage chemotaxis towards the HIV secreted tat protein [405, 406]. In all of these studies, the inhibitory effects of CB_2 agonists was blocked by the CB_2 inverse agonist SR144528.

This negative regulation also extends to chemokine-induced chemotaxis. Chemokines are small molecular weight proteins that play a critical role in the trafficking of leukocytes under normal and pathological conditions [91] and therefore pathways that can modifiy their function are of great clinical interest. 2-AG, AEA, JWH015, JWH133, CP55,940 and WIN55,212-2 have all been shown to inhibit human T cell chemotaxis towards CXCL12 [407–409] and Steffens *et al* demonstrated that Δ9-THC treatment of murine macrophages inhibits their chemotaxis towards CCL2 [334]. Corroborating this discovery, Raborn *et al* found that Δ9-THC and CP55,940

both inhibit macrophage migration towards CCL5 [410]. These data are of importance, as they may explain the multiple observations that activation of CB_2 acts to limit atherosclerotic plaque size and macrophage content [334–337, 339, 341], as CC chemokines are essential for monocyte and macrophage recruitment and dynamics during atherogenesis [327, 330, 331].

Nonetheless, as detailed in section 3.1.6, both cell type differences and functional selectivity may impact on the ability of CB_2 agonists to block immune cell chemotaxis towards other chemoattractants. In a recent study, treatment of murine bone marrow derived dendritic cells with the CB_2 agonist GP1a for 24 or 48 hours had no effect on CCL19-induced chemotaxis [411]. Furthermore, two studies exist demonstrating that Δ9-THC is unable to inhibit human neutrophil chemotaxis towards fMLF [402, 412]. Not only is this in contrast to the previously mentioned findings that fMLF-induced chemotaxis can be blocked by CB_2 activation, it also conflicts with the finding that Δ9-THC can inhibit chemotaxis induced by other chemoattractants. However, as almost all of these studies vary by at least one variable (cell type used, CB_2 agonist used, chemoattractant used) it is difficult to determine whether cell type differences, functional selectivity or another factor is responsible for these documented disparities. Finally, a study by Lunn *et al* found that a CB_2 inverse agonist was able to block CC chemokine-induced cell migration *in vivo* [396]. They developed their own novel CB_2 inverse agonist named Sch.336, and found that oral administration of the compound blocked CCL2-induced immune cell recruitment to the peritoneal cavity in female B6D2F/1 mice. This is the only study demonstrating that inhibition of CB_2 blocks immune cell chemotaxis towards CC chemokines and adds even further complexity to the role of CB_2 in the regulation of cell migration.

3.2 Rationale for the experiments presented in this chapter

As macrophages play a core role within the induction and continuation of an inflammatory response, and are central to many chronic inflammatory diseases [7,413], understanding the mechanisms that regulate macrophage migration are of great clinical interest. However to date, no study has examined whether CB_2 acts as a chemoattractant receptor in macrophages and, as detailed above, it is unwise to extrapolate results obtained from other leukocyte populations onto macrophages.

Furthermore, it has been proposed that activation of CB_2 inhibits macrophage chemotaxis towards CC chemokines, explaining the beneficial role of CB_2 within atherosclerosis. However the exact role regulatory role that CB_2 plays in modulating macrophage chemotaxis towards CC chemokines and other chemoattractants remains understudied. Finally, as all previous reports only use a limited range of CB_2 agonists to explore how CB_2 impacts immune cell migration, comparisons between their results is not possible and the extent and importance of functional selectivity within CB_2-mediated chemotaxis remains unknown.

Therefore, the experimental aims of this chapter are to:

- Use a wide panel of commercially available and chemically diverse CB_2 agonists to elucidate whether CB_2 is a chemoattractant receptor in primary murine macrophages
- Determine whether functional selectivity at CB_2 plays any role in this process
- Discover whether activation of CB_2 inhibits CC chemokine-induced macrophage chemotaxis

3.3 Results

Before the results of my thesis begin, it is important to note that some of the data presented in chapters 3 and 4 have been published in an article entitled: 'Primary Macrophage Chemotaxis Induced by Cannabinoid Receptor 2 Agonists Occurs Independently of the CB_2 Receptor' in the journal Scientific Reports, of which I am the first author [414]. This work is covered by a Creative Commons Attribution 4.0 International License, which permits its reproduction in this thesis. I wish to state that I am the person responsible for the creation of any material, be it text or figure, reproduced throughout this thesis.

3.3.1 The CB_2 selective agonists JWH133 and HU308 are chemoattractants for bio-gel elicited PECs

To date, all studies that have examined whether the endocannabinoid system regulates chemotaxis have used single time point chemotaxis assays, the mainstay being the modified Boyden chamber [415]. As a chemotaxis methodology the modified Boyden chamber has a number of limitations, chief among these being the ability to only measure migration at a single time point. To overcome this issue, I employed a novel chemotaxis technology that allows cellular migration to be followed in real-time. This is achieved by measuring electrical impedance across a gold electrode that covers the underside of a Boyden chamber-style filter. This impedance is converted into a parameter known as Cell Index (CI; see section 2.5 for details), with increasing CI equating to higher numbers of migrated cells [343].

Real-time chemotaxis analysis found that the widely used, potent and selective CB_2 agonists JWH133 and HU308 (10 μM) acted as chemoattractants for murine bio-gel elicited PECs, with both cannabinoids eliciting approximately a 2.5 fold increase in CI versus vehicle alone and reaching peak CI after approximately 1.5 hours (Fig 3.1A). Compared to the chemokine CCL5 (5 nM), both JWH133 and

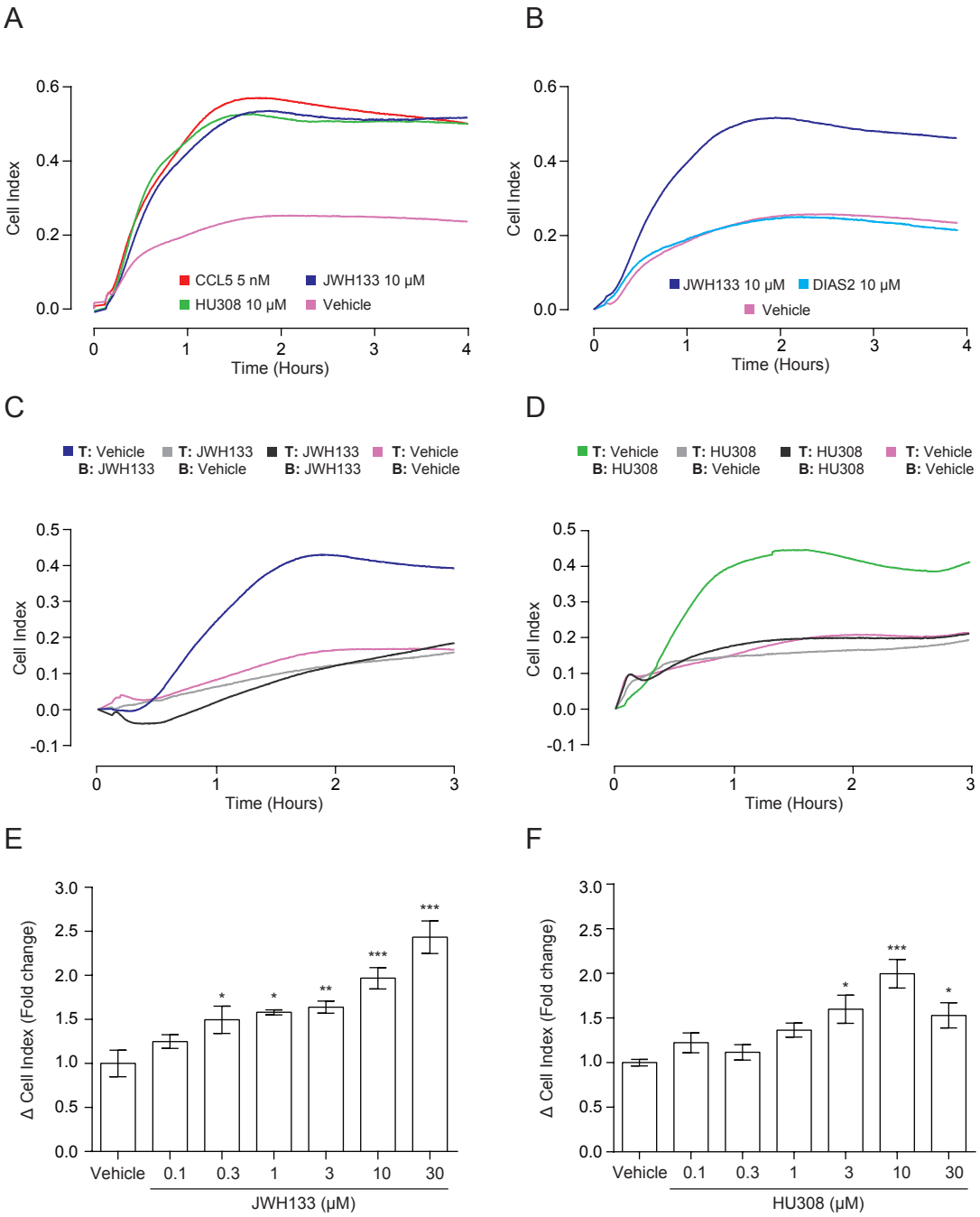

Figure 3.1 The CB_2 selective agonists JWH133, HU308 and DIAS2 differ in their ability to induce the directed migration of murine PECs. (A-F) Bio-gel elicited murine PECs (4 x 10^5) were placed into the upper chamber of a CIM-16 plate and allowed to migrate to the compound indicated for 3-4 hours at 37°C, 5% CO_2. Real-time chemotaxis analysis found that JWH133 and HU308 (A), but not DIAS2 (B) (all 10 μM), elicit PEC chemotaxis. Chemokinetic analysis, comparing all combinations of vehicle or cannabinoid (10 μM) in the top (T) and bottom (B) chambers, demonstrated that (C) JWH133 and (D) HU308 both induced true chemotaxis. Data are mean real-time traces from one experiment with 4 technical replicates per condition, and are representative of 2 independent biological replicates. (E and F) Concentration response analysis found that both JWH133 and HU308 elicit PEC chemotaxis in a concentration-dependent manner. Data are mean± SEM, n = 4 biological replicates with 3-4 technical replicates per condition. Statistical analysis was conducted by one-way ANOVA with Dunnett's multiple comparisons correction. * P <0.05, ** P <0.01 *** P <0.001, comparing all samples to vehicle control.

HU308 displayed similar chemotaxis kinetics and maximal responses, albeit with reduced potency (Fig 3.1A). Interestingly however, in comparison to JWH133 and HU308, DIAS2 (a selective and potent CB_2 agonist developed in our lab [229]) was unable to elicit murine PEC chemotaxis (Fig 3.1B).

Further analysis of both ligands demonstrated that JWH133 and HU308 did not induce fugetaxis (migration away from a soluble ligand - top chamber: 10 μM cannabinoid, bottom chamber: vehicle) or chemokinesis (non-directional migration stimulated by a soluble ligand - 10 μM cannabinoid in top and bottom chamber), as migration kinetics under these conditions closely mimicked vehicle alone (Fig 3.1C and D, respectively). Moreover, JWH133 and HU308 induced chemotaxis in a concentration-dependent manner (Fig 3.1E and F, respectively). Taken together, these experiments demonstrate that JWH133 and HU308 are true chemoattractants for primary murine PECs, whereas our novel CB_2 agonist, DIAS2, is not.

3.3.2 Macrophages are the dominant population in bio-gel elicited PECs that are being measured in real-time chemotaxis

We initially selected bio-gel as our eliciting agent as the literature suggests that this method allows recovery of large cell numbers with 50-60% macrophage purity [416]. However, when analysing the cell composition of bio-gel elicited PECs by flow cytometry, I consistently found that macrophages (defined as $F4/80^+$, $7/4^-$) only comprised around 20% of the cellular composition of bio-gel elicited PECs (Fig 3.2A). The predominant population was $F4/80^-$ and $7/4^+$ (Fig 3.2A; approximately 50% of all cells), which comprised mostly of neutrophils (Fig 3.2B; defined as $Ly6G^+$, $7/4^+$). Interestingly, when I used a second independent batch of bio-gel for cell elicitation, I found that this had no effect on the composition of the bio-gel PECs, with macrophages and neutrophils still comprising around 20% and 40% respectively of the cells present (Fig 3.2C and D).

I next decided to examine whether the facility where the animals were housed

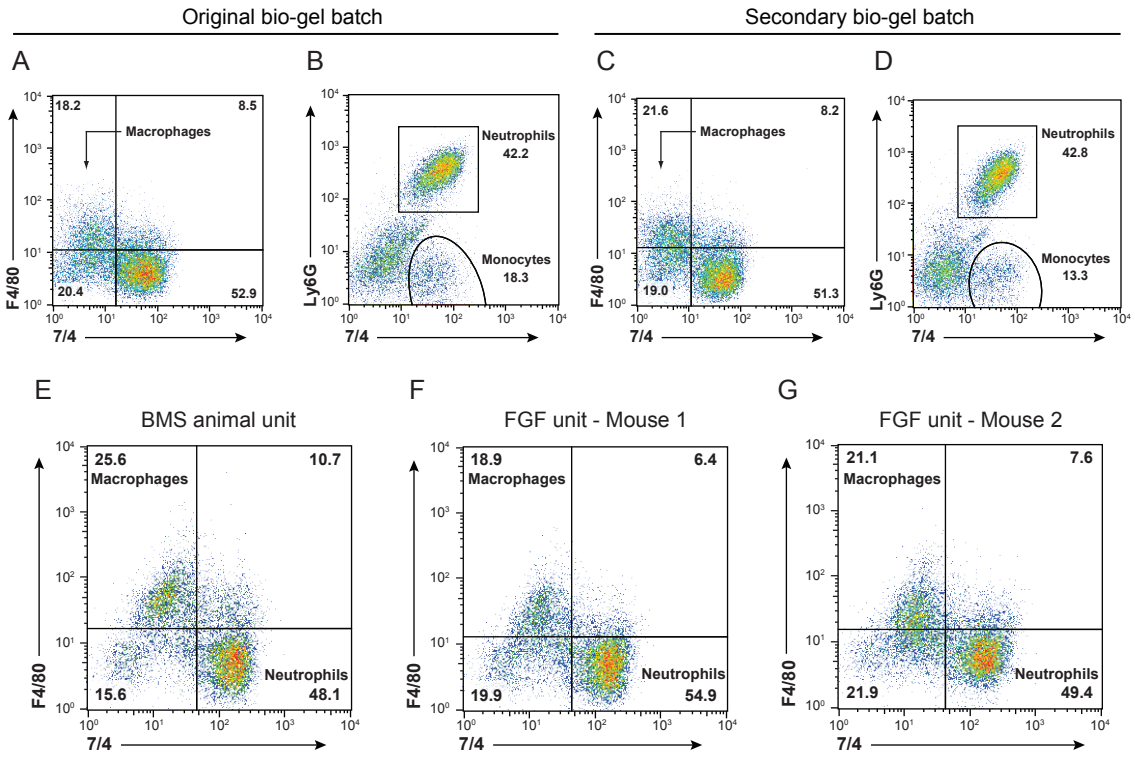

Figure 3.2 The bio-gel batch or the animal housing facility used have no effect on the cellular composition of bio-gel elicited murine PECs. Flow cytometry analysis of the macrophage (defined as F4/80$^+$, 7/4$^-$ cells), monocyte (Ly6G$^-$, 7/4$^+$) and neutrophil (F4/80$^-$, 7/4$^+$ or Ly6G$^+$, 7/4$^+$) content of PECs from male C57BL/6J mice injected with (A and B) our original bio-gel batch or (C and D) a different secondary bio-gel batch. Flow cytometry analysis of the macrophage and neutrophil content of PECs from a male C57BL/6J mouse (E) housed in the BMS animal facility (where all of our animal colonies are housed) or male C57BL/6J mice (F and G) housed in the FGF animal unit. Data are representative flow cytometry plots from independent animals.

had an effect on the composition of bio-gel elicited PECs, as it has been shown that C57BL/6J animals housed in different facilities can have significant differences in the composition of their gut microbiota and that the specific composition of the gut flora can impact on the inflammatory response [417]. Analysis of the composition of bio-gel elicited PECs from a mouse housed in our animal unit (BMS unit: Fig 3.2E) and two animals housed in a second independent unit (FGF unit: Fig 3.2F and G) found that in all cases, neutrophils formed the predominant cell population. Macrophage content was very similar between all animals, with these cells comprising around 20% of bio-gel elicited PECs. Therefore, this data demonstrates that bio-gel elicitation yields mostly neutrophils and not macrophages as previously thought, and that this neutrophil population occurs regardless of what facility the animals are housed in or which batch of bio-gel beads is used for peritoneal cell elicitation.

In light of this result, I next wanted to examine which cells present in bio-gel elicited PECs were contributing to the CI signal in the real-time chemotaxis assay. I began by enriching macrophages from bio-gel elicited PECs using an overnight adherence selection process. Bio-gel elicited PECs before selection contained mostly neutrophils (Fig 3.3A), but after selection contained no neutrophils (<1%) and were strongly enriched for macrophages (Fig 3.3B; ∼80%). Real-time chemotaxis analysis of macrophages enriched from bio-gel PECs demonstrated that both JWH133 and HU308 (10 μM) robustly induced their directed migration, with a large CI signal observed (Fig 3.3C). CCL5 (5 nM) was used as a positive control (Fig 3.3C). To further probe the ability of macrophages to migrate towards JWH133 and HU308, I next used intraperitoneal injection of thioglycollate to elicit a large macrophage population (∼70%) with minimal neutrophils (Fig 3.3D). Real-time chemotaxis analysis found that JWH133 and HU308 significantly induced thioglycollate elicited macrophage chemotaxis (Fig 3.3E and F).

Initial attempts at isolating bio-gel elicited neutrophils proved difficult, so instead I used murine bone marrow neutrophils to examine neutrophil migration in the real-time chemotaxis assay. My isolation protocol resulted in a highly pure population

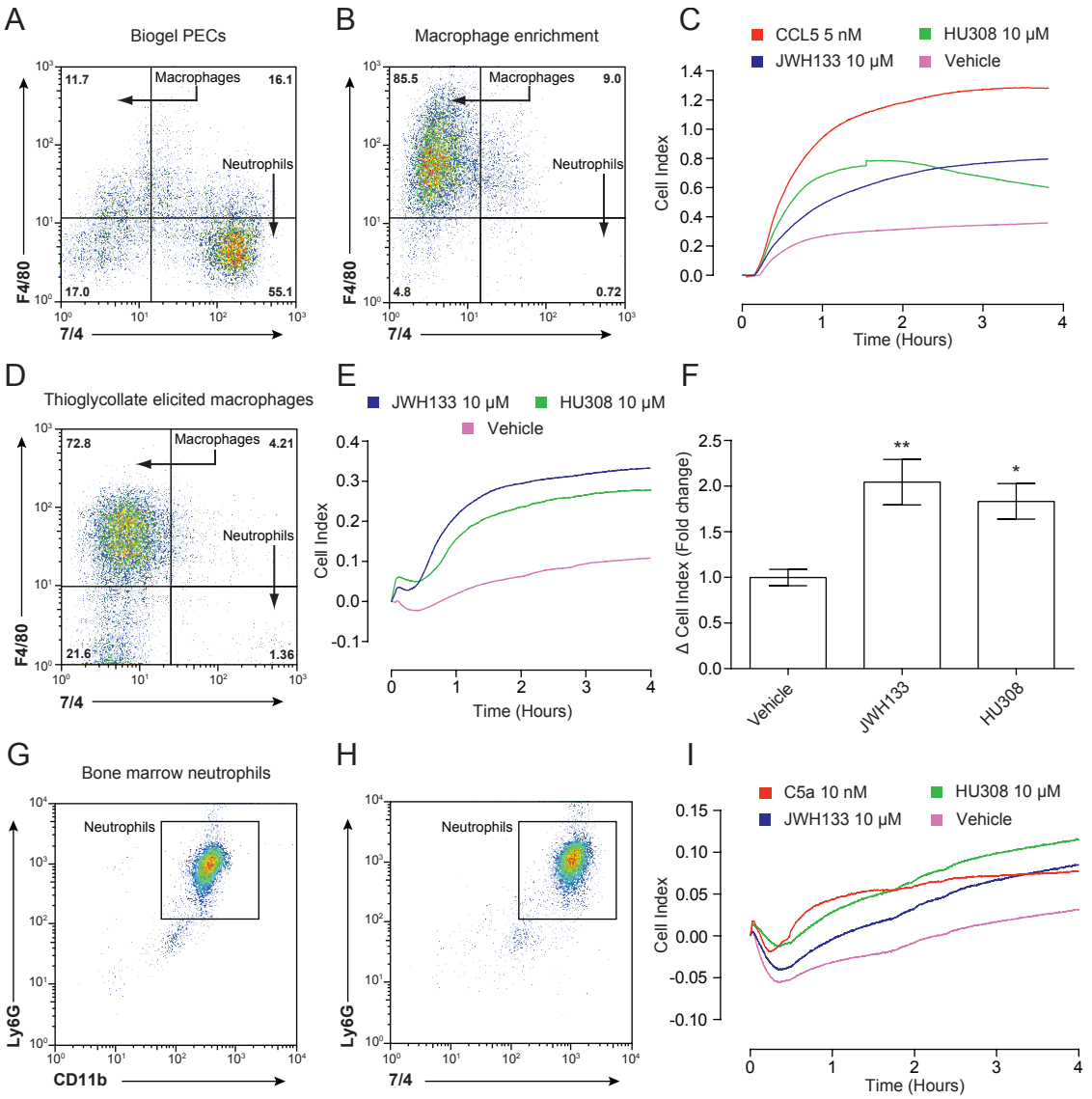

Figure 3.3 Macrophages are the dominant cell population in bio-gel elicited PECs that migrate toward CB_2 agonists. (A) Flow cytometry analysis demonstrated that neutrophils are the major cell population within bio-gel elicited PECs, whereas macrophages and monocytes form only a minor population. (B) Macrophages were enriched from bio-gel elicited PECs using overnight adherence. Flow cytometry analysis demonstrated that this process strongly enriched macrophages and removed neutrophils. (C) Enriched macrophages (2 x 10^5) were placed into the upper chamber of a CIM-16 plate and allowed to migrate for 4 hours at 37°C, 5% CO_2 toward vehicle (0.3% DMSO), 5 nM chemokine or 10 μM cannabinoid. Data show mean trace of 3-4 technical replicates per condition. (D) Flow cytometry analysis demonstrated that macrophages are the main cell population elicited by intraperitoneal injection of 4% thioglycollate. (E and F) Thioglycollate elicited macrophages (2 x 10^5) were placed into the upper chamber of a CIM-16 plate and allowed to migrate for 4 hours at 37°C, 5% CO_2 toward vehicle (0.3% DMSO) or 10 μM cannabinoid. (E) Representative chemotaxis trace of thioglycollate elicited macrophage migration towards JWH133, HU308 or vehicle. Data show mean trace of 3-4 technical replicates per condition. (F) Quantification demonstrated that JWH133 and HU308 significantly induced thioglycollate elicited macrophage chemotaxis. Data are mean± SEM, n = 4-6 biological replicates with 3-4 technical replicates per condition. (G and H) Neutrophils were isolated from murine bone marrow and (I) were placed into the upper chamber of a CIM-16 plate (2 x 10^5 cells/well) and allowed to migrate for 4 hours at 37°C, 5% CO_2 toward vehicle (0.3% DMSO), 10 nM C5a or 10 μM cannabinoid. Data show mean trace of 3-4 technical replicates per condition. Statistical analysis was conducted by one-way ANOVA with Dunnett's multiple comparisons correction. * P <0.05, ** P <0.01, comparing all samples to vehicle control.

of neutrophils (Fig 3.3G and H; >95%), however when these cells were used in the real-time chemotaxis system, the CI signal seen with JWH133, HU308 or the anaphylatoxin C5a, a well known neutrophil chemoattractant, did not exceed 0.1 (Fig 3.3I). Therefore, I believe that neutrophils do not score highly in the real-time chemotaxis system, and are unlikely to contribute to the observed CI signal when using bio-gel PECs. It is important to note that this does not mean neutrophils do not migrate towards the cannabinoids, it simply means that these cells are not measured by the real-time system and can therefore be discounted as a population that contributes to the CI observed. Instead, I believe that these data demonstrate that macrophages can migrate towards JWH133 and HU308 and these are the predominant population in bio-gel elicited PECs that are being measured in real-time chemotaxis analysis.

3.3.3 Only a subset of CB_2 agonists act as chemoattractants for murine macrophages

In order to examine the generality of CB_2 agonist-induced chemotaxis, I expanded my list of ligands to include a range of widely used and commercially available compounds active at CB_2, and their structures can be seen in figure 1.3. Based on results obtained with JWH133 and HU308, I selected 10 μM as the initial screening concentration, as this caused robust and reproducible macrophage chemotaxis. As shown in figure 3.4, CB_2 agonists fall into two distinct classes, with the majority (9/14 ligands tested) unable to induce chemotaxis. Nonetheless, alongside JWH133 and HU308, which significantly induced chemotaxis by 2 and 2.3 fold respectively, I discovered that L-759,633, L-759,656 and SER601 also acted as macrophage chemoattractants (Fig 3.4A). As shown in the representative traces, L-759,656, SER601 (10 and 1 μM) and L-759,633 (10 μM) gave robust increases in CI versus cells migrating towards vehicle alone (Fig 3.4B, C and D). Whereas SER601 mirrored the chemotactic response of JWH133 and HU308, L-759,633 and L-759,656 differed kinetically eliciting a slower chemotactic response, with peak CI reached between 2-2.5 hours, and were

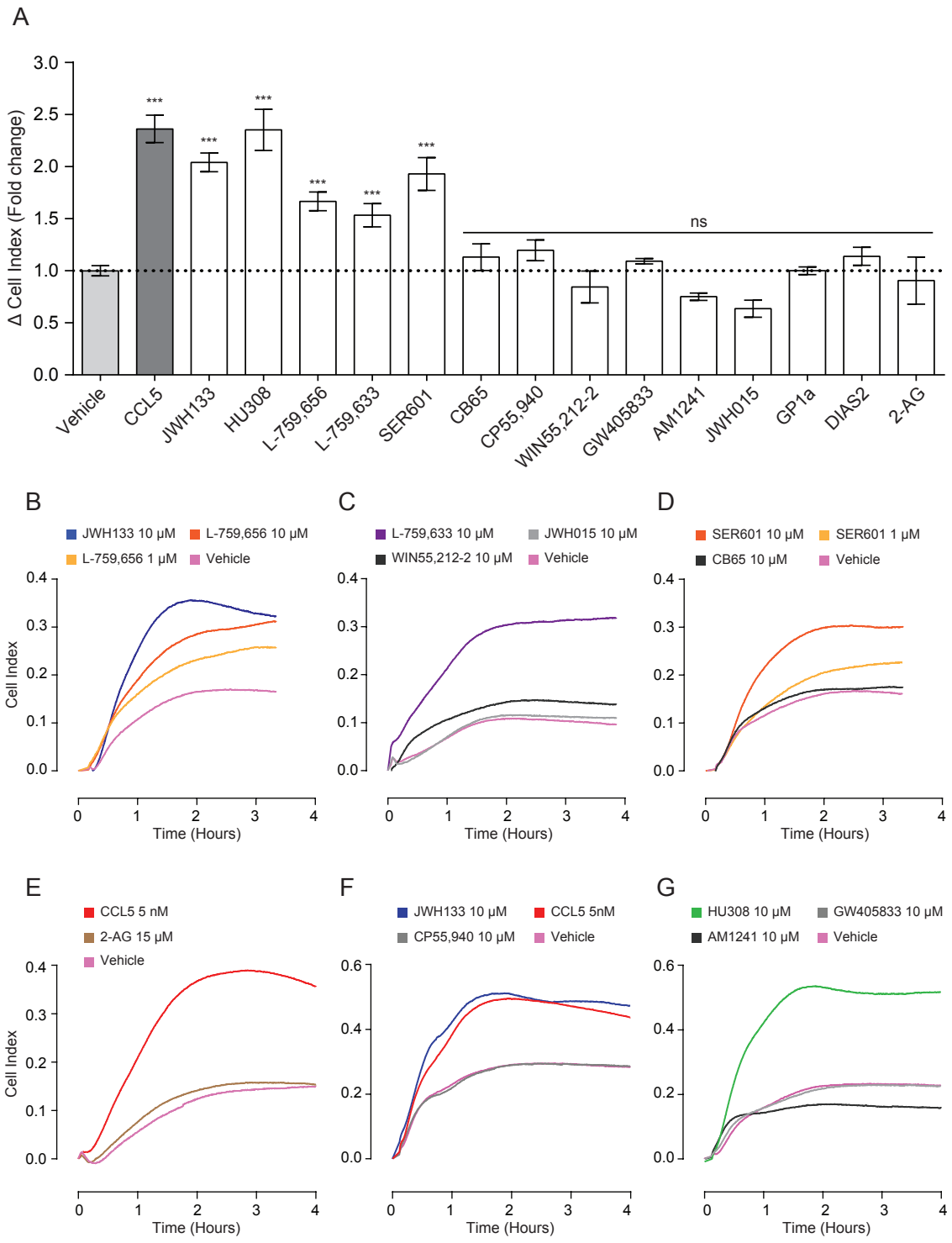

Figure 3.4 Only a subset of CB_2 agonists are macrophage chemoattractants. (A-G) Bio-gel elicited murine PECs (4 x 10^5) were placed into the upper chamber of a CIM-16 plate and allowed to migrate towards vehicle (0.3% DMSO), 5 nM CCL5 or cannabinoid (all 10 or 1 μM, except 2-AG which was used at 15 μM) for 3-4 hours at 37°C, 5% CO_2. (A) Only CCL5, JWH133, HU308, L-759,633, L-759,656 and SER601 acted as macrophage chemoattractants. Data are mean± SEM, n = 3-26 biological replicates with 3-4 technical replicates per condition. (B-G) Representative traces of chemotaxis positive and chemotaxis negative CB_2 agonists. Data show mean trace of 3-4 technical replicates per condition. Statistical analysis was conducted by one-way ANOVA with Dunnett's multiple comparisons correction. ns P >0.05, *** P <0.001, comparing all samples to vehicle control.

slightly less efficacious, inducing chemotaxis 1.7 fold versus vehicle (Fig 3.4A). The aminoalkylindoles, (WIN55,212-2, JWH015, AM1241 and GW405833; Fig 3.4C and G), the non-classical cannabinoid CP55,940 (Fig 3.4F), the tricyclic pyrazole GP1a (Fig 3.4A), the quinolone-3-carboxamide CB65 (Fig 3.4D), the endocannabinoid 2-AG (Fig 3.4E) and our novel CB_2 agonist DIAS2 were all found to be negative for chemotaxis (Fig 3.4A).

To corroborate these findings, I employed another impedance based assay that monitors cytoskeletal rearrangements which occur downstream of receptor activation in real-time [418–420], thereby providing an independent, but complementary, functional readout to chemotaxis. The representative traces shown in figures 3.5A and B demonstrate the kinetics and concentration dependence of JWH133 and HU308-elicited macrophage cell spreading. Concentration response analysis determined EC_{50} values of 5.3 and 1.6 μM for JWH133 and HU308, respectively (Fig 3.5C) and found that L-759,656 and SER601 also induced concentration-dependent macrophage cytoskeletal rearrangement with EC_{50} values of 7.3 and 2.4 μM respectively (Fig 3.5D). The chemotaxis negative CB_2 ligands DIAS2 (Fig 3.5C), CB65 (Fig 3.5D), GP1a, GW405833 (Fig 3.5E), AM1241 and CP55,940 (Fig 3.5F) were unable to induce macrophage spreading at any concentration.

In summary, using real-time analysis I have shown that only a subset of CB_2 agonists act as primary murine macrophage chemoattractants and that only chemotaxis positive compounds are capable of inducing changes in macrophage morphology.

3.3.4 PI3K signalling is essential for CB_2 agonist-induced macrophage chemotaxis

As PI3K is critical for chemotaxis [421], I wanted to examine whether CB_2 agonist-induced macrophage chemotaxis relied on the PI3K signalling pathway. Both JWH133 and HU308 (10 μM) caused a significant increase in the levels of phosphorylated Akt, a surrogate marker for PI3K activity, in bio-gel enriched macrophages (Fig 3.6A and

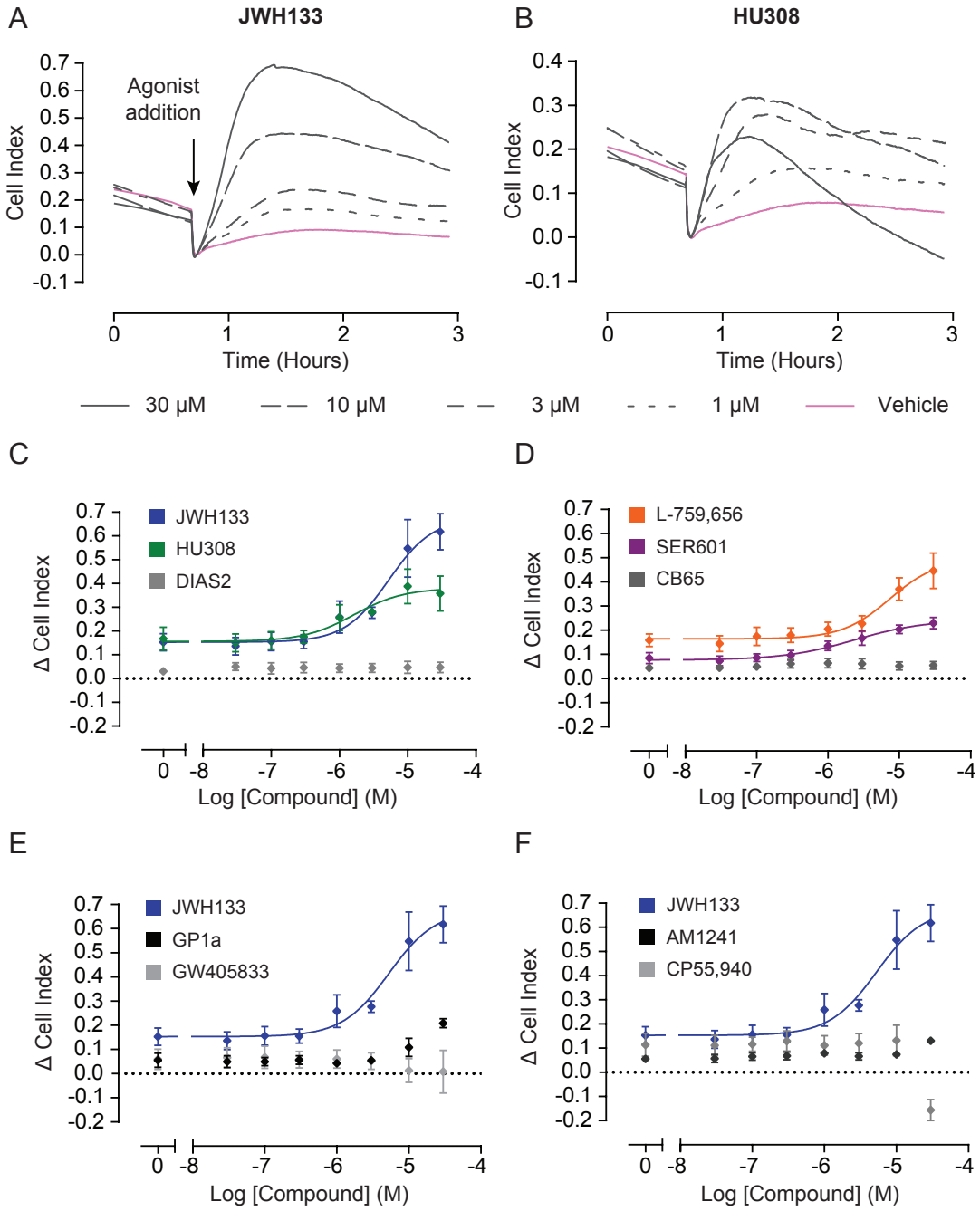

Figure 3.5 Chemotaxis positive CB_2 agonists induce concentration-dependent cytoskeletal rearrangements in primary murine macrophages. (A-F) Bio-gel elicited PECs (5 x 10^4) were placed into a 96 well E-plate allowed to adhere for 2-3 hours at 37°C, 5% CO_2. Afterwards, cells were stimulated with either vehicle (0.3% DMSO) or cannabinoid at the indicated concentration. Representative raw traces showing cell responses to (A) JWH133 and (B) HU308 (30, 10, 3 and 1 μM). Data are mean traces from one experiment with 2-3 technical replicates per condition. Concentration response quantification demonstrated that (C) JWH133, HU308, (D) L-759,656 and SER601 caused macrophage cytoskeletal rearrangement in a concentration-dependent manner, with EC_{50} values of 5.3, 1.6, 7.3 and 2.4 μM respectively. In contrast, (C) DIAS2, (D) CB65, (E) GP1a, GW405833, (F) AM1241 and CP55,940 failed to elicit a response at any concentration (JWH133 curve is shown for comparison). Data are mean± SEM, n = 3 biological replicates with 2-3 technical replicates per condition. A 4-parameter non-linear regression model was fitted to each data set using GraphPad Prism.

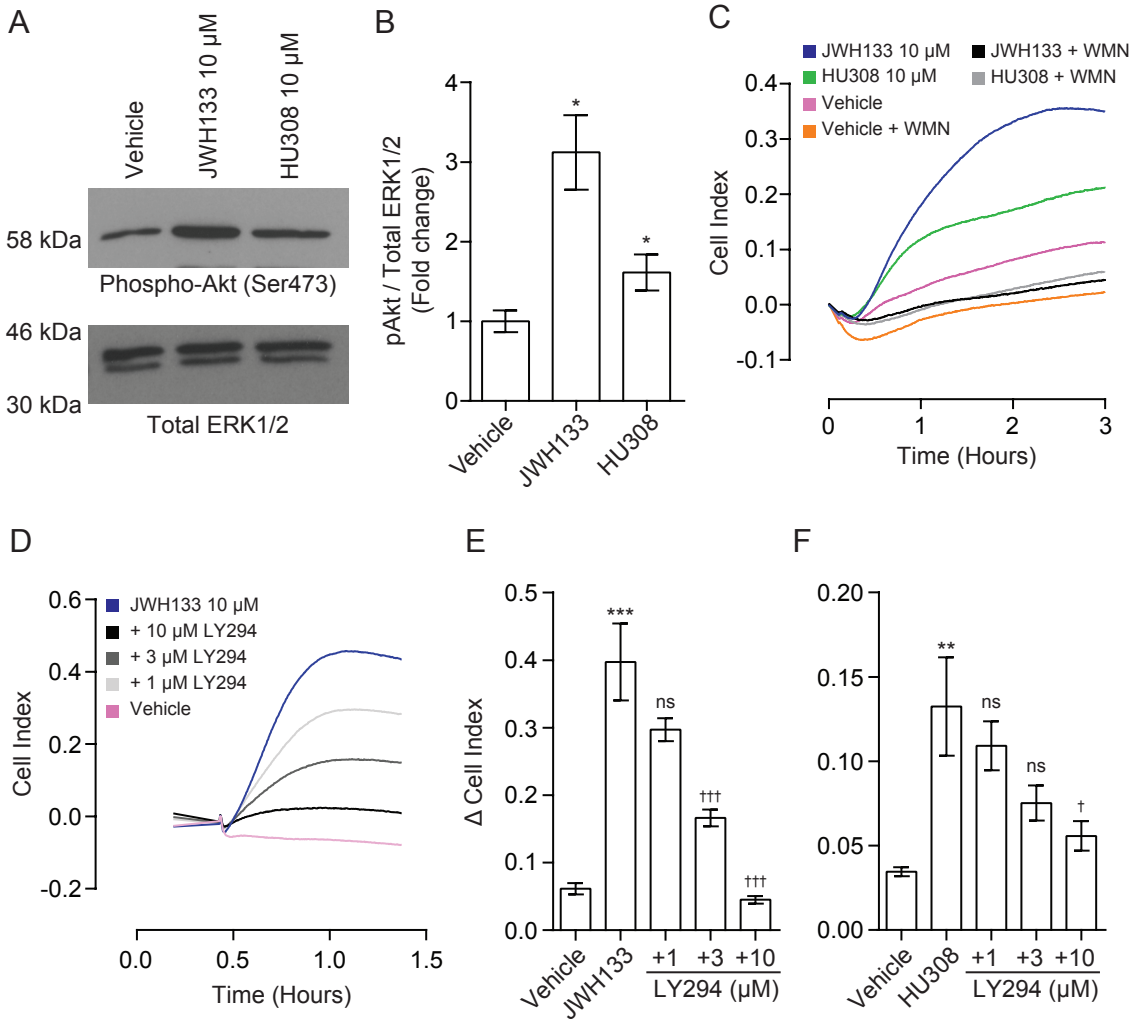

Figure 3.6 PI3K signalling is essential for JWH133 and HU308-induced murine macrophage chemotaxis. Bio-gel elicited enriched macrophages were stimulated with either vehicle (0.3% DMSO), JWH133 or HU308 (both 10 μM) for 30 min at 37°C, 5% CO_2. (A) Relative levels of phosphorylated Akt and total ERK1/2 were determined by western blotting. (B) Densitometric analysis of JWH133 and HU308-induced Akt phosphorylation (Normalised to total ERK1/2 levels). Data are mean± SEM, n = 5 biological replicates. (C) Bio-gel elicited PECs were treated with either vehicle (1% DMSO) or 200 nM wortmannin (WMN) for 1 hour at 37°C, 5% CO_2 prior to being placed into the upper chamber of a CIM-16 plate. Cells were then allowed to migrate towards vehicle (0.3% DMSO), JWH133 or HU308 (both 10 μM) for 3-4 hours at 37°C, 5% CO_2. Data are mean of one independent experiment and are representative of n = 3 biological replicates. (D-F) Bio-gel elicited PECs were placed into a 96 well E-plate allowed to adhere for 2-3 hours at 37°C, 5% CO_2. Afterwards, cells were treated with either vehicle or LY294002 at the indicated concentration prior to stimulation with vehicle (0.3% DMSO), JWH133 or HU308 (both 10 μM). (D) Representative trace showing the effect of LY294002 on JWH133-induced cytoskeletal rearrangements. Quantification demonstrated that LY294002 inhibited (E) JWH133 and (F) HU308-induced cell spreading in a concentration-dependent manner. Data are mean± SEM, n = 3 biological replicates with 3-4 technical replicates per condition. Statistical analysis was conducted by one-way ANOVA with Dunnett's multiple comparisons correction. * P <0.05, ** P <0.01, *** P <0.001, comparing all samples to their vehicle control. ns P >0.05, † P <0.05, ††† P <0.001, compared to cannabinoid alone.

B). Additionally, when bio-gel elicited PECs were treated with 200 nM wortmannin (a broad spectrum, irreversible PI3K inhibitor) their migration towards JWH133 or HU308 was fully inhibited (Fig 3.6C). Furthermore LY294002, another PI3K inhibitor, blocked both JWH133 (Fig 3.6D and E) and HU308 (Fig 3.6F) induced macrophage cytoskeletal rearrangement in a concentration-dependent manner. Taken together, these data demonstrate that CB_2 agonist-induced macrophage cytoskeletal rearrangement and chemotaxis absolutely relies on PI3K signalling.

3.3.5 Screening for activity of the CB_2 ligand panel reveals functional selectivity at CB_2

As it has been previously reported that ligands active at CB_2 display functional selectivity, defined as the ability of different ligands at the same receptor to each activate distinctive downstream signalling pathways [398], I wanted to examine whether this phenomenon explained why only a subset of CB_2 agonists were able to act as macrophage chemoattractants. To begin, I tested the ability of the CB_2 ligands to reduce the levels of intracellular cAMP in CHO cells expressing human CB_2; the hallmark of $G_{i/o}$-coupled GPCR activation. JWH133, HU308, L-759,633, L-759,656, JWH015, AM1241 and DIAS2 all acted as full CB_2 agonists, causing concentration-dependent reductions in forskolin-induced intracellular cAMP levels (Fig 3.7A, B and C). The non-selective, CB_1/CB_2 agonists CP55,940 and WIN55,212-2 also acted as full agonists, eliciting concentration-dependent inhibition of cAMP production (Fig 3.7B). GW405833, previously reported as a partial CB_2 agonist, had no effect on intracellular cAMP levels at any concentration tested (Fig 3.7C). Interestingly, the supposed CB_2 agonists GP1a, CB65 and SER601 acted as inverse agonists in this assay system, with CB65 being almost as efficacious as the CB_2 inverse agonist SR144528 (Fig 3.7D).

Next I examined the ability of the CB_2 ligands to cause β-arrestin recruitment specifically to CB_2 using CHO cells expressing murine CB_2. CP55,940 was the only

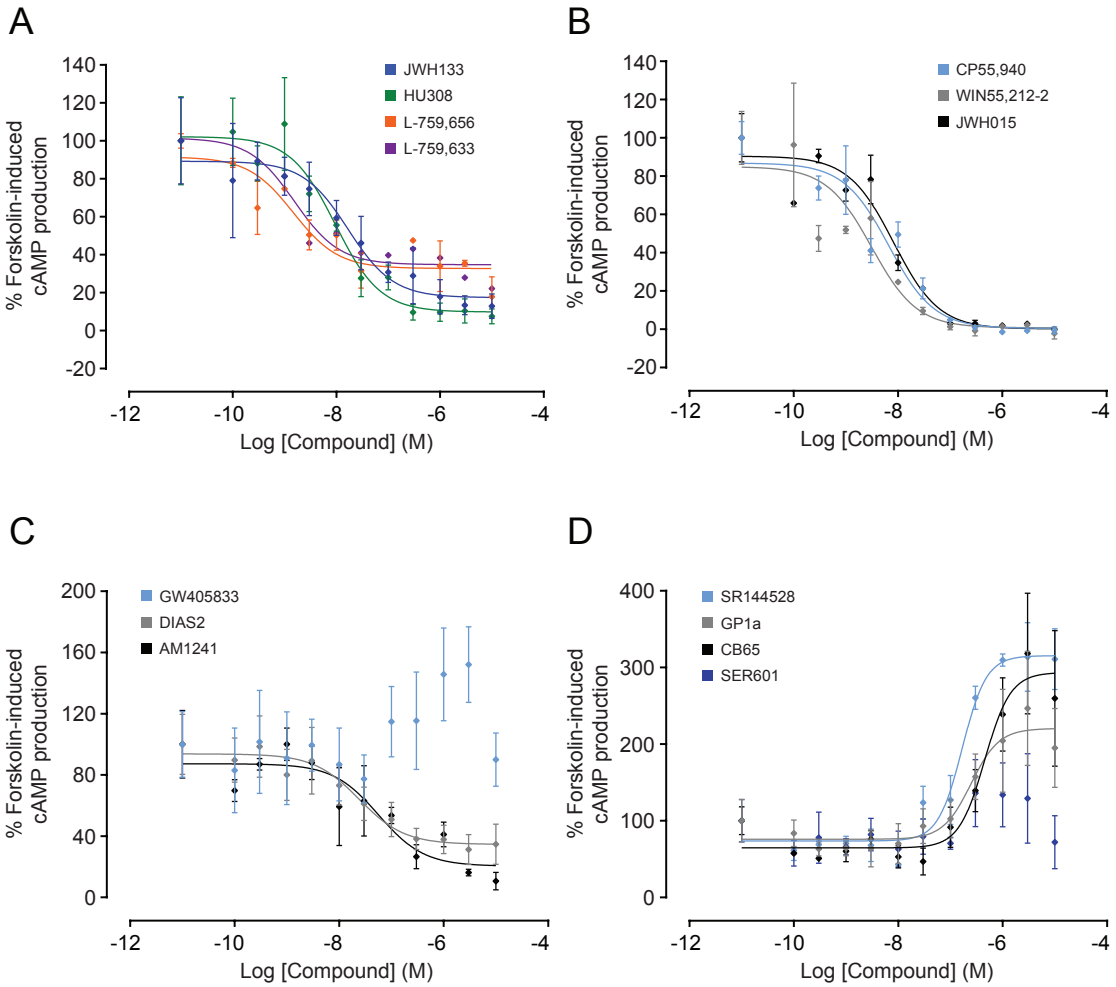

Figure 3.7 Measurement of intracellular cAMP levels demonstrates activity of the cannabinoid ligands at CB_2. Intracellular cAMP levels were measured using Discoverx cAMP Hunter™ eXpress kits. CHO-K1 cells expressing human CB_2 were stimulated with either vehicle (1.2% DMSO with 20 μM forskolin) or cannabinoid at the indicted concentration for 30 min at 37°C, 5% CO_2. Concentration response analysis demonstrated that (A) JWH133, HU308, L-759,633 and L-759,656 all acted as CB_2 agonists with IC_{50} values of 17, 10, 1.5 and 1.5 nM respectively. Furthermore, (B) CP55,940, WIN55,212-2, JWH015, (C) DIAS2 and AM1241 also acted as full CB_2 agonists with IC_{50} values of 7, 3, 8, 24 and 57 nM respectively, whereas GW405833 had no effect on cAMP levels. (D) SR144528, GP1a and CB65 all acted as CB_2 inverse agonists, causing an increase in intracellular cAMP production with EC_{50} values of 180, 260 and 530 nM respectively. SER601 acted as a partial inverse agonist with an EC_{50} value of 100 nM. Data are mean± SEM, n = 2 independent experiments with 2-3 technical replicates per concentration. A 3-parameter non-linear regression model was fitted to each data set using GraphPad Prism.

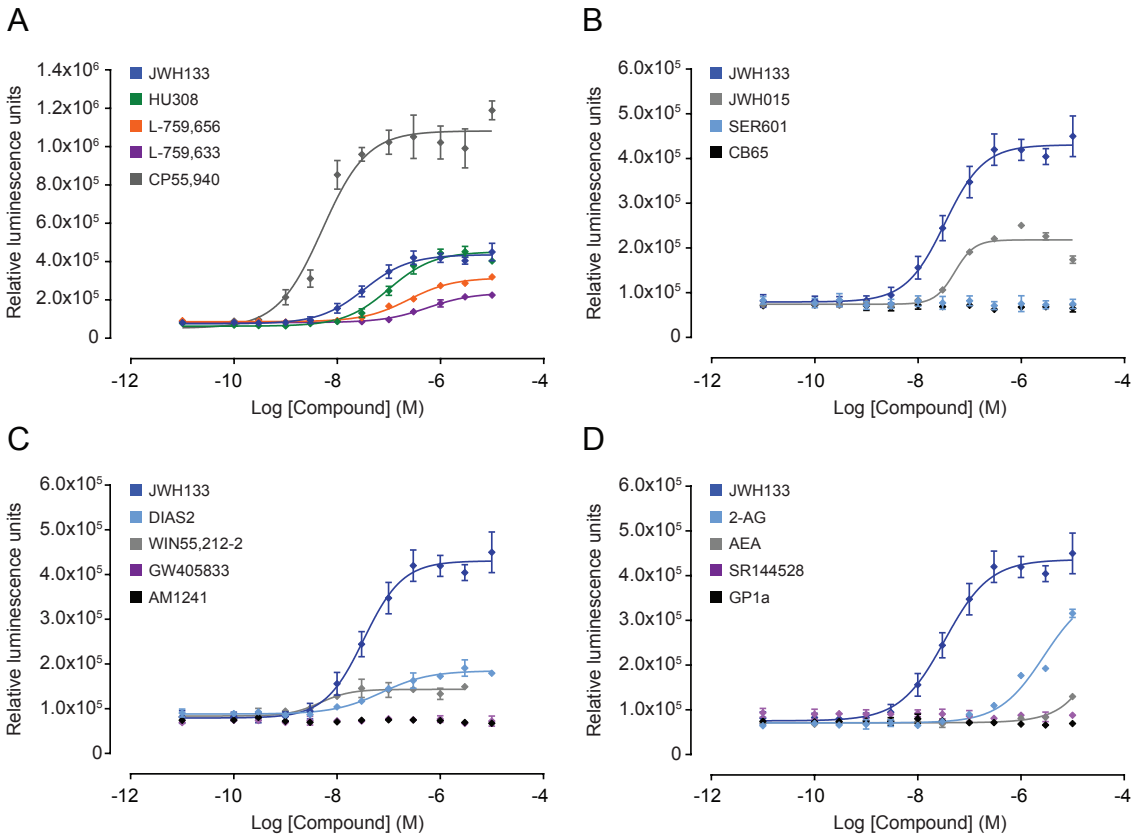

Figure 3.8 CB_2 ligands display marked variation in their ability to recruit β-arrestin to CB_2. β-arrestin recruitment to CB_2 was measured using Discoverx PathHunter™ eXpress β-arrestin assay kits. CHO-K1 cells expressing murine CB_2 were stimulated with either vehicle (1% DMSO) or cannabinoid at the indicated concentration for 30 min at 37°C, 5% CO_2. (A) CP55,940 acted as a full agonist for β-arrestin recruitment to CB_2, with an EC_{50} of 5 nM, whereas JWH133, HU308, L-759,656 and L-759,633, (B) JWH-015, (C) DIAS2, WIN55,212-2 and (D) 2-AG all acted as partial agonists, with EC_{50} values of 33, 100, 240, 560, 51, 74, 4.7 and 2800 nM respectively. (B) SER601, CB65, (C) AM1241, GW405833, (D) AEA, GP1a and SR144528 all had no effect on β-arrestin recruitment to CB_2. Data are mean± SEM, n = 2 independent experiments with 2-3 technical replicates per concentration. A 3-parameter non-linear regression model was fitted to each data set using GraphPad Prism.

ligand to act as a full agonist, eliciting marked concentration-dependent β-arrestin recruitment (Fig 3.8A). JWH133, HU308, L-759,633, L-759,656 (Fig 3.8A), JWH015 (Fig 3.8B), WIN55,212-2, DIAS2 (Fig 3.8C) and 2-AG (Fig 3.8D) all acted as partial agonists with varying degrees of efficacy. SER601, CB65 (Fig 3.8B), AM1241, GW405833 (Fig 3.8C), GP1a, AEA, and SR144528 (Fig 3.8D) all had no effect on β-arrestin recruitment to CB_2. This therefore demonstrates that there is functional selectivity amongst this agonist population, however no obvious grouping containing only the chemotaxis positive compounds emerged from this functional screening.

3.3.6 CB_2 selective agonists induce primary macrophage chemotaxis independently of CB_2

To examine the reliance of CB_2 agonist-induced migration on $G\alpha_{i/o}$ protein activation, bio-gel elicited PECs were incubated with 200 ng/ml PTX for 90 min prior to real-time chemotaxis analysis. Following PTX treatment, migration towards JWH133, HU308, L-759,656 and SER601 (all 10 μM) was significantly inhibited (Fig 3.9A), demonstrating that macrophage chemotaxis towards CB_2 agonists absolutely requires $G\alpha_{i/o}$ activation. Chemerin (5 nM), a chemoattractant protein that acts via the GPCR ChemR23 [422], was used as a PTX control (Fig 3.9A). I next used SR144528 to pharmacologically probe chemotaxis reliance on CB_2 signalling. Surprisingly, pre-treatment with 1 μM SR144428 had no effect on macrophage chemotaxis towards JWH133 and HU308 (Fig 3.9B). However, SR144528 did cause a significant 30% increase in PEC migration toward 5 nM CCL5 (Fig 3.9B). To rule out inactivity at CB_2, I tested the ability of SR144528 to antagonise JWH133 and HU308-induced CB_2 activation by measuring cAMP levels in CHO cells expressing CB_2. JWH133 and HU308 acted as agonists at all concentrations, whereas SR144528 alone (1 μM) acted as an inverse agonist, significantly increasing forskolin-induced cAMP levels (Fig 3.9C and D). Pre-incubation with SR144528 for 30 min prior to agonist addition significantly reversed JWH133 and HU308-induced CB_2 activation at 10, 3 and 1 μM (Fig 3.9C and D).

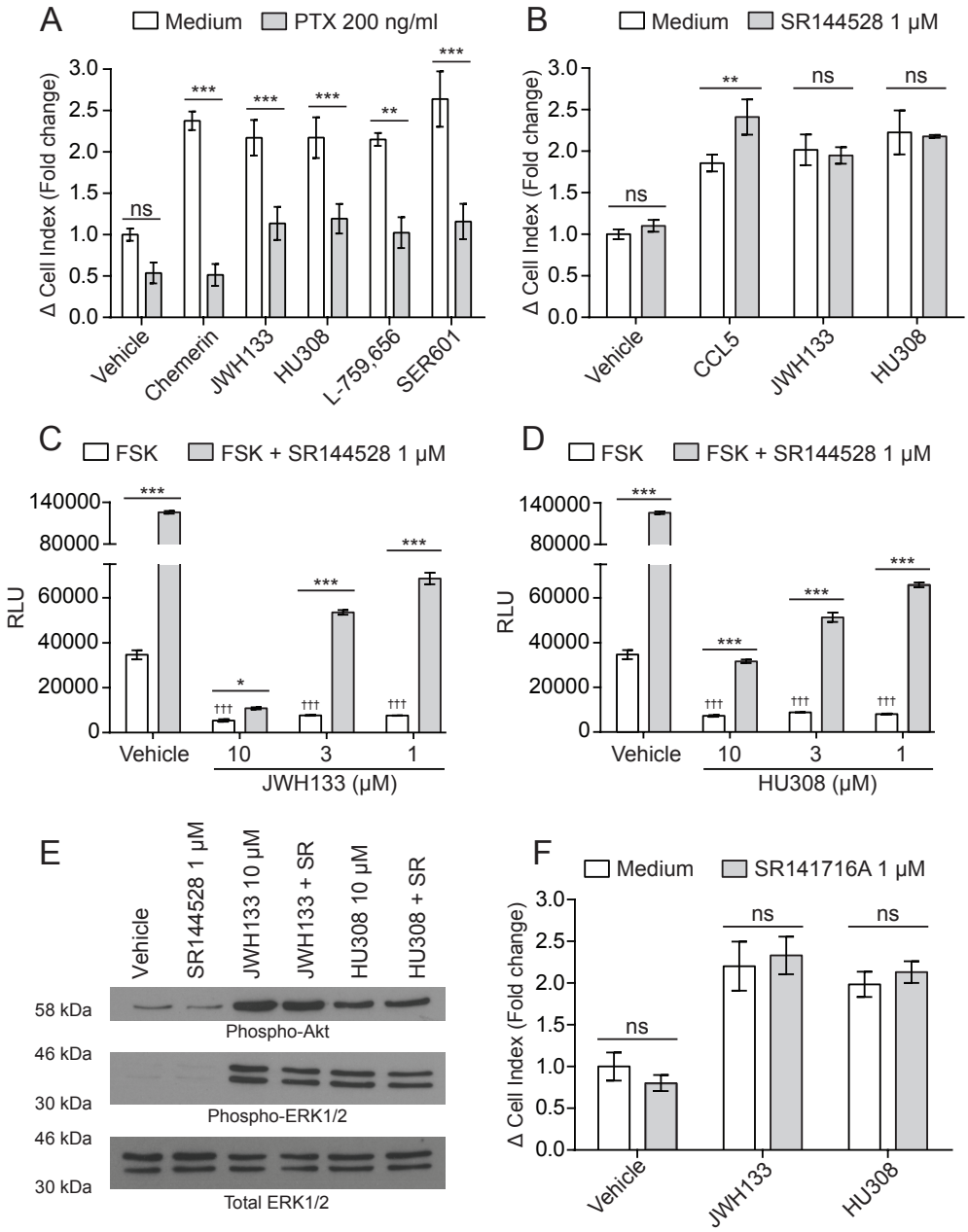

Figure 3.9 Macrophage chemotaxis towards CB_2 selective agonists is blocked by pertussis toxin, but not by CB_2 or CB_1 inverse agonists. Bio-gel elicited PECs were incubated with either vehicle, (A) 200 ng/ml pertussis toxin (PTX) for 90 min or (B) 1 μM SR144528 for 30 min at 37°C, 5% CO_2. Following treatment, cells were allowed to migrate for 3-4 hours at 37°C, 5% CO_2 toward vehicle, chemerin, CCL5 (5 nM) or 10 μM cannabinoid. Data are mean± SEM, n = 3-11 biological replicates with 3-4 technical replicates per condition. (C and D) CHO-K1 cells expressing human CB_2 were incubated for 30 min at 3°C, 5% CO_2 with either vehicle or SR144528 (1 μM). Following treatment, vehicle, JWH133 (C) or HU308 (D) was added in assay buffer containing forskolin (FSK - 20 μM) and cells incubated for 30 min at 37°C, 5% CO_2 before the addition of the detection reagents. Data are mean± SEM, n = 6. (E) Bio-gel elicited enriched macrophages were stimulated with either vehicle, or 10 μM cannabinoid ± 1 μM SR144528. Relative levels of phosphorylated Akt, ERK1/2 and total ERK1/2 were determined by western blotting. Blot is representative of n = 3 independent biological replicates. (F) Bio-gel elicited murine PECs were incubated with either vehicle or 1 μM SR141716A for 30 min at 37°C, 5% CO_2. Following treatment, cells were allowed to migrate for 3-4 hours at 37°C, 5% CO_2 toward vehicle or 10 μM cannabinoid. Data are mean± SEM, n = 4 biological replicates with 3-4 technical replicates per condition. For all data, statistical analysis was conducted by two-way ANOVA with Sidak's multiple comparisons correction. ns P >0.05, * P <0.05, ** P <0.01, *** P <0.001, for indicated comparisons. † † † P <0.001, compared to vehicle + FSK alone.

To further study the ability of SR144528 to antagonise JWH133 and HU308-induced signalling I examined Akt and ERK1/2 phosphorylation in bio-gel elicited enriched macrophages, as CB_2 agonism has been previously reported to activate these kinase pathways [149]. JWH133 and HU308 (10 μM) both caused substantial Akt and ERK1/2 phosphorylation in comparison to vehicle alone. However, SR144528 (1 μM) pre-treatment had no effect on the activation of either pathway (Fig 3.9E). SR144528 alone gave no increase in the levels of phospho-Akt or ERK1/2 and total ERK1/2 levels confirmed equal protein loading across all samples (Fig 3.9E). Although bio-gel elicited macrophages do not express CB_1 mRNA, I wanted to confirm that CB_1 was not responsible for CB_2 agonist-induced macrophage chemotaxis, as some of these ligands can activate CB_1 at high concentrations [131, 423]. Pre-treatment with 1 μM SR141716A (a CB_1 receptor inverse agonist [230]) for 30 min prior to real-time chemotaxis analysis had no effect on JWH133 or HU308-induced macrophage chemotaxis and SR141716A alone did not affect migration (Fig 3.9F).

To conclusively establish whether CB_2 agonist-induced macrophage chemotaxis occurs independently of CB_2, real-time chemotaxis analysis was conducted using bio-gel elicited PECs isolated from CB_2 null mice (B6.129P2-Cnr2^{tm1Dgen}/J mice from Jackson laboratories). Remarkably, 10 μM JWH133, HU308, L-759,656 and SER601 significantly induced $CB_2^{-/-}$ macrophage chemotaxis (Fig 3.10A and B). As demonstrated by the real-time traces in figure 3.10A, JWH133 and HU308 retained similar kinetic chemotaxis profiles compared to WT cells. Pre-treatment of $CB_2^{-/-}$ PECs with PTX significantly inhibited macrophage chemotaxis towards both JWH133 and HU308 (Fig 3.10C).

Following this result, I wanted to examine whether JWH133 and HU308 could still activate intracellular signalling in the absence of CB_2. Stimulation of bio-gel elicited enriched $CB_2^{-/-}$ macrophages with 10 μM JWH133 or HU308 resulted in a significant increase in the levels of phosphorylated ERK1/2 (Fig 3.10D). Chemotaxis positive CB_2 agonists retained their ability to induce cytoskeletal rearrangements in $CB_2^{-/-}$ macrophages, whereas chemotaxis negative agonists had no effect, replicating

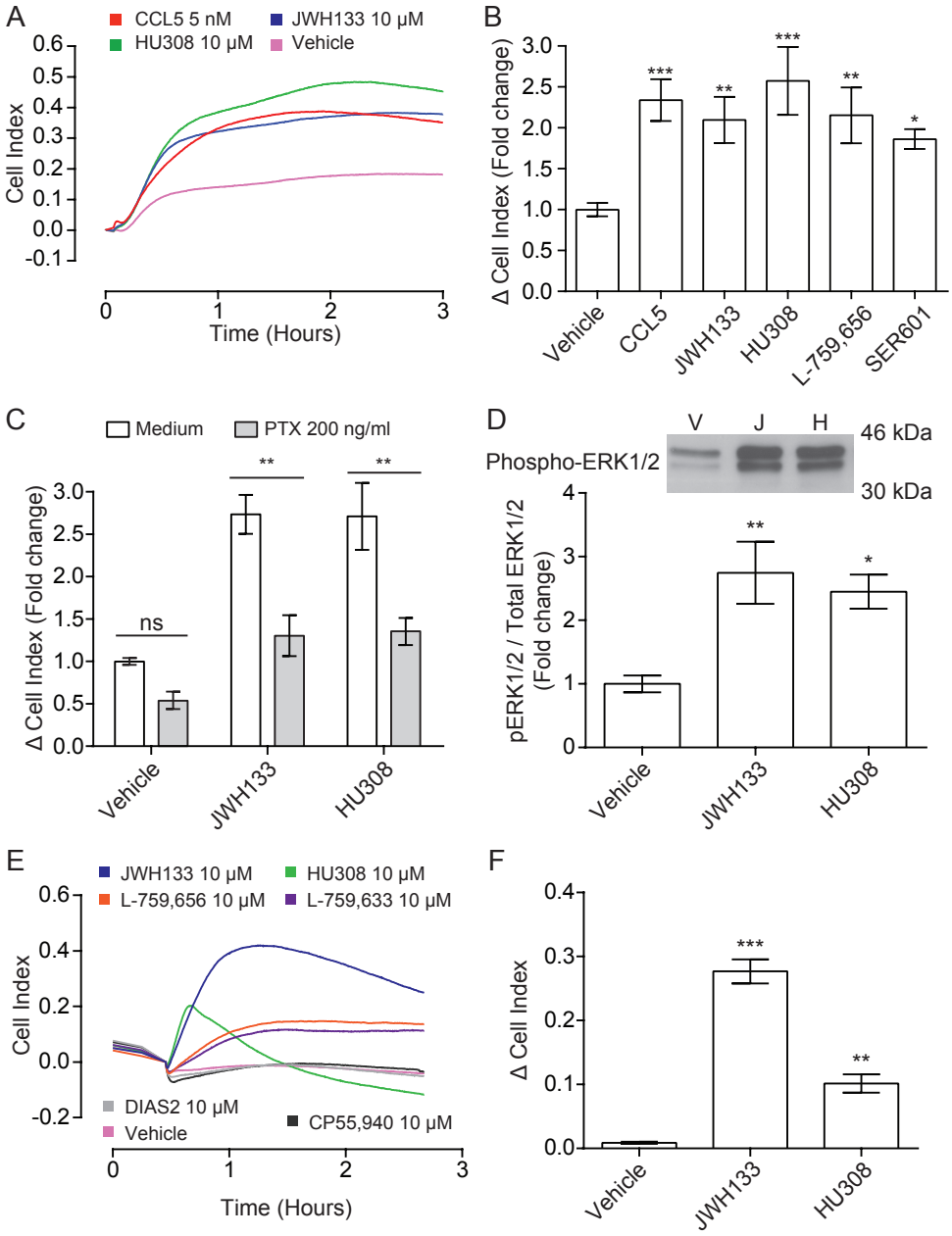

Figure 3.10 JWH133, HU308 and L-759,656 are chemoattractants for $CB_2^{-/-}$ primary macrophages. $CB_2^{-/-}$ bio-gel elicited PECs were allowed to migrate for 3-4 hours towards vehicle (0.3% DMSO), 5 nM CCL5 or 10 μM cannabinoid. (A) Representative real-time chemotaxis trace. (B) Quantification demonstrated that CCL5, JWH133, HU308 and L-759,656 significantly induced $CB_2^{-/-}$ macrophage chemotaxis. Data are mean± SEM, n = 5-15 biological replicates with 3-4 technical replicates per condition. (C) Treatment of $CB_2^{-/-}$ bio-gel elicited PECs with PTX (200 ng/ml for 90 min) significantly reduced JWH133 and HU308-induced macrophage chemotaxis (both 10 μM). Data are mean± SEM, n = 3 biological replicates with 2-3 technical replicates per condition. (D) Bio-gel elicited enriched $CB_2^{-/-}$ macrophages were stimulated with either vehicle (0.3% DMSO) or 10 μM cannabinoid. Western blotting and densitometric analysis confirmed that JWH133 and HU308 significantly elicited ERK1/2 phosphorylation. Data are mean± SEM, n = 6 biological replicates. (E and F) Bio-gel elicited $CB_2^{-/-}$ PECs were placed into a 96 well E-plate and allowed to adhere for 2 hours before being stimulated with either vehicle (0.3% DMSO) or cannabinoid (10 μM). (E) Representative real-time trace. (F) Quantification demonstrated that JWH133 and HU308 significantly elicited cell spreading in $CB_2^{-/-}$ macrophages. Data are mean± SEM, n = 4-5 biological replicates with 3-4 technical replicates per condition. Statistical analysis was conducted by one-way ANOVA with Dunnett's multiple comparisons correction (B, D and F) or by two-way ANOVA with Sidak's multiple comparisons correction (C). * P <0.05, ** P <0.01, *** P <0.001, comparing all samples to vehicle control.

the WT results (Fig 3.10E). Quantification of JWH133 and HU308 activity at 10 μM is shown in figure 3.10F. Taken together, these results demonstrate that JWH133 and HU308 activate at least one $G_{i/o}$-coupled GPCR, which is not CB_1 or CB_2, to elicit macrophage cytoskeletal rearrangement and directed migration.

3.3.7 JWH133 and HU308 enhance chemokine-induced macrophage chemotaxis in a CB_2 independent manner

Previous work has shown that activation of CB_2 inhibits chemokine-induced chemotaxis [334, 410]. Therefore, in light of the finding that JWH133 and HU308 are macrophage chemoattractants, I set out to discover whether they affect chemokine-induced macrophage chemotaxis. Interestingly, the presence of 10 μM JWH133 alongside 5 nM CCL2 (Fig 3.11A) or CCL5 (Fig 3.11B) in the lower chamber of the chemotaxis plate (gold line) resulted in a marked increase in peak CI compared to either CCL2, CCL5 (red line) or JWH133 (blue line) alone. Quantification of chemotaxis affirmed that whilst CCL2, CCL5 and JWH133 alone significantly induced macrophage migration, the combination of chemokine and JWH133 elicited a macrophage chemotactic response significantly larger than either chemokine or cannabinoid alone (Fig 3.11C and D). HU308 (10 μM) also caused a similar enhancement, when added alongside CCL5 (5 nM) (Gold line - Fig 3.11E and F).

I next assessed CB_2 dependency by conducting the same combinatorial chemotaxis experiments using bio-gel elicited PECs isolated from $CB_2^{-/-}$ mice. Genetic deletion of CB_2 had no effect on the ability of JWH133 to enhance chemokine-induced macrophage chemotaxis, as when added alongside CCL2 (Fig 3.12A) or CCL5 (Fig 3.12B) the peak CI reached by $CB_2^{-/-}$ macrophages was significantly greater than that reached when exposed to chemokine or JWH133 alone (Fig 3.12C and D). Furthermore, HU308 (10 μM) also enhanced 5 nM CCL2 (Fig 3.12E) and 5 nM CCL5 (Fig 3.12F)-induced $CB_2^{-/-}$ macrophage chemotaxis, resulting in a substantial increase in peak CI compared to chemokine or HU308 alone.

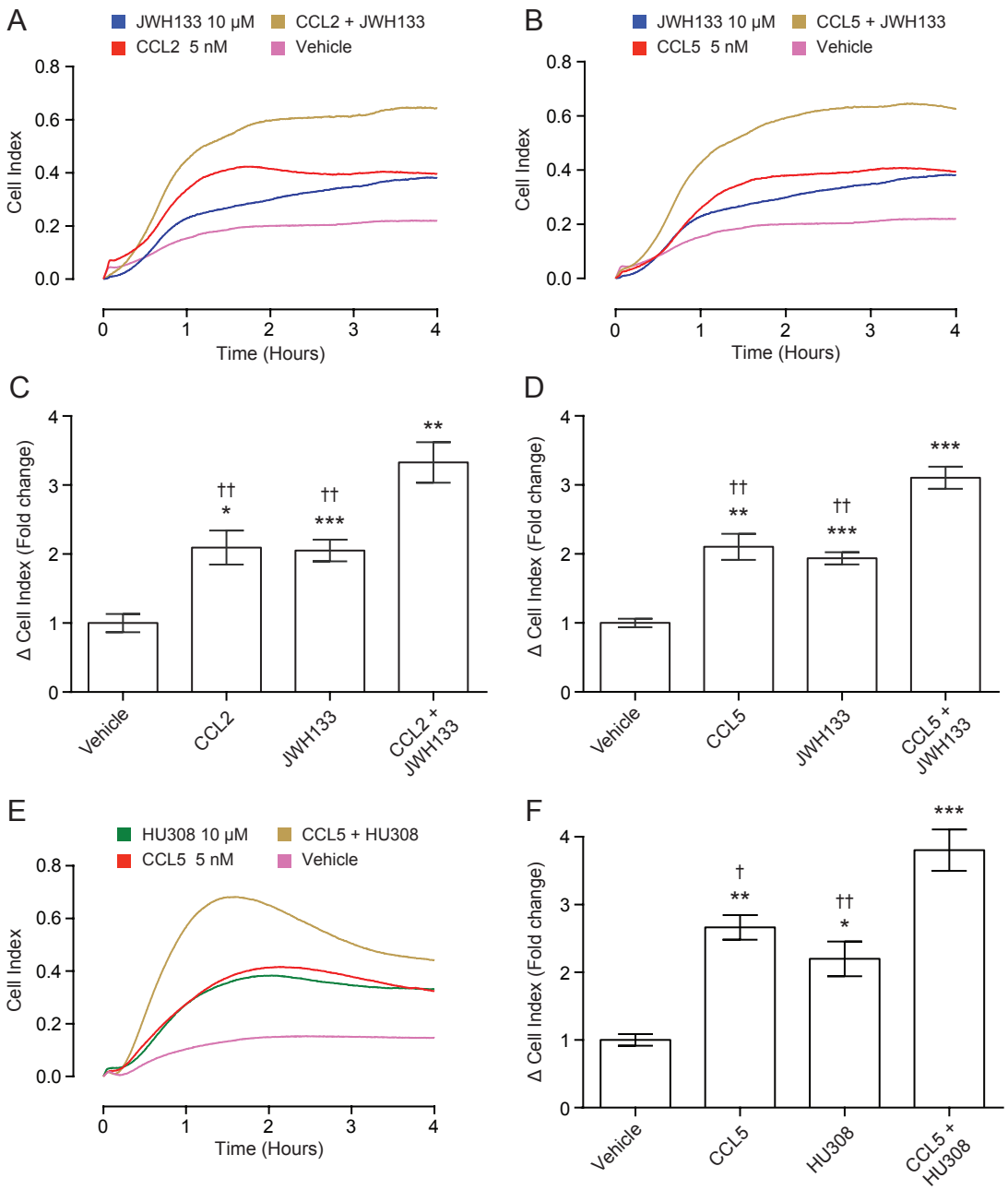

Figure 3.11 JWH133 and HU308 enhance chemokine-induced murine macrophage chemotaxis. Bio-gel elicited murine PECs (4 x 10^5) were placed into the upper chamber of a CIM-16 plate and allowed to migrate for 4 hours at 37°C, 5% CO_2 towards vehicle (0.3% DMSO), chemokine alone, cannabinoid alone or chemokine plus cannabinoid. JWH133 (10 μM) significantly enhanced (A and C) 5 nM CCL2 and (B and D) 5 nM CCL5-induced macrophage chemotaxis. (E and F) HU308 (10 μM) also significantly enhanced 5 nM CCL5-induced macrophage chemotaxis. Data are mean± SEM, (C and D) n = 4, (F) n = 3 biological replicates with 3-4 technical replicates per condition. Statistical analysis was conducted by one-way ANOVA with Dunnett's multiple comparisons correction. * P <0.05, ** P <0.01, *** P <0.001, comparing all samples to vehicle control. † P <0.05, †† P <0.01, comparing all samples to chemokine plus cannabinoid.

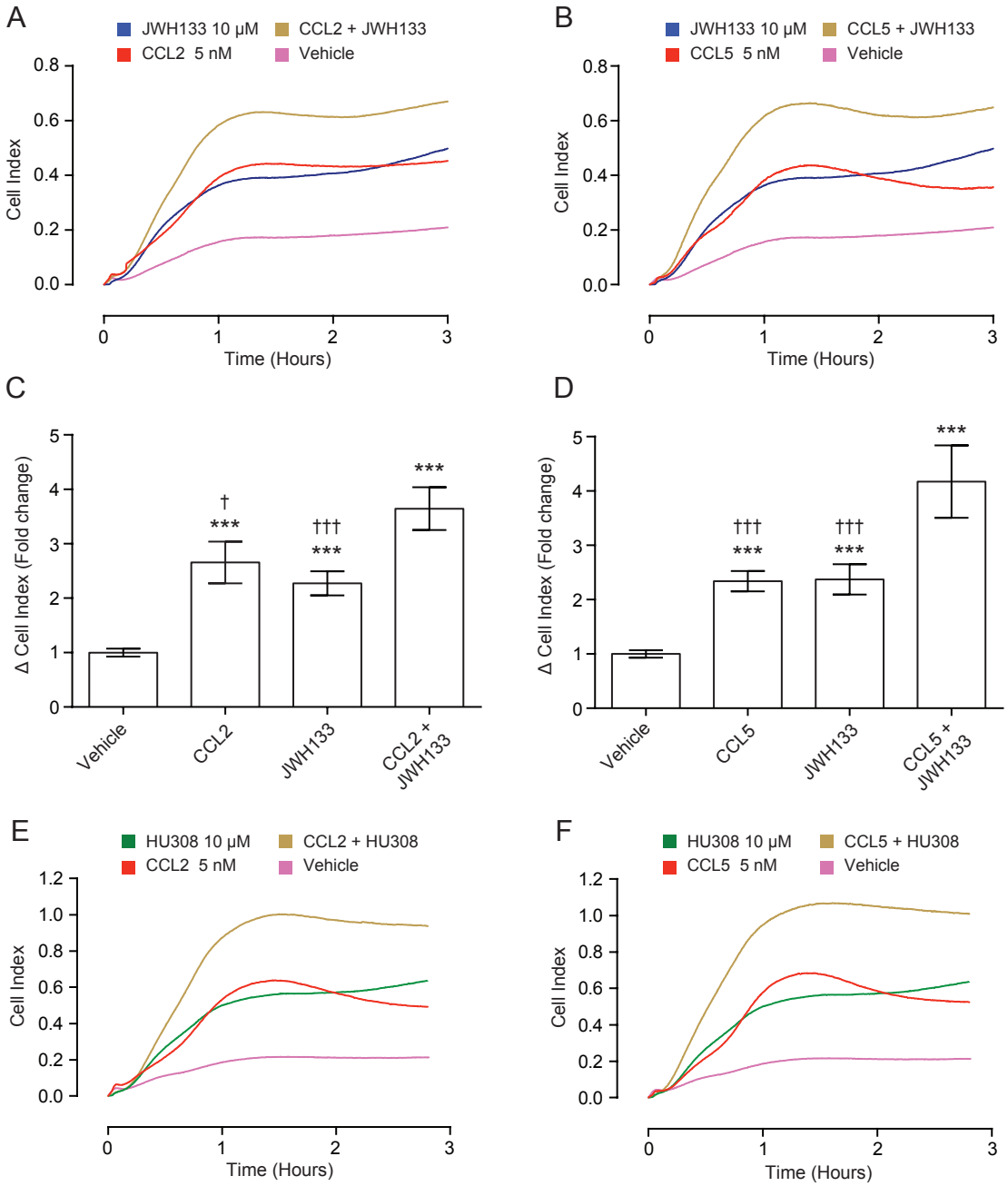

Figure 3.12 JWH133 and HU308 enhance chemokine-induced chemotaxis of $CB_2^{-/-}$ macrophages Biogel-elicited murine PECs from $CB_2^{-/-}$ mice (4 x 10^5) were placed into the upper chamber of a CIM-16 plate and allowed to migrate for 3 hours at 37°C, 5% CO_2 towards vehicle (0.3% DMSO), chemokine alone, cannabinoid alone or chemokine plus cannabinoid. JWH133 (10 μM) significantly enhanced (A and C) 5 nM CCL2 and (B and D) 5 nM CCL5-induced $CB_2^{-/-}$ macrophage chemotaxis. Data are mean± SEM, n = 3-18 biological replicates with 3-4 technical replicates per condition. Statistical analysis was conducted by one-way ANOVA with Dunnett's multiple comparisons correction. *** P <0.001, comparing all samples to vehicle control. † P <0.05, † † † P <0.001, comparing all samples to chemokine plus cannabinoid. (E and F) HU308 (10 μM) also potentiated 5 nM CCL2 and 5 nM CCL5-induced $CB_2^{-/-}$ macrophage chemotaxis. Data are representative traces from one experiment with 3-4 technical replicates per condition.

3.3.8 JWH133 and HU308 enhance C5a-induced macrophage chemotaxis

I was interested to discover if JWH133 and HU308 are generally able to enhance chemotaxis, or whether this effect is specific to CC chemokines. To address this, I used C5a as the chemoattractant; a short peptide generated from activation of the complement cascade that is a potent macrophage chemoattractant. When used alone C5a induced robust macrophage chemotaxis (Fig 3.13A and B), however when in the presence of JWH133 or HU308, macrophage chemotaxis was significantly greater than that caused by C5a alone (Fig 3.13A and B).

As both JWH133 and HU308 are chemoattractants in their own right, I wanted to examine whether the same enhanced chemotaxis would be seen if two different macrophage chemoattractants were placed together in the lower chamber of the chemotaxis plate. For this I selected CCL2 and CCL5, as I had been using these throughout my study. As expected, both CCL2 and CCL5 (10 nM) acted as chemoattractants, but when combined together macrophage chemotaxis was clearly enhanced (Fig 3.13C).

3.3.9 The CB_2 inverse agonist SR144528 acts as a macrophage chemoattractant

In figure 3.9B, I found that the CB_2 inverse agonist SR144528 significantly increased CCL5-induced macrophage chemotaxis, and a representative trace from those experiments is shown in figure 3.14A. As I have demonstrated that the chemotaxis positive ligands JWH133 and HU308 also increased chemokine-induced macrophage chemotaxis, I hypothesised that SR144528 might also act as a macrophage chemoattractant, thereby explaining why SR144528 enhanced CCL5-induced chemotaxis. When used at a concentration of 10 μM, the same as that of JWH133 and HU308, SR144528 induced thioglycollate elicited macrophage chemotaxis (Fig 3.14B). Furthermore,

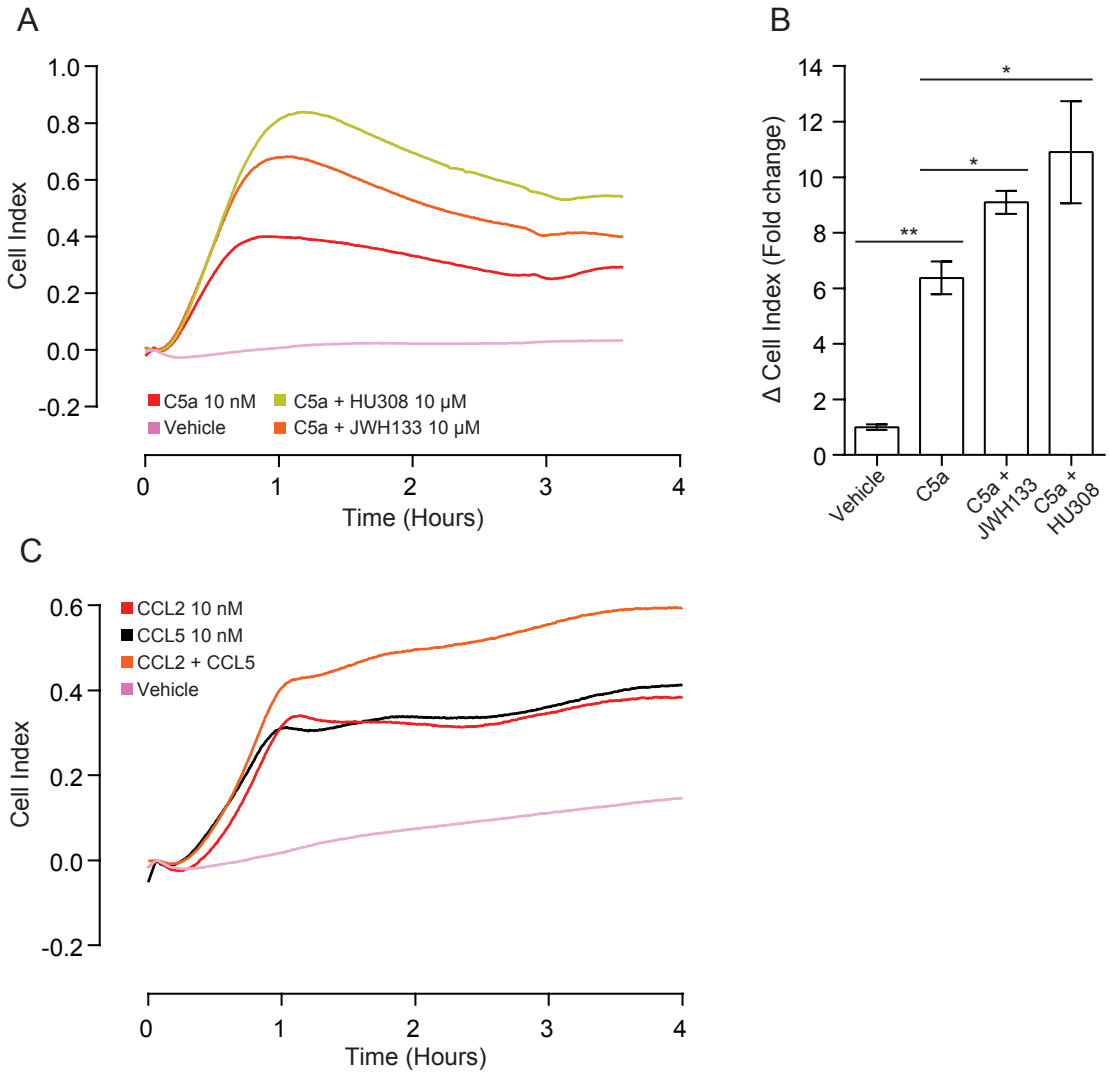

Figure 3.13 JWH133 and HU308 enhance C5a-induced chemotaxis. (A) Bio-gel elicited PECs (4 x 10^5) were placed into the upper chamber of a CIM-16 plate and allowed to migrate for 3-4 hours at towards vehicle (0.3% DMSO), C5a alone (10 nM), or C5a plus JWH133 or HU308 (both 10 μM). (B) Quantification demonstrated that, in comparison to C5a alone, macrophage chemotaxis is significantly increased when C5a is in the presence of JWH133 or HU308. Data are mean± SEM, n = 4 biological replicates with 3-4 technical replicates per condition. (C) Bio-gel elicited PECs were placed into the upper chamber of a CIM-16 plate and allowed to migrate for 3-4 hours at towards vehicle, CCL2 or CCL5 alone (both 10 nM), or CCL2 and CCL5. Data are the mean of 3-4 technical replicates per condition. Statistical analysis was conducted using one-way ANOVA with Sidak's multiple comparisons correction. * P <0.05, ** P <0.01, for indicated comparisons.

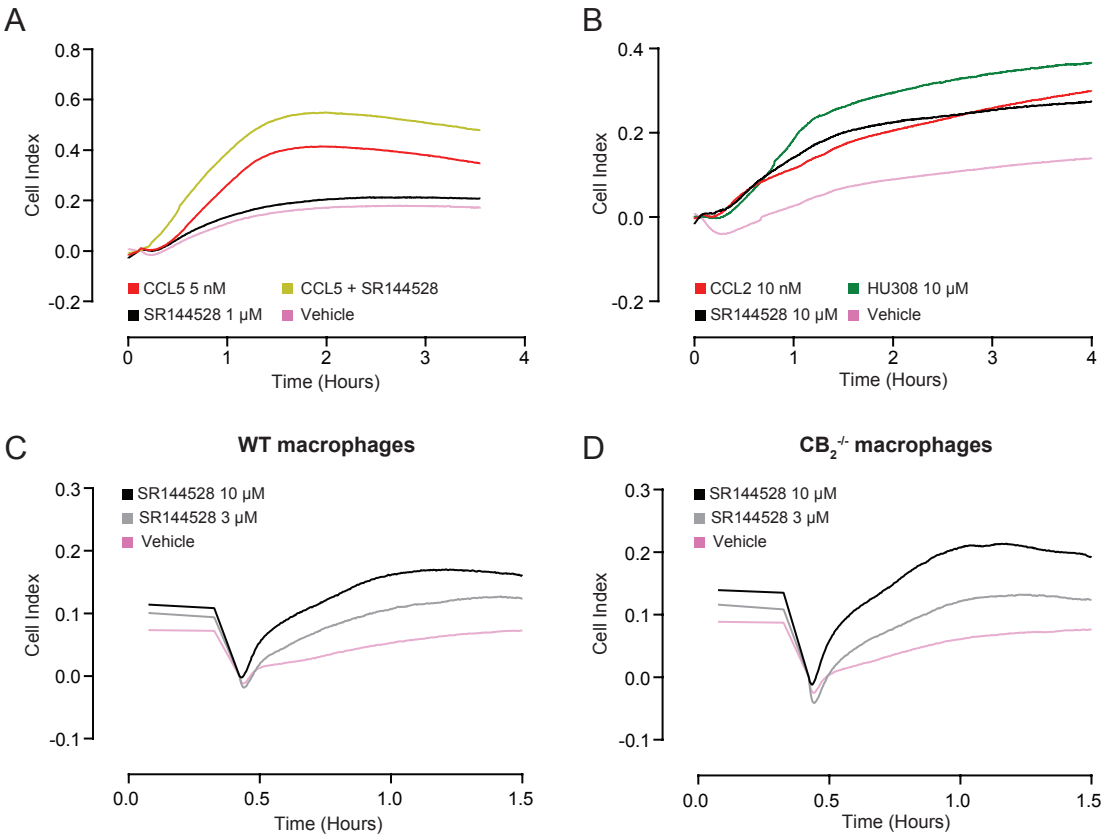

Figure 3.14 The CB_2 inverse agonist SR144528 acts as a macrophage chemoattractant. (A) Bio-gel elicited PECs were treated with either vehicle or 1 μM SR144528 for 30 min at 37°C, 5% CO_2. Following treatment, cells were allowed to migrate for 3-4 hours at 37°C, 5% CO_2 toward vehicle or 5 nM CCL5. SR144528 (1 μM) was also added in the lower chamber alongside the indicated chemoattractant in the respective wells. Data are the mean of 3-4 technical replicates per condition. (B) Thioglycollate elicited macrophages were placed into the upper chamber of a CIM-16 plate and were allowed to migrate for 3-4 hours at 37°C, 5% CO_2 towards vehicle, CCL2 (10 nM), HU308 or SR144528 (both 10 μM). Bio-gel elicited PECs from (C) WT or (D) $CB_2^{-/-}$ mice were placed into a 96 well E-plate allowed to adhere for 2-3 hours at 37°C, 5% CO_2. Afterwards, cells were stimulated with either vehicle (0.3% DMSO) or SR144528 at the indicated concentration. Data are mean traces from one experiment with 3-6 technical replicates per condition.

SR144528 induced concentration-dependent macrophage cytoskeletal rearrangement, as determined by electrical impedance, in WT (Fig 3.14C) and $CB_2^{-/-}$ (Fig 3.14D) macrophages. Taken together, this data demonstrate that the CB_2 inverse agonist SR144528 is capable of inducing macrophage spreading and chemotaxis, in a CB_2 independent manner.

3.3.10 CP55,940 and DIAS2 do not negatively regulate chemokine-induced macrophage chemotaxis

Given that JWH133 and HU308 clearly activate a $G_{i/o}$-coupled receptor that is not CB_2, this makes it difficult to evaluate whether specific activation of CB_2 negatively regulates chemokine-induced macrophage chemotaxis. To overcome this issue, I used the potent, but importantly chemotaxis negative, CB_2 agonists CP55,940 and DIAS2 to further probe how CB_2 agonism affects CC chemokine mediated macrophage migration. The addition of 1 μM DIAS2 alongside either 5 nM CCL2 or CCL5 had no effect on chemokine-induced macrophage chemotaxis (Fig 3.15A). Furthermore, 1 μM CP55,940 alongside 5 nM CCL5 also had no effect on macrophage migration (Fif 3.15B - White bars). As CP55,940 is a mixed CB_1/CB_2 agonist, the experiment was repeated using bio-gel elicited PECs isolated from $CB_2^{-/-}$ mice. Again, 1 μM CP55,940 had no effect on CCL5-induced macrophage chemotaxis (Fig 3.15B - Grey bars). Potentially, these negative results could be ascribed to using an insufficient concentration of DIAS2 and CP55,940. Therefore, real-time chemotaxis experiments were conducted using 10 μM agonist alongside 5 nM CCL5. However, even at this concentration, both DIAS2 (Fig 3.15C) and CP55,940 (Fig 3.15D) had no effect on CCL5-induced macrophage migration, as the kinetic profiles in the presence of each compound closely mirrored that of CCL5 alone. Therefore, these data do not support the hypothesis that CB_2 activation negatively regulates chemokine-induced macrophage chemotaxis.

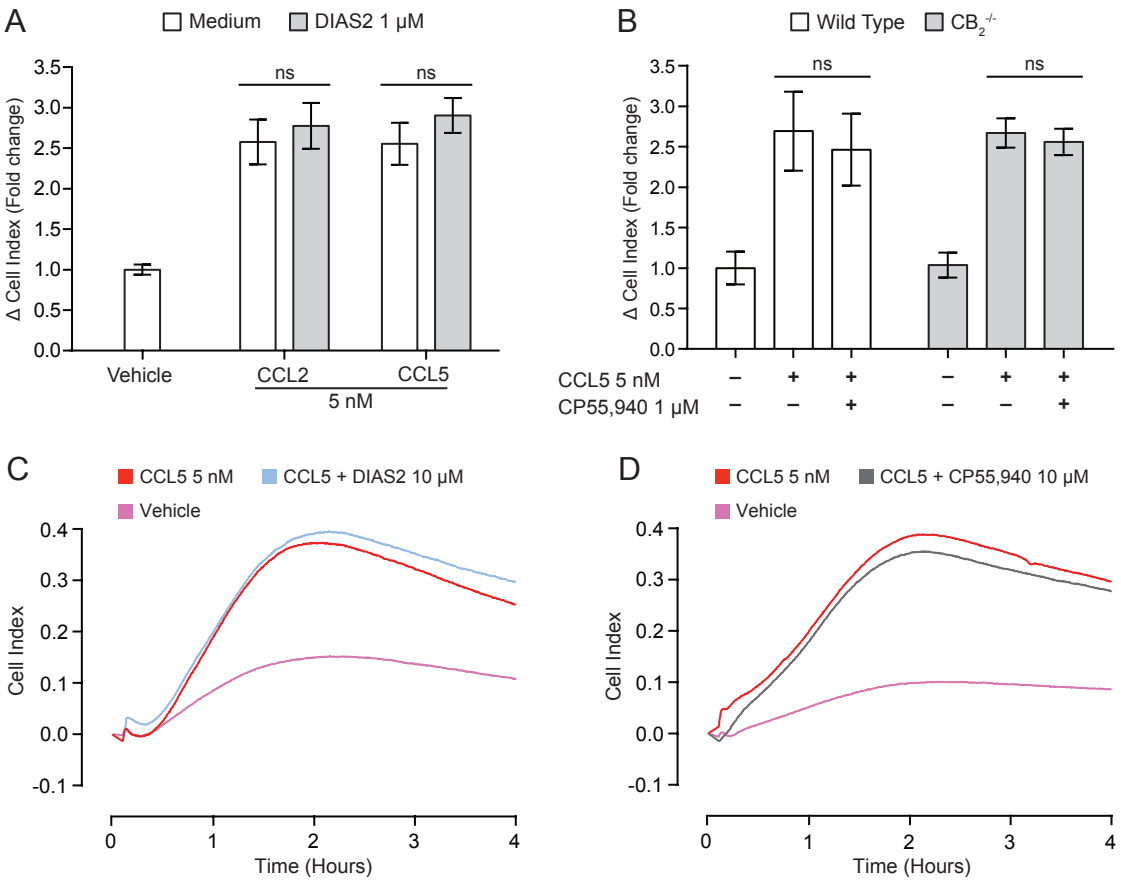

Figure 3.15 CP55,940 and DIAS2 do not negatively regulate chemokine-induced murine macrophage chemotaxis. Biogel-elicited murine PECs (4 x 10^5) were placed into the upper chamber of a CIM-16 plate and allowed to migrate for 4 at 37°C, 5% CO_2 hours toward vehicle (0.3% DMSO), chemokine alone, cannabinoid alone or chemokine plus cannabinoid. (A) DIAS2 (1 μM) did not inhibit 5 nM CCL2 and CCL5-induced macrophage chemotaxis. (B) CP55,940 (1 μM) did not inhibit 5 nM CCL5-induced chemotaxis in WT or $CB_2^{-/-}$ murine macrophages. Data are mean± SEM, (A) n = 3, (B) n = 4 biological replicates with 3-4 technical replicates per condition. Statistical analysis was conducted by two-way ANOVA with Sidak's multiple comparisons correction. ns P >0.05. (C and D) Neither 10 μM DIAS2 nor 10 μM CP55,940 inhibited CCL5-induced (5 nM) macrophage chemotaxis. Data are mean real-time traces from one experiment, representative of 2 independent biological replicates with 3-4 technical replicates per condition.

3.4 Discussion

I began this results chapter with two aims; firstly to discover whether CB_2 acts as a chemoattractant receptor in primary murine macrophages and secondly to examine whether activation of CB_2 inhibits macrophage chemotaxis towards CC chemokines.

With respect to the first aim, I believe that this is the first study to address whether activation of CB_2 causes the directed migration of primary murine macrophages. By using real-time measurements of both cell morphology and migration, I have found that only a subset of CB_2 agonists act as chemoattractants for primary murine macrophages. Furthermore, I demonstrated that functional selectivity was present within the agonist cohort, but could not explain why only certain CB_2 agonists acted as macrophage chemoattractants. Instead, I found that although CB_2 agonist-induced chemotaxis was PTX sensitive, pharmacological inhibition or genetic ablation of CB_2 had no effect on cellular signalling or macrophage migration. Therefore, this provides the first evidence that the widely used CB_2 agonists JWH133, HU308, L-759,633, L-759,656 and SER601 have off-target effects at a non-CB_1/CB_2 $G_{i/o}$-coupled GPCR, a finding that has wide ranging implications for the entire cannabinoid field, and conclusively demonstrates that CB_2 is not a macrophage chemoattractant receptor.

With respect to my second aim, I found no evidence that activation of CB_2 negatively regulates CC chemokine-induced macrophage chemotaxis. When adding JWH133 or HU308 alongside a CC chemokine, an increase in chemotaxis was observed as opposed to a reduction. This is perhaps expected as both of these agonists are macrophage chemoattractants. However, addition of the chemotaxis negative CB_2 agoinsts DIAS2 or CP55,940 alongside a CC chemokine, also had no effect on the chemotactic response observed. Therefore, I conclude that immediate activation of CB_2 does not inhibit CC chemokine-induced primary macrophage chemotaxis.

I am confident that throughout this study I am specifically measuring macrophage chemotaxis, despite the fact that the bio-gel elicited PECs were comprised mostly of neutrophils. Without enrichment 4 x 10^5 bio-gel elicited PECs were used per chemotaxis well and CI signals for JWH133 and HU308 peaked at approximately 0.4. After macrophage enrichment of bio-gel elicited PECs, 2 x 10^5 cells were used per well, half that of bio-gel elicited PECs, yet JWH133 and HU308 reached peak CIs of approximately 0.8, double that of bio-gel elicited PECs, and retained similar kinetic chemotaxis profiles. Therefore as macrophages comprise 20-25% of bio-gel elicited PECs and 100% of enriched macrophages, the CI signal per cell between the two populations is almost identical (approximately 5 x 10^{-6} CI/cell), strongly implying that macrophages are the primary contributor to the observed CI. Furthermore, thioglycollate elicited macrophages used at 2 x 10^5 cells per well displayed chemotaxis kinetics and peak CI signals similar to the enriched macrophages. Importantly, the thioglycollate elicited peritoneal macrophage preparations did not contain neutrophils.

Concomitantly, murine neutrophils isolated from bone marrow only elicited a weak CI signal that never exceeded 0.1, when migrating towards the potent neutrophil chemoattractant C5a. This data mirrors those obtained by Cano *et al* who found that neutrophil chemotaxis towards IL-8 could not be measured using the same real-time chemotaxis system, unless the underside of the wells were coated with the extracellular matrix component fibronectin [424]. As I only used uncoated chemotaxis plates, I believe that bio-gel elicited neutrophils only contribute a negligible component to the observed CI signal as they cannot efficiently adhere to the underside electrode. It is important to note that this does not mean that neutrophils do not migrate towards the CB_2 agonists, just that their migration cannot be measured using the xCELLigence real-time chemotaxis system. Taken together, I am confident that macrophages, and not neutrophils, are the dominant population in bio-gel elicited PECs that are being measured in the real-time chemotaxis assay.

Multiple lines of evidence support the hypothesis that CB_2 agonist induced

macrophage migration is indeed *bona fide* chemotaxis that relies on GPCR signalling, rather than a non-specific off-target effect of these ligands. JWH133 and HU308 both elicit macrophage migration in a concentration-dependent manner and checkerboard analysis demonstrates that they do not cause fugitaxis or chemokinesis. Instead macrophages move towards the compound in a directional manner, the definition of chemotaxis. Additionally, all chemotaxis positive compounds elict concentration-dependent macrophage cytoskeletal rearrangement, a process fundamental to directed migration. Further evidence that these CB_2 agonists elicit true chemotaxis comes from the finding that JWH133 and HU308 cause Akt phosphorylation (a marker for PI3K activity) and that inhibition of PI3K blocks JWH133 and HU308-induced cytoskeletal rearrangement and migration. Therefore, these CB_2 agonists activate and rely on PI3K, a signalling pathway critical for the control of directed cellular migration (see section 3.1.3). Finally, when JWH133 or HU308 were added alongside CCL2, CCL5 or C5a, increased macrophage chemotaxis was observed in comparison to any of the chemoattractants alone. Addition of both CCL2 and CCL5 in the lower chamber of the chemotaxis assay also resulted in a similar increase in macrophage chemotaxis, therefore the additive effect of JWH133 and HU308 alongside other chemoattractants likely reflects the fact that these compounds elicit chemotaxis in their own right.

Initially I assumed that the ability of only a subset of CB_2 agonists to induce macrophage chemotaxis was due to functional selectivity at CB_2. This phenomenon, where different ligands at the same receptor can activate distinct downstream signalling pathways, is well documented for agonists acting at CB_2 and previous studies demonstrating that 2-AG acts as a chemoattractant, also found that that the synthetic CB_2 agonists WIN55,212-2 and CP55,940 failed to elicit any migratory response [390, 393, 397]. When examining signalling pathways downstream of CB_2 activated by the agonists in this study, functional selectivity was evident in the ligand cohort, as they varied in their ability to recruit β-arrestin to the receptor. Corroborating previous results, CP55,940 caused the greatest recruitment

of β-arrestin and JWH133, HU308, L-759,633 and L-759,656 all acted as partial agonists. However, SER601 caused no recruitment at any concentration and the chemotaxis negative JWH015 caused β-arrestin recruitment to levels comparable to chemotaxis positive ligands. Therefore, ability to recruit β-arrestin did not correlate with ability to cause macrophage chemotaxis.

Evidence that functional selectivity, and indeed CB_2 itself, might not be responsible for why only a subset of CB_2 agonists act as macrophage chemoattractants came from the discovery that SER601 did not act as a CB_2 agonist in any of the signalling assays used, despite being able to elicit macrophage chemotaxis. Furthermore, as the CB_2 inverse agonist SR144528 also caused macrophage migration, this provided further doubt that activation of CB_2 was responsible for the observed chemotaxis. Confirmation that CB_2 was not needed came from the finding that CB_2 agonist-induced macrophage chemotaxis was unaffected by pharmacological inhibition or genetic deletion of CB_2. Instead these results, combined with the finding that CB_2 agonist-induced chemotaxis is PTX sensitive, demonstrate that the synthetic CB_2 agonists JWH133, HU308, L-759,633, L-759,656 and SER601 likely activate at least one $G_{i/o}$-coupled receptor distinct from CB_2, to elicit directed cellular migration. This finding is not without precedent, as a non-CB_1/CB_2 receptor has been implicated in the negative regulation of fMLF-induced chemotaxis by endo and phytocannabinoids [402]. The profile of the receptor identified by McHugh *et al* does not match the putative GPCR from our study, however their observation demonstrates that novel receptors involved in chemotaxis modulation by cannabinoids may be more numerous than presently thought.

Chemical analysis of the agonists used in this study provides some evidence that JWH133, HU308, L-759,633, L-759,656 and SER601 all have a specific mechanism at the same off-target site. JWH133, HU308, L-759,633 and L-759,656 are all structurally related, being based on the phytocannabinoid Δ9-THC. Furthermore, the chemotaxis positive ligands are all highly lipophillic, having high cLogP values. As similar compounds normally have similar biological activity [425], this implies

that they share a common mode of action. However as SER601 and SR144528 were also macrophage chemoattractants and these two compounds are structurally distinct from the other chemotaxis positive ligands, it is unlikely that the ability of only some CB_2 ligands to induce chemotaxis relies solely on their physicochemical properties. Indeed CP55,940, which has a similar structure and lipophilicity to the chemotaxis positive compounds, and CB65, which is structurally related to SER601, were unable to induce directed migration. Therefore it is likely the case that both CP55,940 and CB65 violate the steric constraints of the off-target site rendering them inactive and unable to induce directed migration. Nonetheless, as all of the chemotaxis positive compounds have been screened or designed to be active at CB_2 it is reasonable to assume that some aspect of what makes a CB_2 ligand crosses over onto the novel receptor implicated in this chapter. However, exactly what these attributes may be will remain unknown until the off-target receptor is identified.

Regardless of the exact nature of the receptor, I believe my finding that JWH133, HU308, L-759,633, L-759,656 and SER601 are more promiscuous than currently thought has wide-ranging implications for the cannabinoid field as a whole. Numerous endogenous and plant derived cannabinoids have been shown to activate a multitude of receptors other than CB_1 or CB_2, however to my knowledge this is the first report that these synthetic agonists have off-target effects of functional consequence in disease relevant primary cells. This is of importance as JWH133 and HU308 are among the agonists most frequently used to assess the selective activation of CB_2 [131]. However their reputation as selective agonists, cemented by historical compound characterisation for CB_1/CB_2 activity in transfected cell systems overexpressing either cannabinoid receptor, has meant that many studies do not employ stringent controls when using these ligands.

A cursory search of the literature found multiple examples of JWH133 and HU308 being used in both primary cell assays and *in vivo* disease models without receptor antagonism or CB_2 deletion to confirm CB_2 dependence [273, 282, 299, 426–432]. The off-target effects of JWH133 and HU308 may mean that results obtained in

these studies have been erroneously attributed solely to the activation of CB_2. Additionally, many of the above models have a strong inflammatory component and, as macrophages are key players during inflammation [1, 43], the macrophage localised GPCR implicated in this study has likely confounded observed results. Indeed this receptor may even explain current findings in the literature. For example, the previously mentioned chemoattractant ability of JWH133 for human monocytes was not confirmed to absolutely depend on CB_2 [389]. In light of my data I speculate that, rather than CB_2, the novel receptor implicated in this chapter may be responsible for JWH133-mediated chemotaxis of human monocytes.

Interestingly, and in contrast with a myriad of studies, I found that 2-AG was unable to act as a macrophage chemoattractant. This is not the first report that 2-AG is unable to elicit chemotaxis, as Oka *et al* found that 2-AG did not cause the directed migration of human neutrophils [392], and hints that this disparity could be due to cell type differences in CB_2 biology. However it could also be due to species differences in CB_2 pharmacology. Multiple CB_2 ligands have been shown to display different binding affinities and functional efficacies between the human, rat and murine receptors [147, 433]. Furthermore, AM1241 has been demonstrated to have entirely different pharmacology between species as it behaves as an agonist at human CB_2, but an inverse agonist at the rat and murine receptors [434]. As no study currently exists comparing CB_2 mediated chemotaxis of multiple cell types from different species, it is difficult to conclude how much these variables impact on the role of CB_2 in the regulation of leukocyte migration. Regardless, my work highlights that caution should be employed when extrapolating results obtained from one cell type or species onto another.

When examining whether CB_2 agonists can inhibit CC chemokine-induced macrophage chemotaxis, I found that when JWH133 and HU308 were added alongside CC chemokines, macrophage chemotaxis was enchanced. As mentioned above, this is not surprising as they are themselves chemoattractants. Therefore, I used the chemotaxis negative, but potent, CB_2 agonists CP55,940 and DIAS2 to address

whether CB_2 activation dampens macrophage chemotaxis. Interestingly, I found that CP55,940 and DIAS2 had no effect on CC chemokine-induced macrophage chemotaxis and this directly conflicts with the only other reports examining the effect of CB_2 activation of CC chemokine-induced migration in murine macrophages. Δ9-THC has been shown to inhibit macrophage migration towards CCL2 [334] and CCL5 [410], and this inhibitory effect was subsequently found to extend to synthetic cannabinoids, as CP55,940 also inhibits CCL5-induced macrophage chemotaxis [410]. However, these previous works all used an extended cannabinoid pre-incubation of 3-4 hours before macrophages were exposed to CC chemokines. As long pre-incubations of murine macrophages or human monocytes with Δ9-THC or JWH015 respectively, have been shown to cause a significant reduction in macrophage chemokine receptor mRNA levels and surface expression [334, 389], this potentially explains how prolonged CB_2 activation inhibits CC chemokine-induced macrophage chemotaxis.

However, as both Δ9-THC and CP55,940 are not endogenous cannabinoids, the only way they can be present *in vivo* is after exogenous administration. Therefore it is difficult to imagine a scenario whereby monocytes/macrophages would be exposed to these agonists for 3-4 hours prior to being stimulated to migrate by CC chemokines, as they surely would be administered after any inflammatory disease has presented clinically. Therefore, the clinical relevance of these above findings is called into question. To address this, I made a conscious decision to expose the macrophages to cannabinoid and chemokine simultaneously and as migration was measured in real time over at least a 4 hour time period, chemokine receptor desensitization following CB_2 activation should have become apparent within this time frame. Instead, no differences in CC chemokine-induced chemotaxis were observed in the presence of DIAS2 or CP55,940, even at time points up to 6 hours. Therefore, I believe that the finding that phyto- or synthetic cannabinoids can negatively regulate CC chemokine-induced macrophage chemotaxis may not manifest *in vivo*. Whether the endogenous cannabinoids have the same effect remains unstudied. However, it is currently accepted that endocannabinoids are synthesised on demand when

needed, so again prolonged cell exposure to these endogenous ligands may also not be possible. Additionally, the levels of endocannabinoids in various anatomical sites under physiological an pathological conditions are very poorly understood, so further work is clearly needed to uncover whether these agonists have the correct signalling and spatio-temporal properties to negatively regulate macrophage chemotaxis.

3.4.1 Limitations of this study

One limitation with this study is that I have only used one real-time methodology to measure macrophage chemotaxis. Whilst the advantages of using real-time chemotaxis systems over traditional single time point assays are numerous, it is still desirable to use multiple real-time methods to study chemotaxis. This is because no single method is perfect and therefore using mulitple assays allows greater understanding of leukocyte migratory behaviour. For example, as the xCELLigence system measures movement of cells through a membrane, it does not allow other chemotaxis parameters to be measured, such as distance migrated or the velocity and directionality of migration. However, the IBIDI μ-slide chemotaxis assay allows measurement of these parameters, as chemotaxis is followed in real-time using time lapse microscopy [435]. However, this system is not without its limitations as well; a maximum of around 40 cells can be tracked per condition, quantification is time consuming and each slide only allows for three separate chemotaxis conditions. This therefore strengthens the idea that no single chemotaxis assay provides the perfect system for studying migration.

A further limitation of the xCELLigence system is that it cannot measure the migration of non-adherent cell types, as the CI signal relies on cells adhering onto the gold electrode present in each well. Whilst for my work this proved beneficial as the neutrophil population in bio-gel elicited PECs could not score, for others this may provide a serious limitation. In the future it would be of great interest to me to discover whether neutrophils also migrate towards the same CB_2 agonists as

macrophages and to do this I would have to use a different chemotaxis methodology. A classical transwell system would allow measurement of non-adherent cell migration, but suffers from being a single time point readout. Instead, the recently released IncuCyte ZOOM® system provides an elegant way of measuring the chemotaxis of non-adherent cell types in real-time (See their website for details [436]). It uses a Boyden-chamber style 96 well plate, combined with microscopy and advanced image analysis to identify cells on the filter. For non-adherent cell, the system measures the loss of cells from the top surface; a measure of how many have migrated through the pores.

Another limitation of this study is that I only used a limited range of primary macrophage populations. I focussed mainly on bio-gel elicited macrophages, as these are easy to obtain in large numbers [416]. Also, as they are cells that have differentiated *in vivo* they are more likely to represent *in vivo* macrophage behaviour in comparison to macrophage populations differentiated *in vitro*, such as bone marrow-derived macrophages. However, there are a wide range of different tissue resident macrophages throughout the body and each are programmed by their local niche to behave differently and perform tissue specific functions [40, 42, 43]. In the future, I would like to isolate macrophages from different tissues and discover whether they also migrate towards the CB_2 agonists identified in this study. I would hypothesise that tissue resident macrophages would migrate towards the chemotaxis positive CB_2 agonists, as I found that JWH133 and HU308 acted as chemoattractants for thioglycollate elicited macrophages.

Furthermore, I would also like to study different leukocyte populations to discover how many different immune cell types will migrate towards the CB_2 agonists. This would aid in the identification of the GPCR responsible for CB_2 agonist-induced chemotaxis, as the identifying the GPCR complement of positive and negative immune cell populations will allow narrowing of the candidate receptor pool.

Chapter 4

Identification of the off-target GPCR(s) responsible for CB_2 agonist-induced macrophage chemotaxis

4.1 Introduction

4.1.1 Drug promiscuity - Off-target effects of small molecules

Over the last 30 years, the 'holy grail' of drug discovery has commonly been held to be the identification and generation of compounds with a high degree of specificity towards their intended target. It is hoped that minimising or eliminating the actions of a drug at other targets will limit unwanted, adverse effects of a compound. However, it is now thought that almost all small molecule drugs likely interact with multiple targets. By analysing databases containing functional data for a large number of small molecules, evaluations of drug promiscuity are now being made. Paolini *et al* examined 276,122 compounds annotated in an in-house database and found that 35% had more than one target [437]. Furthermore, Hu *et al* analysed

33,778 compounds meeting strict inclusion criteria from the ChEMBL database and similarly found that 38.4% had 2 or more targets [438]. However, when considering currently approved drugs only, the best estimates show that on average they have 7 targets [439, 440], with 84% having 2 or more targets and 40-50% having 5 or more targets [438, 441]. However, it is important to note that these numbers vary depending on the datasets used, the compounds included in the analysis and the way promiscuity is defined.

However, it is now becoming increasingly apparent that that these statistics likely underestimate how many off-target effects current approved drugs and other small molecule compounds actually have [440]. Obviously the number of targets a drug is found to have depends on how many targets the small molecule has been tested against, and historically drug discovery has relied on using target-centric screening methods [442]. This is especially true for ligands acting at cannabinoid receptors, as agonist/antagonist discovery has focussed heavily on the binding and/or activity of a ligand at CB_1 versus CB_2. Whilst this has undoubtedly provided compounds very selective for either receptor, this screening is so narrow that any off-target effects of these synthetic ligands will have been missed. As approximately 3000 of the 20-25,000 genes that make up the human genome [443] have been predicted to have attributes that make them 'druggable' - defined as having properties beneficial for interaction with drug-like compounds [444, 445], and no compound to date has been screened against anywhere near that number of targets, it is highly likely that the number of targets any given small molecule possesses is higher than currently thought.

4.1.2 Adverse drug reactions - The negative side of drug off-target effects

Generally, off-target effects are considered undesirable as they can cause unwanted adverse side effects sometimes seen when small molecules are used clinically. Although

many drugs have side effect profiles that are tolerated when used by patients, adverse drug reactions (ADRs) cause an estimated 100,000 deaths per year, with 2 million patients suffering with serious side effects [446]. Numerous licensed drugs have been withdrawn from sale after they have been found to cause serious adverse effects or even death due to unwanted ADRs [447], for example the CB_1 inverse agonist rimonabant (See section 1.8.7 for more details), causing large societal and financial costs. However, the prototypical off-target that has been responsible for the withdrawal of multiple therapeutics is drug interactions with the hERG potassium channel. hERG is a voltage-gated potassium channel that is required for action potential repolarisation in the heart and its inhibition results in, the now infamous, QT interval prolongation that in turn can led to fatal arrhythmias [448]. A classic example is the drug terfenadine that was developed as a histamine H1-receptor antagonist for the treatment of allergies [449]. It was approved for clinical usage in 1985, but eventually was linked to QT interval prolongation, arrhythmia and sudden death [450]. It was subsequently found that terfenadine is a potent inhibitor of hERG, having an IC_{50} in the low nanomolar range and it was eventually withdrawn from sale in 1998 [451–453]. Multiple drug classes with diverse chemical structures have now been demonstrated to block hERG function and it is now common practise for pharmaceutical companies to test all clinical candidates for activity at the hERG potassium channel [454].

4.1.3 Drug repurposing - The positive side of drug off-target effects

However, the off-target effects of small molecules can also be used in a positive way, as they underlie the basis of drug repurposing; the process of finding new clinical usages for existing drugs that are outside of their original indications [455]. Drug repurposing efforts have been rapidly increasing due to the multiple benefits that this process can potentially offer to the drug discovery process. Traditional drug discovery, going from lead identification through to licensing, takes between 10-17 years, has a success rate of less than 10% [456, 457] and is currently estimated to

cost 2.6 billion US dollars [458]. By finding new uses for already existing compounds, the process of drug discovery can not only be sped up but also de-risked as multiple stages of the drug-development pipeline, such as drug manufacturing, toxicology and even phase I and II trials, may have already been completed, allowing a faster route to the clinic (estimated between 3-12 years) and a greater understanding of the safety profile of the compound [457, 459].

There are multiple instances of drug repurposing in the literature [459], however a classic success story comes from sildenafil, marketed by Pfizer as Viagra. Sildenafil is an inhibitor of phosphodiesterase 5 (PDE5) and was orignially intended as a treatment for angina, as it was hoped that PDE5 inhibition would result in increased coronary blood flow by causing dilation of the coronary artery [460]. Sildenafil failed a phase II clinical trial for the treatment of angina, but was instead found to cause the unintended side effect of persistent penile erection [457]. Sildenafil was demonstrated to be an effective treatment for erectile dysfunction and was introduced into the clinic in 1998 [461]. Another high profile case is that of thalidomide; the infamous morning sickness medication, originally marketed in 1957, that also caused severe birth defects [462]. Thalidomide has now been licensed for the treatment of erythema nodosum laprosum and also multiple myeloma [463]. More recently, I myself found that the angiotensin II receptor antagonist losartan acts as an anti-thrombotic by inhibiting the platelet collagen receptor, GPVI [464].

4.1.4 Off-target effects of cannabinoids

Despite the high degree of specificity for CB_1 or CB_2 that has been achieved for cannabinoid receptor ligands, many studies over the last decade have detailed off-target activities of various endo, phyto and synthetic cannabinoids (excellently reviewed in [131]). The targets identified include multiple GPCRs, ligand and voltage gated ion channels as well as ligand activated transcription factors, and serve to highlight the fact that cannabinoid receptor ligands are more promiscuous than

might be appreciated from reading current cannabinoid receptor review articles and primary research papers.

4.1.5 Off-target effects at GPCRs

GPR55

Originally identified in 1999, GPR55 has high expression in the striatum of the brain and it is now commonly thought that its endogenous ligand is lysophosphatidyl inositol, as this lipid has been shown to activate GPR55 in a range of assays [465, 466]. However, it has also been demonstrated that GPR55 can be activated by multiple cannabinoid ligands and is believed responsible for many off-target effects of cannabinoids [467]. These discoveries were initially surprising as GPR55 shares little sequence identity with either CB_1 (13.5%) or CB_2 (14.4%) [468] and lacks the proposed cannabinoid binding pocket seen in both CB_1 and CB_2 [469, 470]. Nevertheless, a seminal paper by Ryberg *et al* published in 2007 demonstrated that AEA, 2-AG, Δ9-THC, CP55,940, CBD and abnormal-cannabidiol (Abn-CBD) all stimulate GTPγS activity in HEK293 cells expressing GPR55 with EC_{50} values in the nanomolar range [471]. Corroborating this finding, others have shown that AEA, Δ9-THC and JWH015 cause increases in intracellular Ca^{2+} levels in HEK293 cells expressing GPR55 [472, 473]. However, it seems not all cannabinoid ligands are capable of activating GPR55 as WIN55,212-2 is unable to stimulate GTPγS activity or Ca^{2+} signalling in GPR55 transfected cells [471]. However, this lack of signalling could be due to functional selectivity. Despite the fact that AEA and CP55,940 are able to cause β-arrestin recruitment to GPR55, 2-AG, Δ9-THC, CBD and Abn-CBD (all compounds active in the GTPγS assay) were unable to elicit β-arrestin recruitment [474, 475]. Unfortunately, the degree of functional selectivity of cannabinoid ligands acting at GPR55 is uncertain as so far no study has directly compared multiple ligands in multiple functional assays. Furthermore, the significance of these results in primary cells and tissues is currently lacking, however

it is clear from these data that numerous cannabinoid ligands are active at GPR55.

GPR18

GPR18, previously an orphan GPCR discovered in 1997, is highly expressed in the spleen, testis and bone marrow [476] and has recently received attention as a potential cannbinoid receptor due to the discovery that it binds and is activated by *N*-arachidonoylglycine (NAGly); a metabolite of AEA [477]. In GPR18 expressing cells, NAGly has been shown to cause Ca^{2+} signalling and phosphorylation of ERK1/2 in a PTX sensitive manner, alongside both Δ9-THC and Abn-CBD [478]. Additionally, NAGly and Abn-CBD cause the directed migration of GPR18 transfected HEK293 cells and the BV-2 murine microglial cell line, with GPR18 dependence confirmed using siRNA knockdown [479, 480], and NAGly and Δ9-THC induce the migration of a human endometrial cell line in a GPR18-dependent manner [481]. Interestingly, JWH015, JWH133, CP55,940 and WIN55,212-2 were unable to cause endometrial cell chemotaxis. This result suggests that functional selectivity may impact this ligand cohort in a manner similar to GPR55. Further support of this hypothesis comes from the finding that Δ9-THC causes β-arrestin recruitment to GPR18, whereas NAGly, AEA, CBD and Abn-CBD all have no effect [478]. However, due to a lack of studies specifically examining functional selectivity of cannabinoids at GPR18, the extent of this phenomenon at this receptor remains unclear. Regardless, it is clear that cannabinoids active at CB_1 and CB_2 are also active at GPR18. Interestingly for my work, NAGly has been shown to induce apoptosis in the macrophage RAW264.7 cell line in a PTX and GPR18-dependent manner [482], highlighting that cannabinoid compounds acting at GPR18 can impact on macrophage function.

Other GPCRs targeted by cannabinoids

Whilst the majority of the literature regarding the off-target effects of cannabinoids at GPCRs focusses on GPR55 and GPR18, there are a few studies demonstrating that

endo and phytocannabinoids have effects at various other GPCRs [131]. Δ9-THC and CBD have been shown to act as allosteric modulators of δ and μ-opioid receptors, as they displace radiolabelled ligand binding at these receptors in a non-competitive manner [483, 484], whilst the CB_1 inverse agonist rimonabant displaces ligand binding at μ- and κ-opioid receptors in a competitive manner [485, 486]. Further to this, AEA has been demonstrated to inhibit ligand binding at both M_1 and M_4 muscarinic acetylcholine receptors and displace radiolabelled muscarinic agonists in human cerebrocortical membrane preparations in a non-competitive manner at micromolar concentrations [487, 488]. AEA, 2-AG and rimonobant have all been found to allosterically inhibit ligand binding at the adenosine A_3 receptor [489] and additionally, rimonobant inhibits binding of ligands at α_{2A}- and α_{2C}-adrenergic receptors, angiotensin AT_1 receptors, prostanoid EP_4 receptors 5-HT_6 receptors and finally tachykinin NK_2 receptors [131].

The putative endothelial cannabinoid receptor

Work conducted by Járai *et al* in 1999 found that both AEA and Abn-CBD cause the vasodilation of murine mesenteric vasculature in a CB_1 and CB_2-independent manner [490]. Furthermore, this vasodilation was sensitive to the removal of the endothelium from the vessel, leading to the conclusion that an endothelial receptor, that is not CB_1 or CB_2, is responsible for the observed vasodilation. Since this discovery numerous studies have shown that AEA and Abn-CBD cause vasodilation of rat, murine and human vessels from different anatomical locations. Importantly, alongside demonstrating independence of CB_1 and CB_2, these studies show that AEA and Abn-CBD induced vasodilation is PTX sensitive, implying that a non-CB_1/CB_2 $G_{i/o}$-coupled GPCR is responsible for this effect (see [491]). It has been claimed that GPR55 and/or GPR18 might be the true identity of the endothelial cannabinoid receptor [479, 492], however the pharmacological profiles of GPR55 and GPR18 do not match that of the endothelial receptor [131] and the vasodilatory effects of Abn-CBD persist in $GPR55^{-/-}$ animals [493]. Clearly further work is required

to uncover the true identity of the endothelial cannabinoid receptor. Nevertheless, taken together these above studies demonstrate that numerous endo, phyto and synthetic cannabinoids target a range of GPCRs other than CB_1 or CB_2.

4.1.6 Off-target effects at non-GPCR targets

Peroxisome proliferator-activated receptors

Peroxisome proliferator-activated receptors (PPARs) are nuclear restricted proteins that function as ligand activated transcription factors, whereby ligand binding causes their dimerisation with the retinoid X receptor, DNA binding and transcriptional regulation [494]. There are three PPAR isoforms, PPARα, PPARβ and PPARγ, and it is not surprising that cannabinoids target these proteins as their classical agonists are all lipid-like compounds. Whilst the activity of cannabinoid compounds at PPARβ has not been tested, AEA, Δ9-THC, WIN55,212-2 and rimonobant all act as agonists of PPARα in the low micromolar range [495, 496]. Additionally, AEA, 2-AG, Δ9-THC, CP55,940, WIN55,212-2 and rimonobant all act as agonists at PPARγ, again in the low micromolar range [495, 496].

Transient receptor potential channels

The TRP family consists of membrane ion channels with a common protein topology; six transmembrane spanning domains containing a non-selective cation pore [497]. The TRP family comprises six subgroups and these are involved in sensing a large range of stimuli, including temperature, pain, osmotic pressure and various noxious stimuli [498]. Currently, endocannabinoids have been demonstrated to interact with six different TRP members spanning three different subgroups. TRPV1 was the first TRP protein to be cloned and famously binds capsaicin, naturally found in chilli peppers, to cause the classic sensation of 'heat' [499]. It is now well established that cannabinoids can bind and activate TRPV1, as multiple studies have shown that

AEA, CBD, HU201 and JWH015 all act as TRPV1 agonists (see [131]). Alongside, CBD, cannabinol, Δ9-THC and CP55,940 have been demonstrated to activate TRPV2 in HEK293 cells overexpressing this protein and CBD has been shown to activate TRPV2 in primary rat dorsal root ganglion neurones [500]. Furthermore, micromolar concentrations of CBD and Δ9-THC active TPRV3 in HEK293 cells overexpressing the rat TPRV3 channel [501] and AEA, 2-AG and CBD can bind and activate the TRPV4 channel [501, 502]. Additionally, cannabinoids can also agonise TRP channels from different subgroups, as AEA, Δ9-THC, cannabinol, WIN55,212-2 and AM1241 all act as TRPA1 agonists in transfected cell systems [503–505], and WIN55,212-2 and AM1241 are also active in primary cells, agonising TRPA1 in primary neuronal cultures [504]. However, cannabinoids do not only act as TRP agonists, as they have been found to inhibit the function of TRPM8. TRPM8 is involved in temperature sensation and can bind methanol, which causes the 'cooling' effect of this compound [506, 507]. Recent data has found that AEA, Δ9-THC and CBD potently antagonise methanol-induced rises in intracellular Ca^{2+} levels in both HEK293 cells expressing TRPM8 and in primary dorsal root ganglion neurones, displaying IC_{50} values in the nanomolar range [503, 508].

Voltage-gated Na^+ channels

Numerous studies exist demonstrating that cannabinoids can inhibit the function of voltage-gated Na^+ channels (Na_Vs). AEA, 2-AG, CP55,940 and WIN55,212-2 all inhibit Na_Vs in synaptosomes isolated from rat brain [509–512]. Furthermore, WIN55,212-2 has been demonstrated to inhibit Na_Vs in rat ganglionic neuronal cultures [513] whereas AEA was shown to antagonise Na_Vs not only in rat dorsal root ganglion neurones [514], but also in rat ventricular myocytes [515]. Recently, evidence for cannabinoid blockade on murine and human Na_Vs has been provided by Hill *et al* who found that CBD blocks Na_Vs in human and murine neuronal cell cultures, but also that CBD specifically blocks $Na_V1.1$. $Na_V1.2$ and $Na_V1.5$ in CHO cells expressing these channels [516].

Voltage-gated K^+ channels

A wide range of K^+ channels are blocked by multiple cannabinoids. Both AEA and 2-AG have been demonstrated to inhibit the function of K_{ATP} channels with IC_{50} values in the low micromolar range [517, 518]. Alongside these findings, CP55,940, WIN55,212-2 and rimonabant have been shown to inhibit the TASK-1 K^+ channel [131]. Alongside TASK-1, AEA has also been found to inhibit the TASK-3 and TREK-1 K^+ channels [131, 519]. Furthermore, a variety of K_V voltage-gated K^+ channels are blocked by cannabinoids, with $K_V1.2$ inhibited by AEA and Δ9-THC [520], $K_V1.5$ inhibited by AEA and 2-AG [521, 522], $K_V3.1$ blocked by AEA [523] and finally $K_V4.3$ inhibited by both AEA and 2-AG [524]. Although most of these above studies were conducted using transfected cell systems, cannabinoid blockade of K_V channels has been demonstrated in primary tissues. In patch clamping experiments, AEA and WIN55,212-2 inhibit K^+ currents in a CB_1/CB_2-independent manner in both retinal ganglion cells and rat aorta smooth muscle cells with IC_{50} values in the micromolar range [525, 526].

Voltage-gated Ca^{2+} channels

A wide range of voltage-gated Ca^{2+} channels are also inhibited by various cannabinoid ligands. Of the T-type Ca^{2+} channels, $Ca_V3.1$, $Ca_V3.2$ and $Ca_V3.3$ have all been shown to be antagonised by AEA, Δ9-THC, CBD and NAGly in both transfected cells and primary murine sensory neurones [131]. Furthermore, native T-type Ca^{2+} channels are also blocked by Δ9-THC [527] and WIN55,212-2 has been shown to block Ca^{2+} transients in rat retinal glial cells with an IC_{50} of 4 μM [528]. These glial cells were shown to express the $Ca_V1.2$, $Ca_V3.1$, $Ca_V3.2$ and $Ca_V3.3$ channels and importantly WIN55,212-2 blockade of Ca^{2+} transients was CB_1/CB_2-independent [528]. Further to this, 2-AG blocks L-type and P-type Ca^{2+} channels, AEA blocks L-, N-, P- and PQ-type Ca^{2+} channels and WIN55,212-2 has been shown to inhibit N-, P- and PQ-type Ca^{2+} channels [515, 529–531].

Ligand-gated ion channels

Alongside the voltage-gated ion channels, cannabinoids have also been demonstrated to inhibit ligand-gated ion channels. The 5-hydroxytryptamine 3 (5-HT_3) receptor is a ligand-gated ion channel permeable to Na^+, K^+ and Ca^{2+} and its activation by 5-HT can be antagonised by AEA, Δ9-THC, CP55,940, WIN55,212-2 amd JWH015 [131, 532]. Numerous isoforms of nicotinic acetlycholine receptors can also be inhibited by cannabinoid ligands. As their name implies, these ion channels are activated by nicotine alongside their endogenous ligand acetlycholine, and are mainly permeant to Na^+ and K^+. The first evidence that cannabinoids can directly inhibit nicotinic acetlycholine receptors came from Oz *et al* who demonstrated that in *Xenopus* oocytes expressing α_7-nicotinic acetlychoine receptors AEA, 2-AG and CP55,940 all inhibited acetlycholine binding with IC_{50} values of 229, 168 and 2700 nM respectively [533–535]. Recent work has now shown that cannabinoid blockade of α_7-nicotinic acetlycholine receptors also occurs in primary tissue, as Mahgoub *et al* not only demonstrated that CBD can inhibit acetlycholine function in *Xenopus* oocytes expressing α_7-nicotinic acetlycholine receptors, but also found that this subtype was blocked by CBD in rat hippocampal neurones [536]. Furthermore, other nicotinic acetlycholine receptor subtypes are targeted by cannabinoids as WIN55,212-2 inhibits native nicotinic acetlycholine receptors ($IC_{50} = 3\ \mu M$) in rat ganglionic neurones [537] and the α_4/β_2 nicotinic acetlycholine receptor is antagonised in both overexpressing cells and in synaptosomes isolated from rat thalamus by AEA [538, 539].

4.2 Rationale for the experiments presented in this chapter

In my previous chapter, I have clearly demonstrated that compounds classically thought to be specific CB_2 agonists, in fact elicit macrophage chemotaxis by activating at least one other non-CB_1/CB_2 GPCR. This provides the first report of an off-target effect for many of the synthetic cannabinoids used in this study. As this off-target action impacts upon macrophage chemotaxis, a crucial cellular function, and these cells play a key role in multiple inflammatory pathologies, identification of the off-target GPCR(s) will not only allow a greater understanding of cannabinoid biology and CB_2 ligand pharmacology, but may afford a new therapeutic target for the management of inflammatory diseases.

Therefore, the experimental aims of this chapter are to:

- Characterise the expression profile of GPCRs in bio-gel elicited macrophages
- Functionally test the ability of JWH133 and HU308 to activate candidate GPCRs
- Use ligand-directed virtual screening, combined with medicinal chemistry and photoaffinity labelling, to discover and develop novel tool compounds that will aid in the identification of the off-target GPCR(s)

It is important to note that I did not personally synthesise any of the novel tool compounds that were generated in order to carry out my final aim. These were all synthesised by students in the Department of Chemistry, namely Rebecca Hancock, Minjun Yang and Ryan Davies. Instead, I was involved in discussions surrounding the direction of the SAR studies and I conducted the biological testing of the compounds using primary murine macrophages.

4.3 Results

4.3.1 Bio-gel elicited macrophages express 124 GPCRs

In order to discover the GPCR(s) responsible for the off-target effects of the chemotaxis positive CB_2 agonists, I wanted to firstly identify exactly which GPCRs bio-gel elicited macrophages express. This will allow the narrowing of the candidate GPCR pool and will also allow results obtained using different approaches to be cross-checked against this GPCR expression profile. I isolated macrophages from bio-gel elicited PECs by adhesion, extracted total mRNA and made cDNA. I then used a 384 well murine GPCR expression array from Applied Biosystems to determine their receptor expression complement. The expression cutoff Ct value was set at 32, above which genes were deemed not expressed.

Of the 354 receptors present on the array, 124 GPCRs were deemed to be present in bio-gel elicited macrophages, with varying degress of expression. Example RT-PCR cuvres for GPCRs covering the expression range seen are shown in figure figure 4.1. Breaking these GPCRs into different expression groups, sixteen were very highly expressed (Ct values of up to 23) and reassuringly this group contained many macrophage-associated GPCRs; for example Emr1 (F4/80) and C5aR1, whose RT-PCR traces are shown in figure 4.1A and B respectively, and also CCR1, 2 and 5, C3aR, CXCR4, and FPR1 [47]. 25 receptors were expressed at a high level (Ct values of greater than 23 but less than 25), with this group containing the putative cannabinoid receptor GPR18 and CB_2, with an average Ct values of 24.8 (Fig 4.1C and D), alongside other macrophage-associated receptors such as CX_3CR1 (fractalkine receptor). Thirty four GPCRs were expressed at a medium level (Ct values of greater than 25 but less then 29) and example traces for GPR120 and CCR3, both members of this group, can be seen in figure 4.1E and F. Forty nine GPCRs were found to be expressed at a low level (Ct values greater than 29 but lower than 32), including GPR55 (Fig 4.1G), and 230 were deemed not to be expressed (either

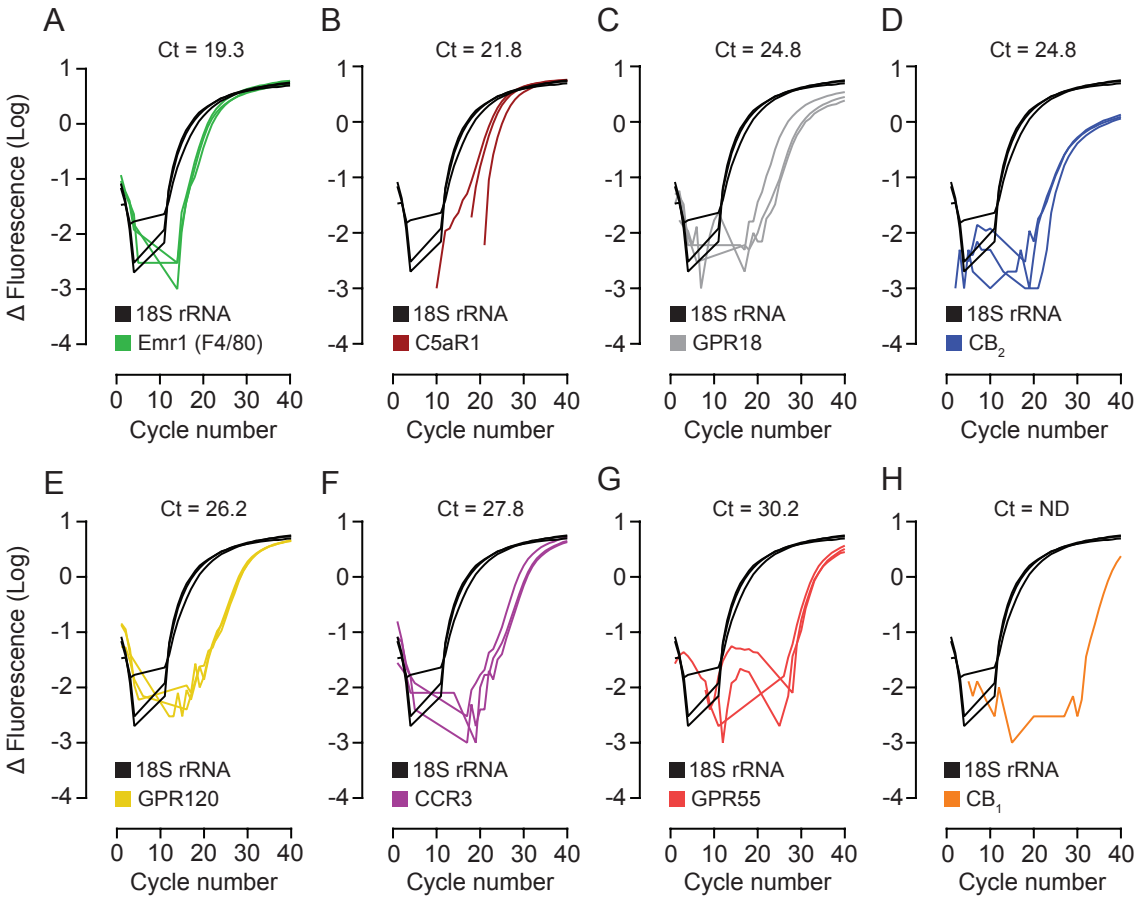

Figure 4.1 Representative real-time PCR traces of selected GPCRs from the bio-gel macrophage GPCR expression array. cDNA was prepared from enriched bio-gel macrophages and GPCR expression determined by RT-PCR using a 384-well murine GPCR Taqman GPCR expression array. Representative RT-PCR curves for (A) Emr1 (F4/80), (B) C5aR1, (C) GPR18, (D) CB_2, (E) GPR120, (F) CCR3, (G) GPR55 and (H) CB_1, with the Ct value for each GPCR. The RT-PCR curves for the 18S rRNA housekeeping control are shown for comparison (black lines). Each curve is derived from one biological replicate, with n = 3 experiments shown. For (H) two of the three experiments had no detectable signal.

as they had a Ct value of greater than 32, or no expression was detectable in the assay) with CB_1 being an important example (Fig 4.1H). This data is summarised in Table 4.1. Therefore, this GPCR expression profile serves as an important starting point for the identification of the GPCR(s) responsible for CB_2 agonist-induced macrophage chemotaxis.

Expression Category	**Ct Value Range**	**Count**
Very high	Less than 23	16
High	23 to 25	25
Medium	25 to 29	34
Low	29 to 32	49
Total receptors expressed		**124**
Not expressed	Over 32 or not detected	230
Total receptors in the assay		**354**

Table 4.1 Bio-gel macrophage GPCR expression summary.

4.3.2 GPR18 and GPR55 are not responsible for the off-target effects of JWH133 and HU308

A body of literature exists implicating both GPR18 and GPR55 as potential cannabinoid receptors [131, 467, 477]. Since I found that both receptors were expressed in bio-gel elicited macrophages (Fig 4.1C and G) and activation of GPR55 by L-α-lysophosphatidylinositol causes the directed migration of human breast cancer cells [540] and GPR18 has been shown to mediate 2-AG-induced chemotaxis of a microglial cell line [479, 480], I set out to determine whether either receptor was responsible for the off-target effects of JWH133 and HU308. N-terminal tagged receptor constructs were transfected into CHO cells using electroporation and surface receptor levels determined by flow cytometry after approximately 16 hours. In comparison to cells transfected with empty vector (blue histogram), CB_2 (Fig

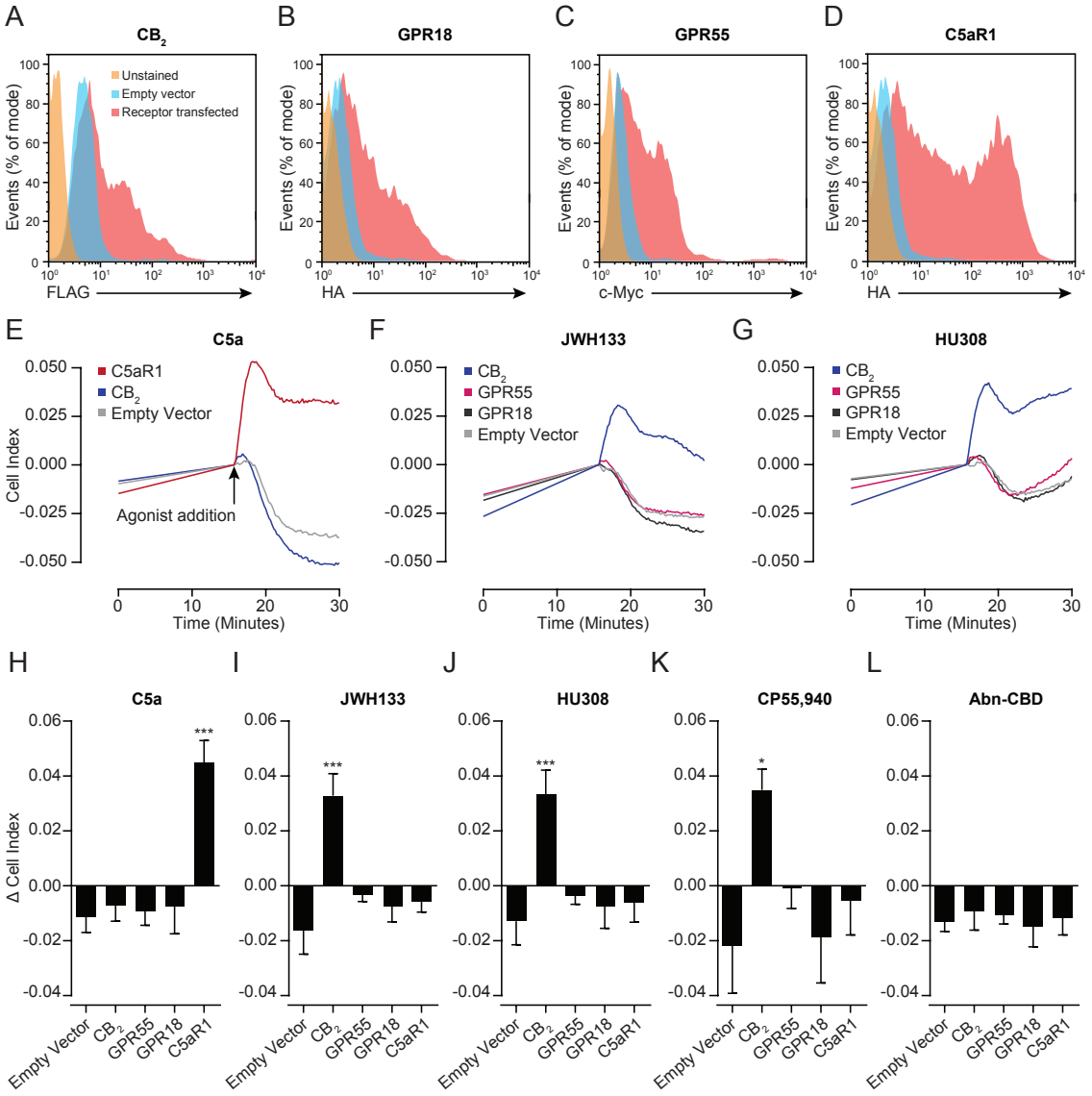

Figure 4.2 JWH133 and HU308 do not elicit cytoskeletal rearrangements in CHO cells expressing murine GPR18 or GPR55. CHO cells (1 x 10^6) were mixed with 2 μg of empty or GPCR-containing vector, transfected via electroporation and left overnight at 37°C, 5% CO_2 to allow tagged GPCR expression. (A-D) GPCR surface levels were determined by flow cytometry and representative histograms are shown. Cells transfected with empty vector alone were used to determine non-specific antibody staining. (A) FLAG-CB_2, (B) HA-GPR18 and (C) c-Myc-GPR55 all had similar expression levels. (D) HA-C5aR1 was used as a positive control and displayed high surface levels. (E-L) Transfected CHO cells were plated into a 96 well E-plate (25,000 cells) and left overnight at 37°C, 5% CO_2 to reach a stable baseline. Afterwards, cells were stimulated with vehicle (0.3% DMSO), C5a (10 nM) or cannabinoid (10 μM). (H) Quantification of C5a-induced responses found that only C5aR1 transfected cells responded to C5a (10 nM; E - Representative trace). JWH133 (F and I), HU308 (G and J) and CP55,940 (K) only caused significant responses in CB_2 transfected cells. Importantly, cells transfected with GPR18 or GPR55 did not respond to either JWH133 or HU308 (I and J). Abnormal-cannabidiol (Abn-CBD; 10 μM) did not elicit a response in any of the GPCR transfected cells (L). Data are mean± SEM, n = 3-6 biological replicates with 2-3 technical replicates per condition. Statistical analysis was conducted by one-way ANOVA with Dunnett's multiple comparisons correction. * P <0.05, *** P <0.001, comparing all samples to empty vector transfected cells.

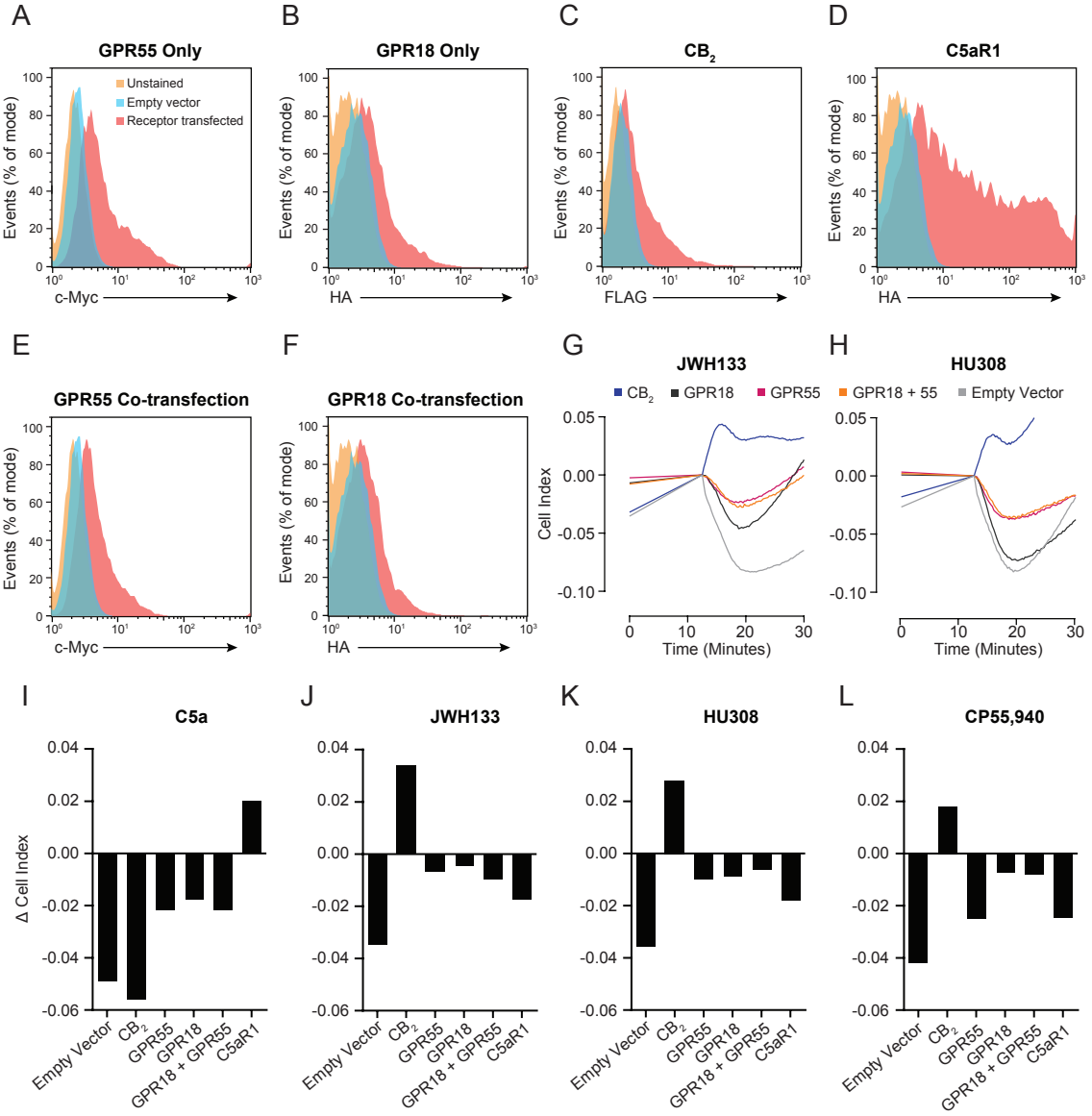

Figure 4.3 JWH133 and HU308 do not elicit cytoskeletal rearrangements in CHO cells co-expressing murine GPR18 or GPR55. (A-F) CHO cells (1 x10^6) were mixed with 2 μg empty vector, GPCR vector alone or GPR18 and GPR55 expression vectors, transfected by electroporation and left overnight at 37°C 5% CO_2 to allow tagged receptor expression. Cells were then stained with anti-tag antibodies and surface GPCR expression for (A) GPR55, (B) GPR18, (C) CB_2, (D) C5aR1 or (E and F) GPR55 and GPR18 co-transfected cells determined by flow cytometry. Cells transfected with empty vector were used to determine non-specific antibody staining (blue histogram). (G-L) Transfected CHO cells were plated into a 96 well E-plate (25,000 cells) and left overnight at 37°C, 5% CO_2 to reach a stable baseline. Afterwards, cells were stimulated with vehicle (0.3% DMSO), C5a (10 nM) or cannabinoid (10 μM). Representative traces of cells transfected with empty vector (light grey line) CB_2 (blue line), GPR18 (black line), GPR55 (pink line) or GPR55 and GPR18 together (orange line) stimulated with (G) JWH133 or (H) HU308. (I) Quantification of C5a-induced responses found that only cells transfected with C5aR1 responded to C5a. Quantification of (J) JWH133, (K) HU308 and (L) CP55,940-induced responses found that only cells transfected with CB_2 responded to cannabinoid treatment. Data are mean only, n = 1 biological replicate with 2-3 technical replicates per condition.

4.2A), GPR18 (Fig 4.2B) and GPR55 (Fig 4.2C) transfected cells had surface expression (red histogram) that was comparable across all three GPCRs (∼50% positive). C5aR1 transfected CHO cells (selected as a positive control) had very high surface receptor levels (Fig 4.2D; ∼75% positive). I then measured the ability of the chemotaxis positive CB_2 agonists JWH133 and HU308, the chemotaxis negative ligand CP55,940 and C5a to induce cytoskeletal rearrangement in receptor transfected cells. Stimulation with 10 nM C5a (Representative trace − Fig 4.2E) elicited significant positive signalling in C5aR1 transfected cells only (Fig 4.2H), confirming the assay worked as intended. Stimulation of cells with 10 μM JWH133 (Fig 4.2F and I), HU308 (Fig 4.2G and J) or CP55,940 (Fig 4.2K) only caused significant cytoskeletal rearrangement in CB_2 transfected cells. Abn-CBD caused no response in any of the receptor transfected cells (Fig 4.2L).

As multiple GPCRs can form homo/hetrodimers that can modulate downstream signalling at either, or both receptors, and cannabinoid receptors including CB_1, CB_2 and GPR55 have been demonstrated to form hetrodimers [541–544], I wanted to examine whether the co-expression of GPR18 and GPR55 is needed for the off-target effects of CB_2 agonists. When transfected into CHO cells singularly, GPR55 (Fig 4.3A) and GPR18 (Fig 4.3B) had similar surface expression levels, which were comparable to that of CB_2 transfected cells (Fig 4.3C). When co-transfected, GPR55 (Fig 4.3E) and GPR18 (Fig 4.3F) were both detectable on the cell surface and at comparable levels to cells transfected with either receptor alone (GPR55 - Fig 4.3A vs E; GPR18 Fig 4.3B vs F). As seen previously, C5aR1 transfected cells had very high surface receptor expression (Fig 4.3D) and C5a only elicited positive signalling in these cells (Fig 4.3I). Stimulation with 10μM JWH133 (Fig 4.3G and J), HU308 (Fig 4.3H and K) or CP55,940 (Fig 4.3L) only caused positive signalling in CB_2 transfected CHO cells; cells co-transfected with GPR18 and GPR55 did not respond to any of the ligands tested (Fig 4.3G-L). Taken together, this data suggest that GPR18 and GPR55, both of which are expressed in bio-gel elicited macrophages, are not responsible for the off-target effects of JWH133 and HU308.

4.3.3 Functional screening of JWH133 at 241 human GPCRs

In an attempt to find the receptor responsible for CB_2 agonist-induced macrophage chemotaxis, the ability of JWH133 (10 μM) to induce β-arrestin recruitment at 241 GPCRs was examined using the Discoverx PathHunter® eXpress β-Arrestin GPCR Assay system. The screen was split into two halves, the first being the GPCRMax panel, which contains CHO cells transfected with GPCRs that have well characterised agonists (Fig 4.4A - 168 receptors) and the second being the OrphanMax panel, which contains orphan GPCRs (Fig 4.4B - 73 receptors). Both reassuringly and unfortunately, JWH133 only gave robust β-arrestin recruitment in CB_1 and CB_2 transfected CHO cells (Fig 4.4A). Additionally, JWH133 was unable to induce β-arrestin recruitment in GPR18 or GPR55 transfected CHO cells (Fig 4.4B).

4.3.4 Functional testing of lipid binding GPCRs expressed in bio-gel elicited macrophages

These data, when combined with the GPCR expression array results detailed in table 4.1, allowed me to narrow down the list of candidate GPCRs that could be the off-target receptor. To begin, there were 46 receptors that were expressed in bio-gel elicited macrophages that were not included in the Discoverx β-arrestin screen. Next, there were 20 receptors that were not included on the expression array or in the functional screening. Therefore I have no functional data and limited expression data for these GPCRs and therefore, 66 receptors remain as viable candidates (notwithstanding the potential limitations of these experiments that will be discussed at the end of this chapter).

However, this number is still too large for me to screen all of these receptors for activity using CHO cells, as I did with GPR18 and GPR55. Instead, and as the endocannbinoids are lipids and the synthetic cannabinoids are highly lipophilic, I

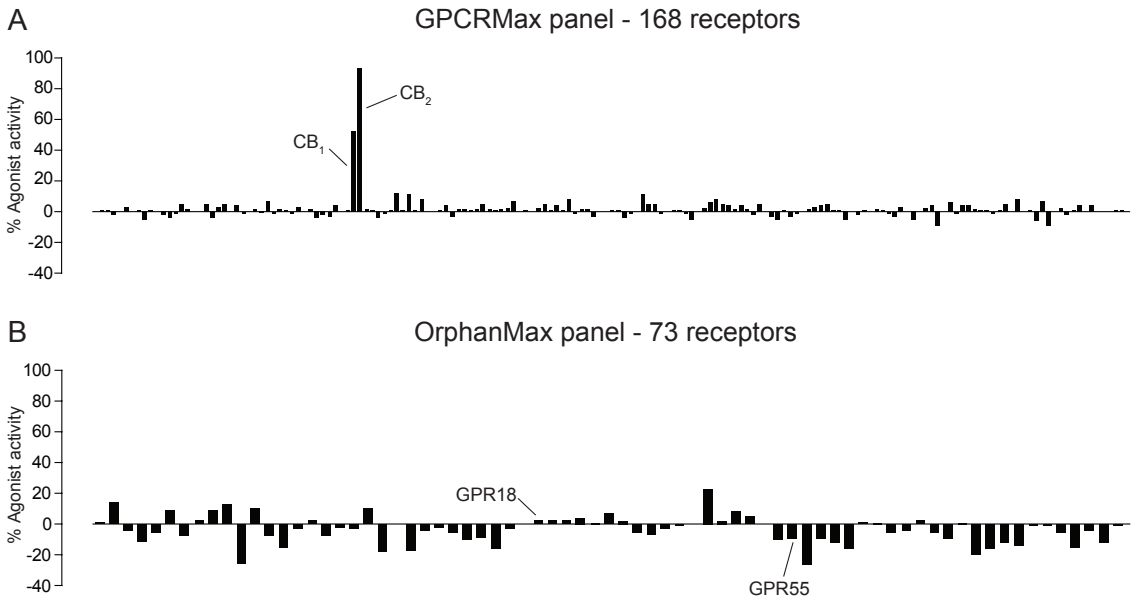

Figure 4.4 Out of 241 GPCRs, JWH133 only elicits β-arrestin recruitment at CB_1 and CB_2. JWH133 (10 μM) was tested for its ability to induce β-arrestin recruitment at 241 GPCRs, split over two panels, using the Discoverx PathHunter® eXpress β-Arrestin GPCR Assay system. (A) The GPCRMax panel was comprised of GPCRs with known and validated ligands. For this panel % Agonist activity is calculated as 100% x (mean of test sample − mean of vehicle control) / (mean MAX control ligand − Mean of vehicle control). JWH133 only caused β-arrestin recruitment at CB_1 and CB_2. (B) The OrphanMax panel was comprised of GPCRs without validated ligands. For this panel % Agonist activity is calculated as 100% x (mean of test sample − mean of vehicle control) / (mean of vehicle control). JWH133 did not elicit β-arrestin recruitment at either GPR18 or GPR55. Data are mean of technical duplicates.

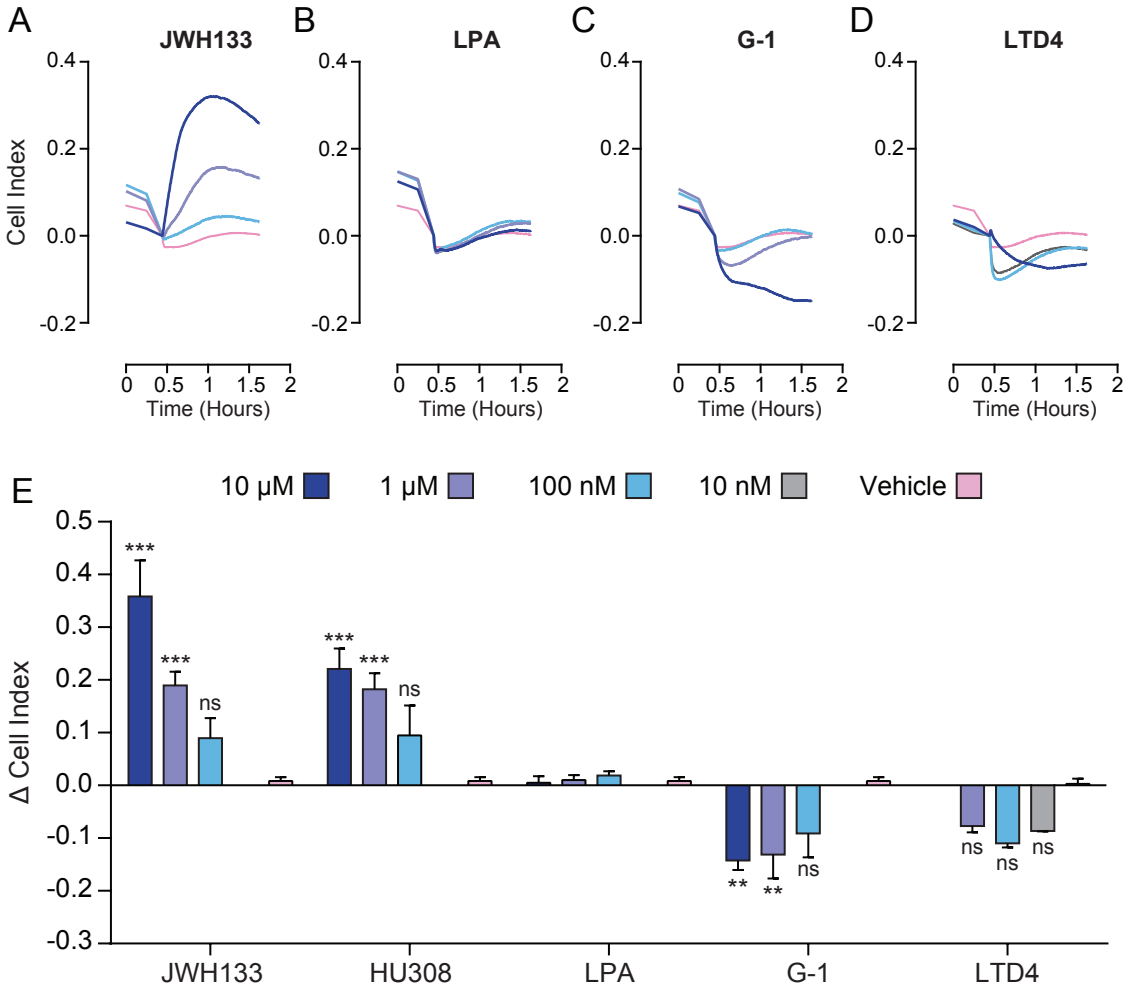

Figure 4.5 LPAR1, LPAR5, GPER1, CYSLTR1 and CYSLTR2 agonists do not elicit cytoskeletal responses similar to JWH133 or HU308 in bio-gel elicited macrophages. Bio-gel elicited PECs (5 x 10^4) were placed into a 96 well E-plate allowed to adhere for 2-3 hours at 37°C, 5% CO_2. Afterwards, cells were stimulated with vehicle (0.3% DMSO), HU308, (A) JWH133, (B) lysphosphatidic acid (LPA - a LPAR1 and 5 agonist), (C) G-1 (a GPER1 agonist) or (D) Leukotriene D4 (LTD4 - a CYSLTR1 and 2 agonist) at the indicated concentration. (E) Quantification of cytoskeletal rearrangement demonstrates that JWH133 and HU308 both cause positive changes in CI signal in a concentration-dependent manner. LPA, G-1 and LTD4 did not cause the same positive cytoskeletal signal. Data are mean+ SEM, n = 2-3 biological replicates with 2-3 technical replicates per condition. Statistical analysis was conducted by two-way ANOVA with Sidak's multiple comparisons correction. ns P >0.05, ** P <0.01, *** P <0.001.

decided to narrow down the candidate list by focussing on lipid binding GPCRs that met the following criteria; A lipid binding receptor that was determined to be expressed in bio-gel elicited macrophages, but was not included in the Discoverx β-arrestin functional screen. There are approximately 43 GPCR in the mouse that have been previously annotated as having lipid or lipid-like agonists, but only 5 of these met the above criteria. These were: Cysteinyl leukotriene receptor (CYSLTR) 1 and 2, G-protein coupled estrogen receptor 1 (GPER1) and lysophosphatidic acid receptor (LPAR) 1 and 5.

I began by attempting to transfect each receptor into CHO cells using pcDNA3.1 expression vectors, and then testing the ability of JWH133 and HU308 to elicit cytoskeletal rearrangement in these cells, as I had done with GPR18 and GPR55. However, expression of most of these receptors was poor to none in the CHO cell system and therefore I could not use this as a screening assay (data not shown). Instead, I decided to test whether agonists for these lipid GPCRs would elicit a cytoskeletal response kinetically similar to that induced by JWH133 or HU308 in bio-gel elicited macrophages. If a response was obtained with a similar magnitude and kinetics to the cannabinoids then this would hint that the compounds may be activating the same pathway(s). As I had seen previously, both JWH133 and HU308 caused positive changes in CI signal compared to vehicle alone, in a concentration-dependent manner (Fig 4.5A and E). However, lysophosphatidic acid (LPA), an agonist for both LPAR1 and LPAR5, did not elicit a cytoskeletal response at any concentration tested (Fig 4.5B and E). Furthermore, both G-1 (an agonist for GPER1) and leukotriene D4 (LTD4 - an agonist for both CYSLTR1 and 2) had an opposite response to JWH133 and HU308, causing a decrease in the CI signal, with the former reaching statistical significance (Fig 4.5C, D and E). Since no compound tested mimicked the response of JWH133 or HU308, it can be concluded that it is unlikely that LPAR1, LPAR5, GPER1, CYSLTR1 or CYSLTR2 is the macrophage receptor responsible for CB_2 agonist-induced macrophage chemotaxis.

4.3.5 Ligand based virtual screening discovers a novel chemoattractant chemical scaffold

As all efforts undertaken so far failed to identify the receptor responsible for CB_2 agonist-induced macrophage chemotaxis, I decided to take a different approach to hopefully increase the chance of finding the responsible receptor. In collaboration with Professor Angela Russell's group from the Department of Chemistry at the University of Oxford, ligand-directed virtual screening, combined with photoaffinity labelling, was chosen as an alternative approach for target identification.

Ligand-directed virtual screening relies on the hypothesis that compounds with similar shape and electrostatic properties have similar activities [425]. Therefore by comparing the chemical properties of a library of compounds against known active compounds, it is hoped that compounds closely matched to the input ligand(s) will retain the activity of interest [545]. Importantly, these compounds may have an entirely different 2 dimensional chemical scaffold and may provide a novel starting point for understanding a target or further drug discovery efforts.

Photoaffinity labelling involves the addition of a photoreactive group onto a compound of interest that is capable of covalently binding to any nearby molecule when irradiated with a specific wavelength of light [546]. Hopefully, the highly reactive intermediate species generated upon irradiation will covalently bond to the protein target of the small molecule. Alongside the photoreactive group, a reporter tag is normally incorporated into the compound, such as a biotin label, to allow for the enrichment and identification of covalently bound proteins. In order to incorporate both the photaffinity and reporter labels, detailed structure-activity relationship (SAR) studies are required to uncover areas of the lead scaffold where chemical modifications can be made without compromising on activity [546]. Furthermore, this approach has been used with success to uncover the targets of orphan compounds and examine ligand interactions with multiple GPCRs [546,547], providing confidence that this is a viable approach for GPCR identification. Importantly, this affords

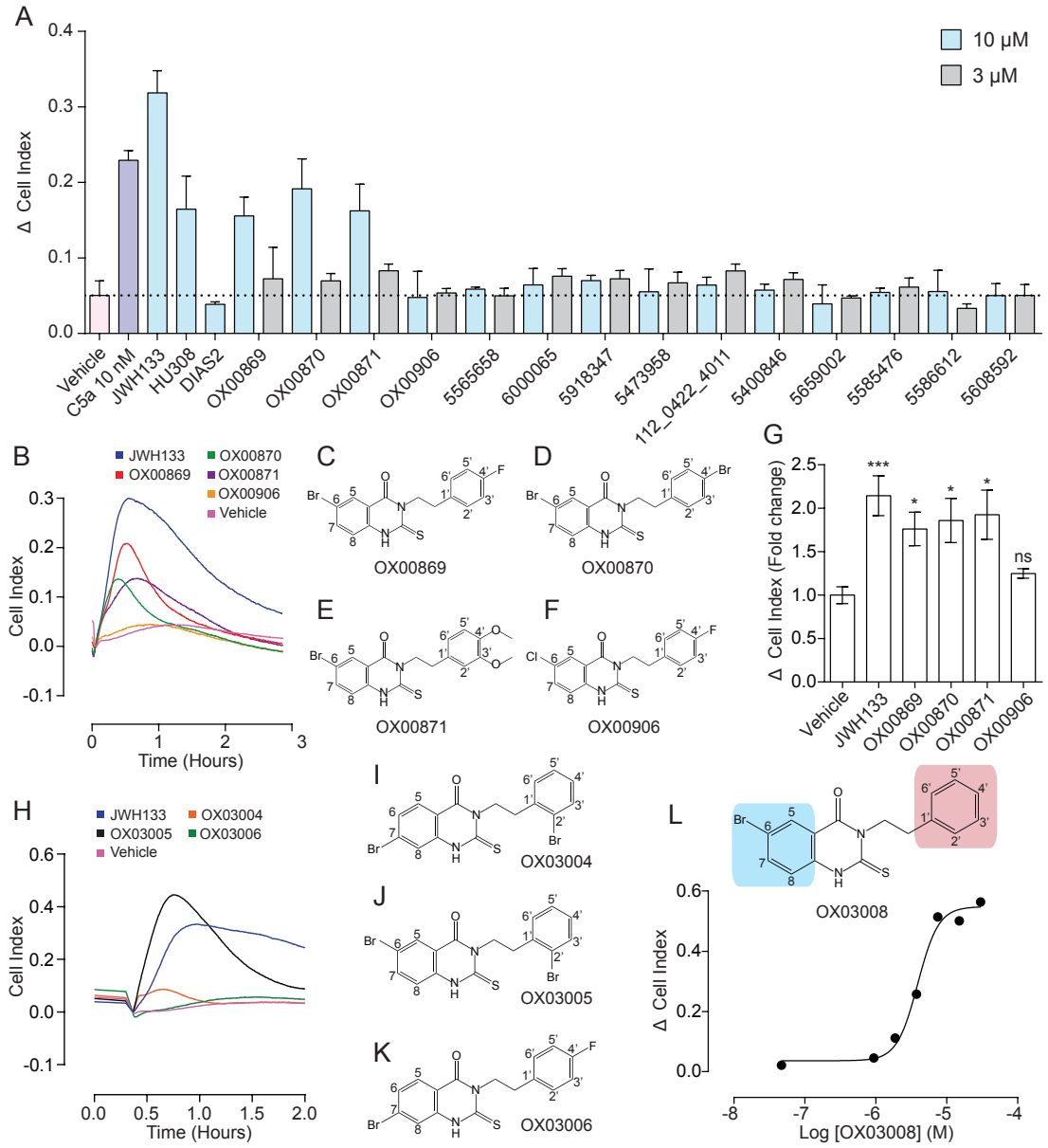

Figure 4.6 Virtual screening identifies a novel chemical scaffold that retains chemoattractant properties. Bio-gel elicited PECs were plated into a 96 well E-plate and allowed to adhere for 2-3 hours, after which they were stimulated with (A) vehicle (0.3% DMSO), C5a (10 nM), cannabinoid, or the top ranked hits from the virtual screen (10 and/or 3 μM) and the elicited response quantified. OX00869, -870 and -871 were the only compounds tested that gave a positive response. Interestingly, the chemically related compound OX00906 was inactive. A representative trace is shown in (B). Data are mean+ SD, n = 1 biological replicate with 3 technical replicates per condition. The chemical structures of OX00869, -870, -871 and -906 are shown in (C), (D), (E) and (F) respectively. Carbon numbering for important carbon atoms in the left hand side and right hand side phenyl rings is displayed for each compound. (G) Bio-gel elicited PECs were allowed to migrate towards vehicle (0.3% DMSO), OX00869, -870, -871 or -906 (10 μM) for 3-4 hours. Quantification found that JWH133, OX00869 and -870, -871 significantly induced macrophage chemotaxis. Data are mean± SEM, n = 4 biological replicates with 2-3 technical replicates per condition. (H) Bio-gel elicited PECs were stimulated with vehicle, JWH133, OX03004, -3005 or -3006 (10 μM) and cytoskeletal activity measured. The chemical structures of OX03004, -3005 and -3006 are shown in (I), (J) and (K) respectively. (L) Bio-gel elicited PECs were stimulated with vehicle or OX03008 at the indicated concentrations and cytoskeletal activity measured. The chemical structure of OX03008 is shown as an insert. Data are mean only from n = 1 representative biological replicate with 3 technical replicates for condition. Statistical analysis was conducted by one-way ANOVA with Dunnett's multiple comparisons correction. ns P >0.05, * P <0.05, *** P <0.001.

an unbiased method to identify the target responsible for CB_2 agonist-induced chemotaxis as it does not rely on pre-selection of candidate receptors. Furthermore, if the ligands have multiple GPCR targets this will also be uncovered as bio-gel elicited macrophages will be used for the cross-linking experiments.

Therefore an initial ligand based virtual screen was conducted in collaboration with Rebecca Hancock from the Department of Chemistry. The chemotaxis positive CB_2 agonists JWH133, HU308, L-759,656 and SER601 were modelled in 3D into their lowest energy conformation, due to the absence of known binding poses, and each used as the bait compound for a ligand-directed virtual screen. A library containing approximately 25,000 compounds was then compared against each reference ligand and ranked from high to low based on their combo score; a composite measure of how similar the test compound is to the reference ligand in both three dimensional shape and overall charge distribution. The top ranking compounds were then selected for functional testing using the 96 well cytoskeletal rearrangement assay.

The initial screen was conducted by testing ligands at 10 and 3 μM, to provide a measure of how concentration-dependent any activity seen may be, and three compounds were identified that caused macrophage cytoskeletal rearrangement with similar efficacy to that of HU308 (Fig 4.6A). These were OX00869, OX00870 and OX00871 and a representative trace of their activity in the cytoskeletal rearrangement assay can be seen in figure 4.1B. All of these compounds belonged to the same chemical class, being 2-thioxo-2,3-dihydroquinazolin-4(1H)-ones, and their 2 dimensional structures can be seen in figures 4.6C-E. OX00869, OX00870 and OX00871 all have a bromine at the 6 position on the left hand side phenyl ring but seem to tolerate different chemical constituents on the right hand side phenyl ring. Interestingly OX00906, which also belongs to the same chemical class and has a chlorine at the 6 position rather than a bromine (Fig 4.6F), did not induce macrophage cytoskeletal rearrangement (Fig 4.6A and B). Real-time chemotaxis analysis found that OX00869, OX00870 and OX00871 significantly induced macrophage chemotaxis with a similar efficacy to JWH133, whereas OX00906 was unable to act as a macrophage

chemoattractant (Fig 4.6G; all compounds tested at 10 μM). Importantly, this result highlights that hits in the cytoskeletal rearrangement screening assay translate into the real-time macrophage chemotaxis assay.

Next a further series of compounds were synthesised based on the initial hits to begin to understand the activity of the 2-thioxo-2,3-dihydroquinazolin-4(1H)-one series. OX03005 caused macrophage cytoskeletal rearrangement to a greater extent to that of JWH133, whereas OX03004 and OX03006 had minimal to no activity (Fig 4.6H). As opposed to OX03005 (Fig 4.6J) and the previous active compounds, the inactive OX03004 (Fig 4.6I) and OX03006 (Fig 4.6K) have a bromine at the 7 position on the left hand side phenyl ring, rather than the 6 position. Removal of any additional groups on the right hand side phenyl ring yielded OX03008, which caused concentration-dependent macrophage cytoskeletal rearrangement with an EC_{50} of 4 μM and the greatest efficacy seen so far in the series (Fig 4.6L - maximum ΔCI signal of $\sim$0.5). This therefore became the lead compound for more detailed SAR studies. For the purpose of this chapter, I will refer to the left hand side (LHS - Fig 4.6 - highlighted in blue) phenyl group, and the right hand side (RHS - Fig 4.6L - highlighted in red) phenyl group, when discussing the SAR studies conducted. We focussed on these two areas for compound SAR, as these are the easiest to functionalise.

4.3.6 SAR studies on the 2-thioxo-2,3-dihydroquinazolin-4(1H)-one series

To further examine the effect of bromine substitutions on the LHS phenyl ring, OX03009 was synthesised; an analogue of OX03008 that has a bromine at the 7 position rather than the 6 position (Fig 4.7A and B). Functional testing found that OX03009 was unable to elicit macrophage cytoskeletal rearrangement (Fig 4.7C). As chemical modifications are not tolerated at any point other than the 6 position on the LHS phenyl ring, this seemed the only position where the addition of a photoreactive

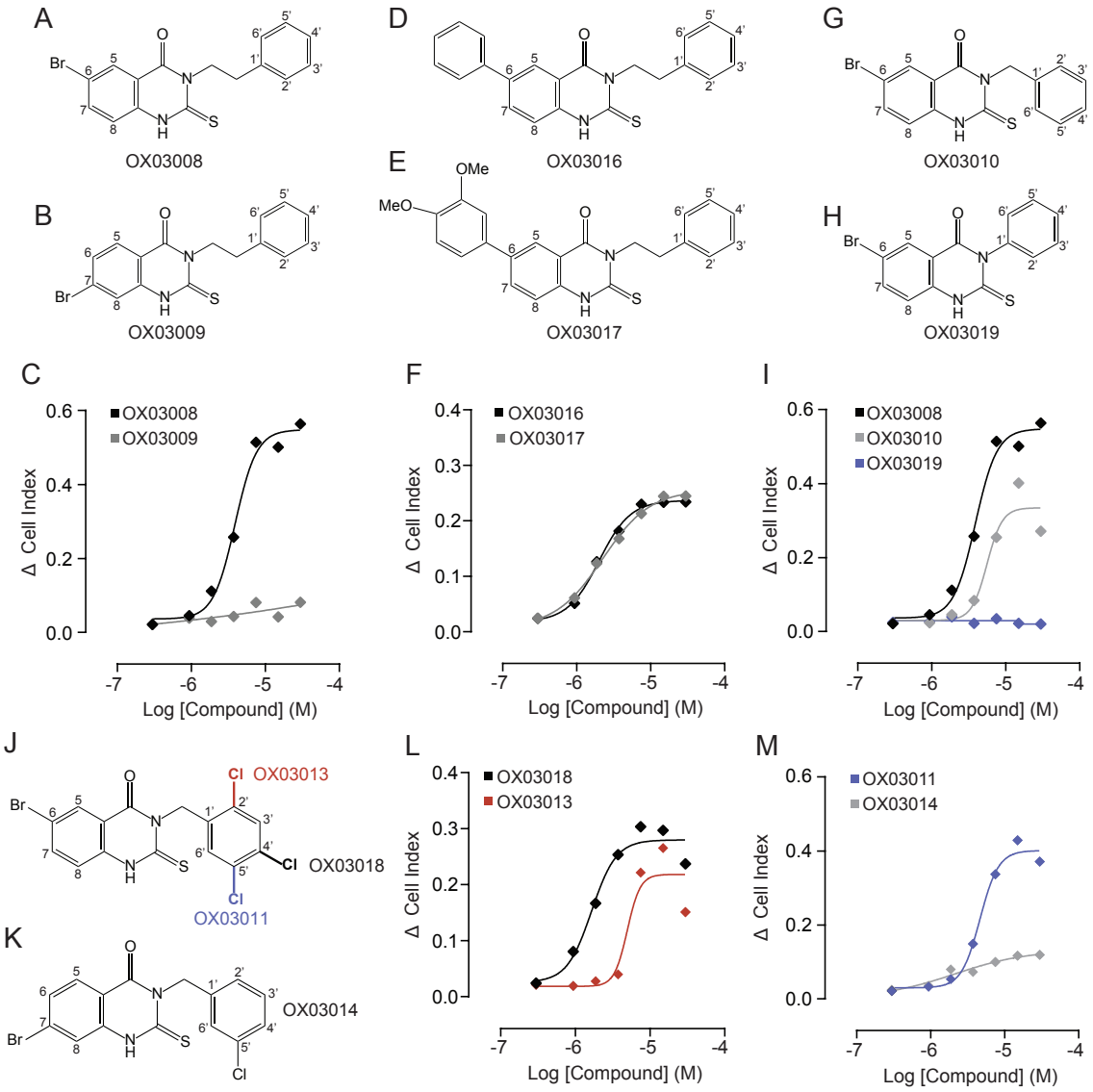

Figure 4.7 Structure activity relationship studies surrounding the 2-thioxo-2,3-dihydroquinazolin-4(1H)-one scaffold. (C, F, I, L and M) Bio-gel elicited PECs (5 x 10^4) were plated into a 96 well E-plate and allowed to adhere for 2-3 hours to reach a stable baseline prior to ligand stimulation. The chemical structures of (A) OX03008 and (B) OX03009. (C) Bio-gel PECs were stimulated with OX03008 or OX03009 at the indicated concentrations and changes in CI signal quantified. The chemical structures of (D) OX03016 and (E) OX03017. (F) Bio-gel PECs were stimulated with OX03016 or OX3017 at the indicated concentration and changes in CI signal quantified. (J) The chemical structures OX03011, OX03013, OX03018 and (K) OX03014. Bio-gel PECs were stimulated with (L) OX03013, OX03018, (M) OX03011 or OX03014 at the indicated concentrations and changes in CI signal quantified. Data are mean only, n = 1 biological replicate with 2 technical replicates per condition. For all compounds, atom numbers for important carbon atoms are shown. A 4-parameter non-linear regression model was fitted to the corresponding data sets using GraphPad Prism.

or reporter group might be tolerated. Therefore to examine how tolerant this position may be, large sterically bulky groups were added at the 6 position to determine what effect this would have on activity, with OX03016 containing a phenyl group (Fig 4.7D) and OX03017 containing a dimethoxyphenyl group (Fig 4.7E). Despite these large additions, both compounds retained activity, with slightly reduced efficacy, but comparable potency, to OX03008 (Fig 4.7F - EC_{50} values of 2 and 2.3 μM for OX03016 and OX03017 respectively). This therefore indicates that this position would be suitable for the addition of a functional group.

All of the compounds in the series so far have a 2 carbon chain linking the RHS phenyl group to the chemical core. Unfortunately however, this makes them difficult to work with as the precursor compounds required for their synthesis are hard to obtain as they can be used to make compounds currently controlled by the Home Office. To try and overcome this issue, compounds were synthesised with different carbon chain lengths to see what effect this would have on activity. OX03010 contains one carbon in the linking chain (Fig 4.7G), whereas OX03019 has no linking chain at all (Fig 4.7H). Interestingly, decreasing the chain length from 2 down to 0 caused a step reduction in activity, with OX03008 being the most active, OX03010 having intermediate activity and OX03019 displaying no activity at all (Fig 4.7I). However, as the reduction in activity was modest going from 2 to 1 carbon atoms in the linker, and the EC_{50} was very similar to OX03008 (5.6 μM), it was decided to adopt the one carbon linker for future SAR work to maximise the speed and ease of compound synthesis.

4.3.7 SAR studies on the right hand side phenyl group

Alongside the LHS phenyl group, the RHS phenyl group was an obvious place for functionalisation, given the route of compound synthesis and the fact that compounds detailed in figures 4.6C, D, E and J have numerous substitutions around this ring without reduced activity. We began by substituting chlorine groups around the RHS

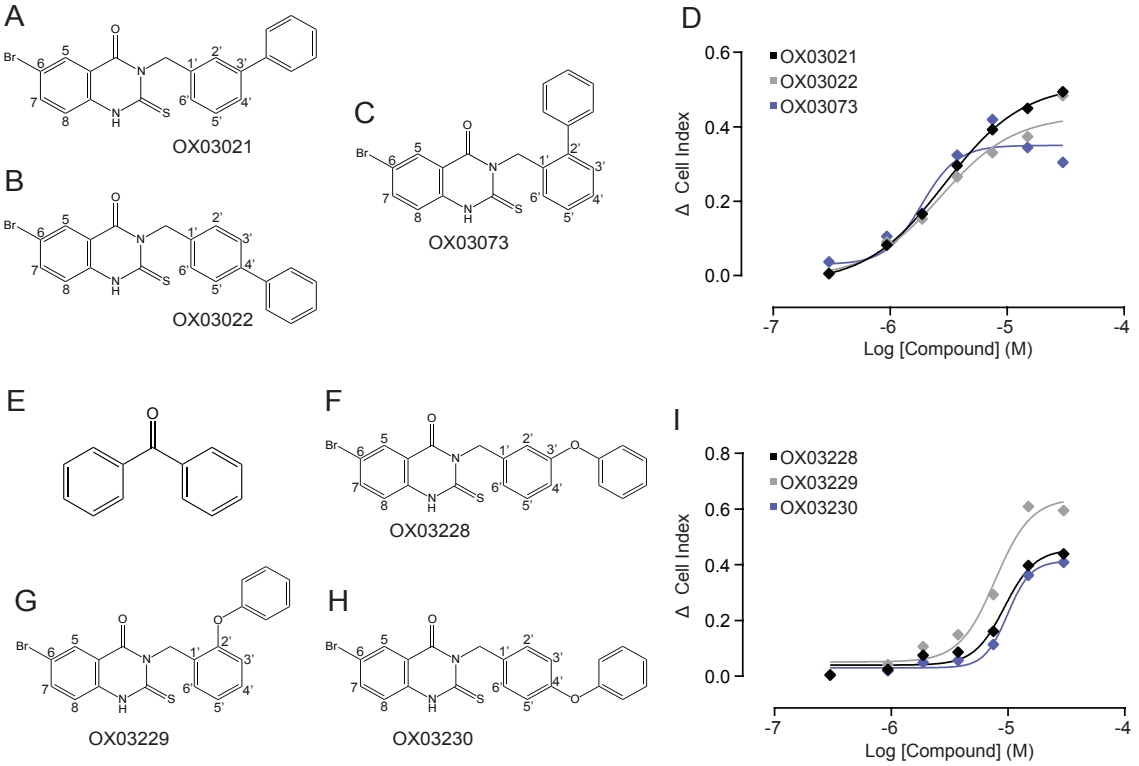

Figure 4.8 SAR studies on the right hand side of the 2-thioxo-2,3-dihydroquinazolin-4(1H)-one scaffold identify positions suitable for the addition of a photoaffinity group. Bio-gel elicited PECs (5 x 10^4) were plated into a 96 well E-plate and allowed to adhere for 2-3 hours to reach a stable baseline prior to ligand stimulation. The chemical structures of (A) OX03021, (B) OX03222 and (C) OX03073. (D) Bio-gel elicited PECs were stimulated with OX03021, OX03022 or OX03073 at the indicated concentrations and the change in CI signal quantified. (E) The chemical structure of the photoreactive benzophenone group. The chemical structures of (F) OX03228, (G) OX03229 and (H) OX03230. (I) Bio-gel elicited PECs were stimulated with OX03228, OX03229 or OX03230 at the indicated concentrations and the change in CI signal quantified. Data are mean only, n = 1 biological replicate with 2 technical replicates per condition. A 4-parameter non-linear regression model was fitted to the corresponding data sets using GraphPad Prism.

and synthesised OX03013, OX03018 and OX03011 with chlorine at the 2', 4' and 5' positions respectively, and a bromine at the 6 position (Fig 4.7J). OX03014 was also synthesised containing a chlorine at the 5' position, but a bromine at the 7 position (Fig 4.7K). Functional testing found that chlorine substitution had no effect on compound efficacy (Fig 4.7L and M). The potency of OX03011 and OX03013 was similar to that of OX03010, with EC_{50} values of 4.6 and 5 μM respectively, whereas OX03018 had an almost 3-fold increase in potency compared to OX03010, with an EC_{50} value of 1.7 μM. As previous, the presence of a bromine at the 7 position on the LHS caused a marked reduction in activity (OX03014; Fig 4.7M).

To begin to understand where a photoreactive group may be placed on the RHS phenyl ring, sterically bulky phenyl groups were added at various positions to see what effect this would have on compound activity. OX03021 (Fig 4.8A), OX03022 (Fig 4.8B) and OX03073 (Fig 4.8C) have phenyl groups added at the 3', 4' and 2' positions respectively. Functional analysis found that all three compounds caused concentration-dependent macrophage cytoskeletal rearrangement with EC_{50} values of 3, 2.8 and 2.1 μM for OX03021, OX03022 and OX03073 respectively (Fig 4.8D). Interestingly, all three were more efficacious than their parent compound OX03010. As large bulky groups can be easily accommodated at multiple positions around the RHS phenyl ring, this seemed like the ideal area of the compound for the addition of the photoreactive group. There are three main types of photoactive groups that are commonly used; phenylazide, phenyldiazirine and benzophenone [546]. Due to the chemistry of the 2-thioxo-2,3-dihydroquinazolin-4(1H)-one scaffold, the benzophenone is the simplest group to add to the RHS and its chemical structure is shown in figure 4.8E. To mimic not only the steric bulk, but also the charge imparted by the oxygen atom in the benzophenone group, compounds were generated containing an oxygen-linked phenyl group on the RHS. OX03228 (Fig 4.8F), OX03229 (Fig 4.8G), and OX3230 (Fig 4.8H) have this group at the 3', 2' and 4' positions respectively. Functional testing found that the compounds were highly efficacious, giving ΔCI signals as high as 0.8 (Fig 4.8I), however all three were approximately half as potent

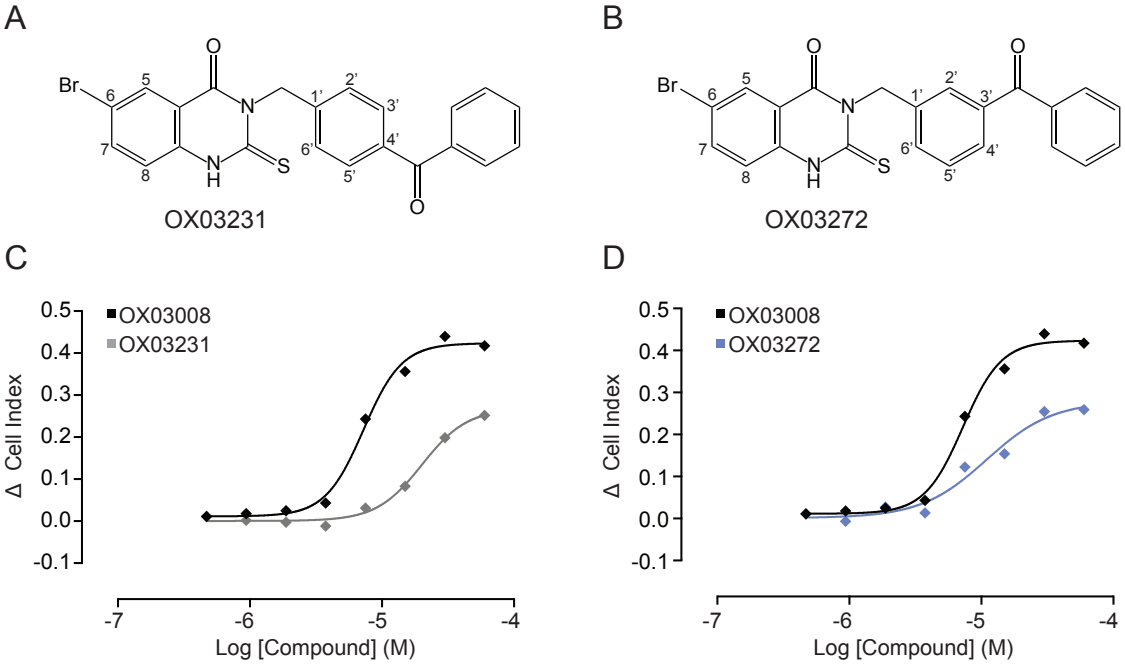

Figure 4.9 Compounds with a photoreactive benzophenone group at the 3' or 4' position in the right hand phenyl ring retain the ability to elicit macrophage cytoskeletal rearrangement. The chemical structures of (A) OX03231 and (B) OX03272. (C and D) Bio-gel elicited PECs (5 x 10^4) were plated into a 96 well E-plate and allowed to adhere for 2-3 to reach a stable baseline prior to ligand stimulation. Bio-gel elicited PECs were stimulated with (C) OX03231 or (D) OX03272, alongside OX03008 at the indicated concentrations and cytoskeletal changes measured. Data are mean only, n = 1 biological replicate with 2 technical replicates per condition. A 4-parameter non-linear regression model was fitted to the corresponding data sets using GraphPad Prism.

as the parent compound OX03010, with EC_{50} values of 9.3, 7.8 and 9.9 μM for OX03228, OX03229 and OX03230 respectively. Nonetheless, these results imply that a benzophenone photoactive group will be tolerated at any of these RHS positions.

4.3.8 Compounds containing the photoactive benzophenone group retain functional activity

In light of the above findings, two compounds were synthesised containing the benzophenone photoactive group on the RHS. OX03231 (Fig 4.9A) and OX03272 (Fig 4.9B) contain a benzophenone group at the 4' or 3' position respectively. Functional testing found that OX03231 (Fig 4.9C) and OX03272 (Fig 4.9D) elicited concentration-dependent macrophage cytoskeletal rearrangement with EC_{50} values of 20 and 10 μM respectively. Although not as efficacious as OX03008 or the benzophenone mimics, the compounds retained enough activity to be able to be used in future cross-linking experiments. Furthermore it should be noted that the ΔCI signal seen with these compounds of around 0.3 is comparable to that of the original hit compounds, as well as JWH133, which all acted as macrophage chemoattractants.

4.4 Discussion

I began this results chapter with three aims; firstly to characterise the GPCR expression profile of bio-gel elicited macrophages, secondly to functionally test any candidate receptors to determine whether JWH133 or HU308 act as agonists at these GPCRs and finally to use ligand-directed virtual screening, combined with medicinal chemistry and photoaffinity labelling, to discover and develop novel tool compounds that will aid in the identification of the off-target GPCR(s).

With respect to my first aim, I found that bio-gel elicited macrophages express 124 GPCRs, excluding sensory receptors, over a wide range of expression levels. There have been a few studies that have determined the GPCR expression profile of

different macrophage populations, with the first conducted by Lattin *et al* in 2008, who examined GPCR expression in murine bone marrow-dervived and thioglycollate elicited macrophages [548]. However the concordance of this study with my results was low as the authors found that only 66 GPCRs were expressed. Furthermore, I found that 10 of these were not expressed in bio-gel macrophages, leaving 56 common GPCRs and a total expression overlap of 45%. Further to this, studies conducted in 2012 and 2013 examined the GPCR expression profile of human alveolar macrophages and human monocyte-derived macrophages, with either population expressing 156 and 82 GPCRs respectively [549, 550]. Thirteen of the receptors deemed expressed in human alveolar macrophages do not have orthologs in mouse and 54 were not expressed in bio-gel macrophages, leaving 89 common GPCRs; an expression overlap of 72% with my results. Of the receptors expressed in human monocyte-derived macrophages, 15 have no mouse counterparts and 14 were not expressed in bio-gel macrophages, leaving 67 common GPCRs; an expression overlap of 54%.

The high degree of difference between my results and these other studies is likely due to the fact that macrophages from different tissues and species were used in each of the studies. It is now well established that the gene expression profiles of macrophages isolated from different tissues are distinct from one another and are shaped by their local microenvironment to allow these cells to perform niche specific functions [40–42]. For example I found CCR2 to be highly expressed in bio-gel macrophages and Lattin *et al* also found that CCR2 was expressed in thioglycollate elicited macrophages. However, CCR2 was not found to be expressed in human alveolar macrophages. This is consistent with the findings of Lavin *et al* who found that CCR2 is highly expressed in mouse monocytes, but not in murine alveolar macrophages [40]. As both bio-gel and thioglycollate are elicited cells differentiated from monocytes, this would explain why they would have CCR2 expression, as this receptor is highly important for monocyte recruitment to sites of inflammation [121]. However alveolar macrophages, like almost all tissue-resident macrophages, are not derived from blood monocytes and are instead seeded into the lung before birth [551],

thereby explaining why they have little or no expression of CCR2.

However, macrophages from different tissue origins also share a common set of genes that allow them to perform core macrophage-specific functions. This is evident when comparing my results with the three studies detailed above, as 33 GPCRs were expressed in all of the macrophage populations examined. Included in this list are many macrophage-associated genes that are important for macrophage function, such as the complement receptors C3aR1 and C5aR1, the CC chemokine receptors CCR1 and CCR5, CXCR4, leukotriene B4 receptor 1 and also the chemerin receptor ChemR23 [47]. Interestingly however, there are multiple orphan GPCRs expressed by all macrophage populations, including GPR146, GPR160, GPR85 and GPRC5B. Currently very little is known about these receptors and even less is known about how they impact macrophage function, however as they seem to be conserved across different macrophage populations it can be speculated that they may control important macrophage function(s).

With regards to my second aim, the GPCR expression data immediately highlighted two candidate receptors to take forward for functional screening; GPR55 and GPR18. As detailed in the introduction, both of these GPCRs have been put forward as potential cannabinoid receptors, as they bind and are activated by a wide range of endo-, phyto- and synthetic cannabinoids, and both have been previously demonstrated to mediate directed cellular migration [467, 477]. However, both JWH133 and HU308 were unable to induce cytoskeletal rearrangements in CHO cells expressing GPR18 or GPR55 and JWH133 did not elicit β-arrestin recruitment at either receptor. In both assays, the cannabinoids were shown to activate CB_2, so compound inactivity does not explain their lack of activty at GPR55 or GPR18. Consequently, both were ruled out as the GPCR responsible for CB_2 agonist-induced macrophage chemotaxis. Further support of this hypothesis comes from McHugh *et al* who found that although NAGly induced human endometrial cell migration and intracellular signalling in a GPR18-independent manner, JWH133 and other synthetic cannabinoids had no effect in any assay examined [481]. This therefore

means that JWH133 is unable to activate GPR18 in this cell line to cause chemotaxis, thereby corroborating the hypothesis that GPR18 is not the receptor responsible for CB_2 agonist-induced chemotaxis.

Alongside GPR18 and GPR55, I also considered lipid binding GPCRs and receptors phylogenetically related to CB_2. As cannabinoid ligands are highly lipophillic, I reasoned that it is likely that the off-target receptor is a lipid binding GPCR structurally similar to CB_2. There are approximately 43 GPCRs in mouse that have been previously annotated as having lipid ligands and CB_2 phylogenetically clusters with 11 other class A GPCRs [131]. These are LPAR1, LPAR2, LPAR3, the sphingosine-1-phosphate receptors 1, 2, 3, 4 and 5 and the orphan receptors GPR3, GPR6 and GPR12. I could immediately rule out GPR3, 6 and 12 as these were not expressed in bio-gel macrophages, and although all S1PRs were expressed, none were active in the JWH133 GPCR β-arrestin screening assay. Furthermore it has been previously shown that AEA and 2-AG can elicit β-arrestin recruitment at S1PR1 [474], providing further evidence that S1PR1 is not the off-target receptor, as 2-AG was unable to elicit macrophage chemotaxis. Of the remaining phylogenetically related GPCRs, only LPAR1 stood out as a candidate to examine further, as this was expressed in bio-gel elicited macrophages but not included in the Discoverx β-arrestin screen.

Next considering lipid GPCRs in general, I decided that I would functionally test any lipid GPCR that was deemed expressed in bio-gel macrophages but was not tested in the functional screen. Alongside LPAR1, four more receptors fit this criteria and these were: LPAR5 (another lysophosphatidic acid receptor phylogenetically distant to CB_2 but interestingly similar to GPR55), GPER1 and CYSLTR1 and CYSLTR2. Unfortunately however functional testing of each receptor proved impossible as sufficient receptor expression could not be obtained using transfected CHO or HEK cells. Instead I decided to take a different approach and stimulated bio-gel elicited macrophages with agonists for these lipid GPCRs to see whether any mimicked the cytoskeletal response seen in primary macrophages stimulated with JWH133

or HU308. However, none of the agonists tested gave similar responses to JWH133 or HU308 and in fact the GPER1 agonist G-1 and the CYSLTR1/2 agonist LTD4 gave responses opposite to that of the cannabinoids. These data imply that none of these lipid binding GPCRs are the off-target receptor(s), however further studies are required to confirm this conclusion.

My final aim of this chapter was to identify novel chemoattractant chemical scaffolds and use photoaffinity labelling to identify their target protein(s), and I have made substantial progress towards completing this objective. In collaboration with the Department of Chemistry, SAR studies on conducted on a novel chemical scaffold discovered to cause macrophage cytoskeletal rearrangement and chemotaxis has allowed the rational design and synthesis of compounds that retain functional activity, but also contain a photoreactive benzophenone group. This approach has been used with success to probe GPCR-ligand interactions, with photoaffinity labelling being used to study ligand binding to the β adrenergic receptor, the A_{2A} adenosine receptor, dopamine receptors, VPAC2, $mGlu_5$ and the kisspeptin receptor GPR54 [546,547,552–554], and therefore I believe that this is a viable and importantly unbiased approach for GPCR identification.

The SAR studies described in the chapter were instrumental in elucidating that the right hand side of the 2-thioxo-2,3-dihydroquinazolin-4(1H)-one scaffold was the most likely place where a photoreactive group would be tolerated, as the addition of sterically bulky and/or electronegative groups had only a minor impact on compound activity. However, it also provided additional evidence that active compounds and CB_2 agonists specifically activate a receptor to cause macrophage cytoskeletal rearrangement, as in all cases, movement of only one atom, the Br from the 6 position to the 7 position of the LHS ring, resulted in ablation of compound activity (OX00869 vs OX03006; OX03005 vs OX03004; OX03008 vs OX03009). The complete loss of function seen with this minor chemical modification likely means that a receptor ligand binding site with specific steric/electrochemical constraints is the target of these compounds. This is of importance, as so far the only direct

evidence that a receptor is responsible for the off-target effects of CB_2 agonists is my finding that CB_2 agonist-induced macrophage chemotaxis is PTX sensitive.

The next step for this project is to add a biotin tag to the benzophenone containing compounds, so that once UV cross-linking has been performed, any proteins covalently bound can be recovered and identified by mass spectroscopy. The SAR experiments demonstrate that the 6 position on the LHS ring would be the most logical point for biotin addition as large bulky groups are well tolerated at this position, having minimal impact on compound activity. However, once synthesised compound activity will have to be tested to ensure it is still able to induce macrophage cytoskeletal rearrangement and chemotaxis.

4.4.1 Limitations of this study

Although providing as unbiased a readout as possible for JWH133 activity at multiple GPCRs, the β-arrestin GPCR functional screen is not a comprehensive assay of all GPCRs. According to the International Union of Basic and Clinical Pharmacology GPCR database, mice have 358 GPCRs, excluding sensory receptors [555]. As 24 of the GPCRs in the human β-arrestin screen do not exist in mouse, this therefore means that I have no functional data for 141 GPCRs. However, of these receptors, 121 were present on the murine GPCR array and 75 were found to be not expressed. This therefore means that I have mRNA expression, but no functional data for 46 receptors and no expression or functional data for 20 receptors.

However, it is important to note that the negative result from the β-arrestin GPCR functional screen with JWH133 does not conclusively prove that none of the 217 GPCRs tested that have mouse othologs are responsible for the off-target effects of the synthetic CB_2 agonists. Human GPCRs were used for the GPCR screen (as murine versions were not available) and therefore species differences between human and mouse receptor pharmacology could explain the negative result. As mentioned in the discussion of chapter three, differences in cannabinoid ligand pharmacology

between species has been previously documented. Nonetheless, JWH133 agonised human CB_1 and CB_2 in the screen, demonstrating that this compound behaved as expected at these receptors, and JWH133 has been shown to act as a chemoattractant for human monocytes, at the same concentrations used in my work [389]. This therefore implies that JWH133 does activate the receptor responsible for CB_2 agonist-induced chemotaxis in human cells. Despite this however, functional selectivity may mean that JWH133 does not cause β-arrestin recruitment at its off-target GPCR. The differential abilities of cannabinoid agonists to elicit β-arrestin recruitment to CB_2 has been well documented [152] and even extends to DIAS2, the novel CB_2 agonist developed in my laboratory [229], as DIAS2 does not cause β-arrestin recruitment to CB_2, despite being a full agonist in the CB_2 cAMP assay. Therefore this could potentially explain why no hits were found in the GPCR screen.

Importantly, recent work has shown that established CB_2 ligands can behave differently in primary tissue as opposed to recombinant cellular systems as in human, rat and mouse spleen, AM1241 behaves as an agonist, whereas in CHO cells expressing human CB_2 it acts as an inverse agonist [434]. Therefore although JWH133 acts as an agonist at the GPCR responsible for CB_2 agonist-induced chemotaxis in primary murine macrophages, there is no guarantee that JWH133 will display the same pharmacology in the *in vitro* system used for the β-arrestin screen. The reason for this difference is likely due to multiple factors, including differences in receptor expression levels, coupling and the expression of accessory proteins needed for receptor function. Furthermore, these disparities between primary and transfected cell systems also impacts the GPR55 and GPR18 functional screening I conducted using receptor expression in CHO cells. Although C5aR1 and CB_2 transfected cells responded in the functional screen, this is not a guarantee that GPR55 and GPR18 will do the same when stimulated with JWH133 or HU308. To further strengthen the conclusion that GPR55 or GPR18 are not responsible for CB_2 agonist-induced macrophage chemotaxis, siRNA mediated knock-down of either receptor in murine macrophages could be conducted to examine their role in primary cells.

There are also some potential limitations when considering the photoaffinity labelling approach for target identification. Despite the fact that photoreactive probes have been used to examine ligand-receptor interactions at multiple GPCRs [547], the experiment might fail for technical reasons, such as poor labelling efficiency, low target abundance and/or inefficient recovery of covalently linked targets. If this happens, and the issue cannot be solved, then alternative approaches for target identification may need to be considered. One such approach would be to use siRNA pools against the entire murine GPCR complement in primary macrophages to knock-down GPCR expression in primary macrophages and look for inhibition of JWH133-induced signalling.

However this also is not without its limitations as macrophages can be challenging to transfect and incomplete knock-down of gene expression could lead to false negative results. Next, the cross-linking experiments may yield false positive hits, with the final photoreactive compounds covalently binding to proteins other than their actual cellular target. To try and overcome this, a negative photoreactive control will be produced with a bromine group at the 7 position, rather than the 6 position, as having a bromine at this position fully ablates activity. Cross-linking will then be performed with both negative and positive compounds, allowing any common hits to be ignored.

Finally, the novel compounds identified in this chapter may not have the same target as the chemotaxis positive CB_2 agonists. The fact that they have the same effect in macrophage functional assays does not necessarily mean that they have the same target, so activity of JWH133 and HU308 will have to be confirmed at any hits identified from the UV-cross linking experiments to conclude that any targets identified are responsible for CB_2 agonist-induced macrophage chemotaxis.

Chapter 5

Innate immune mobilisation in $CB_2^{-/-}$ animals

5.1 Introduction

5.1.1 Animal models for studying the inflammatory response

As inflammation is involved in, or central to, a vast array of pathologies, understanding the inflammatory process itself and the role it plays within disease is of great importance. Generally, the models used to study inflammation fall into two groups: Firstly the reductionist and simplistic models that are used to examine the inflammatory response, or a particular aspect of it in isolation, and secondly those that also aim to mimic the histopathology of human disease. Both are important for our understanding of the fundamentals of inflammation and how it impacts on disease. Therefore, I will now introduce some common animals models used to study the inflammatory response and inflammatory diseases. This is not intended to be an exhaustive list, but instead to provide a sample of the range of inflammatory models available.

5.1.2 The dorsal air pouch inflammation model

The first usage of the dorsal air pouch inflammation model came in 1953, whereby a pouch was created on the back of a rat to allow for inflammatory cell recruitment to be studied [556]. Since then the model has been refined and standardised and involves two dorsal subcutaneous injections of air, one on day zero and one on day three, which results in the formation of a dorsal air pouch. After 7 days the pouch lining, which is two to three cells thick, resembles granulation tissue and is comprised mainly of fibroblast-like cells, mast cells and macrophages [557, 558]. Furthermore after 7 days the pouch is well vascularised, making it ideal for studying immune cell recruitment during an inflammatory response [559]. Due to the composition of the pouch lining itself, it is thought that the most similar *bona fide* anatomical site *in vivo* is the synovial joint.

The main advantages of the dorsal air pouch model are that it is technically simple to set up, offers a defined and easy to access site for inflammogen injection and inflammatory exudate collection and that it can be used with a range wide of inflammatory stimuli depending on the type of inflammatory response desired. Furthermore the air pouch is amenable for histological analysis. Classically both zymosan and carrageenan are used as the pouch inflammatory insult, with both causing a rapid and predominant influx of neutrophils followed by a smaller monocyte wave at later time points [557,560]. However other inflammogens such as monosodium urate (MSU) crystals and LPS have also been used [561–563].

Additionally, injection of specific chemokines or chemoattractant proteins into the air pouch can be used to study the recruitment of specific leukocyte populations *in vivo*. Importantly this is made possible by the fact that the basal air pouch contains relatively few cells, contrasting with other anatomical sites used in inflammatory models. IL-1β, IL-8, C5a and S100A8/9 have been used to specifically study neutrophil recruitment [562, 564–566], Eotaxin to study eosinophil recruitment [567, 568] and CCL2 to generate a monocyte specific influx into the air pouch [566].

Furthermore, recently published work demonstrates how the air pouch can be used to model the resolution phase of an inflammatory response. Apoptotic neutrophils injected into a dorsal air pouch caused the subsequent recruitment of inflammatory monocytes [569]. Interestingly it was found that annexin A1, produced by these apoptotic neutrophils, was responsible for this monocyte influx, demonstrating a previously unrecognised role of annexin A1 in the resolution of inflammation [569].

5.1.3 Peritonitis models of inflammation

Peritonitis is the inflammation of the peritoneum; a cavity formed from a monolayer of mesothelial cells that contains the abdominal organs. Due to its ease of access, injection of an inflammatory stimulus into the peritoneal cavity is widely used to study the acute inflammatory response [570]. Alongside the mesothelium, the peritoneum contains approximately three million resident cells, consisting of macrophages, B cells, T cells and dendritic cells [570, 571], and all contribute to the initiation of an inflammatory response. Importantly, cells recruited to the peritoneal cavity and inflammatory mediators produced during the inflammatory response can be easily recovered by peritoneal lavage.

Peritoneal injection of LPS, thioglycollate and MSU crystals have been used to cause peritoneal inflammation [570, 572–576], however the most commonly employed inflammogen is zymosan [577]. This yeast cell wall component is recognised by the receptors TLR2 and Dectin-1 and leads to a reproducible acute inflammatory response with an initial influx of neutrophils peaking around 4 hours, a later wave of monocytes peaking between 16 to 24 hours, and resolution of the acute phase response by 96 hours [577]. Importantly as this model is self-resolving, it is increasingly being used to study the process of inflammation resolution and has increased our understanding of many pro-resolving mediators such as the resolvins, lipoxin A4, chemerin and annexin A1 [129, 578]. This model has also been used to examine the pathways important for inflammatory cell recruitment. For example, genetic deletion of CCR2

has been shown to blunt monocyte recruitment [31, 579], whereas genetic deletion of CXCR2 has been shown to blunt neutrophil recruitment [580], in the thioglycollate peritonitis model. Additionally, and in a similar fashion to the dorsal air pouch, specific cytokines, chemokines and chemoattractant molecules have been injected into the air pouch to assess the role they play in leukocyte recruitment and this list includes TNF-α, CXCL1 and CXCL2, C5a, LTB4 and fMLF [581–584].

5.1.4 Carrageenan-induced paw oedema

One of the hallmalks of an acute inflammatory response is oedema; an increase of fluid and protein content at an inflammatory site due to greater local vascular permeability, inflammatory mediator production and leukocyte recruitment [6]. Carrageenan-induced paw oedema is widely used acute inflammatory model, and as the name suggests, is characterised by a swelling of the inflamed paw normally measured by water displacement (plethysmometry) [585]. Carrageenan (1-3%) is injected into the bottom of the paw and this induces a classic acute inflammatory response with a range of inflammatory mediators produced that cause a first wave of neutrophil recruitment and oedema that peaks at 4-6 hours [586,587]. A second phase then develops around 48-72 hours after carrageenan injection, with a more intense oedema and macrophages, eosinophils and lymphocytes observed in the paw [586,587]. Importantly the contralateral paw can be used as a control, receiving a vehicle only injection, allowing for a paired analysis to be performed which results in increased statistical power. Finally, this model has been validated for the identification of novel anti-inflammatory compounds, as known anti-inflammatories such as indomethacin and dexamethasone inhibit carrageenan-induced leukocyte recruitment and paw oedema [587, 588]. Indeed multiple studies exist examining the anti-inflammatory actions of many different classes of compounds using this model [585, 589–591].

5.1.5 Mouse ear oedema models

Acute inflammatory oedema can be also be induced in the ear by the topical or intradermal application of an inflammatory stimulus. A wide range of inflammatory agents such as cantharidin, capsaicin, zymosan and carrageenan can be used to elicit an inflammatory response that, in a manner similar to the carrageenan-induced paw odema, has a first phase peaking at 6 hours and a second phase peaking at 24 hours [592, 593]. Typically ear weight is used as a measure of oedema, but inflammatory mediators and leukocytes present in the ear can also be quantified. Being a skin inflammation model, this can be used to mimic various inflammatory pathologies of the skin such as psoriasis, dermatitis and eczema and allows the testing of topical application of anti-inflammatory compounds; the preferred route of administration for treating skin inflammation [592–594]. Finally, alongside being simple to perform, another advantage of this model is that the contralateral ear can be used as a control allowing the benefits of paired analysis as previously mentioned.

5.1.6 LPS-induced endotoxemia

Intraperitoneal or intravenous injection of LPS, a major component of the outer membrane of gram negative bacteria, elicits a rapid and systemic inflammatory response via the activation of TLR4 [265]. Low dose LPS injection causes a rapidly resolving response, whereas injection of higher LPS concentrations leads to a prolonged inflammatory state and even death [267]. The inflammatory response is normally quantified by measuring the levels of pro-inflammatory mediators in the serum and these usually peak quickly at approximately 2 hours after LPS administration and then rapidly return to basal levels [270]. However, neutrophil recruitment to organs such as the lungs and the liver can also provide a readout of systemic inflammation. The benefits of this model are that it is easy to perform, quick and highly reproducible given that the type and quality of the LPS used can be tightly controlled.

5.1.7 Chemically-induced intestinal inflammation models

In humans, chronic inflammation of the intestines is the underlying cause of IBD, a classification that encompasses both UC and CD [250]. In animals, intestinal inflammation that mimics the pathology and clinical symptoms of IBD can be induced by the administration of a variety of chemical agents, with the most commonly used being DSS and TNBS [595]. DSS induces inflammation by damaging the gut epithelial cells, which leads to the breakdown of the epithelial barrier and exposure of the gut microbiota to the lamina propria. This causes activation of TLR signalling on resident macrophage and dendritic cell populations and a robust inflammatory response involving both the innate and adaptive immune system. DSS-induced intestinal inflammation is thought to most closely resemble human UC [596, 597]. In contrast, TNBS is thought to most closely mimic CD, with experimental animals displaying many of the pathological and clinical symptoms of CD. TNBS is administered directly into the colon where it modifies host proteins to make them immunogenic to the immune system. This causes a predominantly T_H1-mediated immune response with recruitment of $CD4^+$ T cells along with neutrophils, monocytes and macrophages into the lamina propria [250, 595–597]. In both models, disease severity can be assessed by change in body weight, colon weight, colon length, histological scoring for tissue damage, local and systemic inflammatory mediator production and also local immune cell recruitment. Importantly both acute and chronic inflammation of the gut can be studied in these models by changing the concentration and administration routine of the inflammogen. For example, the addition of 1-5% DSS to the drinking water for 1 week induces an acute inflammatory response, whereas prolonged administration over 2 months leads to advanced chronic inflammation of the gut [598].

5.2 Rationale for the experiments presented in this chapter

As introduced in chapter 1, there is a large body of work demonstrating that activation of CB_2 is anti-inflammatory in a range of animal models of inflammation [163], many of which I have introduced above. Currently, the exact mechanism underlying this beneficial effect remains unknown, however one hypothesis put forward is that activation of CB_2 blocks immune cell chemotaxis and recruitment to sites of inflammation, thereby dampening the inflammatory response.

However, in chapter 3 I have shown that CB_2 does not play a role in regulating macrophage chemotaxis. In light of this finding, I wanted to further understand whether CB_2 regulates the migration and trafficking of other immune cell populations, but I could not explore this using CB_2 ligands due to the off-target effect I have documented in chapter 3 of my thesis. Instead I chose to compare immune cell trafficking between WT mice and animals that are genetically null for CB_2 in an *in vivo* model of acute inflammation to explore the role that CB_2 plays, if any, in regulating immune cell recruitment and migration during an inflammatory response. I have chosen to focus on the dorsal air pouch model of innate immune cell recruitment, as it is an acute model that is reliable and easy to perform and has not previously been used with $CB_2^{-/-}$ animals.

Therefore, the experimental aims of this chapter are to:

- Compare immune cell trafficking and the acute inflammatory response of WT and $CB_2^{-/-}$ animals using the dorsal air pouch inflammation model
- To understand the mechanistic basis behind any difference that may be seen between WT and $CB_2^{-/-}$ animals

5.3 Results

5.3.1 WT and $CB_2^{-/-}$ mice have no difference in their baseline air pouch cellular composition

To understand how CB_2 regulates immune cell trafficking *in vivo*, I decided to use the dorsal air pouch inflammation model with zymosan as the inflammatory stimulus. This is because, as described in section 5.1.2, the dorsal air pouch offers a trafficking site largely devoid of a typical resident cell population and is easy to access for inflammatory stimulus injection and subsequent collection of the inflammatory exudate. Furthermore, zymosan was chosen as the inflammatory insult as this agent is commonly used to elicit an inflammatory response in multiple models of inflammation, including the dorsal air pouch model [557,560]. It is important to note that unless otherwise specified, female animals were used for the dorsal air pouch experiments, initially due to limitations in the numbers of $CB_2^{-/-}$ animals available and to minimise animal wastage; a central principle of the 3Rs.

To begin to compare the inflammatory response between WT and $CB_2^{-/-}$ female animals, I first analysed the immune cell composition of the dorsal air pouch under baseline conditions using flow cytometry. The surface markers used I used to define each immune cell population can be found in table 5.1 and the flow cytometry gating strategy can be seen in figure 5.1.

Cell Type	**Surface Markers Used**
Neutrophils	CD45, CD11b, Ly6G, Ly6C, 7/4
Ly6C^{lo} monocytes	CD45, CD11b, CD115, Ly6C^{lo}
Ly6C^{hi} monocytes	CD45, CD11b, CD115, Ly6C^{hi}
Macrophages	CD45, CD11b, F4/80, 7/4 negative
Eosinophils	CD45, CD11b, F4/80^{mid}, Siglec-F
Continued on next page	

Table 5.1 – continued from previous page

Cell Type	Surface Markers Used
Mast cells	CD45, CD11b, Siglec-F, FcϵRIα
T cells	CD45, CD3
B cells	CD45, CD19, B220
B-1 cells	CD45, CD19, B220 negative

Table 5.1 Surface markers used for leukocyte identification.

Quantification of the cells present in the dorsal air pouch under basal conditions found that there was no difference in the total number of $CD45^+$ cells between WT (white bars) and $CB_2^{-/-}$ (grey bars) animals, with there being around 1.2 to 1.4 million $CD45^+$ cells in total (Fig 5.1A, I and Fig 5.2A). When examining myeloid cell populations, neutrophils were found in the pouches of both WT and $CB_2^{-/-}$ animals, with there being around 200,000 to 250,000 cells making up 20 to 23% of the total $CD45^+$ cells present (Fig 5.1C, K and Fig 5.2B). Both $Ly6C^{lo}$ and $Ly6C^{hi}$ monocytes were also found in the dorsal air pouch under baseline conditions (Fig 5.1D and L) and there was no difference in their total number between the genotypes with 220,000 to 250,000 $Ly6C^{lo}$ and 45,000 to 50,000 $Ly6C^{hi}$ monocytes comprising 16 to 20% and 3.5 to 4.5% of total $CD45^+$ cells respectively (Fig 5.2C and D).

Eosinophils were also present in both genotypes (Fig 5.1E, F, M and N) but again, there was no difference in the total number between WT and $CB_2^{-/-}$ animals, with 230,000 to 250,000 eosinophils comprising 15% of the total $CD45^+$ cell population (Fig 5.2E). $F4/80^+$ macrophages were found in the basal pouch (Fig 5.1E and M), with the total number present the same between the genotypes with 420,000 to 520,000 macrophages comprising 20 to 28% of the total $CD45^+$ cells present (Fig 5.2F). Interestingly, no mast cells were found in the pouch at baseline in either WT or $CB_2^{-/-}$ animals (Fig 5.1F and N).

When examining lymphocytes, no B cells were found in the baseline pouch of WT or $CB_2^{-/-}$ animals (Fig 5.1G and O), but a small T cell population was present

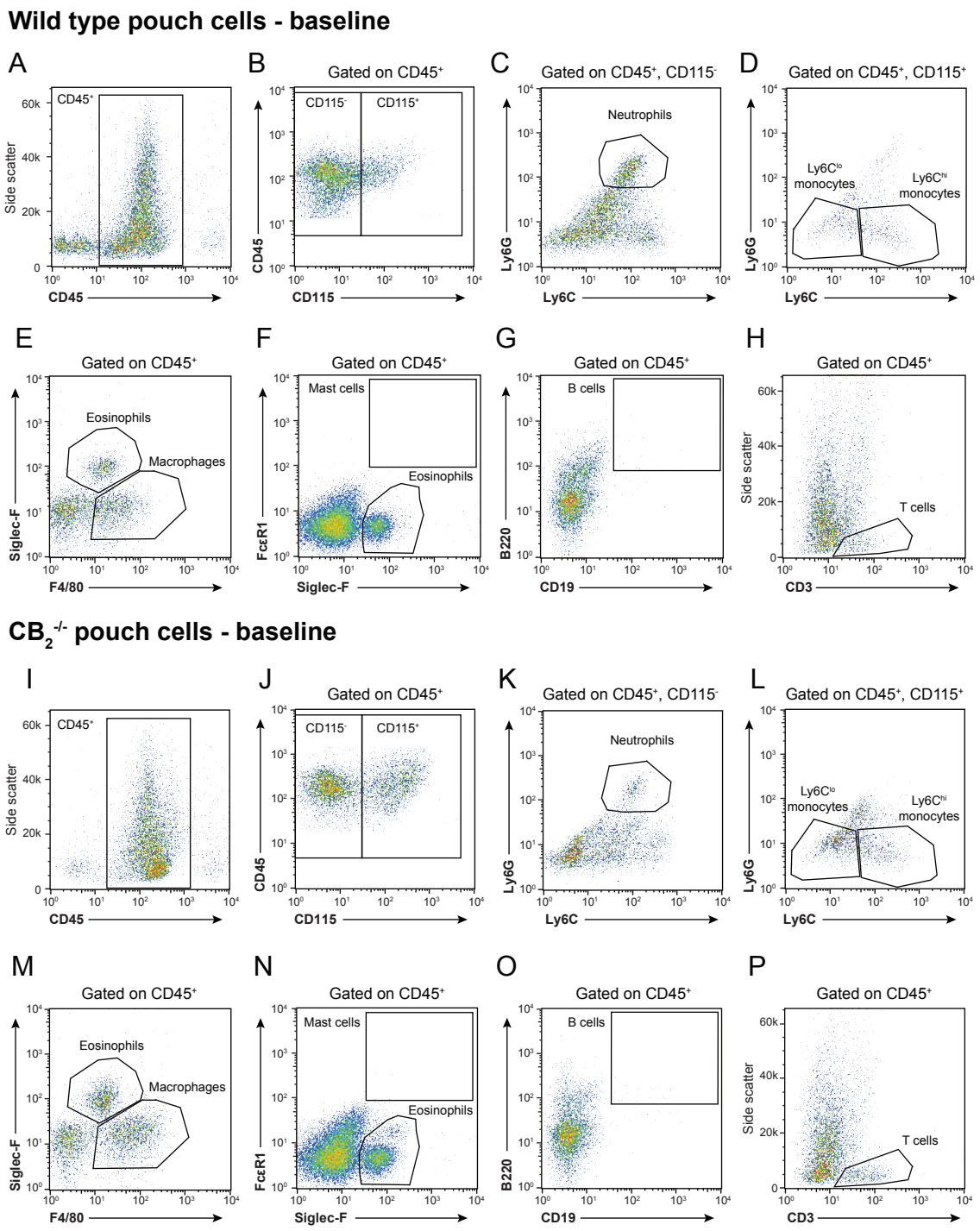

Figure 5.1 Baseline analysis of cells present in day 6 dorsal air pouches in WT and $CB_2^{-/-}$ mice by flow cytometry. Day 6 dorsal air pouches in WT or $CB_2^{-/-}$ animals were lavaged with 3 ml PBS containing 2 mM EDTA and the cells present analysed by flow cytometry. Dot plots showing (A) $CD45^+$ cells, (B) $CD45^+$, CD115 - and + cells, (C) $Ly6C^{lo}$ and $Ly6C^{hi}$ monocytes, (D) neutrophils, (E and F) Eosinophils, (E) $F4/80^+$ macrophages and (F) the lack of mast cells in WT pouches. (G) Dot plots showing the lack of B cells (as no staining for either B220 or CD19) in WT pouches. (H) Dot plots showing $CD3^+$ T cells in WT pouches. Dot plots showing (I) $CD45^+$ cells, (J) $CD45^+$, CD115 - and + cells, (K) $Ly6C^{lo}$ and $Ly6C^{hi}$ monocytes, (L) neutrophils, (M and N) Eosinophils, (M) $F4/80^+$ macrophages and (N) the lack of mast cells in $CB_2^{-/-}$ pouches. (O) Dot plots showing the lack of B cells in $CB_2^{-/-}$ pouches. (P) Dot plots showing $CD3^+$ T cells in $CB_2^{-/-}$ pouches. Dot plots are representative of n = 5-11 independent animals per group.

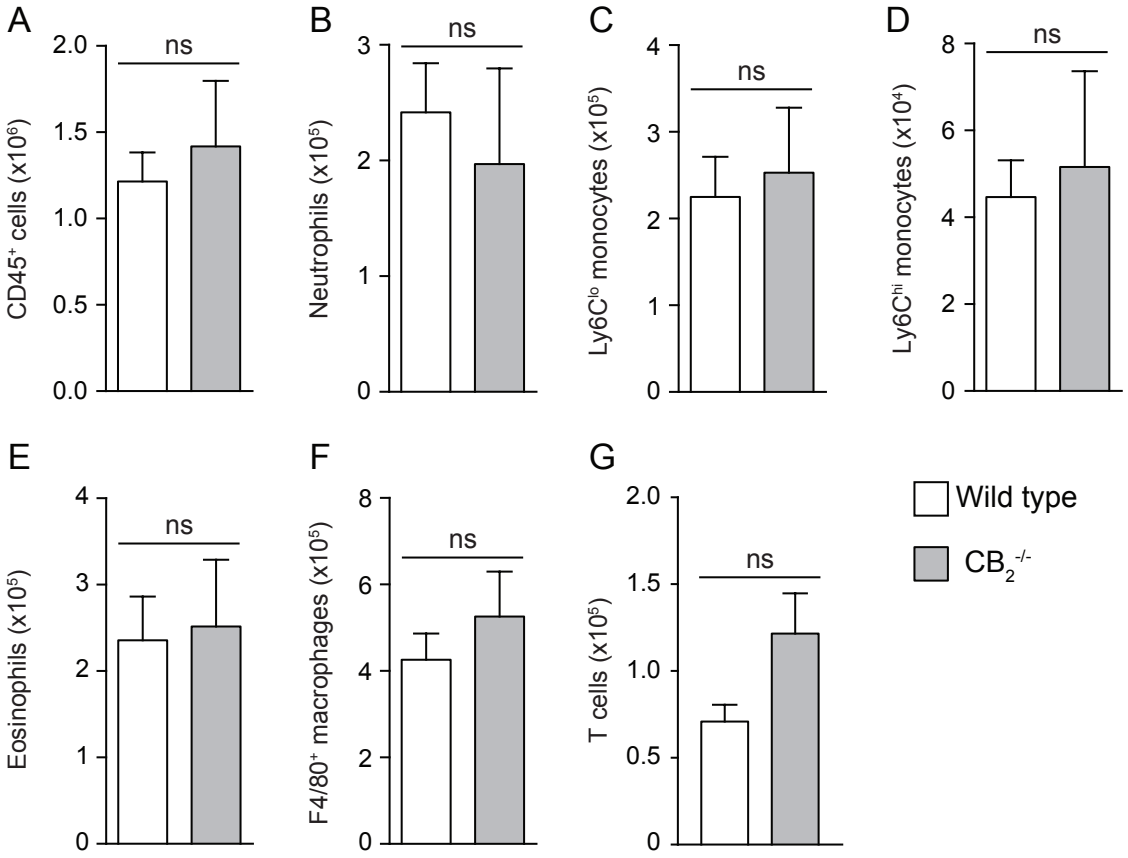

Figure 5.2 There is no difference in the baseline leukocyte composition of day 6 dorsal air pouches between WT and $CB_2^{-/-}$ mice. Day 6 dorsal air pouches in WT or $CB_2^{-/-}$ animals were lavaged with 3 ml PBS containing 2 mM EDTA and total cell counts and populations present determined by flow cytometry. (A) Total $CD45^+$ cells, (B) Neutrophils, (C) $Ly6C^{lo}$ monocytes, (D) $Ly6C^{hi}$ monocytes, (E) Eosinophils, (F) $F4/80^+$ macrophages and (G) T cells in WT (white bars) and $CB_2^{-/-}$ (grey bars) pouches under baseline conditions. Data are mean+ SEM, n = 5-11 independent animals per group. Statistical analysis was conducted using the unpaired student's t-test. ns $P > 0.05$.

(Fig 5.1H and P). Quantification found that there was no difference in the number of $CD3^+$ T cells between WT and $CB_2^{-/-}$ animals with 70,000 to 120,000 total T cells present comprising 3.5 to 6.6% of the total $CD45^+$ cells (Fig 5.2G). Taken together, these data demonstrate that there is a small and varied leukocyte population present in the dorsal air pouch under basal conditions, which is the same size and composition in both WT and $CB_2^{-/-}$ animals.

5.3.2 $CB_2^{-/-}$ animals with dorsal air pouches have increased B cell numbers in their blood under basal conditions

Next I wanted to examine whether there was any difference in the composition of leukocytes in the blood between WT and $CB_2^{-/-}$ animals with dorsal air pouches under baseline conditions. Concentrating on myeloid cells in the blood, neutrophils (Fig 5.3A and C), $Ly6C^{lo}$ and $Ly6C^{hi}$ monocytes (Fig 5.3B and D) in both WT and $CB_2^{-/-}$ animals were identified by flow cytometry. Quantification of the populations present found that there was no difference in the number of $CD45^+$ cells (Fig 5.3E), neutrophils (Fig 5.3F), $Ly6C^{lo}$ monocytes (Fig 5.3G) or $Ly6C^{hi}$ (Fig 5.3H) monocytes per ml of blood between WT (white bars) and $CB_2^{-/-}$ (grey bars) animals under basal conditions. Moving onto blood lymphocytes, B cells (Fig 5.4A and C) and T cells (Fig 5.4B and D) in WT and $CB_2^{-/-}$ animals were also identified by flow cytometry. Quantification found that there were significantly more B cells in the blood of $CB_2^{-/-}$ animals (Fig 5.4E) compared to WT, whereas there was no difference in the number of T cells per ml of blood between the genotypes (Fig 5.4F).

5.3.3 $CB_2^{-/-}$ animals have an exaggerated acute inflammatory response in the zymosan-induced dorsal air pouch inflammation model

To assess whether genetic deletion of CB_2 effects the acute inflammatory response, I began by examining immune cell recruitment to the dorsal air pouch of WT and $CB_2^{-/-}$ mice 6 hours after pouch injection of 100 μg of zymosan. In both WT and

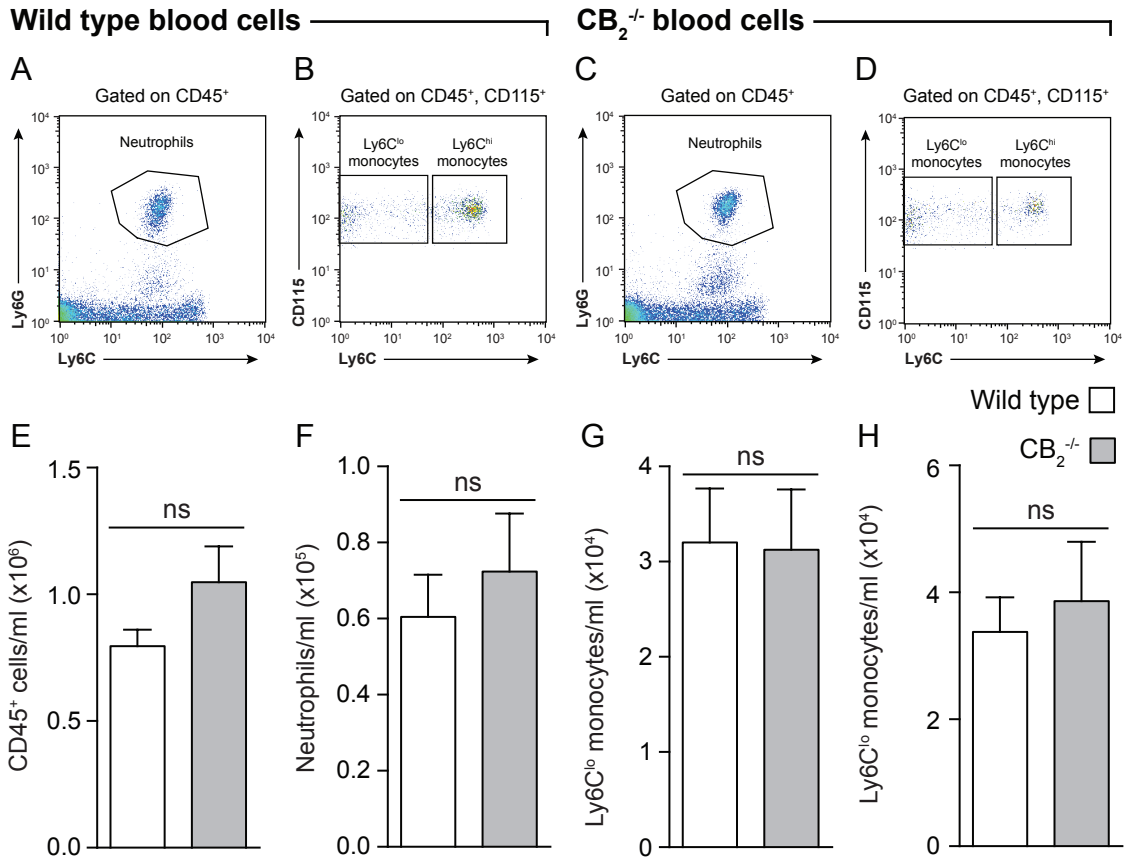

Figure 5.3 There are no differences in the myeloid cell populations present in the blood of WT and $CB_2^{-/-}$ mice with day 6 dorsal air pouches under baseline conditions. Blood was taken from mice with day 6 dorsal air pouches under baseline conditions and cells counts and populations present determined by flow cytometry. Representative dot plots of blood (A) neutrophils and (B) Ly6C^{lo} and Ly6C^{hi} monocytes in WT mice. Representative dot plots of blood (C) neutrophils and (D) Ly6C^{lo} and Ly6C^{hi} monocytes in $CB_2^{-/-}$ mice Quantification of the numbers of (E) CD45$^+$ cells, (F) neutrophils, (G) Ly6C^{lo} and (H) Ly6C^{hi} monocytes per ml of blood in WT (white bars) and $CB_2^{-/-}$ (grey bars) animals. Data are mean+ SEM, n = 5-11 independent animals per group. Statistical analysis was conducted using the unpaired student's t-test. ns P >0.05.

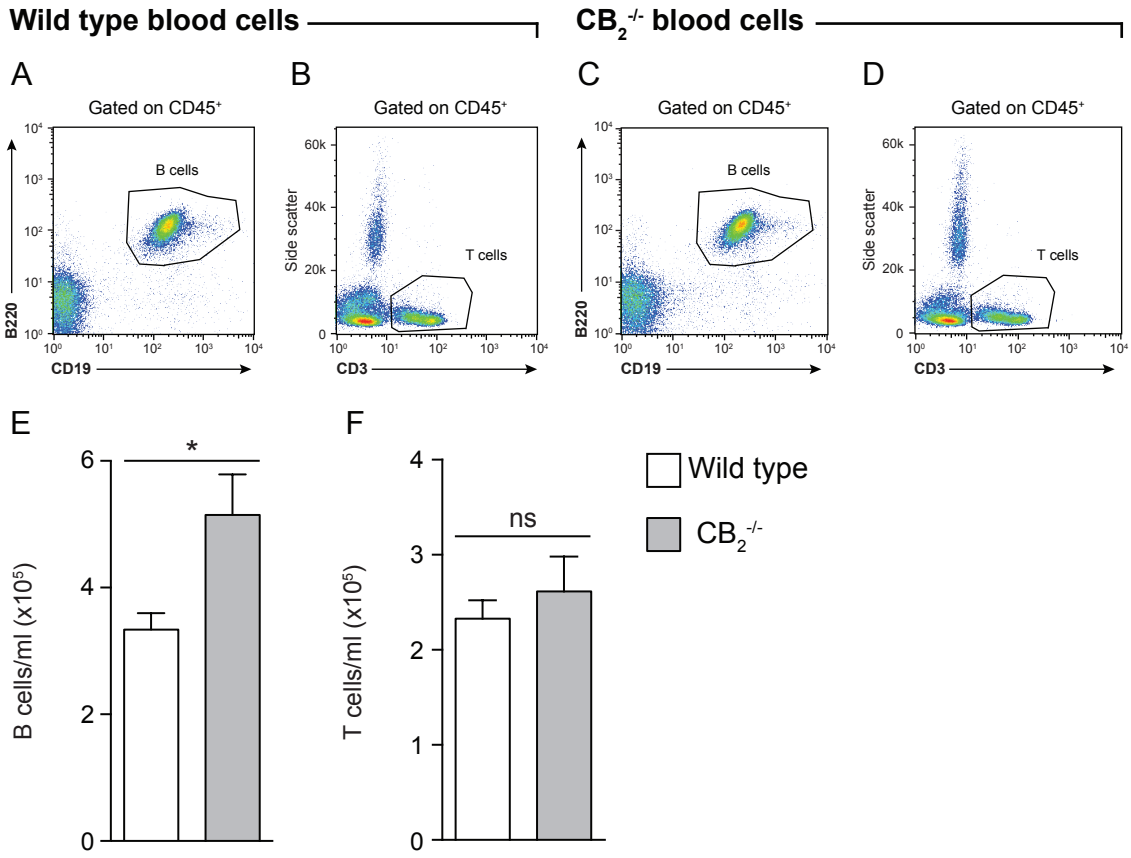

Figure 5.4 $CB_2^{-/-}$ mice have increased B cell, but not T cell, numbers in their blood under baseline conditions compared to WT animals. Blood was taken from mice with day 6 dorsal air pouches under baseline conditions and cells counts and populations present determined by flow cytometry. Representative dot plots of blood (A) B cells and (B) T cells in WT mice. Representative dot plots of blood (C) B cells and (D) T cells in $CB_2^{-/-}$ mice. Quantification of the number of (E) B cells and (F) T cells per ml of blood in WT (white bars) and $CB_2^{-/-}$ (grey bars) animals. Data are mean+ SEM, n = 5-11 independent animals per group. Statistical analysis was conducted using the unpaired student's t-test. ns $P > 0.05$, * $P < 0.05$.

$CB_2^{-/-}$ animals, neutrophils were the dominant cell population present 6 hours after zymosan challenge (Fig 5.5A and E respectively), comprising 60 to 70% of all $CD45^+$ cells, in both WT and $CB_2^{-/-}$ mice. Both $Ly6C^{lo}$ and $Ly6C^{hi}$ monocytes were present, but comprised a minor fraction of all $CD45^+$ cells (Fig 5.5B and F) in both WT and $CB_2^{-/-}$ mice. No B cells (Fig 5.5C and G) or T cells (Fig 5.5D and H) were found in the dorsal air pouch of either genotype at this time point. Quantification of total cell counts in the dorsal air pouch 6 hours after zymosan injection demonstrated that $CB_2^{-/-}$ animals had significantly higher numbers of $CD45^+$ cells and neutrophils compared to WT animals (Fig 5.5I - 4.6 vs 17.1 $x10^6$ cells and Fig 5.5J - 3.3 vs 12.3 $x10^6$ cells). There was no significant difference in the number of $Ly6C^{lo}$ or $Ly6C^{hi}$ monocytes between the genotypes (Fig 5.5K and L). I next examined the number of leukocytes present in the blood of these animals 6 hours after injection of zymosan into the dorsal air pouch and found that there was no difference in the numbers of $CD45^+$ cells (Fig 5.6A), neutrophils (Fig 5.6B), $Ly6C^{lo}$ monocytes (Fig 5.6C), $Ly6C^{hi}$ monocytes (Fig 5.6D), B cells (Fig 5.6E) or T cells (Fig 5.6F) per ml of blood between the genotypes.

Quantification of inflammatory mediators present in the lavage fluid from the dorsal air pouch showed that the levels of the cytokine IL-6 and the CC chemokines CCL2 and CCL4 were significantly higher in $CB_2^{-/-}$ animals 6 hours after zymosan injection (Fig 5.7A, B and C respectively). CXCL1, CXCL2 and CXCL5, chemokines classically involved in neutrophil recruitment, were present at relatively low levels and there was no difference in the amounts present between the genotypes (Fig 5.7D, E and F). Interestingly, the levels of CXCL10 and MMP-9 in the pouch exudate were significantly higher in $CB_2^{-/-}$ animals 6 hours after zymosan challenge (Fig 5.7G and H).

To further examine the role of CB_2 in the acute phase of the inflammatory response, I next compared WT and $CB_2^{-/-}$ animals 16 hours after dorsal air pouch injection with 100 μg of zymosan. As seen with the 6 hour time point, neutrophils were the dominant leukocyte population present, but now comprised 80% of all $CD45^+$

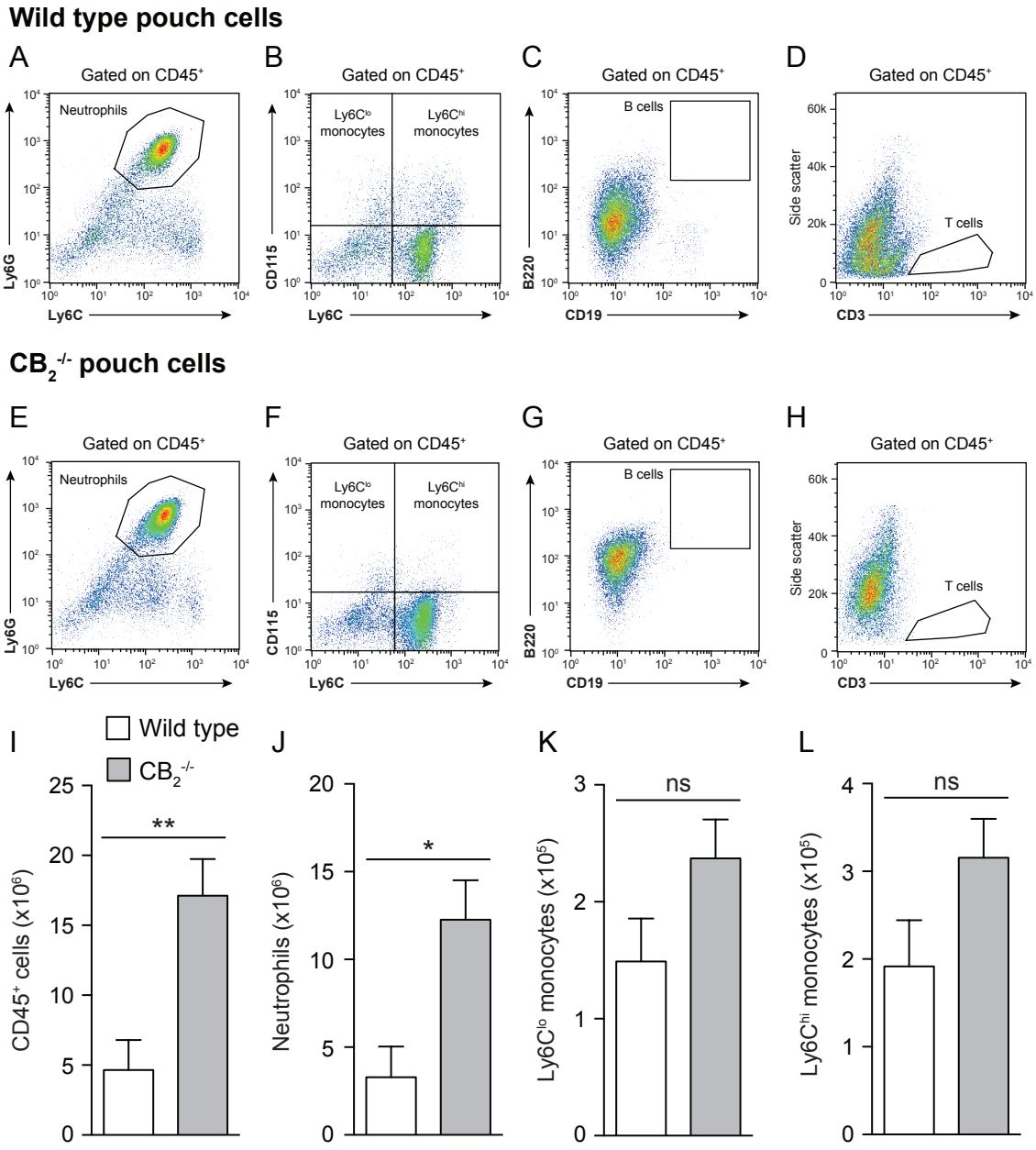

Figure 5.5 $CB_2^{-/-}$ mice have increased air pouch neutrophil recruitment 6 hours after zymosan injection. The dorsal air pouches of WT or $CB_2^{-/-}$ mice were injected with 100 μg zymosan and 6 hours later the pouches lavaged and total cell counts and populations present determined by flow cytometry. Representative dot plots of (A) neutrophils, (B) Ly6C^{lo} and Ly6C^{hi} monocytes, (C) B cells and (D) T cells in the dorsal air pouch of WT mice 6 hours after zymosan injection. Representative dot plots of (E) neutrophils, (F) Ly6C^{lo} and Ly6C^{hi} monocytes, (G) B cells and (H) T cells in the dorsal air pouch of $CB_2^{-/-}$ mice 6 hours after zymosan injection. Quantification of the number of (I) CD45$^+$ cells, (J) neutrophils, (K) Ly6C^{lo} or (L) Ly6C^{hi} monocytes recruited to the dorsal air pouch 6 hours after zymosan injection in WT (white bars) and $CB_2^{-/-}$ (grey bars) animals. Data are mean+ SEM, n = 7-11 independent animals per group. Statistical analysis was conducted using the unpaired student's t-test. ns P >0.05, * P <0.05, ** P <0.01.

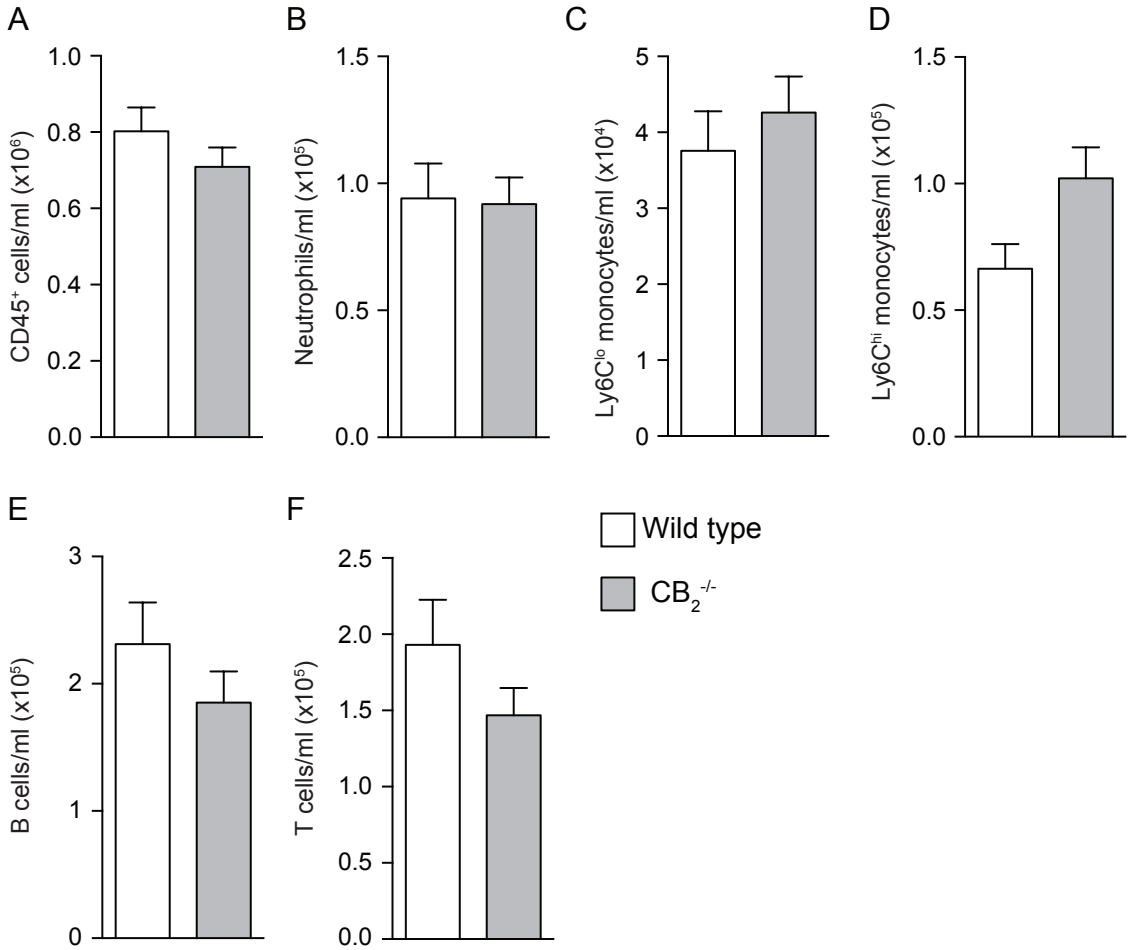

Figure 5.6 There are no differences in blood leukocyte numbers between WT and $CB_2^{-/-}$ mice 6 hours after pouch zymosan injection. Blood was taken from WT or $CB_2^{-/-}$ animals 6 hours after zymosan injection into the dorsal air pouch and cell counts and populations present determined by flow cytometry. There was no difference in the numbers of (A) $CD45^+$ cells, (B) neutrophils, (C) $Ly6C^{lo}$ monocytes, (D) $Ly6C^{hi}$ monocytes, (E) B cells or (F) T cells per ml of blood between WT (white bars) or $CB_2^{-/-}$ (grey bars) animals 6 hours after pouch zymosan injection. Data are mean+ SEM, n = 7-11 independent animals per group. Statistical analysis was conducted using the unpaired student's t-test. ns $P > 0.05$.

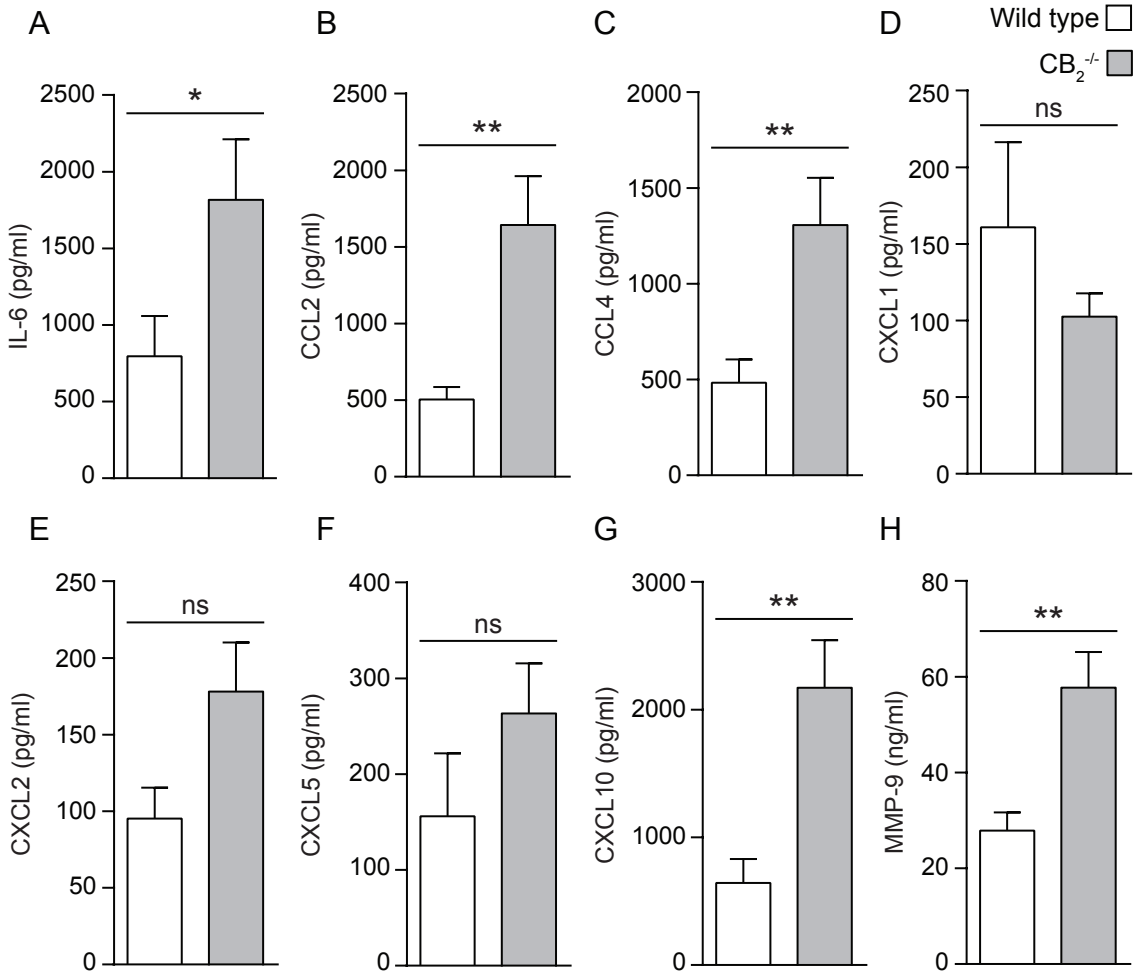

Figure 5.7 $CB_2^{-/-}$ mice have significantly higher levels of pro-inflammatory mediators in the dorsal air pouch 6 hours after zymosan injection compared to WT animals. The dorsal air pouches of WT or $CB_2^{-/-}$ mice were injected with 100 μg zymosan and 6 hours later the pouches lavaged and the concentration of inflammatory mediators present determined by ELISA. $CB_2^{-/-}$ mice (grey bars) had significantly higher levels of (A) IL-6, (B) CCL2 and (C) CCL4 in the dorsal air pouch 6 hours after zymosan injection compared to WT animals (white bars). There was no difference in the levels of (D) CXCL1, (E) CXCL2 and (F) CXCL5 between the genotypes. However, $CB_2^{-/-}$ mice had significantly higher levels of (G) CXCL10 and (H) MMP-9 in the dorsal air pouch 6 hours after zymosan injection compared to WT animals. Data are mean+ SEM, n = 7-11 independent animals per group. Statistical analysis was conducted using the unpaired student's t-test. ns $P > 0.05$, * $P < 0.05$, ** $P < 0.01$.

cells in both WT and $CB_2^{-/-}$ mice (Fig 5.8A and C). Alongside the small $Ly6C^{lo}$ monocyte population, a much more substantial $Ly6C^{hi}$ inflammatory monocyte population was present in the pouch, comprising 10% of all $CD45^+$ cells in both WT and $CB_2^{-/-}$ mice (Fig 5.8B and D). Quantification of total cell counts demonstrated that $CB_2^{-/-}$ animals had significantly higher air pouch numbers of $CD45^+$ cells and neutrophils compared to WT animals 16 hours after zymosan challenge (Fig 5.8E - 13.6 vs 27.7 $x10^6$ cells and Fig 5.8F - 10.5 vs 22.3 $x10^6$ cells). Interestingly for both genotypes, the numbers of $CD45^+$ cells and neutrophils were higher than those seen at the 6 hour time point. There was a trend towards increased $Ly6C^{lo}$ monocyte recruitment in the $CB_2^{-/-}$ animals, but this was not significant (Fig 5.8G). However, there were significantly more $Ly6C^{hi}$ inflammatory monocytes present in the pouch of $CB_2^{-/-}$ animals 16 hours after zymosan injection (Fig 5.8H). As with the 6 hour time point, no B cells or T cells were found in the dorsal air pouch at the 16 hour time point (data not shown).

Quantification of the number of leukocytes present in the blood of these animals found that there was no difference in the numbers of $CD45^+$ cells (Fig 5.9A), neutrophils (Fig 5.9B), $Ly6C^{lo}$ monocytes (Fig 5.9C), $Ly6C^{hi}$ monocytes (Fig 5.9D), B cells (Fig 5.9E) or T cells (Fig 5.9F) per ml of blood between the genotypes 16 hours after pouch zymosan injection. Furthermore, IL-6, CCL2, CXCL1, CXCL2 and CXCL5 were not detectable in the air pouch lavage fluid 16 hours after zymosan challenge.

Taken together, these data demonstrate that mice lacking CB_2 have an exaggerated acute inflammatory response in the zymosan-induced dorsal air pouch inflammation model, as significantly higher numbers of neutrophils and $Ly6C^{hi}$ inflammatory monocytes, as well as significantly higher levels of multiple pro-inflammatory proteins, are found in the dorsal air pouch of $CB_2^{-/-}$ animals at both 6 and 16 hours post zymosan challenge.

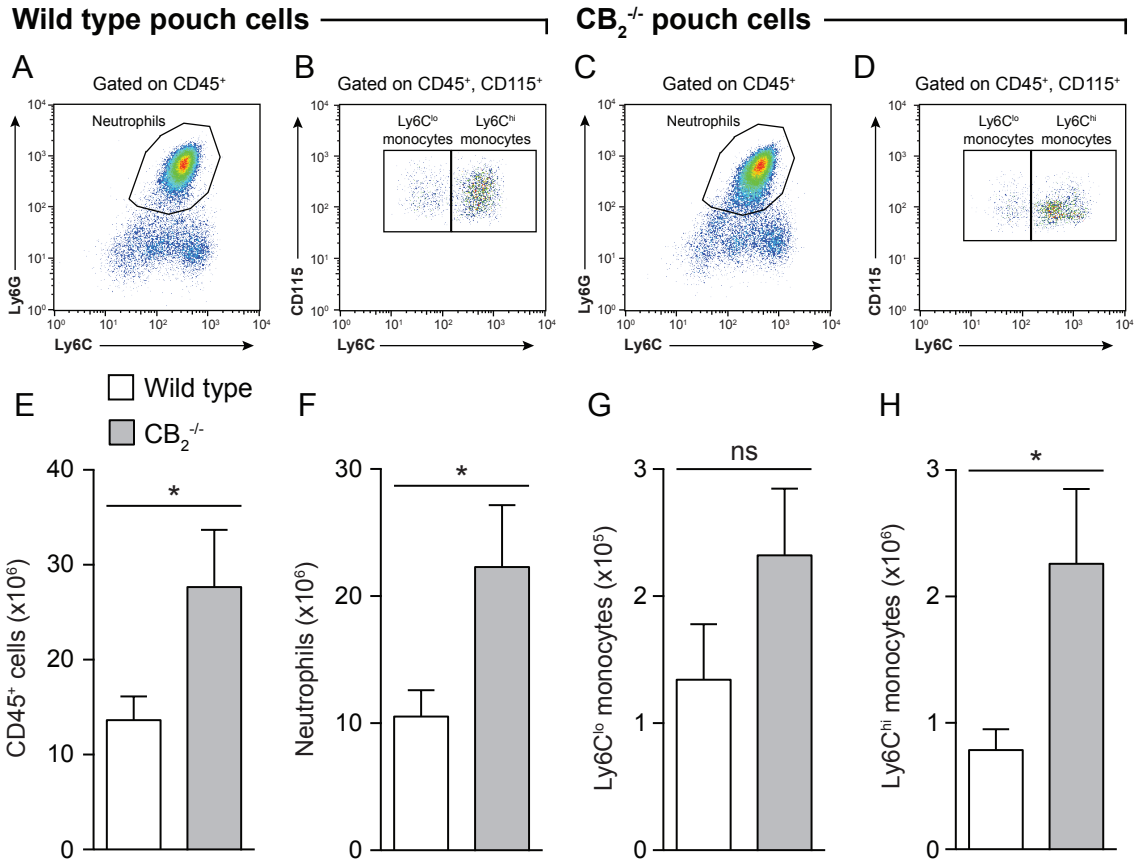

Figure 5.8 $CB_2^{-/-}$ mice have significantly more myeloid cells recruited to the dorsal air pouch 16 hours after zymosan injection compared to WT animals. The dorsal air pouches of WT or $CB_2^{-/-}$ mice were injected with 100 μg zymosan and 16 hours later the pouches lavaged and total cell counts and populations present determined by flow cytometry. Representative dot plots of (A) neutrophils and (B) $Ly6C^{lo}$ and $Ly6C^{hi}$ monocytes in the dorsal air pouch of WT mice 16 hours after zymosan injection. Representative dot plots of (C) neutrophils and (D) $Ly6C^{lo}$ and $Ly6C^{hi}$ monocytes in the dorsal air pouch of $CB_2^{-/-}$ and mice 16 hours after zymosan injection. Quantification of the number of (E) $CD45^+$ cells, (F) neutrophils (G) $Ly6C^{lo}$ and (H) $Ly6C^{hi}$ monocytes recruited to the dorsal air pouch 16 hours after zymosan injection in WT (white bars) and $CB_2^{-/-}$ (grey bars) animals. Data are mean+ SEM, n = 6-8 independent animals per group. Statistical analysis was conducted using the unpaired student's t-test. ns $P > 0.05$, * $P < 0.05$.

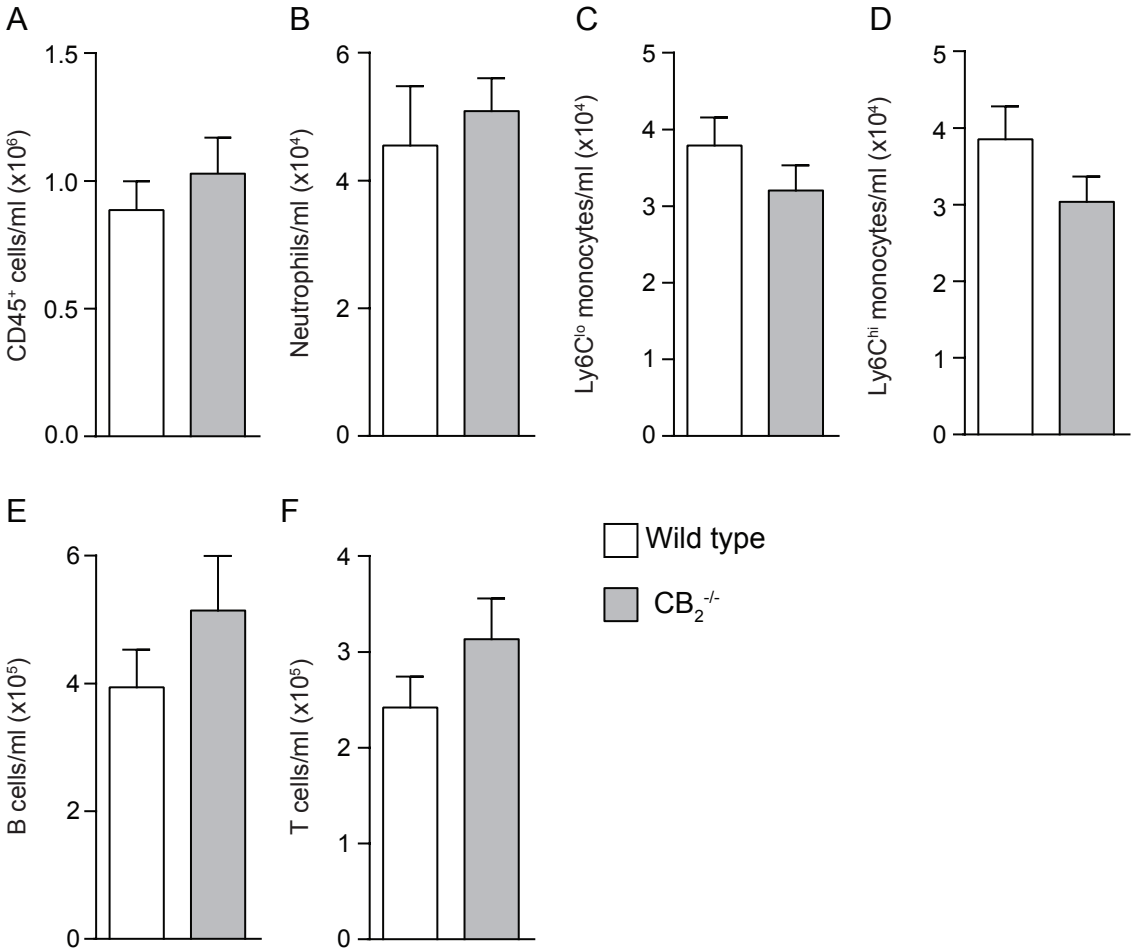

Figure 5.9 There are no differences in blood leukocyte numbers between WT and $CB_2^{-/-}$ mice 16 hours after pouch zymosan injection. Blood was taken from WT or $CB_2^{-/-}$ animals 16 hours after zymosan injection (100 μg) into the dorsal air pouch and cell counts and populations present determined by flow cytometry. There was no difference in the numbers of (A) $CD45^+$ cells, (B) neutrophils, (C) $Ly6C^{lo}$ monocytes, (D) $Ly6C^{hi}$ monocytes, (E) B cells or (F) T cells per ml of blood between WT (white bars) or $CB_2^{-/-}$ (grey bars) animals 16 hours after pouch zymosan injection. Data are mean+ SEM, n = 6-8 independent animals per group. Statistical analysis was conducted using the unpaired student's t-test. ns $P > 0.05$.

5.3.4 There is no difference in the inflammatory response between WT and $CB_2^{-/-}$ animals 2 hours after zymosan challenge

To understand exactly when this inflammatory phenotype manifests, and to search for mechanistic insights into the increased neutrophil recruitment seen in $CB_2^{-/-}$ mice 6 and 16 hours after zymosan challenge, I next assessed leukocyte recruitment and inflammatory mediator production in the dorsal air pouch, as well as blood leukocyte numbers, in WT and $CB_2^{-/-}$ animals 2 hours after zymosan challenge. Even at this short time point, the majority of leukocytes present in the pouch exudate were neutrophils, forming 50% of all $CD45^+$ cells in both WT and $CB_2^{-/-}$ mice (Fig 5.10A and C). Interestingly, a proportionally large $Ly6C^{hi}$ inflammatory monocyte population was seen at this time point, accounting for approximately 25% of all $CD45^+$ cells in both WT and $CB_2^{-/-}$ mice (Fig 5.10B and D). However, quantification revealed that there was no difference in the number of $CD45^+$ cells (Fig 5.10E), neutrophils (Fig 5.10F) or $Ly6C^{hi}$ inflammatory monocytes (Fig 5.10G) present in the pouch of WT or $CB_2^{-/-}$ animals 2 hours after zymosan challenge. Quantification of the number of leukocytes present in the blood of these animals 2 hours after injection of zymosan into the dorsal air pouch found that there was no difference in the numbers of $CD45^+$ cells (Fig 5.11A), neutrophils (Fig 5.11B), $Ly6C^{lo}$ monocytes (Fig 5.11C), $Ly6C^{hi}$ monocytes (Fig 5.11D), B cells (Fig 5.11E) or T cells (Fig 5.11F) per ml of blood between the genotypes.

When examining inflammatory mediators present in the dorsal air pouch 2 hours after zymosan challenge, I found that there was no difference in the levels of IL-6 (Fig 5.12A), CCL2 (Fig 5.12B) or CCL4 (Fig 5.12C) between the genotypes. Interestingly, the CXC chemokines CXCL1, 2 and 5 were present at high levels, especially CXCL1, likely explaining why neutrophils are the predominant cell type recruited in this model, however there was no difference in their levels between WT and $CB_2^{-/-}$ animals (Fig 5.12D, E and F). Finally, there was no difference between the genotypes in the concentration of CXCL10 in the pouch 2 hours after zymosan challenge (Fig

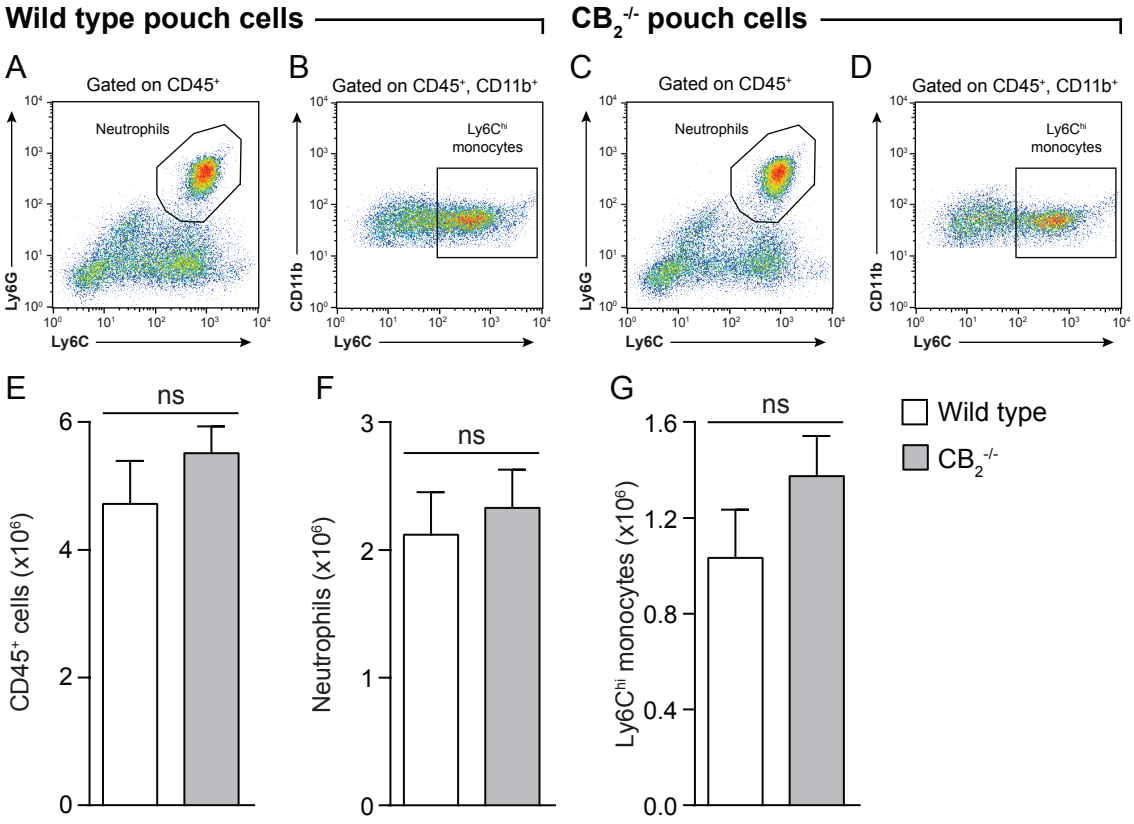

Figure 5.10 There is no difference in pouch myeloid cell recruitment between WT and $CB_2^{-/-}$ animals 2 hours after zymosan injection. The dorsal air pouches of WT or $CB_2^{-/-}$ mice were injected with 100 μg zymosan and 2 hours later the pouches lavaged and total cell counts and populations present determined by flow cytometry. Representative dot plots of (A) neutrophils and (B) Ly6C^{hi} monocytes in the dorsal air pouch of WT mice 2 hours after zymosan injection. Representative dot plots of (C) neutrophils and (D) Ly6C^{hi} monocytes in the dorsal air pouch of $CB_2^{-/-}$ mice 2 hours after zymosan injection. Quantification of the number of (E) CD45$^+$ cells, (F) neutrophils and (G) Ly6C^{hi} monocytes recruited to the dorsal air pouch 2 hours after zymosan injection in WT (white bars) and $CB_2^{-/-}$ (grey bars) animals. Data are mean+ SEM, n = 9-10 independent animals per group. Statistical analysis was conducted using the unpaired student's t-test. ns P >0.05.

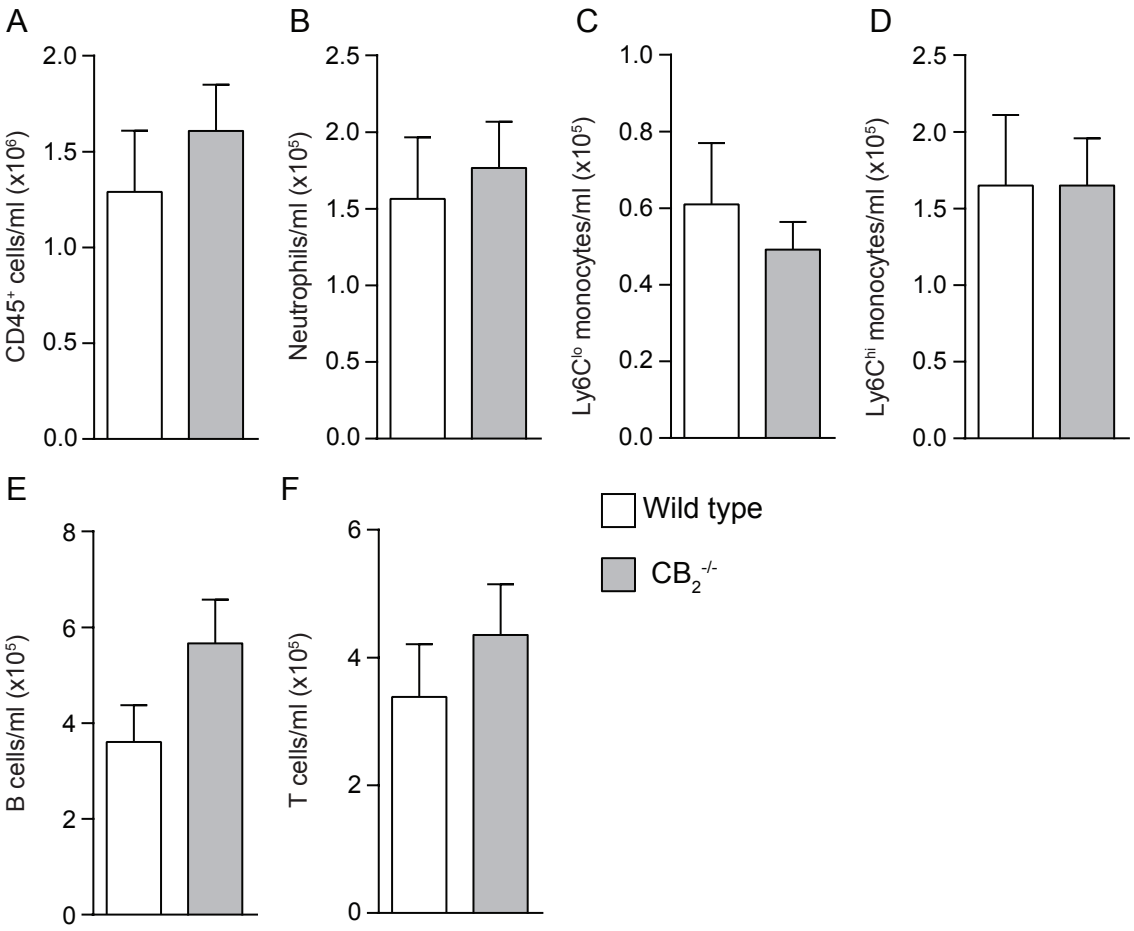

Figure 5.11 There are no differences in blood leukocyte numbers between WT and $CB_2^{-/-}$ mice 2 hours after pouch zymosan injection. Blood was taken from WT or $CB_2^{-/-}$ animals 2 hours after injection of 100 μg zymosan into the dorsal air pouch and cell counts and populations present determined by flow cytometry. There was no difference in the numbers of (A) $CD45^+$ cells, (B) neutrophils, (C) $Ly6C^{lo}$ monocytes, (D) $Ly6C^{hi}$ monocytes, (E) B cells or (F) T cells per ml of blood between WT (white bars) or $CB_2^{-/-}$ (grey bars) animals 2 hours after pouch zymosan injection. Data are mean+ SEM, n = 9-10 independent animals per group. Statistical analysis was conducted using the unpaired student's t-test. ns $P > 0.05$.

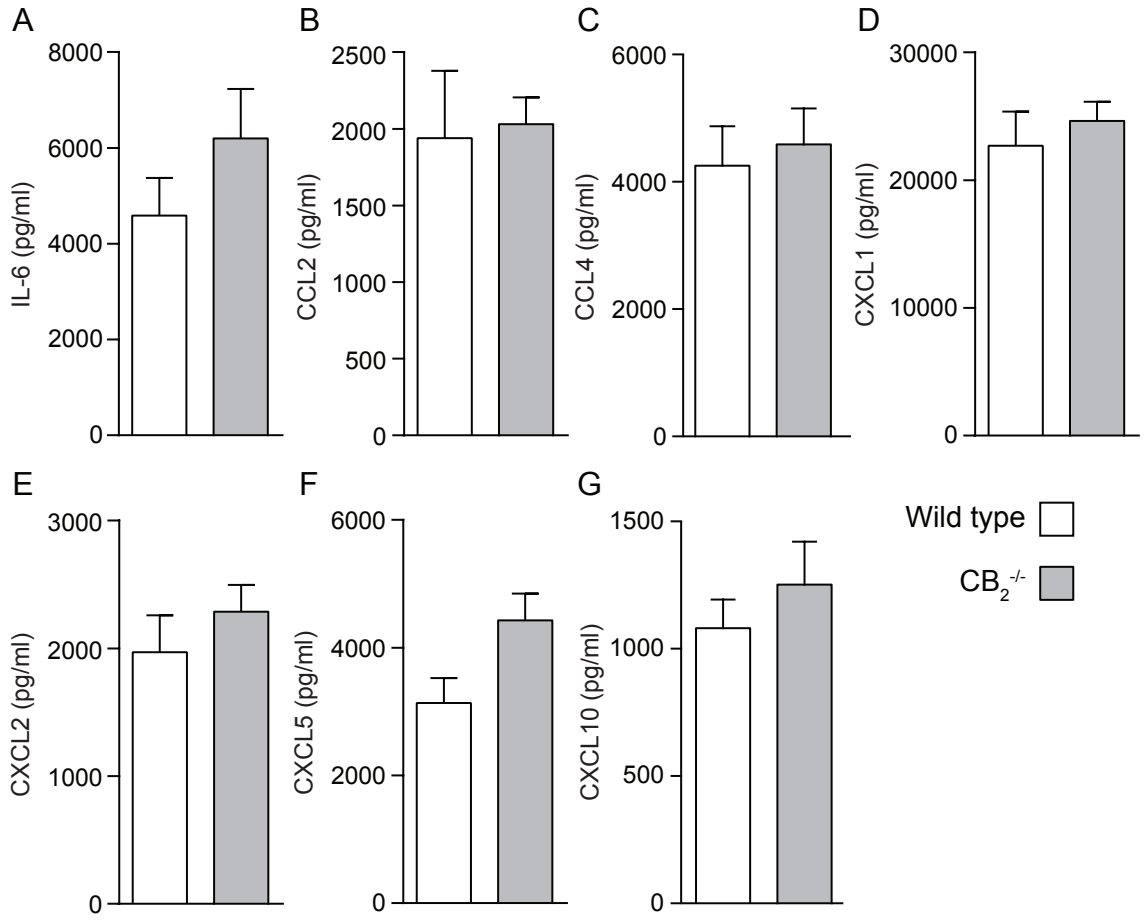

Figure 5.12 There are no differences in the levels of pro-inflammatory mediators in the dorsal air pouch 2 hours after zymosan injection between WT and $CB_2^{-/-}$ animals. The dorsal air pouches of WT or $CB_2^{-/-}$ mice were injected with 100 μg zymosan and 2 hours later the pouches lavaged and the concentration of inflammatory mediators present determined by ELISA. There was no difference in the levels of (A) IL-6, (B) CCL2, (C) CCL4, (D) CXCL1, (E) CXCL2, (F) CXCL5 or (G) CXCL10 in the dorsal air pouch 2 hours after zymosan injection between WT (white bars) and $CB_2^{-/-}$ (grey bars) animals. Data are mean+ SEM, n = 9-10 independent animals per group. Statistical analysis was conducted using the unpaired student's t-test. ns P >0.05.

5.12G). Therefore, these data demonstrate that the difference in neutrophil number during the acute phase response seen between WT and $CB_2^{-/-}$ occurs after the 2 hour time point, and is unlikely due to the presence of higher levels of known neutrophil recruiting chemokines.

5.3.5 $CB_2^{-/-}$ animals have elevated myeloid cell numbers in the dorsal air pouch 48 hours after zymosan challenge

I next wanted to examine whether genetic deletion of CB_2 had any impact on inflammation resolution in the dorsal air pouch inflammation model. To do this, I extended the time course of inflammation by examining the pouch leukocyte populations present 48 hours after dorsal air pouch injection with zymosan. Even at this late time point, neutrophils were still the predominant leukocyte population present, comprising up to 70% of all $CD45^+$ cells in both WT and $CB_2^{-/-}$ animals (Fig 5.13A and E). Alongside $Ly6C^{hi}$ inflammatory monocytes, a sizeable population of $Ly6C^{lo}$ monocytes was present at this time point (Fig 5.13B and F - 9.5-14% of all $CD45^+$ cells for both monocyte subsets). No B cells were found in the pouches of either genotype at this time point (Fig 5.13C and G), however a small population of T cells were present in both WT and $CB_2^{-/-}$ animals, comprising 3.3-5.8% of all $CD45^+$ cells (Fig 5.13D and H).

Quantification of total cell counts found that $CB_2^{-/-}$ animals had significantly higher numbers of $CD45^+$ cells (Fig 5.13I), neutrophils (Fig 5.13J) and $Ly6C^{hi}$ inflammatory monocytes (Fig 5.13L) in the dorsal air pouch 48 hours after zymosan challenge in comparison to WT mice. There was a trend towards more $Ly6C^{lo}$ monocytes in $CB_2^{-/-}$ animals, however this just fell short of reaching significance (Fig 5.13K). Additionally, there was no difference in the total number of T cells present in the pouch 48 hours post zymosan challenge (Fig 5.13M). For both genotypes, the total numbers of $CD45^+$ cells and neutrophils at the 48 hour time point were lower than those seen at 16 hours, whereas the number of $Ly6C^{lo}$ monocytes was higher.

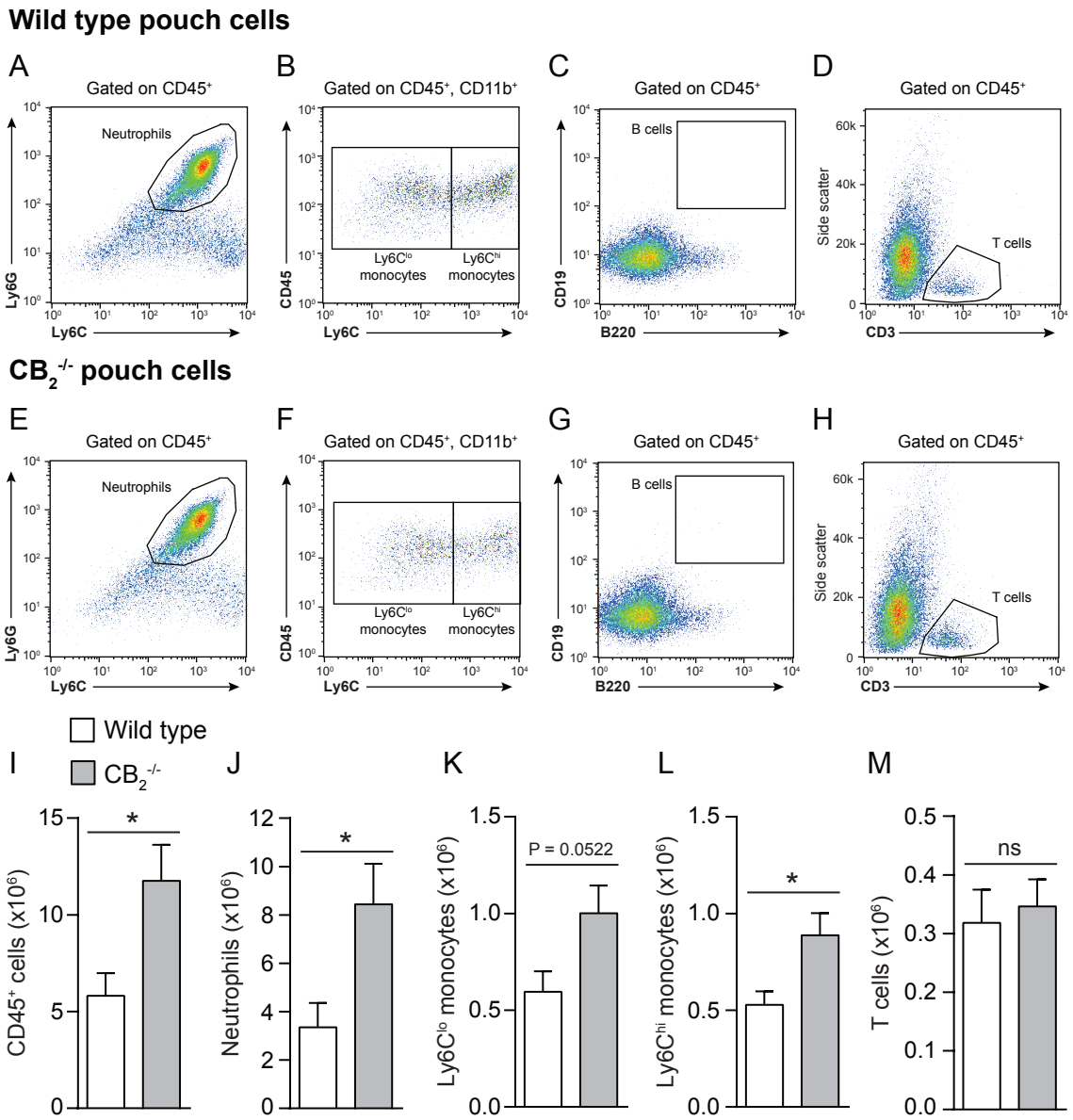

Figure 5.13 $CB_2^{-/-}$ mice have significantly more myeloid cells in the dorsal air pouch 48 hours after zymosan injection compared to WT animals. The dorsal air pouches of WT or $CB_2^{-/-}$ mice were injected with 100 μg zymosan and 48 hours later the pouches lavaged and total cell counts and populations present determined by flow cytometry. Representative dot plots of (A) neutrophils, (B) Ly6C^{lo} and Ly6C^{hi} monocytes, (C) B cells and (D) T cells in the dorsal air pouch of WT mice 48 hours after zymosan injection. Representative dot plots of (E) neutrophils, (F) Ly6C^{lo} and Ly6C^{hi} monocytes, (G) B cells and (H) T cells in the dorsal air pouch of $CB_2^{-/-}$ mice 48 hours after zymosan injection. Quantification of the number of (I) CD45$^+$ cells, (J) neutrophils, (K) Ly6C^{lo} or (L) Ly6C^{hi} monocytes and (M) T cells recruited to the dorsal air pouch 48 hours after zymosan injection in WT (white bars) and $CB_2^{-/-}$ (grey bars) animals. Data are mean+ SEM, n = 5 independent animals per group. Statistical analysis was conducted using the unpaired student's t-test. ns P >0.05, * P <0.05.

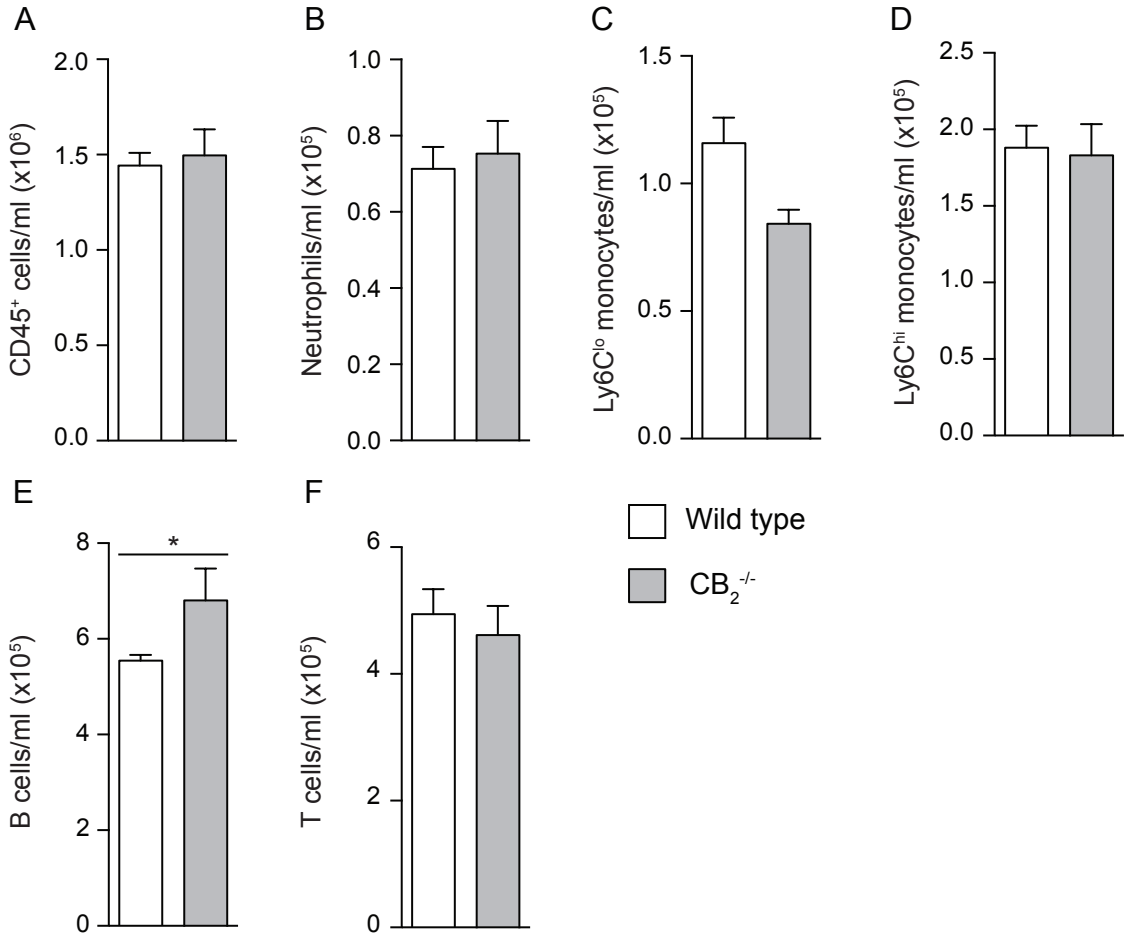

Figure 5.14 $CB_2^{-/-}$ mice have elevated B cell numbers in the blood 48 hours after zymosan injection into the dorsal air pouch. Blood was taken from WT or $CB_2^{-/-}$ animals 48 hours after zymosan injection into the dorsal air pouch and cell counts and populations present determined by flow cytometry. There was no difference in the numbers of (A) $CD45^+$ cells, (B) neutrophils, (C) $Ly6C^{lo}$ monocytes or (D) $Ly6C^{hi}$ monocytes per ml of blood between WT (white bars) or $CB_2^{-/-}$ (grey bars) animals 48 hours after pouch zymosan injection. (E) There were significantly more B cells per ml of blood in $CB_2^{-/-}$ animals 48 hours after zymosan challenge. (F) There was no difference in the number of T cells per ml of blood between WT and $CB_2^{-/-}$ animals 48 hours after zymosan injection. Data are mean+ SEM, n = 5 independent animals per group. Statistical analysis was conducted using the unpaired student's t-test. ns $P > 0.05$, * $P < 0.05$.

When combined with the finding that $CD3^+$ T cells were found in both WT and $CB_2^{-/-}$ pouches, this indicates that this time point falls within the resolution phase of the acute inflammatory response. Analysis of the blood leukocyte composition found that there was no difference in the numbers of $CD45^+$ cells (Fig 5.14A), neutrophils (Fig 5.14B), $Ly6C^{lo}$ monocytes (Fig 5.14C), $Ly6C^{hi}$ monocytes (Fig 5.14D) and T cells (Fig 5.14F) per ml of blood between WT and $CB_2^{-/-}$ animals 48 hours after air pouch zymosan challenge. However, $CB_2^{-/-}$ mice did have a significantly higher B cell count in their blood in comparison to WT mice (Fig 5.14E).

5.3.6 Time course of the zymosan-induced inflammatory response in the dorsal air pouch of WT and $CB_2^{-/-}$ animals

As I have compared the zymosan-induced inflammatory response in the dorsal air pouch of WT and $CB_2^{-/-}$ animals over a range of time points, plotting these data together allows a detailed understanding of the kinetics of the inflammatory response both within and between WT and $CB_2^{-/-}$ animals. The total number of $CD45^+$ cells in the air pouch was low in both genotypes under basal conditions and started to increase after zymosan injection, peaking at 16 hours and then returning towards baseline at 48 hours post zymosan challenge (Fig 5.15A). However in animals lacking CB_2 at 6, 16 and 48 hours post zymosan challenge there were significantly more $CD45^+$ cells present in the pouch when compared to WT animals, demonstrating their exaggerated inflammatory response (Fig 5.15A). The percentage of total cells present that are $CD45^+$ remained consistent throughout the inflammatory time course, with most cells present being leukocytes (Fig 5.15E).

The same kinetics are seen with total neutrophil numbers in the dorsal air pouch, with $CB_2^{-/-}$ animals having significantly higher numbers of neutrophils at 6, 16 and 48 hours post zymosan challenge in comparison to WT animals (Fig 5.15B). The proportion of $CD45^+$ cells that are neutrophils starts at around 20% under basal conditions for both genotypes, but after zymosan challenge this quickly increased,

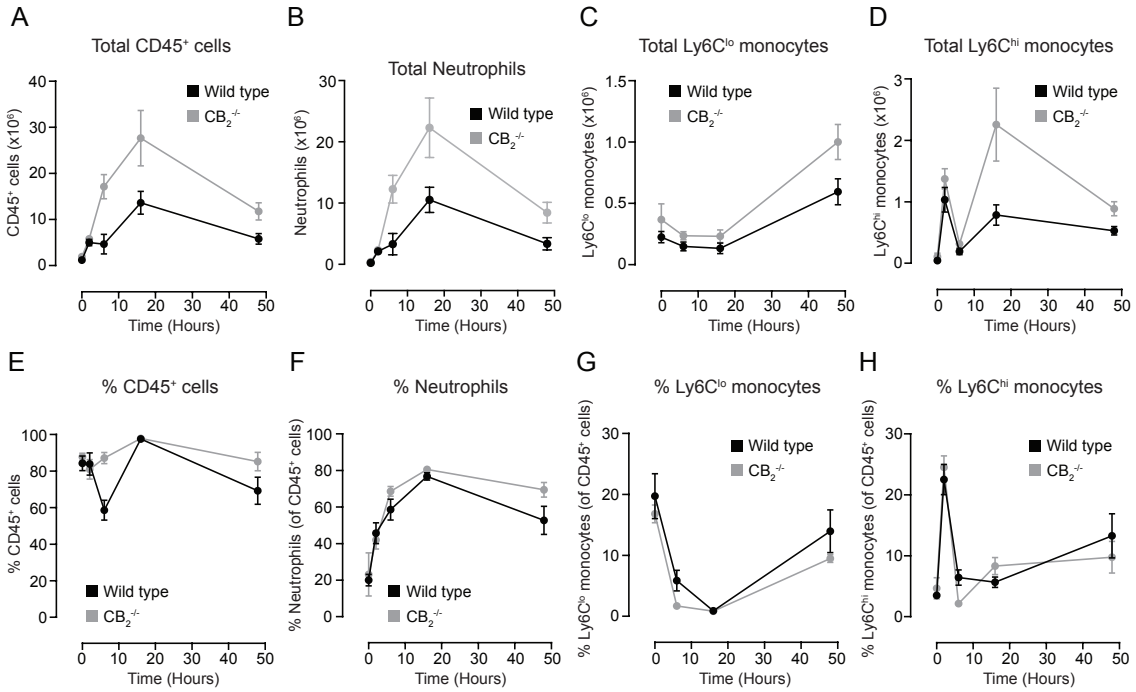

Figure 5.15 Time course of the inflammatory response in the zymosan-induced dorsal air pouch inflammation model in female WT and $CB_2^{-/-}$ animals. The dorsal air pouches of female WT or $CB_2^{-/-}$ mice were injected with 100 μg zymosan and, at the time points indicated, the pouches lavaged and total cell counts and populations present determined by flow cytometry. Time course of the total numbers of (A) $CD45^+$ cells, (B) neutrophils, (C) $Ly6C^{lo}$ and (D) $Ly6C^{hi}$ monocytes in the dorsal air pouch of WT (black) and $CB_2^{-/-}$ (grey) animals following zymosan challenge. Time course of the percentage of total cells that are (E) $CD45^+$ and the percentage of $CD45^+$ cells that are (F) neutrophils, (G) $Ly6C^{lo}$ and (H) $Ly6C^{hi}$ monocytes in the dorsal air pouch of WT (black) and $CB_2^{-/-}$ (grey) animals following zymosan challenge. Data are mean$\pm$ SEM, n = 5-11 independent animals per group.

eventually peaking at 16 hours post challenge, with neutrophils accounting for 80% of all $CD45^+$ cells (Fig 5.15F). This clearly demonstrates how this model of acute inflammation is heavily neutrophil driven. Both $Ly6C^{lo}$ and $Ly6C^{hi}$ monocytes were present under basal conditions, but their kinetics differed markedly. The total number of $Ly6C^{lo}$ monocytes remained relatively constant until 48 hours when an influx was seen in both genotypes (Fig 5.15C), and their proportion of $CD45^+$ cells dropped from basal and began to recover 48 hours after zymosan challenge (Fig 5.15G). However, the number of $Ly6C^{hi}$ monocytes in the pouch rose sharply at 2 hours and returned almost to baseline at 6 hours post zymosan injection in both genotypes (Fig 5.15D), with the same response seen in their proportion of $CD45^+$ cells (Fig 5.15H). Interestingly however, and in contrast to WT mice, there was then a significant influx of inflammatory monocytes in $CB_2^{-/-}$ animals 16 hours post zymosan challenge, with these cells then remaining elevated in $CB_2^{-/-}$ animals at the 48 hour time point (Fig 5.15D).

When comparing the blood leukocyte composition over the time course of the dorsal air pouch inflammation model between WT and $CB_2^{-/-}$ animals, there are few differences in the response between the genotypes. Whilst the proportion of $CD45^+$ cells after blood lysis remained constant throughout (Fig 5.16E), the number of $CD45^+$ cells per ml of blood peaked at 2 hours post dorsal pouch injection of zymosan, returned to baseline and then steadily increased up to 48 hours post zymosan challenge in both genotypes (Fig 5.16A). The number of neutrophils in the blood also peaked 2 hours after zymosan injection before returning to baseline at 16 hours (Fig 5.16B), with similar kinetics seen for the proportionality of neutrophils in the blood (Fig 5.16F). The picture is much the same for both $Ly6C^{lo}$ and $Ly6C^{hi}$ monocytes with an early peak in total numbers and proportionality that returned to baseline at the 16 hour time point (Fig 5.16C and G - $Ly6C^{lo}$ monocytes; Fig5.16D and H - $Ly6C^{hi}$ monocytes). However, in contrast to neutrophils, the number and proportionality of $Ly6C^{lo}$ and Ly6C*hi* monocytes started to increase towards the the 48 hour time point (Fig 5.16B-D and F-H).

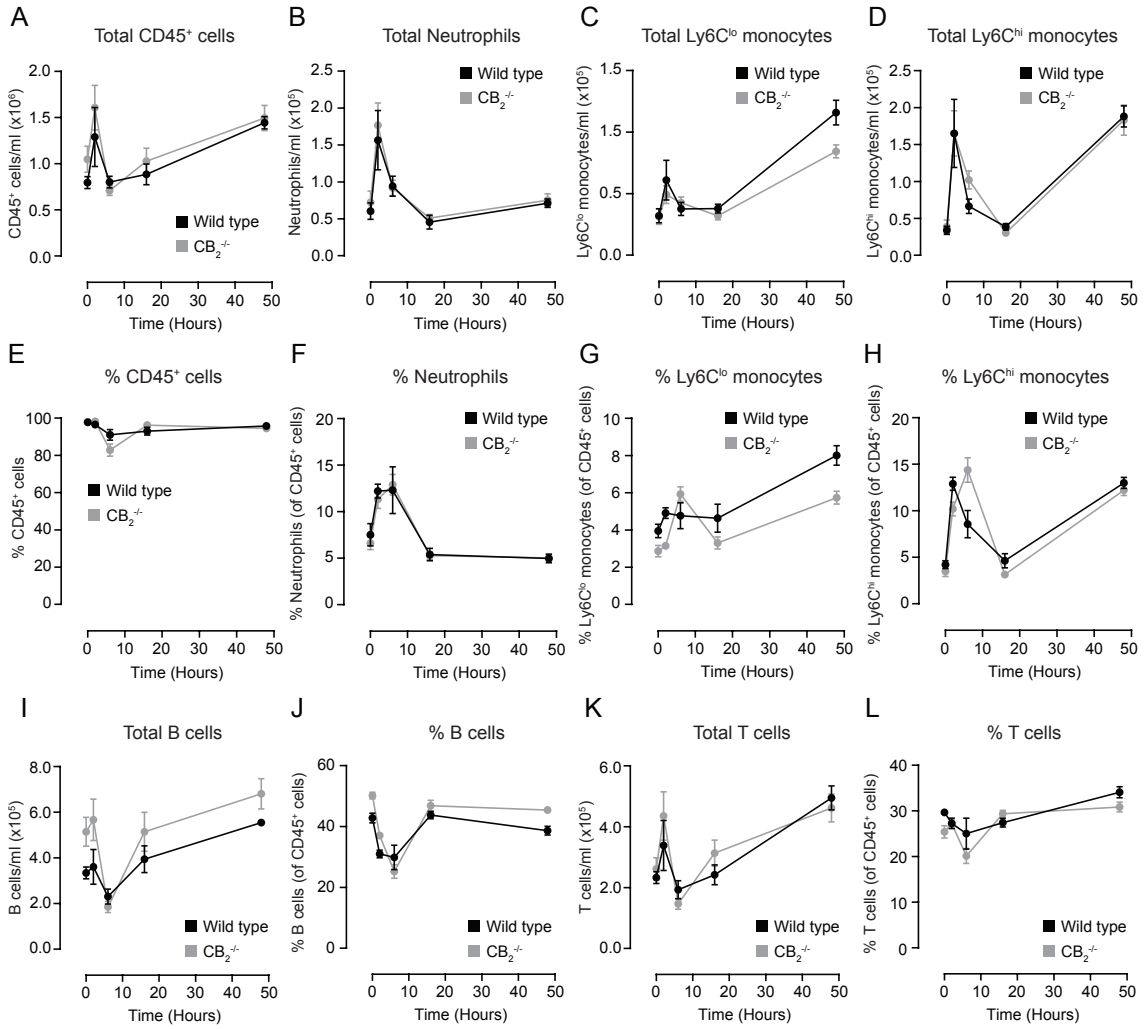

Figure 5.16 Time course of blood leukocyte dynamics in the zymosan-induced dorsal air pouch inflammation model in female WT and $CB_2^{-/-}$ animals. Blood was taken from female WT or $CB_2^{-/-}$ mice at the time points indicated after injection of 100 μg zymosan into the dorsal air pouch. Cell counts and populations present were determined by flow cytometry. Time course of the total numbers of (A) $CD45^+$ cells, (B) neutrophils, (C) $Ly6C^{lo}$ and (D) $Ly6C^{hi}$ monocytes per ml of blood in WT (black) and $CB_2^{-/-}$ (grey) animals following zymosan challenge. Time course of the percentage of total blood cells that are (E) $CD45^+$ and the percentage of $CD45^+$ cells that are (F) neutrophils, (G) $Ly6C^{lo}$ and (H) $Ly6C^{hi}$ monocytes in the blood of WT (black) and $CB_2^{-/-}$ (grey) animals following zymosan challenge. Time course of the total number and percentage of B cells (I and J respectively) and T cells (K and L respectively) in the blood of WT and $CB_2^{-/-}$ animals following zymosan challenge. Data are mean± SEM, n = 5-11 independent animals per group.

When concentrating on the lymphocyte populations, T cells show similar kinetics to those of the myeloid cells, peaking at 2 hours, dipping and then steadily increasing towards 48 hours post zymosan (Fig 5.16K and L). However, B cells show an opposite trend, as their number and proportionality decreased following zymosan injection, reaching a minimum at 6 hours and returning to baseline by the 48 hour time point (Fig 5.16I and J). As previously noted, the number of B cells in the blood was significantly higher in $CB_2^{-/-}$ animals under basal conditions and at 48 hours post zymosan injection (Fig 5.16I).

5.3.7 Male $CB_2^{-/-}$ animals also have an exaggerated acute inflammatory response

So far I have only used female animals in the dorsal air pouch inflammation model. Therefore I wanted to examine whether males display the same phenotype in the air pouch model, as differences in inflammatory responses between male and female animals have been well documented in the literature [599–601]. Therefore, I compared air pouch leukocyte recruitment and inflammatory mediator production between male WT and $CB_2^{-/-}$ animals 6 hours after injection of 100 μg zymosan into the dorsal air pouch.

Mirroring the results seen when using female animals, neutrophils comprised the dominant leukocyte population present in both genotypes 6 hours after zymosan challenge (Fig 5.17A and C) and male $CB_2^{-/-}$ mice had significantly higher numbers of $CD45^+$ cells and neutrophils in the air pouch compared to male WT animals (Fig 5.17E and F). Interestingly however, the effect size seen was smaller than that of the females, due to the increased leukocyte numbers present in the pouch of male WT animals (Fig 5.5I and J vs Fig5.17E and F). Both $Ly6C^{lo}$ and $Ly6C^{hi}$ monocytes were present in the male air pouch (Fig 5.17B and D), but there was no difference in their absolute number between the genotypes 6 hours after zymosan injection (Fig 5.17G and H). Analysis of inflammatory mediators in the pouch lavage fluid 6 hours

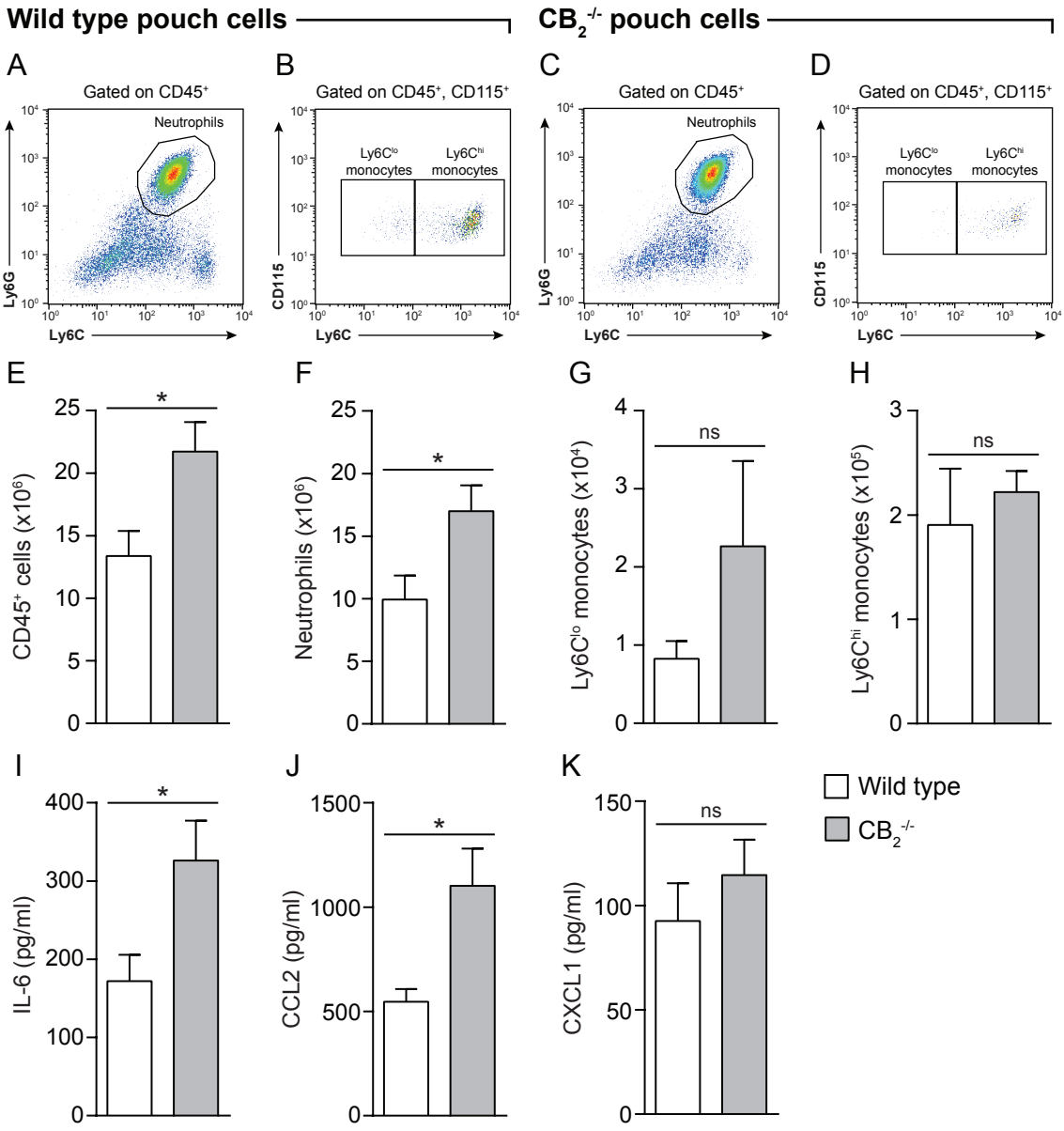

Figure 5.17 Male $CB_2^{-/-}$ animals have an exaggerated acute inflammatory response 6 hours after pouch zymosan injection. The dorsal air pouches of male WT or $CB_2^{-/-}$ mice were injected with 100 μg zymosan and 6 hours later the pouches lavaged and total cell counts and populations present determined by flow cytometry. Representative dot plots of (A) neutrophils and (B) Ly6C^{lo} and Ly6C^{hi} monocytes in the dorsal air pouch of male WT mice 6 hours after zymosan injection. Representative dot plots of (C) neutrophils and (D) Ly6C^{lo} and Ly6C^{hi} monocytes in the dorsal air pouch of male $CB_2^{-/-}$ mice 6 hours after zymosan injection. Quantification of the number of (E) CD45$^+$ cells, (F) neutrophils, (G) Ly6C^{lo} or (H) Ly6C^{hi} monocytes recruited to the dorsal air pouch 6 hours after zymosan injection in male WT (white bars) and $CB_2^{-/-}$ (grey bars) animals. The levels of pro-inflammatory mediators present in the air pouch were determined by ELISA and male $CB_2^{-/-}$ mice had significantly higher levels of (I) IL-6 and (J) CCL2 compared to WT animals. (K) There was no difference in the level of CXCL1 between the genotypes. Data are mean+ SEM, n = 6-8 independent animals per group. Statistical analysis was conducted using the unpaired student's t-test. ns P >0.05, * P <0.05, ** P <0.01.

after zymosan challenge in male animals found that the levels of IL-6 and CCL2 were significantly higher in $CB_2^{-/-}$ mice (Fig 5.17I and J), whereas the level of CXCL1 was very low with no difference between the genotypes (Fig 5.17K), recapitulating the results seen in female animals. Therefore, taken together these data demonstrate that male $CB_2^{-/-}$ animals also have an exaggerated acute inflammatory response 6 hours after zymosan challenge.

5.3.8 Genetic deletion of CB_2 has no effect on the acute inflammatory response in the zymosan-induced peritonitis model

I next wanted to discover whether CB_2 plays a general role in the regulation of an acute inflammatory response. To begin to address this question I examined whether female $CB_2^{-/-}$ mice also have an exaggerated acute inflammatory response in the ZIP model; an inflammatory experimental system well characterised in my laboratory and in the literature. Importantly, as the same gender of animals and inflammatory stimulus will be used as in the dorsal air pouch experiments, this will allow me to compare differences in anatomical site only. To study the acute phase of the ZIP model, I compared leukocyte recruitment and inflammatory mediator production in the peritoneal cavity of female WT and $CB_2^{-/-}$ animals 4 hours after intraperitoneal injection of 100 μg of zymosan, as this is when peak neutrophil numbers are seen.

Interestingly, there was no difference in the number of $CD45^+$ cells present in the peritoneum between the two genotypes (Fig 5.18E). Neutrophils formed the dominant cell population present in both genotypes and a clear $Ly6C^{hi}$ inflammatory monocyte population was also present (Fig 5.18A and C). However there was no difference in the number of neutrophils (Fig 5.18F) or $Ly6C^{hi}$ monocytes (Fig 5.18G) recruited to the peritoneal cavity 4 hours after zymosan injection between WT and $CB_2^{-/-}$ mice. In the peritoneum, both B and B-1 cells were present in both genotypes (Fig 5.18B and D), and although there was no difference in the number of B cells present between the genotypes (Fig 5.18H), there were significantly more B-1 cells in

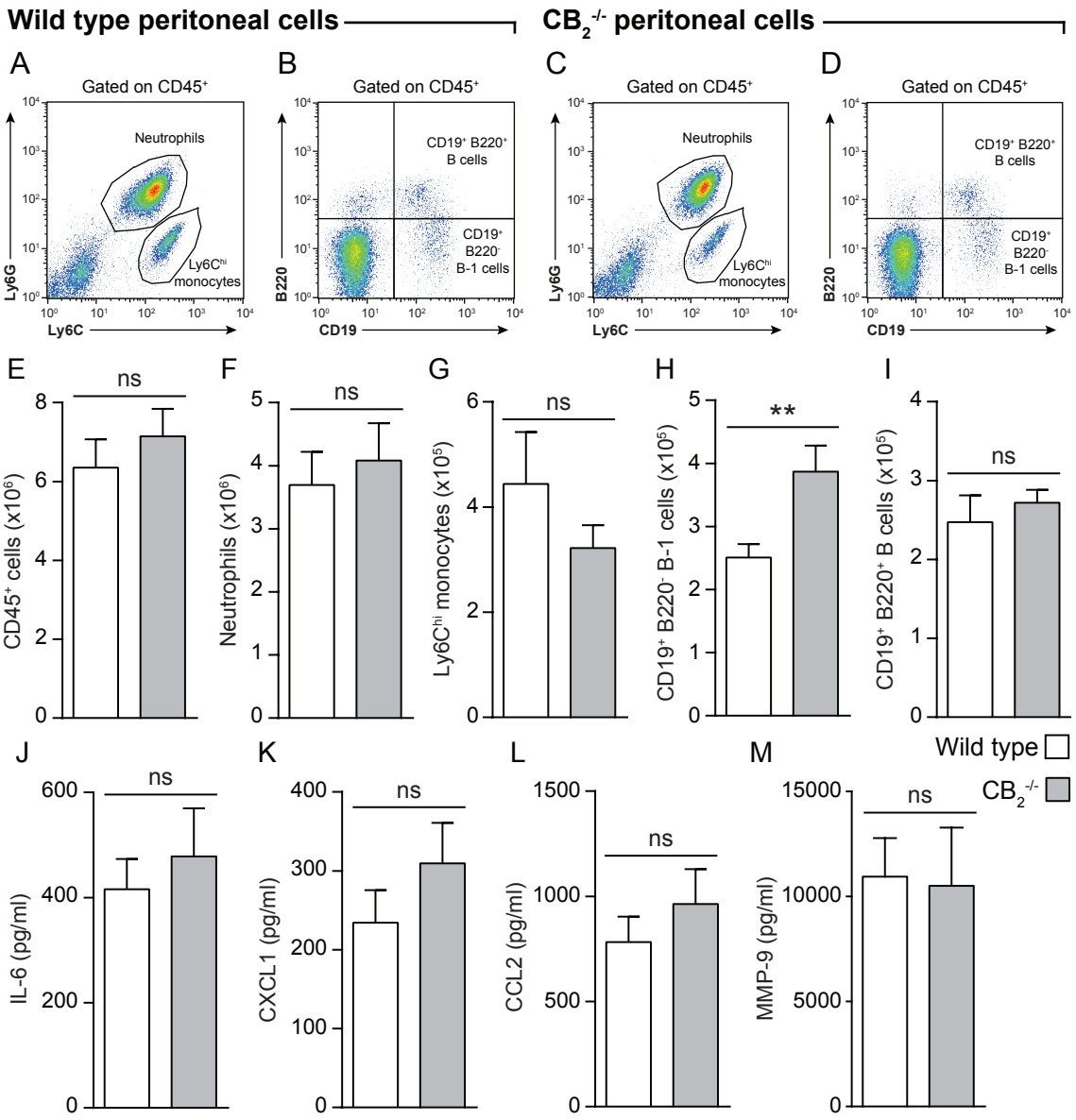

Figure 5.18 Genetic deletion of CB_2 has no effect on the acute inflammatory response in the zymosan-induced peritonitis model. Female WT or $CB_2^{-/-}$ mice were injected intraperitoneally with 100 μg zymosan and 4 hours later the peritoneum was lavaged and total cell counts and populations present determined by flow cytometry. Representative dot plots of (A) neutrophils and Ly6C^{hi} monocytes and (B) CD19$^+$ B220$^-$ B-1 cells and CD19$^+$ B220$^+$ B cells recruited to the peritoneum of WT animals 4 hours after i.p zymosan injection. Representative dot plots of (C) neutrophils and Ly6C^{hi} monocytes and (D) CD19$^+$ B220$^-$ B-1 cells and CD19$^+$ B220$^+$ B cells recruited to the peritoneum of $CB_2^{-/-}$ animals 4 hours after i.p zymosan injection. Quantification of the number of (E) CD45$^+$ cells, (F) neutrophils, (G) Ly6C^{hi} monocytes, (H) CD19$^+$ B220$^-$ B-1 cells and (I) CD19$^+$ B220$^+$ B cells recruited to the peritoneum of WT (white bars) or $CB_2^{-/-}$ (grey bars) animals 4 hours after i.p injection of zymosan. The amounts of pro-inflammatory mediators present in the peritoneal cavity were determined by Luminex or ELISA and no difference in the levels of (J) IL-6, (K) CXCL1, (L) CCL2 or (M) MMP-9 was found between the genotypes. Data are mean+ SEM, n = 9-11 independent animals per group. Statistical analysis was conducted using the unpaired student's t-test. ns P >0.05, ** P <0.01.

the peritoneum of $CB_2^{-/-}$ animals (Fig 5.18I). Analysis of the inflammatory mediators present in the peritoneal lavage fluid 4 hours after zymosan injection found that there was no difference in the levels of IL-6, CXCL1, CCL2 or MMP-9 between the genotypes (Fig 5.18J, K, L and M).

Importantly, the finding that $CB_2^{-/-}$ animals do not have an exaggerated acute inflammatory response in the ZIP model has been confirmed in our lab. A comparison of male WT and $CB_2^{-/-}$ mice found that there was no difference in inflammatory cell recruitment or mediator production between the two genotypes over a wide range of time points (T Kapellos 2016, Personal Communication). Therefore these and my data show that $CB_2^{-/-}$ animals do not have an exaggerated acute inflammatory response in the ZIP model and suggest that CB_2 does not play a generic role in the regulation of inflammation. Instead, it is likely that CB_2 plays a context-dependent role in the regulation of a zymosan-induced inflammatory response.

5.3.9 Lack of CB_2 in the myeloid population is responsible for increased neutrophil recruitment to the dorsal air pouch in $CB_2^{-/-}$ animals

With this in mind, I returned to the female air pouch inflammation model and began searching for a potential mechanism underlying the increased air pouch recruitment of neutrophils in $CB_2^{-/-}$ animals, as understanding the pathway(s) responsible would also shed light on why deletion of CB_2 only exaggerates inflammation in specific anatomical locations. I started by questioning whether deletion of CB_2 in the myeloid or non-myeloid compartment, or both, is responsible for increased neutrophil pouch recruitment, by generating mixed bone marrow chimeric animals following the scheme detailed in figure 5.19A.

This process involved isolating bone marrow cells from $CB_2^{-/-}$ animals, which express the CD45.2 surface antigen, and from WT B6.SJL animals, which are of the black six genetic background but express the CD45.1 surface antigen. These cells were then mixed in equal parts and injected into WT or $CB_2^{-/-}$ animals that had been

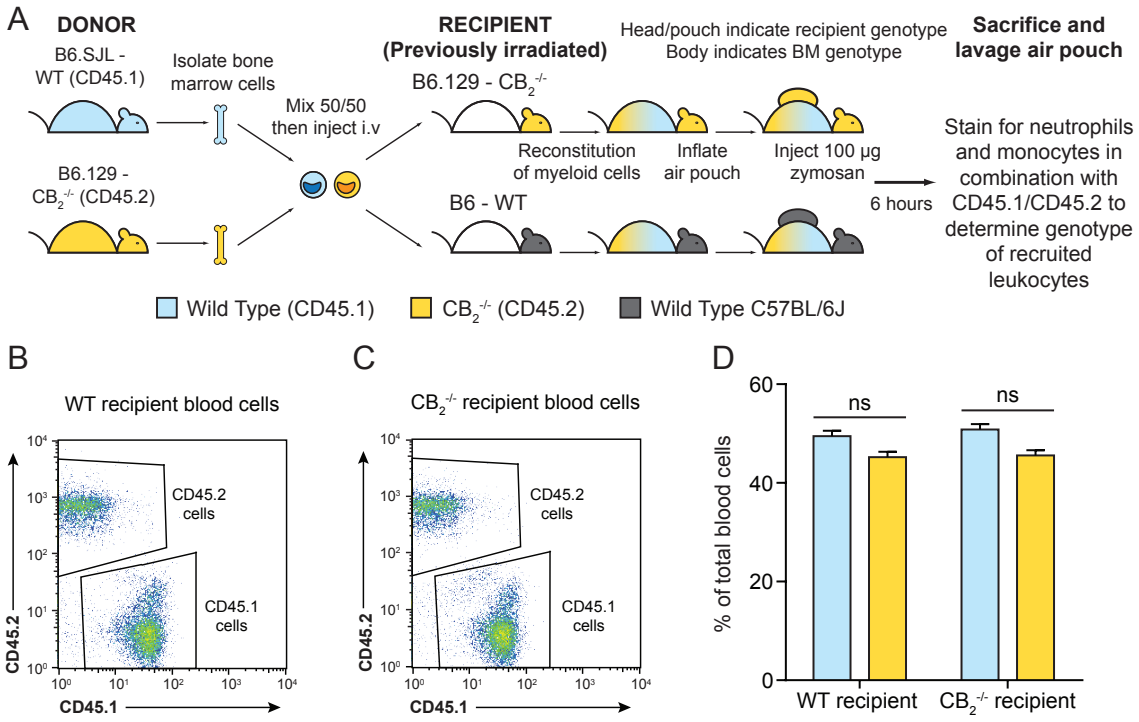

Figure 5.19 Generation of mixed bone marrow chimeric animals. (A) Scheme detailing the strategy used to generate mixed bone marrow chimeric animals. The color of the air pouch and head denotes the recipient genotype and the color of the body denotes the genotype of the bone marrow-derived cells. Bone marrow cells were isolated from B6.SJL WT animals that have the CD45.1 surface antigen (blue) and B6.129 $CB_2^{-/-}$ animals that have the CD45.2 surface antigen (yellow), mixed in equal amounts and then injected intravenously into either C57BL/6J WT or $CB_2^{-/-}$ animals that had previously been irradiated to remove their endogenous bone marrow. The animals were then left to allow reconstitution of the bone marrow and myeloid cell populations and 8-10 weeks later, blood was taken from the tail vein of (B) WT and (C) $CB_2^{-/-}$ recipient animals and the proportion of CD45.1/CD45.2 cells determined by flow cytometry. (D) Quantification demonstrated that there was no significant difference in the proportion of CD45.1/CD45.2 cells in the blood of either the WT or $CB_2^{-/-}$ recipient animals prior to their usage in the dorsal air pouch inflammation model. Data are mean+ SEM, n = 9-11 independent animals per group. Statistical analysis was conducted by two-way ANOVA with Sidak's multiple comparisons correction. ns P >0.05.

previously irradiated to remove their endogenous bone marrow cells. These injected cells re-populate the bone marrow and allow the generation of animals with an equal mix of WT and $CB_2^{-/-}$ bone marrow-derived cells, but WT or $CB_2^{-/-}$ non-myeloid cells (i.e. cells lining the air pouch). As the WT and $CB_2^{-/-}$ myeloid-derived cells are differentially labelled (CD45.1 vs CD45.2), I can therefore simultaneously assess the trafficking of both WT and $CB_2^{-/-}$ neutrophils in WT or CB_2 deficient backgrounds using the dorsal air pouch inflammation model.

Eight weeks after generation of these chimeric animals, and one week before the air pouch inflammation model was performed, tail blood was taken from each animal to assess the relative proportion of CD45.1 to CD45.2 cells in the blood and examine whether the bone marrow re-population had been successful. Representative flow cytometry dot plots of CD45.1 and CD45.2 cells in the blood of WT and $CB_2^{-/-}$ recipient animals can be seen in figures 5.19B and C and quantification demonstrated that there was no difference in the proportion of CD45.1 and CD45.2 cells in the blood of both the WT and $CB_2^{-/-}$ recipient animals after bone marrow reconstitution (Fig 5.19D).

These bone marrow chimeric animals were then used in the dorsal air pouch inflammation model, with pouch leukocyte recruitment examined 6 hours after zymosan injection. There was no difference in the number of total cells recruited to the dorsal air pouch between WT or $CB_2^{-/-}$ recipient animals 6 hours after zymosan challenge (Fig 5.20A). As previous, the majority of cells recruited to the air pouch in both WT and $CB_2^{-/-}$ recipients were neutrophils (Fig 5.20B and E), however this population was made up of proportionally more CD45.2 neutrophils than CD45.1 neutrophils in both recipient genotypes (Fig 5.20C and F). Quantification of the numbers of CD45.1 and CD45.2 neutrophils found that in both WT and $CB_2^{-/-}$ recipients there were significantly more CD45.2 neutrophils than CD45.1 neutrophils recruited to the dorsal air pouch 6 hours after zymosan challenge (Fig 5.20H). A small Ly6C^{hi} monocyte population was also present in both recipient genotypes (Fig 5.20B and E), but this comprised of approximately equal proportions

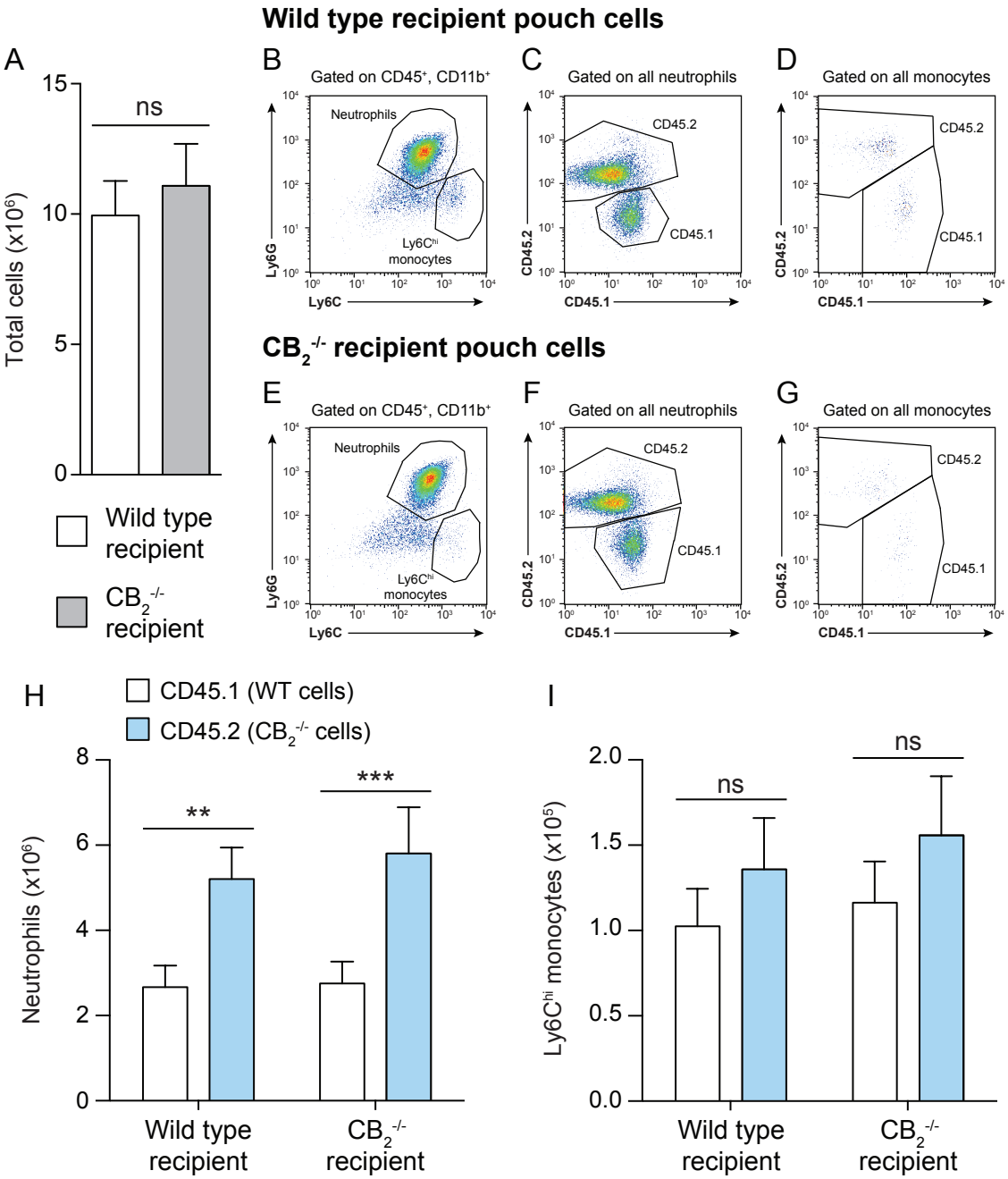

Figure 5.20 Lack of CB_2 in myeloid cells is responsible for increased neutrophil air pouch recruitment in $CB_2^{-/-}$ animals. WT or $CB_2^{-/-}$ bone marrow chimeric animals containing an equal mix of CD45.1 (WT) and CD45.2 ($CB_2^{-/-}$) myeloid cells were used in the dorsal air pouch inflammation model. Six hours after zymosan injection (100 μg), air pouches were lavaged and total cell counts, cell populations present and the relative amounts of CD45.1/CD45.2 cells calculated by flow cytometry. (A) Total cell numbers in the dorsal air pouches of WT (white bars) or $CB_2^{-/-}$ (grey bars) recipient animals 6 hours after zymosan injection. Representative dot plots of (B) total neutrophils and Ly6C^{hi} monocytes and the proportion of (C) neutrophils and (D) Ly6C^{hi} monocytes that were CD45.1 or CD45.2 positive in WT recipient animals. Representative dot plots of (E) total neutrophils and Ly6C^{hi} monocytes and the proportion of (F) neutrophils and (G) Ly6C^{hi} monocytes that were CD45.1 or CD45.2 positive in $CB_2^{-/-}$ recipient animals. (H) Quantification demonstrated that there were significantly more CD45.2 (blue bars) than CD45.1 (white bars) neutrophils recruited to the air pouch of both WT and $CB_2^{-/-}$ animals. (I) There was no difference between the number of CD45.1 and CD45.2 Ly6C^{hi} monocytes recruited to the air pouch of both WT and $CB_2^{-/-}$ animals. Data are mean+ SEM, n = 9-11 independent animals per group. Statistical analysis was conducted by two-way ANOVA with Sidak's multiple comparisons correction. ns P >0.05, ** P <0.01, *** P <0.001.

of CD45.1 and CD45.2 cells (Fig 5.20D and G) and quantification found that in both WT and $CB_2^{-/-}$ recipients there was no difference between the number of CD45.1 and CD45.2 Ly6C^{hi} monocytes in the pouch (Fig 5.20I).

The relative proportion of CD45.1 and CD45.2 neutrophils and Ly6C^{hi} monocytes in the blood of these animals 6 hours after zymosan pouch injection was also examined. The neutrophils and Ly6C^{hi} monocytes present in the blood of both recipient genotypes (Fig 5.21A and D) were comprised of approximately equal proportions of CD45.1 and CD45.2 cells (Neutrophils - Fig 5.21B and E; monocytes - Fig 5.21C and F) and quantification found that there was no difference between the numbers of CD45.1 and CD45.2 neutrophils (Fig 5.21G) and Ly6C^{hi} monocytes (Fig 5.21H) per ml of blood in either WT or $CB_2^{-/-}$ recipient animals. Therefore, this rules out the explanation that the increased number of CD45.2, and therefore $CB_2^{-/-}$, neutrophils in the pouch of both WT and $CB_2^{-/-}$ recipients was due to a disproportionate number of CD45.2 neutrophils in the blood. Instead taken together these data clearly demonstrate that it is the lack of CB_2 on the neutrophils themselves, as opposed to a non-myeloid stromal cell population, that is responsible for the increased trafficking of neutrophils into the dorsal air pouch of $CB_2^{-/-}$ animals.

5.3.10 Genetic deletion of CB_2 has no effect on inflammatory mediator production by air pouch-derived fibroblasts

One implication from the above results is that deletion of CB_2 in the radio-resistant fibroblast-like cells that line the air pouch is not responsible for increased air pouch neutrophil recruitment seen in $CB_2^{-/-}$ animals. To further test this hypothesis, I isolated the cells lining the dorsal air pouch of WT and $CB_2^{-/-}$ mice and examined their response to zymosan *in vitro*.

RT-PCR analysis found that both WT and $CB_2^{-/-}$ pouch lining cells expressed high levels of the fibroblast marker vimentin, confirming that they are indeed fibroblast-like cells (Fig 5.22A). Under basal conditions, CB_2 is expressed by these

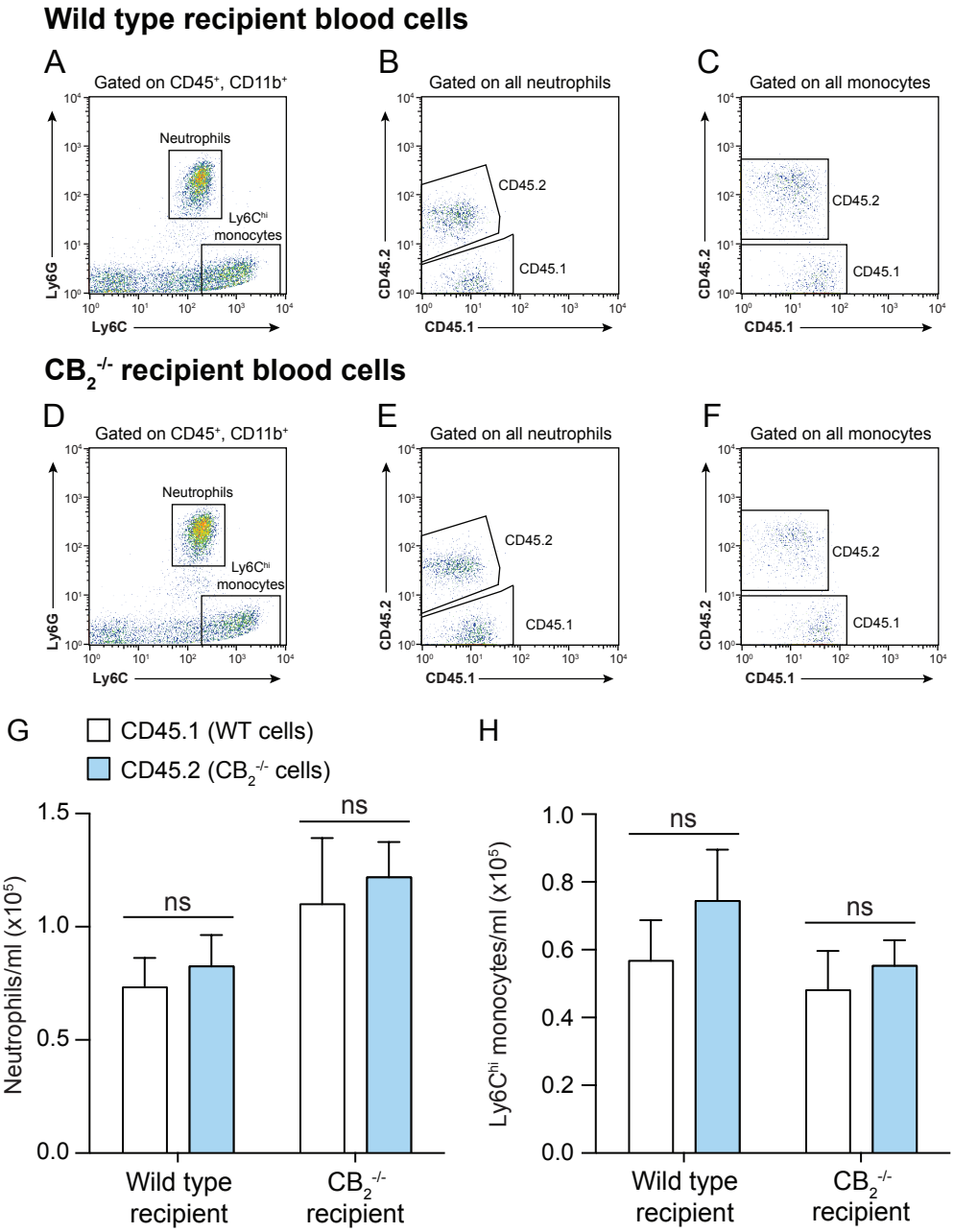

Figure 5.21 There is no difference in the proportion of CD45.1 to CD45.2 neutrophils in the blood of WT or $CB_2^{-/-}$ bone marrow chimera recipient animals 6 hours after zymosan challenge. Blood was taken from WT or $CB_2^{-/-}$ bone marrow chimeric animals 6 hours after dorsal air pouch injection with zymosan (100 μg) and cell counts and populations present were determined by flow cytometry. (A) Representative dot plots of blood neutrophils and Ly6C^{hi} monocytes and the proportion of (B) neutrophils and (C)Ly6C^{hi} monocytes that are CD45.1 or CD45.2 in WT recipient animals. (D) Representative dot plots of blood neutrophils and Ly6C^{hi} monocytes and the proportion of (E) neutrophils and (F) Ly6C^{hi} monocytes that are CD45.1 or CD45.2 in $CB_2^{-/-}$ recipient animals. Quantification of the blood leukocytes present found that there was no difference between the numbers of CD45.1 and CD45.2 (G) neutrophils or (H) Ly6C^{hi} monocytes per ml of blood between WT and $CB_2^{-/-}$ recipient bone marrow chimeric animals. Data are mean+ SEM, n = 9-10 independent animals. Statistical analysis was conducted by two-way ANOVA with Sidak's multiple comparisons correction. ns P >0.05.

cells, but its expression is significantly reduced following stimulation with zymosan for 6 hours (Fig 5.22B). Some residual expression of CB_2 mRNA was detectable in pouch fibroblasts isolated from $CB_2^{-/-}$ mice. Both WT and $CB_2^{-/-}$ pouch fibroblasts expressed TLR-2 (a receptor for zymosan) under basal conditions, and following zymosan treatment its expression increased to a similar level of that seen in bio-gel macrophages (Fig 5.22C). However, WT and $CB_2^{-/-}$ pouch fibroblasts expressed negligible levels of Dectin-1, another zymosan sensing receptor (Fig 5.22D). Stimulation of both WT and $CB_2^{-/-}$ pouch fibroblasts with zymosan caused a significant increase in their production of IL-6, CCL2, CXCL1 and CXCL5, however there was no difference in the levels of any of these inflammatory proteins between the two genotypes (Fig 5.22E-H).

To further strengthen these above results, I examined inflammatory mediator production by air pouch lining tissue explants in response to zymosan stimulation. By keeping the tissue intact I hoped that this would mimic as closely as possible the tissue response that would be elicited *in vivo*. Whilst zymosan stimulation caused a trend towards increased production of IL-6, CCL2, CXCL1 and CXCL5 in both WT and $CB_2^{-/-}$ pouch explants, there was no difference in the levels of any of these inflammatory proteins between the two genotypes (Fig 5.22I-L). It is interesting to note that the level of CXCL1 produced by the air pouch explant tissue is markedly higher than any other mediator, and likely explains the high level of neutrophil recruitment seen in the zymosan-induced air pouch inflammation model.

Therefore in conclusion, these data strengthen the hypothesis that deletion of CB_2 in the pouch lining cells is not responsible for the increased air pouch neutrophil recruitment seen in $CB_2^{-/-}$ animals, as WT and $CB_2^{-/-}$ air pouch-derived fibroblasts and tissue explants produce the same levels of neutrophil recruiting inflammatory mediators in response to zymosan stimulation.

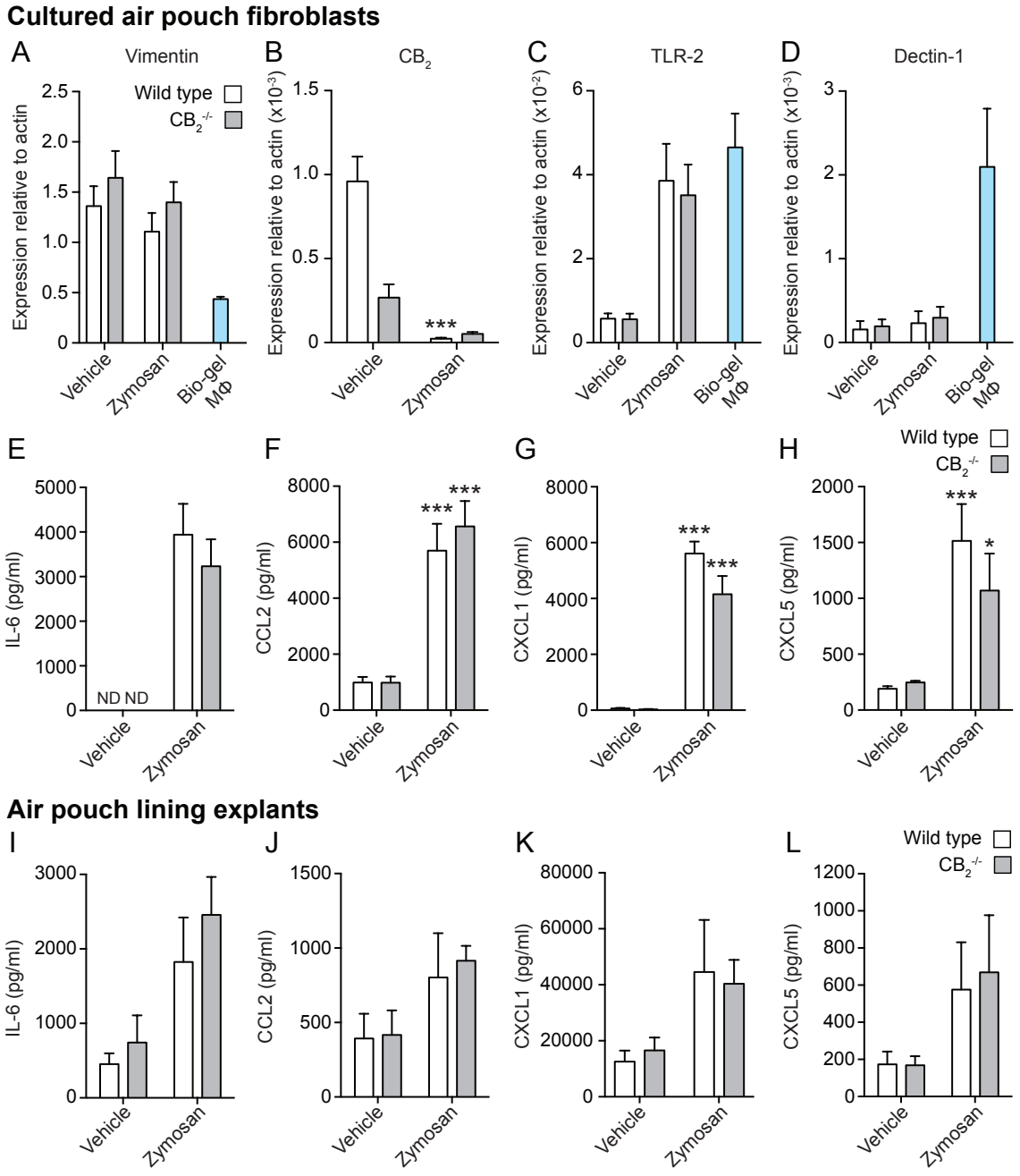

Figure 5.22 Genetic deletion of $CB_2^{-/-}$ in air pouch fibroblasts has no effect on inflammatory mediator production in response to zymosan. Fibroblasts lining the air pouches of WT (white bars) and $CB_2^{-/-}$ (grey bars) mice were stimulated with 10 μg/ml zymosan for 6 hours. Gene expression was measured by RT-PCR and (A) Both WT and $CB_2^{-/-}$ fibroblasts expressed high levels of vimentin. (B) Fibroblasts expressed CB_2, with the levels significantly reduced after zymosan challenge. (C) WT and $CB_2^{-/-}$ fibroblasts expressed TLR-2, with levels increased after zymosan stimulation. (D) WT and $CB_2^{-/-}$ fibroblasts expressed negligible amounts of dectin-1. Bio-gel macrophage gene expression is shown for comparison (blue bars). There was no difference in the levels of (E) IL-6, (F) CCL2, (G) CXCL1 or (H) CXCL5 in the fibroblast culture supernatant, before or after zymosan stimulation, between the genotypes. In all cases zymosan treatment caused a significant increase in mediator production. Data are mean+ SEM, n = 5-7 biological replicates. (I-L) Dorsal air pouch tissue was removed and placed into culture medium with or without zymosan for 3 hours before the supernatants were collected. There was no difference in the levels of (I) IL-6, (J) CCL2, (K) CXCL1 or (L) CXCL5 produced by the air pouch explants between either genotype. Data are mean+ SEM, n = 3-4 biological replicates. Statistical analysis was conducted by two-way ANOVA with Sidak's multiple comparisons correction. ns P >0.05, * P <0.05, *** P <0.001. ND = not detected.

5.4 Discussion

I began this chapter with two aims; firstly to compare immune cell recruitment between WT and $CB_2^{-/-}$ animals using the zymosan-induced dorsal air pouch inflammation model and secondly to investigate the mechanistic basis behind any differences in the acute inflammatory response between WT and $CB_2^{-/-}$ mice.

With regards to the first aim, I found that $CB_2^{-/-}$ animals have increased neutrophil recruitment, in comparison to WT animals, during the acute inflammatory phase of the dorsal air pouch model, and that they still have increased leukocyte numbers in the pouch during the resolution phase of the inflammatory response. Although genetic deletion of CB_2 has been previously shown to result in increased neutrophil trafficking to sites of inflammation during IR injury [310, 315, 319, 324], EAE [283, 286], sepsis [268, 272] and colitis [255], these studies rely on histological analysis of leukocyte/neutrophil tissue recruitment, which is semi-quantitative, or tissue MPO activity that only provides a surrogate readout for how many neutrophils have been recruited to the inflammatory site. Furthermore, these studies only examine a single time point and largely do not examine the mechanistic basis underlying increased neutrophil recruitment. In contrast, my work provides the first example of a fully quantitative analysis of the effect of genetic deletion of CB_2 on neutrophil, and other innate immune cell, recruitment during an acute inflammatory response over a comprehensive inflammation time course. Furthermore, I have provided mechanistic insights into the enhanced acute inflammatory response seen in $CB_2^{-/-}$ animals, which will be discussed later in this section.

The increased pouch neutrophil recruitment seen in $CB_2^{-/-}$ animals is not due to differences in the number of immune cells in the pouch or blood under basal conditions. Importantly, in both the pouch and the blood there was no difference in the number of neutrophils present at baseline. The only difference seen between the two genotypes under basal conditions was the number of B cells per ml of blood. This

result was expected as previous work has demonstrated that naive $CB_2^{-/-}$ animals have increased B cell numbers in the blood, as lack of CB_2 disrupts B cell retention in the marginal zone of the spleen [242, 243]. Furthermore, although B cells numbers drop in both WT and $CB_2^{-/-}$ animals during the acute inflammatory phase, the increased B cell phenotype of $CB_2^{-/-}$ animals is restored at 48 hours, implying that the model is in the resolution phase at this time point.

One interesting finding from my results is that male WT mice had higher numbers of $CD45^+$ cells and neutrophils than female WT mice in the dorsal air pouch 6 hours after zymosan challenge. This result is perhaps not that unexpected as gender has been shown to impact on a range of inflammatory processes such as sepsis, atheroscelrosis, pain, arthritis and autoimmune disease [600, 602–604], and during acute inflammation it has been well documented that male animals mount a more robust inflammatory response than females. In the zymosan-induced peritonitis model, male animals have increased peritoneal recruitment of both neutrophils and monocytes in comparison to female animals [601,605], and this finding also extends to the air pouch inflammation model, as pouch injection of carrageenan into C57BL/6J male animals elicits the influx of approximately 50% more immune cells than in female mice [599].

However, a study by de Coupade *et al* found that it was female animals that had increased leukocyte recruitment in comparison to male mice when LPS was used as the inflammatory insult in the dorsal air pouch [606]. However as animals from the FVB genetic background were used, this may impact on the immune response seen. Indeed, the above study using C57BL/6J animals in the carrageenan air pouch model also found that in other genetic backgrounds there was no difference in neutrophil influx between the genders [599]. Furthermore, it has been demonstrated that there is no difference in inflammatory cell recruitment between males and females in a rat LPS dorsal air pouch model [607], therefore showing that the experimental species used is also an important variable. My results align with the acute inflammatory response seen when using C57BL/6J mice, specifically that males have a greater

inflammatory response than females. However it is clear that multiple factors impact on the immune response between males and females and care should be taken when extrapolating results obtained in experimental animals onto human disease.

With regards to my second aim, I examined the mechanistic basis for the increased neutrophil trafficking seen in $CB_2^{-/-}$ mice. I found that this was due to the lack of CB_2 on the neutrophils themselves, as in the mixed bone marrow chimeria experiments there were always more CD45.2 neutrophils (and hence $CB_2^{-/-}$) in the inflamed pouch regardless of the recipient genotype. This finding is not entirely without precedence, as two studies examining the role of CB_2 in atherosclerosis found that reconstitution of $Ldlr^{-/-}$ or $ApoE^{-/-}$ mice with $CB_2^{-/-}$ bone marrow only, resulted in increased lesional macrophage content, thereby showing that macrophage accumulation in atherosclerotic plaques is caused by the lack of CB_2 on myeloid cells [339, 341]. Additional support for the hypothesis that lack of CB_2 specifically in neutrophils is responsible for their increased air pouch recruitment comes from my findings that there were no differences in the pouch levels of neutrophil chemoattractant chemokines at both 2 and 6 hours post zymosan administration and that there were no differences in zymosan-induced pro-inflammatory mediator production between WT and $CB_2^{-/-}$ pouch fibroblasts or pouch explant tissue.

An obvious explanation for the increased recruitment of $CB_2^{-/-}$ neutrophils is that genetic deletion of CB_2 makes them more responsive to chemoattractants and therefore more likely to migrate. However, previous work conducted in our laboratory has shown that genetic deletion of CB_2 in male animals has no effect on the inflammatory response over a range of time points in the ZIP model (T Kapellos 2016, Personal Communication), and I found that there was no difference in myeloid cell recruitment between female WT and $CB_2^{-/-}$ animals four hours after peritoneal zymosan challenge. Therefore I believe these data suggest it is unlikely that lack of CB_2 in neutrophils generally increases their rate of chemotaxis and migration. Instead, this implies that CB_2 is not a generic regulator of immune cell recruitment, but instead plays a context specific role during an inflammatory

response. I hypothesise that there must be a pathway regulated by, or reliant upon, CB_2 expression in neutrophils that is important for their recruitment into the air pouch, but is less important or not used for entry into the peritoneum.

One pathway of interest to me is the regulation of MMP-9 expression by CB_2 signalling, as I found that there were significantly higher levels of MMP-9 in the dorsal air pouch of $CB_2^{-/-}$ mice 6 hours after zymosan injection. In a study by Adhikary *et al* it was shown that activation of CB_2 does not inhibit dendritic cell chemotaxis *per se*, but instead inhibits their invasive capacity *in vitro* and *in vivo* by downregulating the expression of MMP-9 [411]. Conversely they also demonstrated that $CB_2^{-/-}$ dendritic cells had higher levels of MMP-9, mirroring the results of Netherland *et al* who found that $CB_2^{-/-}$ macrophages also have higher MMP-9 levels and that treatment of WT macrophages with a CB_2 antagonist caused a concentration-dependent increase in MMP-9 expression [337]. Alongside, I found that the level of MMP-9 in the peritoneum of WT mice 4 hours after zymosan injection was 3 times lower than that seen in the air pouch of WT animals 6 hours after zymosan administration. Therefore, this implies that MMP-9 may play a more important role for neutrophil recruitment to the air pouch than the peritoneum.

Taken together, these results inform the hypothesis that inflammatory signalling in the inflamed air pouch drives MMP-9 expression to a greater extent than in the peritoneum, and that the lack of CB_2 signalling in $CB_2^{-/-}$ neutrophils leaves them unable to constrain MMP-9 levels, thereby granting them increased invasive capacity that leads to increased neutrophil influx into the dorsal air pouch. However, additional questions need to be addressed to verify this hypothesis. For example, do $CB_2^{-/-}$ neutrophils have higher levels of MMP-9 in comparison to WT neutrophils and how does expression of MMP-9 in $CB_2^{-/-}$ neutrophils vary between the air pouch and the peritoneum? What pathway drives MMP-9 expression and is this different between the pouch and the peritoneum? Additionally, the use of MMP-9 inhibitors in both the peritoneal and air pouch inflammation models will allow the importance of MMP-9 for immune cell trafficking in each model to be examined.

However, this is not the only hypothesis that can explain my above results. For example, it has been shown that activation of CB_2 can block immune cell migration [388] and JWH133 has been found to inhibit neutrophil chemotaxis towards TNF-α and CXCL2 [316,318]. Therefore, differential production of endocannabinoids between the two anatomical sites could explain why genetic deletion of CB_2 only has an effect in the dorsal air pouch model. This hypothesis implies that the air pouch produces a local concentration of endocannabinoids sufficient to activate CB_2 on neutrophils and block their migration, whereas the peritoneum does not. Currently this explanation remains purely speculative as I have not measured the levels of endocannbinoids present at the two sites. Clearly further work is needed to fully elucidate exactly how lack of CB_2 in neutrophils leads to their enhanced migration into the dorsal air pouch, but not into the peritoneum.

In both WT and $CB_2^{-/-}$ animals, there is a spike of inflammatory Ly6C^{hi} monocyte recruitment into the air pouch seen 2 hours after zymosan injection, which returns to baseline by 6 hours. This seems to be caused by the rapid pouch production of CCL2 and CCL4, which when measured at the 2 hour time point are present at the same level between WT and $CB_2^{-/-}$ mice. In WT animals their levels drop significantly by 6 hours after zymosan injection and likely underpins why Ly6C^{hi} monocyte numbers fall back to basal by this time point. However in $CB_2^{-/-}$ animals, CCL2 and CCL4 remain increased 6 hours after zymosan injection and are likely responsible for the significantly higher number of Ly6C^{hi} inflammatory monocytes in the air pouch of $CB_2^{-/-}$ animals 16 hours after zymosan challenge.

One interesting question that arises from this result is why do inflammatory monocyte numbers fall back to baseline at 6 hours before increasing again at 16 hours in $CB_2^{-/-}$ animals? I believe that the initial production of CC chemokines relies on the pouch resident cells and stroma, whereas the higher levels of CC chemokines seen at 6 hours in $CB_2^{-/-}$ originate from the recruited neutrophils. Therefore as the difference in pouch neutrophil number between the genotypes only begins to manifest 6 hours after zymosan injection, the increased Ly6C^{hi} inflammatory monocyte recruitment

caused by neutrophil-derived chemokines can only happen at later time points.

Interestingly however, this implies that it is not the lack of CB_2 in Ly6C^{hi} monocytes that is responsible for their increased recruitment; a result directly contrasting with the role of CB_2 in neutrophils. Further support for this hypothesis comes from the mixed bone marrow chimera experiments where there was no difference in the number of WT or $CB_2^{-/-}$ Ly6C^{hi} inflammatory monocytes recruited into the dorsal air pouch of either recipient genotype. However, as these experiments were performed 6 hours after zymosan injection they were not designed to directly assess the role of CB_2 in monocyte recruitment. Nevertheless, if true that lack of CB_2 in monocytes does not regulate their recruitment to sites of inflammation, this means that CB_2 also has a cell type dependent role in the regulation of immune cell recruitment, adding even further complexity to how CB_2 and the endocannabinoids act to regulate an inflammatory response.

5.4.1 Limitations of this study

One limitation of this study is that I have only used one inflammogen for examining the role of CB_2 in the regulation of an acute inflammatory response. To be able to fully understand how CB_2 regulates inflammation, a range of inflammatory agents should be used that elicit an inflammatory response by different mechanisms. The range of potential inflammogens is large, but using other TLR ligands like LPS, crystal agents such as MSU that activates the inflammasome and elicits a largely IL-1β driven inflammatory response [608] and even injection of specific chemoattractants, such as CXCL1, CCL2, fMLF and C5a will allow conclusions to be drawn about how broad a role CB_2 plays in the regulation of inflammation. Furthermore, this may identify inflammatory pathologies where therapeutic intervention targeting CB_2 could have clinical value.

A further limitation of this study is that the dorsal air pouch inflammation model is a simple system to examine immune cell recruitment during an inflammatory

response and does not directly model a human disease. Whilst it cannot be doubted that reductionist inflammation models have proved vital to our understanding of an inflammatory response, by their very nature they do not recapitulate the often complex causes and pathologies of human disease. Therefore to fully appreciate the role that CB_2 plays during inflammatory disease I would next like to compare WT vs $CB_2^{-/-}$ animals in an inflammatory disease model.

Perhaps the most obvious model to use would be a rheumatoid arthritis model, as the air pouch is thought to most closely resemble a synovial joint [558, 609]. Both the CIA and the K/BxN serum transfer arthritis models could be used to compare not only immune cell recruitment, but also inflammatory mediator production and joint histology to see whether my results obtained in the dorsal air pouch model translate into a more disease focussed system [290, 610]. I would hypothesise that genetic deletion of CB_2 would result in enhanced leukocyte trafficking and worse disease outcomes, as although $CB_2^{-/-}$ animals have not been used in arthritis disease models to date, it has been shown that activation of CB_2 with synthetic agonists in WT animals decreases artritis score, joint inflammatory mediator production and joint neutrophil and mononuclear cell infiltration in the CIA model [295, 296].

I have not measured the levels of endocannabinoids under baseline and inflammatory conditions in either the dorsal air pouch or the ZIP model. Understanding when, where and which endocannabinoids are produced, and by what cell types, is clearly important for understanding how the endocannabinoid system works and impacts an ongoing inflammatory response. For example, a recent study analysed expression of the components of the endocannabinoid system and endocannabinoids themselves by both macrophages and foam cells and found that all components of the endocannabinoid system are expressed in both macrophages and foam cells [611]. Furthermore macrophages can produce both endocannabinoids, but make 900 times more 2-AG than AEA, and the synthesis of both endocannabinoids is significantly increased as the macrophage becomes a foam cell [611]. Finally, the authors demonstrated that CB_2 activation has anti-inflammatory anti-atherogenic effects, supporting the

hypothesis that CB_2 is a valid target in atherosclerotic lesional foam cells and acts as a protective mechanism within atherosclerosis.

However, measuring the abundance of enocannabinoids in biological samples is not a trivial exercise. In order to achieve this, specialised lipid extraction protocols, combined with high performance liquid chromatography and tandem mass spectrometry is needed [612]. Furthermore, reproducibility of measurements between experiments, combined with the challenges of sample recovery and storage, can lead to decreases in assay accuracy and robustness [613, 614]. Therefore establishing a protocol for the reliable measurement of endocannabinoids will require a large amount of effort and time, that would not have been feasible within the time frame available to me. Nevertheless, having access to such a system in the future will undoubtedly aid research in our laboratory into the endocannabinoid system and the role it plays within inflammation.

Chapter 6

Thesis summary and final discussion

6.1 Key findings

The first aim of my thesis was to use real-time chemotaxis analysis to examine whether CB_2 is a chemoattractant receptor in primary murine macrophages. With regards to this, I made the following key findings:

- Only a subset of CB_2 agonists act as *bona fide* chemoattractants for bio-gel elicited primary murine macrophages.
- At least one non-CB_1/CB_2 $G_{i/o}$-coupled GPCR is responsible for CB_2 agonist-induced macrophage chemotaxis.

The GPCR that mediates CB_2 agonist-induced macrophage chemotaxis still remains unknown, but in trying to uncover its identity I made the following key findings:

- Bio-gel elicited murine macrophages express 124 GPCRs.
- The putative cannabinoid receptors GPR18 and GPR55 are not responsible for CB_2 agonist-induced macrophage chemotaxis.
- It is unlikely that the lipid binding GPCRs LPAR1, LPAR5, CYSLTR1,

CYSLTR2 and GPER1 are responsible for CB_2 agonist-induced macrophage chemotaxis.

- Using a ligand-directed virtual screen, extensive SAR and photoaffinity labelling, a novel UV-crosslinkable bioactive compound was discovered that will hopefully aid in the identification of the target(s) responsible for CB_2 agonist-induced macrophage chemotaxis.

The next aim of my thesis was to use real-time chemotaxis analysis to discover whether activation of CB_2 blocks primary macrophage chemotaxis towards CC chemokines. With regards to this, I made the following key discovery:

- The chemotaxis negative CB_2 agonists CP55,940 and DIAS2 did not inhibit primary murine macrophage chemotaxis towards the CC chemokines, CCL2 and/or CCL5.

The final aim of my thesis was to use the dorsal air pouch acute inflammation model, combined with animals lacking CB_2, to investigate whether CB_2 regulates innate immune cell recruitment to sites of inflammation *in vivo*. With regards to this, I made the following key findings:

- In the zymosan-induced dorsal air pouch inflammation model, female animals genetically deleted for CB_2 have an exaggerated acute inflammatory response with significantly more neutrophils, $Ly6C^{hi}$ inflammatory monocytes and pro-inflammatory mediators present in the pouch during the acute phase.

- Male animals lacking CB_2 also have an exaggerated acute inflammatory response with increased neutrophil numbers and levels of pro-inflammatory mediators in the pouch 6 hours after zymosan challenge.

- It is the lack of CB_2 on the neutrophils themselves that is responsible for the increased zymosan-induced air pouch neutrophil recruitment seen in $CB_2^{-/-}$ animals.

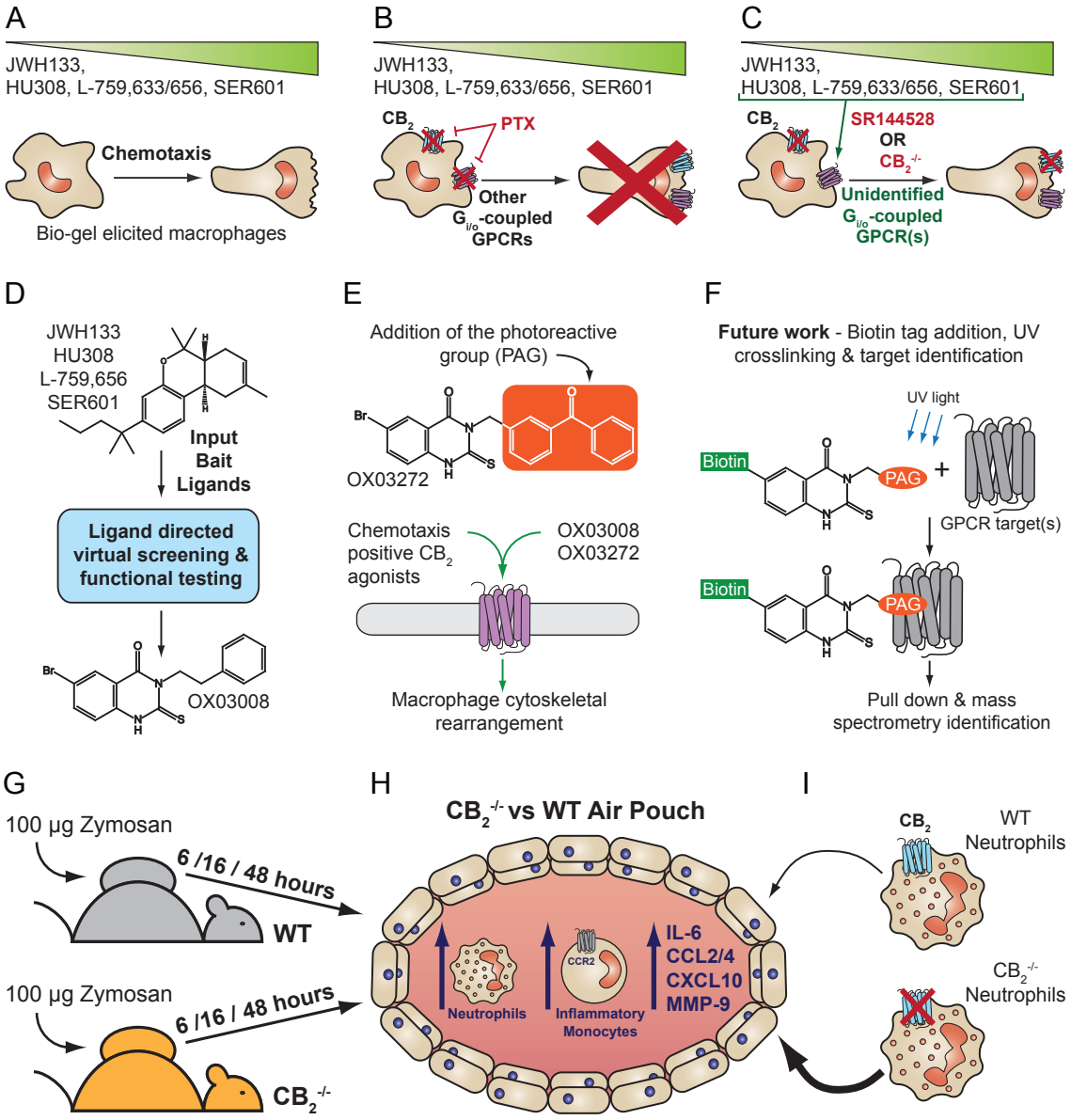

Figure 6.1 Summary of the main findings of my thesis. (A) Only a subset of CB_2 agonists act as chemoattractants for primary bio-gel elicited murine macrophages. CB_2 agonist-induced chemotaxis can be inhibited by pre-treatment of macrophages with (B) pertussis toxin (PTX), but (C) genetic deletion of CB_2 or pharmacological inhibition with SR144528 has no effect on CB_2 agonist-induced chemotaxis. Therefore at least one non-CB_1/CB_2 $G_{i/o}$-coupled GPCR is responsible for CB_2 agonist-induced macrophage chemotaxis. (D) A ligand directed virtual screen using the chemotaxis positive CB_2 agonists, combined with functional screening, identified a novel chemical class with the same bioactivity as the bait ligands, with this class exemplified by OX03008. (E) Extensive SAR studies found that a benzophenone photoaffinity group (PAG) could be added to the core scaffold, yielding the UV-crosslinkable compound OX03272 that retains the same activity as OX03008 and the chemotaxis positive CB_2 agonists. (F) Future work will involve the addition of a biotin label to the scaffold, performing UV crosslinking experiments with bio-gel elicited macrophages and target identification by mass spectrometry. (G) Dorsal air pouches were established in WT and $CB_2^{-/-}$ mice by the dorsal subcutaneous injection of air and were subsequently injected with 100 μg zymosan. (H) Animals genetically deleted for CB_2 have an exaggerated acute inflammatory response, as they have significantly more neutrophils, Ly6C^{hi} inflammatory monocytes and pro-inflammatory mediators present in the pouch after zymosan challenge in comparison to WT animals. (I) Interestingly, it is the lack of CB_2 on the neutrophils themselves that makes them more likely to traffic into the dorsal air pouch, as revealed by the mixed bone marrow chimera experiments.

6.2 How can CB_2 regulate neutrophil, but not macrophage, migration?

One seemingly conflicting finding from my work is that CB_2 does not regulate macrophage chemotaxis, whereas specific deletion of CB_2 in neutrophils results in their increased *in vivo* recruitment to sites of inflammation. One simple explanation for this is that CB_2 plays a cell type-dependent role in the regulation of leukocyte chemotaxis, but precedence for this in the literature is limited. Another explanation however is that rather than regulating leukocyte chemotaxis, CB_2 regulates leukocyte invasiveness.

Indeed, there is current evidence that supports this hypothesis. It has been demonstrated that treatment of murine dendritic cells with the CB_2 agonist GP1a had no effect on their chemotaxis towards CCL12, but blocked their ability to move through a matrigel layer by downregulating their expression of MMP-9 [411]. Furthermore it was shown that $CB_2^{-/-}$ dendritic cells had elevated levels of MMP-9 [411]. As I found that the pouch level of MMP-9 was elevated in $CB_2^{-/-}$ animals, this provides further support for the hypothesis that CB_2 regulates innate immune cell invasiveness *in vivo* by regulating the levels of MMP-9 and potentially other proteases. As I only examined macrophage chemotaxis, and not invasiveness, this explains why I found no role for CB_2 in macrophage directed migration. I would hypothesise that when examining neutrophil chemotaxis *in vitro* that I would see no effect of activation or genetic deletion of CB_2 on chemokine-induced neutrophil migration. Furthermore, I would expect that CB_2 controls the level of MMP-9 and potentially other proteases in macrophages and that this would control their invasiveness *in vivo*. Indeed, it has been shown that $CB_2^{-/-}$ macrophages have increased MMP-9 expression [337] and that specific deletion of CB_2 in the myeloid compartment results in increased atherosclerotic plaque macrophage content [339, 341]. Clearly future work is needed to fully confirm the exact role of CB_2 in the regulation of

innate immune cell chemotaxis and recruitment, and this is currently ongoing in the laboratory.

6.3 Future work

In addition to the future work listed at the end of each chapter, one important area in the cannabinoid field that requires attention is in the generation of tools to allow for the reliable detection of the cannabinoid receptors. Currently, the antibodies available that claim to recognise CB_1 or CB_2 either do not work or are non-specific, and many studies that use them to examine cannabinoid receptor protein levels do not use the correct controls to determine staining specificity. Instead, I propose that the generation of transgenic animals with an epitope tag placed at the N-terminus would provide an elegant solution to this problem. I know that the addition of an N-terminal tag to CB_2 does not ablate its activity and if the CRISPR/Cas9 system were used to generate the transgenic mice, the desired level of precision could be obtained to insert the small epitope tag at the correct position [615]. Importantly as the endogenous gene would be modified, the expression of CB_2 would still be controlled by the endogenous promoter, allowing surface or total levels of CB_2 at any time point or experimental condition to be accurately determined. Obviously this is not a trivial task, but I believe that a tool such as this is sorely needed in the cannabinoid field.

References

[1] R Medzhitov. Origin and physiological roles of inflammation. *Nature*, 454(7203):428–435, 2008.

[2] Taro Kawai and Shizuo Akira. The role of pattern-recognition receptors in innate immunity: update on Toll-like receptors. *Nature Immunology*, 11(5):373–384, may 2010.

[3] Emilie Vénéreau, Chiara Ceriotti, and Marco Emilio Bianchi. DAMPs from Cell Death to New Life. *Frontiers in immunology*, 6:422, 2015.

[4] Derek Gilroy and Roel De Maeyer. New insights into the resolution of inflammation. *Seminars in immunology*, 27(3):161–8, may 2015.

[5] Charles N. Serhan, Nan Chiang, and Thomas E. Van Dyke. Resolving inflammation: dual anti-inflammatory and pro-resolution lipid mediators. *Nature Reviews Immunology*, 8(5):349–361, may 2008.

[6] Maria C. Basil and Bruce D. Levy. Specialized pro-resolving mediators: endogenous regulators of infection and inflammation. *Nature Reviews Immunology*, 16(1):51–67, dec 2015.

[7] C Nathan and A Ding. Nonresolving inflammation. *Cell*, 140(6):871–882, 2010.

[8] Elzbieta Kolaczkowska and Paul Kubes. Neutrophil recruitment and function in health and inflammation. *Nature Reviews Immunology*, 13(3):159–175, feb 2013.

[9] Michael K Richards, Fulu Liu, Hiromi Iwasaki, Koichi Akashi, and Daniel C Link. Pivotal role of granulocyte colony-stimulating factor in the development of progenitors in the common myeloid pathway. *Blood*, 102(10):3562–8, nov 2003.

[10] Niels Borregaard. Neutrophils, from marrow to microbes. *Immunity*, 33(5):657–70, nov 2010.

[11] Tanya N. Mayadas, Xavier Cullere, and Clifford A. Lowell. The Multifaceted Functions of Neutrophils. *Annual Review of Pathology: Mechanisms of Disease*, 9(1):181–218, jan 2014.

[12] T. Tak, K. Tesselaar, J. Pillay, J. A. M. Borghans, and L. Koenderman. What's your age again? Determination of human neutrophil half-lives revisited. *Journal of Leukocyte Biology*, 94(4):595–601, oct 2013.

[13] B Amulic, C Cazalet, G L Hayes, K D Metzler, and A Zychlinsky. Neutrophil function: from mechanisms to disease. *Annu.Rev.Immunol.*, 30(1545-3278 (Electronic)):459–489, 2012.

[14] Warren L. Lee, Rene E. Harrison, and Sergio Grinstein. Phagocytosis by neutrophils. *Microbes and Infection*, 5(14):1299–1306, 2003.

[15] L A Allen and A Aderem. Molecular definition of distinct cytoskeletal structures involved in complement- and Fc receptor-mediated phagocytosis in macrophages. *The Journal of experimental medicine*, 184(2):627–37, aug 1996.

[16] P. Nordenfelt and H. Tapper. Phagosome dynamics during phagocytosis by neutrophils. *Journal of Leukocyte Biology*, 90(2):271–284, aug 2011.

[17] Mikkel Faurschou and Niels Borregaard. Neutrophil granules and secretory vesicles in inflammation. *Microbes and Infection*, 5(14):1317–1327, 2003.

[18] Niels Borregaard, Ole E. Sørensen, and Kim Theilgaard-Mönch. Neutrophil granules: a library of innate immunity proteins. *Trends in Immunology*, 28(8):340–345, 2007.

[19] N Borregaard and J B Cowland. Granules of the human neutrophilic polymorphonuclear leukocyte. *Blood*, 89(10):3503–21, may 1997.

[20] Julien Cachat, Christine Deffert, Stephanie Hugues, et al. Phagocyte NADPH oxidase and specific immunity. *Clinical science (London, England : 1979)*, 128(10):635–48, may 2015.

[21] Christian Bogdan, Martin Röllinghoff, and Andreas Diefenbach. Reactive oxygen and reactive nitrogen intermediates in innate and specific immunity. *Current Opinion in Immunology*, 12(1):64–76, 2000.

[22] Alexander J. Towbin and Ian Chaves. Chronic granulomatous disease. *Pediatric Radiology*, 40(5):657–668, may 2010.

[23] Volker Brinkmann, Ulrike Reichard, Christian Goosmann, et al. Neutrophil extracellular traps kill bacteria. *Science (New York, N.Y.)*, 303(5663):1532–5, mar 2004.

[24] Volker Brinkmann and Arturo Zychlinsky. Neutrophil extracellular traps: is immunity the second function of chromatin? *The Journal of cell biology*, 198(5):773–83, sep 2012.

[25] Diana Boraschi Paola Italiani. From Monocytes to M1/M2 Macrophages: Phenotypical vs. Functional Differentiation. *Frontiers in Immunology*, 5, 2014.

[26] Jan Hettinger, David M Richards, Jenny Hansson, et al. Origin of monocytes and macrophages in a committed progenitor. *Nature immunology*, 14(8):821–30, aug 2013.

[27] M G Cecchini, M G Dominguez, S Mocci, et al. Role of colony stimulating factor-1 in the establishment and regulation of tissue macrophages during postnatal development of the mouse. *Development (Cambridge, England)*, 120(6):1357–72, jun 1994.

[28] Xu-Ming Dai, Gregory R Ryan, Andrew J Hapel, et al. Targeted disruption of the mouse colony-stimulating factor 1 receptor gene results in osteopetrosis, mononuclear phagocyte deficiency, increased primitive progenitor cell frequencies, and reproductive defects. *Blood*, 99(1):111–20, jan 2002.

[29] Frank Rosenbauer and Daniel G. Tenen. Transcription factors in myeloid development: balancing differentiation with transformation. *Nature Reviews Immunology*, 7(2):105–117, feb 2007.

[30] Florent Ginhoux and Steffen Jung. Monocytes and macrophages: developmental pathways and tissue homeostasis. *Nature Reviews Immunology*, 14(6):392–404, may 2014.

[31] Chia-Lin Tsou, Wendy Peters, Yue Si, et al. Critical roles for CCR2 and MCP-3 in monocyte mobilization from bone marrow and recruitment to inflammatory sites. *Journal of Clinical Investigation*, 117(4):902–9, apr 2007.

[32] Natalya V Serbina and Eric G Pamer. Monocyte emigration from bone marrow during bacterial infection requires signals mediated by chemokine receptor CCR2. *Nature Immunology*, 7(3):311–317, mar 2006.

[33] Simon Yona, Ki-Wook Kim, Yochai Wolf, et al. Fate mapping reveals origins and dynamics of monocytes and tissue macrophages under homeostasis. *Immunity*, 38(1):79–91, jan 2013.

[34] Jiyeon Yang, Lixiao Zhang, Caijia Yu, Xiao-Feng Yang, and Hong Wang. Monocyte and macrophage differentiation: circulation inflammatory monocyte as biomarker for inflammatory diseases. *Biomarker research*, 2(1):1, 2014.

[35] Leo M Carlin, Efstathios G Stamatiades, Cedric Auffray, et al. Nr4a1-dependent Ly6C(low) monocytes monitor endothelial cells and orchestrate their disposal. *Cell*, 153(2):362–75, apr 2013.

[36] Cedric Auffray, Darin Fogg, Meriem Garfa, et al. Monitoring of blood vessels and tissues by a population of monocytes with patrolling behavior. *Science*, 317(5838):666–670, aug 2007.

[37] R van Furth and Z A Cohn. The origin and kinetics of mononuclear phagocytes. *The Journal of experimental medicine*, 128(3):415–35, sep 1968.

[38] Daigo Hashimoto, Andrew Chow, Clara Noizat, et al. Tissue-Resident Macrophages Self-Maintain Locally throughout Adult Life with Minimal Contribution from Circulating Monocytes. *Immunity*, 38(4):792–804, apr 2013.

[39] C C Bain, A Bravo-Blas, C L Scott, et al. Constant replenishment from circulating monocytes maintains the macrophage pool in the intestine of adult mice. *Nat Immunol*, 15(10):929–937, 2014.

[40] Yonit Lavin, Deborah Winter, Ronnie Blecher-Gonen, et al. Tissue-resident macrophage enhancer landscapes are shaped by the local microenvironment. *Cell*, 159(6):1312–26, dec 2014.

[41] Emmanuel L Gautier, Tal Shay, Jennifer Miller, et al. Gene-expression profiles and transcriptional regulatory pathways that underlie the identity and diversity of mouse tissue macrophages. *Nature immunology*, 13(11):1118–28, nov 2012.

[42] David Gosselin, Verena M Link, Casey E Romanoski, et al. Environment drives selection and function of enhancers controlling tissue-specific macrophage identities. *Cell*, 159(6):1327–40, dec 2014.

[43] L C Davies, S J Jenkins, J E Allen, and P R Taylor. Tissue-resident macrophages. *Nat Immunol*, 14(10):986–995, 2013.

[44] M. E. Bianchi. DAMPs, PAMPs and alarmins: all we need to know about danger. *Journal of Leukocyte Biology*, 81(1):1–5, oct 2006.

[45] T. H. Mogensen. Pathogen Recognition and Inflammatory Signaling in Innate Immune Defenses. *Clinical Microbiology Reviews*, 22(2):240–273, apr 2009.

[46] Fernando O Martinez and Siamon Gordon. The M1 and M2 paradigm of macrophage activation: time for reassessment. *F1000prime reports*, 6:13, 2014.

[47] J. Lattin, D. A. Zidar, K. Schroder, et al. G-protein-coupled receptor expression, function, and signaling in macrophages. *Journal of Leukocyte Biology*, 82(1):16–32, apr 2007.

[48] Spencer A. Freeman and Sergio Grinstein. Phagocytosis: receptors, signal integration, and the cytoskeleton. *Immunological Reviews*, 262(1):193–215, nov 2014.

[49] Günter Weiss and Ulrich E Schaible. Macrophage defense mechanisms against intracellular bacteria. *Immunological reviews*, 264(1):182–203, mar 2015.

[50] Antonio Sica and Alberto Mantovani. Macrophage plasticity and polarization: in vivo veritas. *The Journal of clinical investigation*, 122(3):787–95, mar 2012.

[51] Peter J Murray and Thomas A Wynn. Protective and pathogenic functions of macrophage subsets. *Nature reviews. Immunology*, 11(11):723–37, nov 2011.

[52] Silvia Nucera, Daniela Biziato, and Michele De Palma. The interplay between macrophages and angiogenesis in development, tissue injury and regeneration. *The International journal of developmental biology*, 55(4-5):495–503, 2011.

[53] L-P Erwig and P M Henson. Clearance of apoptotic cells by phagocytes. *Cell Death and Differentiation*, 15(2):243–250, feb 2008.

[54] T. Lucas, A. Waisman, R. Ranjan, et al. Differential Roles of Macrophages in Diverse Phases of Skin Repair. *The Journal of Immunology*, 184(7):3964–3977, apr 2010.

[55] Helene F. Rosenberg, Kimberly D. Dyer, and Paul S. Foster. Eosinophils: changing perspectives in health and disease. *Nature Reviews Immunology*, 13(1):9–22, nov 2012.

[56] Tae Gi Uhm, Byung Soo Kim, and Il Yup Chung. Eosinophil Development, Regulation of Eosinophil-Specific Genes, and Role of Eosinophils in the Pathogenesis of Asthma. *Allergy, Asthma and Immunology Research*, 4(2):68, 2012.

[57] Yong Mean Park, Bruce S Bochner, JA Boyce, et al. Eosinophil Survival and Apoptosis in Health and Disease. *Allergy, Asthma and Immunology Research*, 2(2):87, 2010.

[58] K J Hamann, R L Barker, R M Ten, and G J Gleich. The molecular biology of eosinophil granule proteins. *International archives of allergy and applied immunology*, 94(1-4):202–9, 1991.

[59] Rossana C N Melo and Peter F Weller. Unraveling the complexity of lipid body organelles in human eosinophils. *Journal of leukocyte biology*, 96(5):703–12, nov 2014.

[60] K Ravi Acharya and Steven J Ackerman. Eosinophil granule proteins: form and function. *The Journal of biological chemistry*, 289(25):17406–15, jun 2014.

[61] Taku Kouro and Kiyoshi Takatsu. IL-5- and eosinophil-mediated inflammation: from discovery to therapy. *International immunology*, 21(12):1303–9, dec 2009.

[62] Patricia C. Fulkerson and Marc E. Rothenberg. Targeting eosinophils in allergy, inflammation and beyond. *Nature Reviews Drug Discovery*, 12(2):117–129, jan 2013.

[63] Rossana C N Melo and Peter F Weller. Piecemeal degranulation in human eosinophils: a distinct secretion mechanism underlying inflammatory responses. *Histology and histopathology*, 25(10):1341–54, oct 2010.

[64] Carine Blanchard and Marc E Rothenberg. Biology of the eosinophil. *Advances in immunology*, 101:81–121, 2009.

[65] Shida Yousefi, Jeffrey A Gold, Nicola Andina, et al. Catapult-like release of mitochondrial DNA by eosinophils contributes to antibacterial defense. *Nature Medicine*, 14(9):949–953, sep 2008.

[66] Myeong Heon Shin, Young Ah Lee, and Duk-Young Min. Eosinophil-mediated tissue inflammatory responses in helminth infection. *The Korean journal of parasitology*, 47 Suppl(Suppl):S125–31, oct 2009.

[67] Jonathan M Swartz, Kimberly D Dyer, Allen W Cheever, et al. Schistosoma mansoni infection in eosinophil lineage-ablated mice. *Blood*, 108(7):2420–7, oct 2006.

[68] N. G. Gebreselassie, A. R. Moorhead, V. Fabre, et al. Eosinophils Preserve Parasitic Nematode Larvae by Regulating Local Immunity. *The Journal of Immunology*, 188(1):417–425, jan 2012.

[69] MichaelF. Gurish and K. Frank Austen. Developmental Origin and Functional Specialization of Mast Cell Subsets. *Immunity*, 37(1):25–33, 2012.

[70] Sara Wernersson and Gunnar Pejler. Mast cell secretory granules: armed for battle. *Nature Reviews Immunology*, 14(7):478–494, jun 2014.

[71] Soman N. Abraham and Ashley L. St. John. Mast cell-orchestrated immunity to pathogens. *Nature Reviews Immunology*, 10(6):440–452, jun 2010.

[72] Theoharis C. Theoharides, Konstantinos-Dionysios Alysandratos, Asimenia Angelidou, et al. Mast cells and inflammation. *Biochimica et Biophysica Acta (BBA) - Molecular Basis of Disease*, 1822(1):21–33, 2012.

[73] Stephen J Galli and Mindy Tsai. IgE and mast cells in allergic disease. *Nature Medicine*, 18(5):693–704, may 2012.

[74] Alasdair M. Gilfillan and Christine Tkaczyk. Integrated signalling pathways for mast-cell activation. *Nature Reviews Immunology*, 6(3):218–230, mar 2006.

[75] Himanshu Kumar, Taro Kawai, and Shizuo Akira. Pathogen recognition by the innate immune system. *International Reviews of Immunology*, 30(1):16–34, jan 2011.

[76] A Poltorak, X He, I Smirnova, et al. Defective LPS signaling in C3H/HeJ and C57BL/10ScCr mice: mutations in Tlr4 gene. *Science (New York, N.Y.)*, 282(5396):2085–8, dec 1998.

[77] Sky W. Brubaker, Kevin S. Bonham, Ivan Zanoni, and Jonathan C. Kagan. Innate Immune Pattern Recognition: A Cell Biological Perspective. *Annual Review of Immunology*, 33(1):257–290, mar 2015.

[78] Petr Broz and Vishva M. Dixit. Inflammasomes: mechanism of assembly, regulation and signalling. *Nature Reviews Immunology*, 16(7):407–420, jun 2016.

[79] Paola Scaffidi, Tom Misteli, and Marco E Bianchi. Release of chromatin protein HMGB1 by necrotic cells triggers inflammation. *Nature*, 418(6894):191–5, jul 2002.

[80] Charles A Dinarello. Historical insights into cytokines. *European journal of immunology*, 37 Suppl 1(Suppl 1):S34–45, nov 2007.

[81] Jun-Ming Zhang and Jianxiong An. Cytokines, inflammation, and pain. *International anesthesiology clinics*, 45(2):27–37, 2007.

[82] C A Feghali and T M Wright. Cytokines in acute and chronic inflammation. *Frontiers in bioscience : a journal and virtual library*, 2:d12–26, jan 1997.

[83] George D. Kalliolias and Lionel B. Ivashkiv. TNF biology, pathogenic mechanisms and emerging therapeutic strategies. *Nature Reviews Rheumatology*, 12(1):49–62, dec 2015.

[84] Priya Darshinee A. Issuree, Thorsten Maretzky, David R. McIlwain, et al. iRHOM2 is a critical pathogenic mediator of inflammatory arthritis. *Journal of Clinical Investigation*, 123(2):928–32, jan 2013.

[85] Calin Popa, Mihai G Netea, Piet L C M van Riel, Jos W M van der Meer, and Anton F H Stalenhoef. The role of TNF-alpha in chronic inflammatory conditions, intermediary metabolism, and cardiovascular risk. *Journal of lipid research*, 48(4):751–62, apr 2007.

[86] Petrus J. W. Naudé, Johan A. den Boer, Paul G. M. Luiten, and Ulrich L. M. Eisel. Tumor necrosis factor receptor cross-talk. *FEBS Journal*, 278(6):888–898, apr 2011.

[87] Peter Norman. Humira: the impending patent battles over adalimumab biosimilars. *Pharmaceutical Patent Analyst*, 5(3):141–145, may 2016.

[88] Jacques Banchereau, Virginia Pascual, and Anne O'Garra. From IL-2 to IL-37: the expanding spectrum of anti-inflammatory cytokines. *Nature Immunology*, 13(10):925–931, sep 2012.

[89] Diana Carolina Torres Palomino and Luciana Cavalheiro Marti. Chemokines and immunity. *Einstein (Sao Paulo, Brazil)*, 13(3):469–73, 2015.

[90] Jason W. Griffith, Caroline L. Sokol, and Andrew D. Luster. Chemokines and Chemokine Receptors: Positioning Cells for Host Defense and Immunity. *Annual Review of Immunology*, 32(1):659–702, mar 2014.

[91] G. E. White, A. J. Iqbal, and D. R. Greaves. CC chemokine receptors and chronic inflammation–therapeutic opportunities and pharmacological challenges. *Pharmacological reviews*, 65(1):47–89, jan 2013.

[92] Brian A Jones, Maria Beamer, and Salahuddin Ahmed. Fractalkine/CX3CL1: a potential new target for inflammatory diseases. *Molecular interventions*, 10(5):263–70, oct 2010.

[93] Jason R Dunkelberger and Wen-Chao Song. Complement and its role in innate and adaptive immune responses. *Cell Research*, 20(1):34–50, jan 2010.

[94] Daniel Ricklin and John D Lambris. Complement in immune and inflammatory disorders: pathophysiological mechanisms. *Journal of immunology (Baltimore, Md. : 1950)*, 190(8):3831–8, apr 2013.

[95] B. Paul Morgan and Claire L. Harris. Complement, a target for therapy in inflammatory and degenerative diseases. *Nature Reviews Drug Discovery*, 14(12):857–877, oct 2015.

[96] Maciej M Markiewski and John D Lambris. The role of complement in inflammatory diseases from behind the scenes into the spotlight. *The American journal of pathology*, 171(3):715–27, sep 2007.

[97] Edward A. Dennis and Paul C. Norris. Eicosanoid storm in infection and inflammation. *Nature Reviews Immunology*, 15(8):511–523, jul 2015.

[98] Bruno L. Diaz, Jonathan P. Arm, B. Samuelsson, et al. Phospholipase A2. *Prostaglandins, Leukotrienes and Essential Fatty Acids*, 69(2-3):87–97, aug 2003.

[99] William W. Busse. Leukotrienes and Inflammation. *American Journal of Respiratory and Critical Care Medicine*, 157(6):S210–S213, jun 1998.

[100] M. Peters-Golden, C. Canetti, P. Mancuso, and M. J. Coffey. Leukotrienes: Underappreciated Mediators of Innate Immune Responses. *The Journal of Immunology*, 174(2):589–594, jan 2005.

[101] C D Funk, G. O. Burr, M. M. Burr, et al. Prostaglandins and leukotrienes: advances in eicosanoid biology. *Science (New York, N.Y.)*, 294(5548):1871–5, nov 2001.

[102] M B Bailie, T J Standiford, L L Laichalk, et al. Leukotriene-deficient mice manifest enhanced lethality from Klebsiella pneumonia in association with decreased alveolar macrophage phagocytic and bactericidal activities. *Journal of immunology (Baltimore, Md. : 1950)*, 157(12):5221–4, dec 1996.

[103] Emanuela Ricciotti and Garret A FitzGerald. Prostaglandins and inflammation. *Arteriosclerosis, thrombosis, and vascular biology*, 31(5):986–1000, may 2011.

[104] D. L. Simmons, Regina M. Botting, and Timothy Hla. Cyclooxygenase Isozymes: The Biology of Prostaglandin Synthesis and Inhibition. *Pharmacological Reviews*, 56(3):387–437, sep 2004.

[105] Craig L Semerad, Fulu Liu, Alyssa D Gregory, Katherine Stumpf, and Daniel C Link. G-CSF is an essential regulator of neutrophil trafficking from the bone marrow to the blood. *Immunity*, 17(4):413–23, oct 2002.

[106] Charlotte Summers, Sara M Rankin, Alison M Condliffe, et al. Neutrophil kinetics in health and disease. *Trends in immunology*, 31(8):318–24, aug 2010.

[107] Q Ma, D Jones, and T A Springer. The chemokine receptor CXCR4 is required for the retention of B lineage and granulocytic precursors within the bone marrow microenvironment. *Immunity*, 10(4):463–71, apr 1999.

[108] Craig W Hendrix, Ann C Collier, Michael M Lederman, et al. Safety, pharmacokinetics, and antiviral activity of AMD3100, a selective CXCR4 receptor inhibitor, in HIV-1 infection. *Journal of acquired immune deficiency syndromes (1999)*, 37(2):1253–62, oct 2004.

[109] Paolo A Hernandez, Robert J Gorlin, John N Lukens, et al. Mutations in the chemokine receptor gene CXCR4 are associated with WHIM syndrome, a combined immunodeficiency disease. *Nature genetics*, 34(1):70–4, may 2003.

[110] Rebecca C Furze and Sara M Rankin. Neutrophil mobilization and clearance in the bone marrow. *Immunology*, 125(3):281–8, nov 2008.

[111] Antje M Wengner, Simon C Pitchford, Rebecca C Furze, and Sara M Rankin. The coordinated action of G-CSF and ELR + CXC chemokines in neutrophil mobilization during acute inflammation. *Blood*, 111(1):42–9, jan 2008.

[112] G Cacalano, J Lee, K Kikly, et al. Neutrophil and B cell expansion in mice that lack the murine IL-8 receptor homolog. *Science (New York, N.Y.)*, 265(5172):682–4, jul 1994.

[113] W A Muller. Getting leukocytes to the site of inflammation. *Veterinary pathology*, 50(1):7–22, jan 2013.

[114] Jordan S. Pober and William C. Sessa. Evolving functions of endothelial cells in inflammation. *Nature Reviews Immunology*, 7(10):803–815, oct 2007.

[115] Klaus Ley, Carlo Laudanna, Myron I. Cybulsky, and Sussan Nourshargh. Getting to the site of inflammation: the leukocyte adhesion cascade updated. *Nature Reviews Immunology*, 7(9):678–689, sep 2007.

[116] Sara Massena, Gustaf Christoffersson, Elina Hjertström, et al. A chemotactic gradient sequestered on endothelial heparan sulfate induces directional intraluminal crawling of neutrophils. *Blood*, 116(11):1924–31, sep 2010.

[117] Mia Phillipson, Jaswinder Kaur, Pina Colarusso, Christie M Ballantyne, and Paul Kubes. Endothelial domes encapsulate adherent neutrophils and minimize increases in vascular permeability in paracellular and transcellular emigration. *PloS one*, 3(2):e1649, 2008.

[118] Abigail Woodfin, Mathieu-Benoit Voisin, and Sussan Nourshargh. Recent developments and complexities in neutrophil transmigration. *Current opinion in hematology*, 17(1):9–17, jan 2010.

[119] W. A. Muller. Mechanisms of Transendothelial Migration of Leukocytes. *Circulation Research*, 105(3):223–230, jul 2009.

[120] Ting Jia, Natalya V Serbina, Katharina Brandl, et al. Additive roles for MCP-1 and MCP-3 in CCR2-mediated recruitment of inflammatory monocytes during Listeria monocytogenes infection. *Journal of immunology (Baltimore, Md. : 1950)*, 180(10):6846–53, may 2008.

[121] Chao Shi and Eric G Pamer. Monocyte recruitment during infection and inflammation. *Nature reviews. Immunology*, 11(11):762–74, nov 2011.

[122] Oliver Soehnlein, Lennart Lindbom, and Christian Weber. Mechanisms underlying neutrophil-mediated monocyte recruitment. *Blood*, 114(21):4613–4623, 2009.

[123] M E Taekema-Roelvink, C Kooten, S V Kooij, E Heemskerk, and M R Daha. Proteinase 3 enhances endothelial monocyte chemoattractant protein-1 production and induces increased adhesion of neutrophils to endothelial cells by upregulating intercellular cell adhesion molecule-1. *Journal of the American Society of Nephrology : JASN*, 12(5):932–940, 2001.

[124] Taunia D Lee, Melva L Gonzalez, Padmasini Kumar, Paula Grammas, and H Anne Pereira. CAP37, a neutrophil-derived inflammatory mediator, augments leukocyte adhesion to endothelial monolayers. *Microvascular research*, 66(1):38–48, jul 2003.

[125] Oliver Soehnlein, Alma Zernecke, Einar E Eriksson, et al. Neutrophil secretion products pave the way for inflammatory monocytes. *Blood*, 112(4):1461–71, aug 2008.

[126] Charles N. Serhan. Pro-resolving lipid mediators are leads for resolution physiology. *Nature*, 510(7503):92–101, jun 2014.

[127] Michelle A Sugimoto, Lirlândia P Sousa, Vanessa Pinho, Mauro Perretti, and Mauro M Teixeira. Resolution of Inflammation: What Controls Its Onset? *Frontiers in immunology*, 7:160, 2016.

[128] ChristopherD. Buckley, DerekW. Gilroy, and CharlesN. Serhan. Proresolving Lipid Mediators and Mechanisms in the Resolution of Acute Inflammation. *Immunity*, 40(3):315–327, 2014.

[129] Almudena Ortega-Gómez, Mauro Perretti, and Oliver Soehnlein. Resolution of inflammation: an integrated view. *EMBO molecular medicine*, 5(5):661–674, may 2013.

[130] Mauro Perretti and Fulvio D'Acquisto. Annexin A1 and glucocorticoids as effectors of the resolution of inflammation. *Nature Reviews Immunology*, 9(1):62–70, jan 2009.

[131] R G Pertwee, A C Howlett, M E Abood, et al. International Union of Basic and Clinical Pharmacology. LXXIX. Cannabinoid receptors and their ligands: beyond CB(1) and CB(2). *Pharmacol Rev*, 62(4):588–631, 2010.

[132] Hui-Chen Lu and Ken Mackie. An Introduction to the Endogenous Cannabinoid System. *Biological Psychiatry*, 79(7):516–525, 2016.

[133] R G Pertwee. Cannabinoid pharmacology: the first 66 years. *British Journal of Pharmacology*, 147 Suppl:S163–71, 2006.

[134] A C Howlett and R M Fleming. Cannabinoid inhibition of adenylate cyclase. Pharmacology of the response in neuroblastoma cell membranes. *Molecular pharmacology*, 26(3):532–8, nov 1984.

[135] A C Howlett. Cannabinoid inhibition of adenylate cyclase. Biochemistry of the response in neuroblastoma cell membranes. *Molecular pharmacology*, 27(4):429–36, apr 1985.

[136] A C Howlett, J M Qualy, and L L Khachatrian. Involvement of Gi in the inhibition of adenylate cyclase by cannabimimetic drugs. *Molecular pharmacology*, 29(3):307–13, mar 1986.

[137] A C Howlett. Regulation of adenylate cyclase in a cultured neuronal cell line by marijuana constituents, metabolites of delta-9-tetrahydrocannabinol, and synthetic analogs having psychoactivity. *NIDA research monograph*, 79:148–57, 1987.

[138] R Mechoulam, J J Feigenbaum, N Lander, et al. Enantiomeric cannabinoids: stereospecificity of psychotropic activity. *Experientia*, 44(9):762–4, sep 1988.

[139] W A Devane, F A Dysarz, M R Johnson, L S Melvin, and A C Howlett. Determination and characterization of a cannabinoid receptor in rat brain. *Molecular pharmacology*, 34(5):605–13, nov 1988.

[140] Lisa A. Matsuda, Stephen J. Lolait, Michael J. Brownstein, Alice C. Young, and Tom I. Bonner. Structure of a cannabinoid receptor and functional expression of the cloned cDNA. *Nature*, 346(6284):561–564, aug 1990.

[141] Sean Munro, Kerrie L. Thomas, and Muna Abu-Shaar. Molecular characterization of a peripheral receptor for cannabinoids. *Nature*, 365(6441):61–65, sep 1993.

[142] Cristina Montero, Nuria Eugenia Campillo, Pilar Goya, and Juan Antonio Páez. Homology models of the cannabinoid CB1 and CB2 receptors. A docking analysis study. *European Journal of Medicinal Chemistry*, 40(1):75–83, 2005.

[143] C M Gérard, C Mollereau, G Vassart, and M Parmentier. Molecular cloning of a human cannabinoid receptor which is also expressed in testis. *The Biochemical journal*, (1):129–34, oct 1991.

[144] Amitabha Chakrabarti, Emmanuel S. Onaivi, and Gautam Chaudhuri. Cloning and sequencing of a cDNA encoding the mouse brain-type cannabinoid receptor protein. *DNA Sequence*, 5(6):385–388, jan 1995.

[145] C Gérard, C Mollereau, G Vassart, and M Parmentier. Nucleotide sequence of a human cannabinoid receptor cDNA. *Nucleic acids research*, 18(23):7142, dec 1990.

[146] A C Howlett, F Barth, T I Bonner, et al. International Union of Pharmacology. XXVII. Classification of cannabinoid receptors. *Pharmacological reviews*, 54(2):161–202, 2002.

[147] David Shire, Bernard Calandra, Murielle Rinaldi-Carmona, et al. Molecular cloning, expression and function of the murine CB2 peripheral cannabinoid receptor. *Biochim Biophys Acta*, 1307(2):132–136, jun 1996.

[148] G Griffin, Q Tao, and M E Abood. Cloning and pharmacological characterization of the rat CB(2) cannabinoid receptor. *The Journal of pharmacology and experimental therapeutics*, 292(3):886–94, mar 2000.

[149] K Mackie. Cannabinoid receptors: where they are and what they do. *Journal of neuroendocrinology*, 20 Suppl 1:10–14, may 2008.

[150] Peter T Nguyen, Cullen L Schmid, Kirsten M Raehal, et al. β-arrestin2 regulates cannabinoid CB1 receptor signaling and adaptation in a central nervous system region-dependent manner. *Biological psychiatry*, 71(8):714–24, apr 2012.

[151] L. Hunyady, P. Gyombolai, E. Boros, and G. Turu. The role of β-arrestin proteins in CB1 cannabinoid receptor endocytosis. 2012.

[152] Brady K Atwood, James Wager-Miller, Christopher Haskins, Alex Straiker, and Ken Mackie. Functional selectivity in CB(2) cannabinoid receptor signaling and regulation: implications for the therapeutic potential of CB(2) ligands. *Molecular pharmacology*, 81(2):250–63, feb 2012.

[153] Debra McGuinness, Asra Malikzay, Richard Visconti, et al. Characterizing cannabinoid CB2 receptor ligands using DiscoveRx PathHunter beta-arrestin assay. *Journal of biomolecular screening*, 14(1):49–58, jan 2009.

[154] K Mackie. Distribution of cannabinoid receptors in the central and peripheral nervous system. *Handbook of experimental pharmacology*, (168):299–325, 2005.

[155] Ivana Svíženská, Petr Dubový, and Alexandra Šulcová. Cannabinoid receptors 1 and 2 (CB1 and CB2), their distribution, ligands and functional involvement in nervous system structures A short review. *Pharmacology, Biochemistry and Behavior*, 2008.

[156] Masanobu Kano, Takako Ohno-Shosaku, Yuki Hashimotodani, Motokazu Uchigashima, and Masahiko Watanabe. Endocannabinoid-mediated control of synaptic transmission. *Physiological reviews*, 89(1):309–80, jan 2009.

[157] J M Witkin, E T Tzavara, and G G Nomikos. A role for cannabinoid CB1 receptors in mood and anxiety disorders. *Behavioural pharmacology*, 16(5-6):315–31, sep 2005.

[158] Katarzyna Starowicz, Natalia Malek, and Barbara Przewlocka. Cannabinoid receptors and pain. *Wiley Interdisciplinary Reviews: Membrane Transport and Signaling*, 2(3):121–132, may 2013.

[159] G Riedel and S N Davies. Cannabinoid function in learning, memory and plasticity. *Handbook of experimental pharmacology*, (168):445–77, 2005.

[160] D Cota, G Marsicano, B Lutz, et al. Endogenous cannabinoid system as a modulator of food intake. *International Journal of Obesity*, 27(3):289–301, mar 2003.

[161] Mauro Maccarrone, Itai Bab, Tamás Bíró, et al. Endocannabinoid signaling at the periphery: 50 years after THC. *Trends in pharmacological sciences*, 36(5):277–96, may 2015.

[162] S Galiegue, S Mary, J Marchand, et al. Expression of central and peripheral cannabinoid receptors in human immune tissues and leukocyte subpopulations. *European journal of biochemistry / FEBS*, 232(1):54–61, aug 1995.

[163] Caroline Turcotte, Marie-Renée Blanchet, Michel Laviolette, and Nicolas Flamand. The CB2 receptor and its role as a regulator of inflammation. *Cellular and Molecular Life Sciences*, pages 1–22, jul 2016.

[164] Sreemanti Basu and Bonnie N Dittel. Unraveling the complexities of cannabinoid receptor 2 (CB2) immune regulation in health and disease. *Immunologic research*, 51(1):26–38, oct 2011.

[165] Brady K Atwood and Ken Mackie. CB2: a cannabinoid receptor with an identity crisis. *British journal of pharmacology*, 160(3):467–79, jun 2010.

[166] M Maccarrone. CB2 receptors in reproduction. *British journal of pharmacology*, 153(2):189–98, jan 2008.

[167] Vincenzo Di Marzo and Dale G. Deutsch. Biochemistry of the Endogenous Ligands of Cannabinoid Receptors. *Neurobiology of Disease*, 5(6):386–404, 1998.

[168] Roger G. Pertwee. Endocannabinoids and their pharmacological actions. In *Endocannabinoids*, volume 231, pages 1–37. Springer International Publishing, 2015.

[169] W A Devane, L Hanus, A Breuer, et al. Isolation and structure of a brain constituent that binds to the cannabinoid receptor. *Science (New York, N.Y.)*, 258(5090):1946–9, dec 1992.

[170] Maria Grazia Cascio and Pietro Marini. Biosynthesis and fate of endocannabinoids. In *Endocannabinoids*, pages 39–58. Springer International Publishing, 2015.

[171] Donmienne Leung, Alan Saghatelian, Gabriel M Simon, and Benjamin F Cravatt. Inactivation of N-acyl phosphatidylethanolamine phospholipase D reveals multiple mechanisms for the biosynthesis of endocannabinoids. *Biochemistry*, 45(15):4720–6, apr 2006.

[172] Jie Liu, Lei Wang, Judith Harvey-White, et al. A biosynthetic pathway for anandamide. *Proceedings of the National Academy of Sciences of the United States of America*, 103(36):13345–50, sep 2006.

[173] Yong-Xin Sun, Kazuhito Tsuboi, Yasuo Okamoto, et al. Biosynthesis of anandamide and N-palmitoylethanolamine by sequential actions of phospholipase A2 and lysophospholipase D. *The Biochemical journal*, 380(Pt 3):749–56, jun 2004.

[174] Gabriel M Simon and Benjamin F Cravatt. Anandamide biosynthesis catalyzed by the phosphodiesterase GDE1 and detection of glycerophospho-N-acyl ethanolamine precursors in mouse brain. *The Journal of biological chemistry*, 283(14):9341–9, apr 2008.

[175] B F Cravatt, D K Giang, S P Mayfield, et al. Molecular characterization of an enzyme that degrades neuromodulatory fatty-acid amides. *Nature*, 384(6604):83–7, nov 1996.

[176] Natsuo Ueda. Endocannabinoid hydrolases. *Prostaglandins & Other Lipid Mediators*, 68:521–534, 2002.

[177] B F Cravatt, K Demarest, M P Patricelli, et al. Supersensitivity to anandamide and enhanced endogenous cannabinoid signaling in mice lacking fatty acid amide hydrolase. *Proceedings of the National Academy of Sciences of the United States of America*, 98(16):9371–6, jul 2001.

[178] Angela B Clement, E Gregory Hawkins, Aron H Lichtman, and Benjamin F Cravatt. Increased seizure susceptibility and proconvulsant activity of anandamide in mice lacking fatty acid amide hydrolase. *The Journal of neuroscience : the official journal of the Society for Neuroscience*, 23(9):3916–23, may 2003.

[179] Natsuo Ueda, Kazuhito Tsuboi, and Toru Uyama. Metabolism of endocannabinoids and related -acylethanolamines: Canonical and alternative pathways. *FEBS Journal*, 280(9):1874–1894, may 2013.

[180] Daniel J. Hermanson, Joyonna C. Gamble-George, Lawrence J. Marnett, and Sachin Patel. Substrate-selective COX-2 inhibition as a novel strategy for therapeutic endocannabinoid augmentation. *Trends in Pharmacological Sciences*, 35(7):358–367, 2014.

[181] Raphael Mechoulam, Shimon Ben-Shabat, Lumir Hanus, et al. Identification of an endogenous 2-monoglyceride, present in canine gut, that binds to cannabinoid receptors. *Biochemical Pharmacology*, 50(1):83–90, jun 1995.

[182] T Sugiura, S Kondo, A Sukagawa, et al. 2-Arachidonoylglycerol: a possible endogenous cannabinoid receptor ligand in brain. *Biochem Biophys Res Commun*, 215(1):89–97, oct 1995.

[183] Tiziana Bisogno, Fiona Howell, Gareth Williams, et al. Cloning of the first sn1-DAG lipases points to the spatial and temporal regulation of endocannabinoid signaling in the brain. *The Journal of cell biology*, 163(3):463–8, nov 2003.

[184] Ying Gao, Dmitry V Vasilyev, Maria Beatriz Goncalves, et al. Loss of retrograde endocannabinoid signaling and reduced adult neurogenesis in diacylglycerol lipase knock-out mice. *The Journal of neuroscience : the official journal of the Society for Neuroscience*, 30(6):2017–24, feb 2010.

[185] Asami Tanimura, Maya Yamazaki, Yuki Hashimotodani, et al. The endocannabinoid 2-arachidonoylglycerol produced by diacylglycerol lipase alpha mediates retrograde suppression of synaptic transmission. *Neuron*, 65(3):320–7, feb 2010.

[186] H Ueda, T Kobayashi, M Kishimoto, T Tsutsumi, and H Okuyama. A possible pathway of phosphoinositide metabolism through EDTA-insensitive phospholipase A1 followed by lysophosphoinositide-specific phospholipase C in rat brain. *Journal of neurochemistry*, 61(5):1874–81, nov 1993.

[187] T Tsutsumi, T Kobayashi, H Ueda, et al. Lysophosphoinositide-specific phospholipase C in rat brain synaptic plasma membranes. *Neurochemical research*, 19(4):399–406, apr 1994.

[188] Shinji Nakane, Saori Oka, Shunsuke Arai, et al. 2-Arachidonoyl-sn-glycero-3-phosphate, an arachidonic acid-containing lysophosphatidic acid: occurrence and rapid enzymatic conversion to 2-arachidonoyl-sn-glycerol, a cannabinoid receptor ligand, in rat brain. *Archives of biochemistry and biophysics*, 402(1):51–8, jun 2002.

[189] T P Dinh, D Carpenter, F M Leslie, et al. Brain monoglyceride lipase participating in endocannabinoid inactivation. *Proceedings of the National Academy of Sciences of the United States of America*, 99(16):10819–24, aug 2002.

[190] Ulrike Taschler, Franz P W Radner, Christoph Heier, et al. Monoglyceride lipase deficiency in mice impairs lipolysis and attenuates diet-induced insulin resistance. *The Journal of biological chemistry*, 286(20):17467–77, may 2011.

[191] Jacqueline L. Blankman, Gabriel M. Simon, and Benjamin F. Cravatt. A Comprehensive Profile of Brain Enzymes that Hydrolyze the Endocannabinoid 2-Arachidonoylglycerol. *Chemistry & Biology*, 14(12):1347–1356, 2007.

[192] Kevin R Kozak, Rajnish A Gupta, John S Moody, et al. 15-Lipoxygenase metabolism of 2-arachidonylglycerol. Generation of a peroxisome proliferator-activated receptor alpha agonist. *The Journal of biological chemistry*, 277(26):23278–86, jun 2002.

[193] Lumír Ondrej Hanus. Pharmacological and therapeutic secrets of plant and brain (endo)cannabinoids. *Medicinal Research Reviews*, 29(2):213–271, mar 2009.

[194] Mahmoud A. ElSohly and Desmond Slade. Chemical constituents of marijuana: The complex mixture of natural cannabinoids. *Life Sciences*, 78(5):539–548, 2005.

[195] John M McPartland, Marnie Duncan, Vincenzo Di Marzo, and Roger G Pertwee. Are cannabidiol and $\Delta(9)$ -tetrahydrocannabivarin negative modulators of the endocannabinoid system? A systematic review. *British journal of pharmacology*, 172(3):737–53, feb 2015.

[196] Y. Gaoni and R. Mechoulam. Isolation, Structure, and Partial Synthesis of an Active Constituent of Hashish. *Journal of the American Chemical Society*, 86(8):1646–1647, apr 1964.

[197] Zdenek Fisar. Phytocannabinoids and endocannabinoids. *Current drug abuse reviews*, 2(1):51–75, jan 2009.

[198] Megan Brafford May and Ashley E Glode. Dronabinol for chemotherapy-induced nausea and vomiting unresponsive to antiemetics. *Cancer management and research*, 8:49–55, 2016.

[199] Melissa E Badowski and Sarah E Perez. Clinical utility of dronabinol in the treatment of weight loss associated with HIV and AIDS. *HIV/AIDS (Auckland, N.Z.)*, 8:37–45, 2016.

[200] Andrew J. Hill, Claire M. Williams, Benjamin J. Whalley, and Gary J. Stephens. Phytocannabinoids as novel therapeutic agents in CNS disorders. *Pharmacology & Therapeutics*, 133(1):79–97, 2012.

[201] R. Mechoulam and Y. Shvo. HashishI. *Tetrahedron*, 19(12):2073–2078, jan 1963.

[202] R G Pertwee. The diverse CB1 and CB2 receptor pharmacology of three plant cannabinoids: delta9-tetrahydrocannabinol, cannabidiol and delta9-tetrahydrocannabivarin. *British journal of pharmacology*, 153(2):199–215, jan 2008.

[203] J M McPartland, M Glass, and R G Pertwee. Meta-analysis of cannabinoid ligand binding affinity and receptor distribution: interspecies differences. *British journal of pharmacology*, 152(5):583–93, nov 2007.

[204] A Thomas, G L Baillie, A M Phillips, et al. Cannabidiol displays unexpectedly high potency as an antagonist of CB1 and CB2 receptor agonists in vitro. *British journal of pharmacology*, 150(5):613–23, mar 2007.

[205] Luciano De Petrocellis, Alessia Ligresti, Aniello Schiano Moriello, et al. Effects of cannabinoids and cannabinoid-enriched Cannabis extracts on TRP channels and endocannabinoid metabolic enzymes. *British journal of pharmacology*, 163(7):1479–94, aug 2011.

[206] Michael Philip Barnes. Sativex: clinical efficacy and tolerability in the treatment of symptoms of multiple sclerosis and neuropathic pain. *Expert opinion on pharmacotherapy*, 7(5):607–15, apr 2006.

[207] Ethan Russo and Geoffrey W Guy. A tale of two cannabinoids: the therapeutic rationale for combining tetrahydrocannabinol and cannabidiol. *Medical hypotheses*, 66(2):234–46, 2006.

[208] Adèle Thomas, Lesley A Stevenson, Kerrie N Wease, et al. Evidence that the plant cannabinoid Delta9-tetrahydrocannabivarin is a cannabinoid CB1 and CB2 receptor antagonist. *British journal of pharmacology*, 146(7):917–26, dec 2005.

[209] R G Pertwee, A Thomas, L A Stevenson, et al. The psychoactive plant cannabinoid, Delta9-tetrahydrocannabinol, is antagonized by Delta8- and Delta9-tetrahydrocannabivarin in mice in vivo. *British journal of pharmacology*, 150(5):586–94, mar 2007.

[210] Cristoforo Silvestri and Vincenzo Di Marzo. Second generation CB1 receptor blockers and other inhibitors of peripheral endocannabinoid overactivity and the rationale of their use against metabolic disorders. *Expert opinion on investigational drugs*, 21(9):1309–22, sep 2012.

[211] Ruth A Ross, Heather C Brockie, Lesley A Stevenson, et al. Agonist-inverse agonist characterization at CB1 and CB2 cannabinoid receptors of L759633, L759656 and AM630. *British Journal of Pharmacology*, 126(3):665–672, feb 1999.

[212] Lawrence S. Melvin, M. Ross Johnson, Charles A. Harbert, George M. Milne, and Albert Weissman. A cannabinoid derived prototypical analgesic. *Journal of Medicinal Chemistry*, 27(1):67–71, jan 1984.

[213] B F Thomas, A F Gilliam, D F Burch, M J Roche, and H H Seltzman. Comparative receptor binding analyses of cannabinoid agonists and antagonists. *The Journal of pharmacology and experimental therapeutics*, 285(1):285–92, apr 1998.

[214] G Griffin, P J Atkinson, V M Showalter, B R Martin, and M E Abood. Evaluation of cannabinoid receptor agonists and antagonists using the guanosine-5'-O-(3-[35S]thio)-triphosphate binding assay in rat cerebellar membranes. *The Journal of pharmacology and experimental therapeutics*, 285(2):553–60, may 1998.

[215] J W Huffman, J Liddle, S Yu, et al. 3-(1',1'-Dimethylbutyl)-1-deoxy-delta8-THC and related compounds: synthesis of selective ligands for the CB2 receptor. *Bioorganic & medicinal chemistry*, 7(12):2905–14, dec 1999.

[216] Roger G Pertwee. Cannabinoid Receptor Ligands. 44(0966), 1993.

[217] Michael A. Eissenstat, Malcolm R. Bell, Thomas E. D'Ambra, et al. Aminoalkylindoles: Structure-Activity Relationships of Novel Cannabinoid Mimetics. *Journal of Medicinal Chemistry*, 38(16):3094–3105, aug 1995.

[218] Thomas E. D'Ambra, Kimberly G. Estep, Malcolm R. Bell, et al. Conformationally restrained analogs of pravadoline: nanomolar potent, enantioselective, (aminoalkyl)indole agonists of the cannabinoid receptor. *Journal of Medicinal Chemistry*, 35(1):124–135, jan 1992.

[219] D R Compton, L H Gold, S J Ward, R L Balster, and B R Martin. Aminoalkylindole analogs: cannabimimetic activity of a class of compounds structurally distinct from delta 9-tetrahydrocannabinol. *The Journal of pharmacology and experimental therapeutics*, 263(3):1118–26, dec 1992.

[220] D R Compton, M R Johnson, L S Melvin, and B R Martin. Pharmacological profile of a series of bicyclic cannabinoid analogs: classification as cannabimimetic agents. *The Journal of pharmacology and experimental therapeutics*, 260(1):201–9, jan 1992.

[221] Kenneth J Valenzano, Laykea Tafesse, Gary Lee, et al. Pharmacological and pharmacokinetic characterization of the cannabinoid receptor 2 agonist, GW405833, utilizing rodent models of acute and chronic pain, anxiety, ataxia and catalepsy. *Neuropharmacology*, 48(5):658–72, apr 2005.

[222] V M Showalter, D R Compton, B R Martin, and M E Abood. Evaluation of binding in a transfected cell line expressing a peripheral cannabinoid receptor (CB2): identification of cannabinoid receptor subtype selective ligands. *The Journal of pharmacology and experimental therapeutics*, 278(3):989–99, sep 1996.

[223] Mohab M Ibrahim, Hongfeng Deng, Alexander Zvonok, et al. Activation of CB2 cannabinoid receptors by AM1241 inhibits experimental neuropathic pain: pain inhibition by receptors not present in the CNS. *Proceedings of the National Academy of Sciences of the United States of America*, 100(18):10529–33, sep 2003.

[224] B B Yao, S Mukherjee, Y Fan, et al. In vitro pharmacological characterization of AM1241: a protean agonist at the cannabinoid CB2 receptor? *British journal of pharmacology*, 149(2):145–54, sep 2006.

[225] Gabriele Murineddu, Paolo Lazzari, Stefania Ruiu, et al. Tricyclic Pyrazoles. 4. Synthesis and Biological Evaluation of Analogues of the Robust and Selective CB ₂ Cannabinoid Ligand 1-(2,4-Dichlorophenyl)-6-methyl- N -piperidin-1-yl- 1,4-dihydroindeno[1,2- c]pyrazole-3-carboxamide. *Journal of Medicinal Chemistry*, 49(25):7502–7512, dec 2006.

[226] Pier Luigi Ferrarini, Vincenzo Calderone, Tiziana Cavallini, et al. Synthesis and biological evaluation of 1,8-naphthyridin-4(1H)-on-3-carboxamide derivatives as new ligands of cannabinoid receptors. *Bioorganic & Medicinal Chemistry*, 12(8):1921–1933, 2004.

[227] Clementina Manera, Veronica Benetti, M. Paola Castelli, et al. Design, Synthesis, and Biological Evaluation of New 1,8-Naphthyridin-4(1 H)-on-3-carboxamide and Quinolin-4(1 H)-on-3-carboxamide Derivatives as CB ₂ Selective Agonists. *Journal of Medicinal Chemistry*, 49(20):5947–5957, oct 2006.

[228] Serena Pasquini, Lorenzo Botta, Teresa Semeraro, et al. Investigations on the 4-Quinolone-3-carboxylic Acid Motif. 2. Synthesis and StructureActivity Relationship of Potent and Selective Cannabinoid-2 Receptor Agonists Endowed with Analgesic Activity in Vivo . *Journal of Medicinal Chemistry*, 51(16):5075–5084, aug 2008.

[229] M Gianella-Borradori, I Christou, C J Bataille, et al. Ligand-based virtual screening identifies a family of selective cannabinoid receptor 2 agonists. *Bioorg Med Chem*, 23(1):241–263, 2015.

[230] Murielle Rinaldi-Carmona, Francis Barth, Michel Héaulme, et al. SR141716A, a potent and selective antagonist of the brain cannabinoid receptor. *FEBS Letters*, 350(2-3):240–244, aug 1994.

[231] M Rinaldi-Carmona, F Barth, J Millan, et al. SR 144528, the first potent and selective antagonist of the CB2 cannabinoid receptor. *The Journal of pharmacology and experimental therapeutics*, 284(2):644–50, feb 1998.

[232] Giancarlo Colombo, Roberta Agabio, Giacomo Diaz, et al. Appetite suppression and weight loss after the cannabinoid antagonist SR 141716. *Life Sciences*, 63(8):PL113–PL117, jul 1998.

[233] Luc F Van Gaal, Aila M Rissanen, André J Scheen, et al. Effects of the cannabinoid-1 receptor blocker rimonabant on weight reduction and cardiovascular risk factors in overweight patients: 1-year experience from the RIO-Europe study. *Lancet (London, England)*, 365(9468):1389–97.

[234] F Xavier Pi-Sunyer, Louis J Aronne, Hassan M Heshmati, et al. Effect of rimonabant, a cannabinoid-1 receptor blocker, on weight and cardiometabolic risk factors in overweight or obese patients: RIO-North America: a randomized controlled trial. *JAMA*, 295(7):761–75, feb 2006.

[235] Luc F Van Gaal, André J Scheen, Aila M Rissanen, et al. Long-term effect of CB1 blockade with rimonabant on cardiometabolic risk factors: two year results from the RIO-Europe Study. *European heart journal*, 29(14):1761–71, jul 2008.

[236] Robin Christensen, Pernelle Kruse Kristensen, Else Marie Bartels, Henning Bliddal, and Arne Astrup. Efficacy and safety of the weight-loss drug rimonabant: a meta-analysis of randomised trials. *Lancet (London, England)*, 370(9600):1706–13, nov 2007.

[237] E. Kirilly, X. Gonda, and G. Bagdy. CB1 receptor antagonists: new discoveries leading to new perspectives. *Acta Physiologica*, 205(1):41–60, may 2012.

[238] Nancy E. Buckley, Kathleen L. McCoy, Éva Mezey, et al. Immunomodulation by cannabinoids is absent in mice deficient for the cannabinoid CB2 receptor. *European Journal of Pharmacology*, 396(2-3):141–149, 2000.

[239] N E Buckley. The peripheral cannabinoid receptor knockout mice: an update. *British journal of pharmacology*, 153(2):309–18, jan 2008.

[240] Jackson. Jackson Laboratory - CB2 knockout animals, 2016.

[241] Deltagen. Deltagen CB2 knockout mouse, 2016.

[242] Sreemanti Basu, Avijit Ray, and Bonnie N Dittel. Cannabinoid receptor 2 is critical for the homing and retention of marginal zone B lineage cells and for efficient T-independent immune responses. *Journal of immunology (Baltimore, Md. : 1950)*, 187(11):5720–32, dec 2011.

[243] Jagan R Muppidi, Tal I Arnon, Yelena Bronevetsky, et al. Cannabinoid receptor 2 positions and retains marginal zone B cells within the splenic marginal zone. *The Journal of experimental medicine*, 208(10):1941–8, sep 2011.

[244] P Pacher and R Mechoulam. Is lipid signaling through cannabinoid 2 receptors part of a protective system? *Progress in Lipid Research*, 50(2):193–211, 2011.

[245] Vincenzo Di Marzo, Nephi Stella, and Andreas Zimmer. Endocannabinoid signalling and the deteriorating brain. *Nature Reviews Neuroscience*, 16(1):30–42, dec 2014.

[246] Michelle Roche and David P Finn. Brain CB2 Receptors: Implications for Neuropsychiatric Disorders. *Pharmaceuticals*, 3(8):2517–2553, aug 2010.

[247] Mohab M Ibrahim, Megan L Rude, Nicola J Stagg, et al. CB2 cannabinoid receptor mediation of antinociception. *Pain*, 122(1-2):36–42, may 2006.

[248] Beat Lutz, Giovanni Marsicano, Rafael Maldonado, and Cecilia J. Hillard. The endocannabinoid system in guarding against fear, anxiety and stress. *Nature Reviews Neuroscience*, 16(12):705–718, nov 2015.

[249] P Pacher and G Kunos. Modulating the endocannabinoid system in human health and disease - successes and failures. *FEBS Journal*, 280(9):1918–1943, 2013.

[250] J. DeVoss and L. Diehl. Murine Models of Inflammatory Bowel Disease (IBD): Challenges of Modeling Human Disease. *Toxicologic Pathology*, 42(1):99–110, jan 2014.

[251] Mireille Alhouayek and Giulio G. Muccioli. The endocannabinoid system in inflammatory bowel diseases: from pathophysiology to therapeutic opportunity. *Trends in Molecular Medicine*, 18(10):615–625, 2012.

[252] Edward S Kimball, Craig R Schneider, Nathaniel H Wallace, and Pamela J Hornby. Agonists of cannabinoid receptor 1 and 2 inhibit experimental colitis induced by oil of mustard and by dextran sulfate sodium. *American journal of physiology. Gastrointestinal and liver physiology*, 291(2):G364–71, aug 2006.

[253] Udai P Singh, Narendra P Singh, Balwan Singh, et al. Cannabinoid receptor-2 (CB2) agonist ameliorates colitis in IL-10(-/-) mice by attenuating the activation of T cells and promoting their apoptosis. *Toxicology and applied pharmacology*, 258(2):256–67, jan 2012.

[254] Martin A Storr, Catherine M Keenan, Hong Zhang, et al. Activation of the cannabinoid 2 receptor (CB2) protects against experimental colitis. *Inflammatory bowel diseases*, 15(11):1678–85, nov 2009.

[255] M A Engel, C A Kellermann, G Burnat, et al. Mice lacking cannabinoid CB1-, CB2-receptors or both receptors show increased susceptibility to trinitrobenzene sulfonic acid (TNBS)-induced colitis. *Journal of physiology and pharmacology : an official journal of the Polish Physiological Society*, 61(1):89–97, feb 2010.

[256] Kalliopi K Gkouskou, Chrysoula Deligianni, Christos Tsatsanis, and Aristides G Eliopoulos. The gut microbiota in mouse models of inflammatory bowel disease. *Frontiers in cellular and infection microbiology*, 4:28, 2014.

[257] Sandra Nell, Sebastian Suerbaum, and Christine Josenhans. The impact of the microbiota on the pathogenesis of IBD: lessons from mouse infection models. *Nature Reviews Microbiology*, 8(8):564–577, aug 2010.

[258] M Sałaga, A Mokrowiecka, P K Zakrzewski, et al. Experimental colitis in mice is attenuated by changes in the levels of endocannabinoid metabolites induced by selective inhibition of fatty acid amide hydrolase (FAAH). *Journal of Crohn's & colitis*, 8(9):998–1009, sep 2014.

[259] M. Alhouayek, D. M. Lambert, N. M. Delzenne, P. D. Cani, and G. G. Muccioli. Increasing endogenous 2-arachidonoylglycerol levels counteracts colitis and related systemic inflammation. *The FASEB Journal*, 25(8):2711–2721, aug 2011.

[260] Martin A. Storr, Catherine M. Keenan, Dominik Emmerdinger, et al. Targeting endocannabinoid degradation protects against experimental colitis in mice: involvement of CB1 and CB2 receptors. *Journal of Molecular Medicine*, 86(8):925–936, aug 2008.

[261] Federico Massa, Giovanni Marsicano, Heike Hermann, et al. The endogenous cannabinoid system protects against colonic inflammation. *The Journal of clinical investigation*, 113(8):1202–9, apr 2004.

[262] Lucia Marquéz, Juan Suárez, Mar Iglesias, et al. Ulcerative colitis induces changes on the expression of the endocannabinoid system in the human colonic tissue. *PloS one*, 4(9):e6893, 2009.

[263] Simon Lal, Neeraj Prasad, Manijeh Ryan, et al. Cannabis use amongst patients with inflammatory bowel disease. *European journal of gastroenterology & hepatology*, 23(10):891–6, oct 2011.

[264] Jessica Ravikoff Allegretti, Andrew Courtwright, Matthew Lucci, Joshua R Korzenik, and Jonathan Levine. Marijuana use patterns among patients with inflammatory bowel disease. *Inflammatory bowel diseases*, 19(13):2809–14, dec 2013.

[265] Jon A. Buras, Bernhard Holzmann, and Michail Sitkovsky. Model organisms: Animal Models of sepsis: setting the stage. *Nature Reviews Drug Discovery*, 4(10):854–865, oct 2005.

[266] Mitchell P Fink. Animal models of sepsis. *Virulence*, 5(1):143–53, jan 2014.

[267] Anthony J. Lewis, Christopher W. Seymour, and Matthew R. Rosengart. Current Murine Models of Sepsis. *Surgical Infections*, 17(4):385–393, aug 2016.

[268] Johannes Tschöp, Kevin R Kasten, Ruben Nogueiras, et al. The cannabinoid receptor 2 is critical for the host response to sepsis. *Journal of immunology (Baltimore, Md. : 1950)*, 183(1):499–505, jul 2009.

[269] Balázs Csóka, Zoltán H Németh, Partha Mukhopadhyay, et al. CB2 cannabinoid receptors contribute to bacterial invasion and mortality in polymicrobial sepsis. *PloS one*, 4(7):e6409, 2009.

[270] Jean A Nemzek, Kelly M S Hugunin, and Mark R Opp. Modeling sepsis in the laboratory: merging sound science with animal well-being. *Comparative medicine*, 58(2):120–8, apr 2008.

[271] Luiz F. Poli-de Figueiredo, Alejandra G. Garrido, Naomi Nakagawa, and Paulina Sannomiya. Experimental models of sepsis and their clinical relevance. *Shock (Augusta, Ga.)*, 30 Suppl 1(Suppl 1):53–59, oct 2008.

[272] Huan Gui, Yang Sun, Zhu-Min Luo, et al. Cannabinoid receptor 2 protects against acute experimental sepsis in mice. *Mediators of inflammation*, 2013:741303, 2013.

[273] J Sardinha, M E M Kelly, J Zhou, and C Lehmann. Experimental cannabinoid 2 receptor-mediated immune modulation in sepsis. *Mediators Inflamm*, 2014:978678, 2014.

[274] J.T. Toguri, R. Moxsom, A.M. Szczesniak, et al. Cannabinoid 2 receptor activation reduces leukocyte adhesion and improves capillary perfusion in the iridial microvasculature during systemic inflammation. *Clinical Hemorheology and Microcirculation*, 61(2):237–249, sep 2015.

[275] Andrew P Robinson, Christopher T Harp, Avertano Noronha, and Stephen D Miller. The experimental autoimmune encephalomyelitis (EAE) model of MS: utility for understanding disease pathophysiology and treatment. *Handbook of clinical neurology*, 122:173–89, 2014.

[276] Cris S Constantinescu, Nasr Farooqi, Kate O'Brien, and Bruno Gran. Experimental autoimmune encephalomyelitis (EAE) as a model for multiple sclerosis (MS). *British journal of pharmacology*, 164(4):1079–106, oct 2011.

[277] I Wirguin, R Mechoulam, A Breuer, et al. Suppression of experimental autoimmune encephalomyelitis by cannabinoids. *Immunopharmacology*, 28(3):209–14, 1994.

[278] W D Lyman, J R Sonett, C F Brosnan, R Elkin, and M B Bornstein. Delta 9-tetrahydrocannabinol: a novel treatment for experimental autoimmune encephalomyelitis. *Journal of neuroimmunology*, 23(1):73–81, jun 1989.

[279] A. Sánchez, A. González-Pérez, P. Galve-Roperh, I. García-Merino. R-(+)-[2,3-Dihydro-5-methyl-3-(4-morpholinylmethyl)-pyrrolo-[1,2,3-de]-1,4-benzoxazin-6-yl]-1-naphtalenylmethanone (WIN-2) ameliorates experimental autoimmune encephalomyelitis and induces encephalitogenic T cell apoptosis: Partial involvement of the CB2. *Biochemical Pharmacology*, 72(12):1697–1706, 2006.

[280] D Baker, G Pryce, J L Croxford, et al. Cannabinoids control spasticity and tremor in a multiple sclerosis model. *Nature*, 404(6773):84–87, mar 2000.

[281] Xiang Ni, Ellen B Geller, Michael J Eppihimer, et al. Win 55212-2, a cannabinoid receptor agonist, attenuates leukocyte/endothelial interactions in an experimental autoimmune encephalomyelitis model. *Multiple sclerosis (Houndmills, Basingstoke, England)*, 10(2):158–64, apr 2004.

[282] Bo-Zong Z Shao, Wei Wei, Ping Ke, et al. Activating cannabinoid receptor 2 alleviates pathogenesis of experimental autoimmune encephalomyelitis via activation of autophagy and inhibiting NLRP3 inflammasome. *CNS Neurosci Ther*, 20(12):1021–1028, dec 2014.

[283] J. Palazuelos, N. Davoust, B. Julien, et al. The CB2 Cannabinoid Receptor Controls Myeloid Progenitor Trafficking: INVOLVEMENT IN THE PATHOGENESIS OF AN ANIMAL MODEL OF MULTIPLE SCLEROSIS. *Journal of Biological Chemistry*, 283(19):13320–13329, may 2008.

[284] Zhi-Yin Lou, Chan Chen, Qing He, Chong-Bo Zhao, and Bao-Guo Xiao. Targeting CB2 receptor as a neuroinflammatory modulator in experimental autoimmune encephalomyelitis. *Molecular Immunology*, 49(3):453–461, 2011.

[285] Sofia Sisay, Gareth Pryce, Samuel J Jackson, et al. Genetic background can result in a marked or minimal effect of gene knockout (GPR55 and CB2 receptor) in experimental autoimmune encephalomyelitis models of multiple sclerosis. *PloS one*, 8(10):e76907, 2013.

[286] Katarzyna Maresz, Gareth Pryce, Eugene D Ponomarev, et al. Direct suppression of CNS autoimmune inflammation via the cannabinoid receptor CB1 on neurons and CB2 on autoreactive T cells. *Nature Medicine*, 13(4):492–497, apr 2007.

[287] G Pryce and D Baker. Control of spasticity in a multiple sclerosis model is mediated by CB1, not CB2, cannabinoid receptors. *British journal of pharmacology*, 150(4):519–25, feb 2007.

[288] R. Ribeiro, F. Yu, J. Wen, A. Vana, and Y. Zhang. Therapeutic potential of a novel cannabinoid agent CB52 in the mouse model of experimental autoimmune encephalomyelitis. *Neuroscience*, 254:427–442, 2013.

[289] D M Lee and M E Weinblatt. Rheumatoid arthritis. *Lancet (London, England)*, 358(9285):903–11, sep 2001.

[290] Darren L. Asquith, Ashley M. Miller, Iain B. McInnes, and Foo Y. Liew. Animal models of rheumatoid arthritis. *European journal of immunology*, 39(8):2040–4, aug 2009.

[291] Marc Feldmann. Timeline: Development of anti-TNF therapy for rheumatoid arthritis. *Nature Reviews Immunology*, 2(5):364–371, may 2002.

[292] Andrea Rubbert-Roth and Axel Finckh. Treatment options in patients with rheumatoid arthritis failing initial TNF inhibitor therapy: a critical review. *Arthritis research & therapy*, 11 Suppl 1(Suppl 1):S1, 2009.

[293] Denise Richardson, Richard G Pearson, Nisha Kurian, et al. Characterisation of the cannabinoid receptor system in synovial tissue and fluid in patients with osteoarthritis and rheumatoid arthritis. *Arthritis research & therapy*, 10(2):R43, 2008.

[294] Steven G Kinsey, Pattipati S Naidu, Benjamin F Cravatt, David T Dudley, and Aron H Lichtman. Fatty acid amide hydrolase blockade attenuates the development of collagen-induced arthritis and related thermal hyperalgesia in mice. *Pharmacology, biochemistry, and behavior*, 99(4):718–25, oct 2011.

[295] Shin Fukuda, Hitoshi Kohsaka, Aiko Takayasu, et al. Cannabinoid receptor 2 as a potential therapeutic target in rheumatoid arthritis. *BMC musculoskeletal disorders*, 15:275, 2014.

[296] Huan Gui, Xia Liu, Li-Rong Liu, Ding-Feng Su, and Sheng-Ming Dai. Activation of cannabinoid receptor 2 attenuates synovitis and joint distruction in collagen-induced arthritis. *Immunobiology*, 220(6):817–822, 2015.

[297] Torsten Lowin, Georg Pongratz, and Rainer H Straub. The synthetic cannabinoid WIN55,212-2 mesylate decreases the production of inflammatory mediators in rheumatoid arthritis synovial fibroblasts by activating CB2, TRPV1, TRPA1 and yet unidentified receptor targets. *Journal of inflammation (London, England)*, 13:15, 2016.

[298] E Selvi, S Lorenzini, E Garcia-Gonzalez, et al. Inhibitory effect of synthetic cannabinoids on cytokine production in rheumatoid fibroblast-like synoviocytes. *Clinical and experimental rheumatology*, 26(4):574–81.

[299] H. Gui, X. Liu, Z.-W. W Wang, et al. Expression of cannabinoid receptor 2 and its inhibitory effects on synovial fibroblasts in rheumatoid arthritis. *Rheumatology (Oxford)*, 53(5):802–809, may 2014.

[300] Theodore Kalogeris, Christopher P Baines, Maike Krenz, and Ronald J Korthuis. Cell biology of ischemia/reperfusion injury. *International review of cell and molecular biology*, 298:229–317, 2012.

[301] H de Groot and U Rauen. Ischemia-reperfusion injury: processes in pathogenetic networks: a review. *Transplantation proceedings*, 39(2):481–4, mar 2007.

[302] Aslan T Turer and Joseph A Hill. Pathogenesis of myocardial ischemia-reperfusion injury and rationale for therapy. *The American journal of cardiology*, 106(3):360–8, aug 2010.

[303] Zhaobin Xu, Jenna Alloush, Eric Beck, and Noah Weisleder. A murine model of myocardial ischemia-reperfusion injury through ligation of the left anterior descending artery. *Journal of visualized experiments : JoVE*, (86), 2014.

[304] Terrance Chiang, Robert O Messing, and Wen-Hai Chou. Mouse model of middle cerebral artery occlusion. *Journal of visualized experiments : JoVE*, (48), 2011.

[305] Qingqing Wei and Zheng Dong. Mouse model of ischemic acute kidney injury: technical notes and tricks. *American journal of physiology. Renal physiology*, 303(11):F1487–94, dec 2012.

[306] Yuta Abe, Ian N Hines, Gazi Zibari, et al. Mouse model of liver ischemia and reperfusion injury: method for studying reactive oxygen and nitrogen metabolites in vivo. *Free radical biology & medicine*, 46(1):1–7, jan 2009.

[307] Demetrios Moris, Sotirios Georgopoulos, Evangelos Felekouras, Efstratios Patsouris, and Stamatios Theocharis. The effect of endocannabinoid system in ischemia-reperfusion injury: a friend or a foe? *Expert opinion on therapeutic targets*, 19(9):1261–75, 2015.

[308] Abdolamir Feizi, Mohammad-Reza Jafari, Farzaneh Hamedivafa, Pouria Tabrizian, and Bijan Djahanguiri. The preventive effect of cannabinoids on reperfusion-induced ischemia of mouse kidney. *Experimental and Toxicologic Pathology*, 60(4):405–410, 2008.

[309] Mohanraj Rajesh, Hao Pan, Partha Mukhopadhyay, et al. Cannabinoid-2 receptor agonist HU-308 protects against hepatic ischemia/reperfusion injury by attenuating oxidative stress, inflammatory response, and apoptosis. *Journal of leukocyte biology*, 82(6):1382–9, dec 2007.

[310] Sándor Bátkai, Douglas Osei-Hyiaman, Hao Pan, et al. Cannabinoid-2 receptor mediates protection against hepatic ischemia/reperfusion injury. *FASEB journal : official publication of the Federation of American Societies for Experimental Biology*, 21(8):1788–800, jun 2007.

[311] Sándor Bátkai, Partha Mukhopadhyay, Bla Horváth, et al. Δ8-Tetrahydrocannabivarin prevents hepatic ischaemia/reperfusion injury by decreasing oxidative stress and inflammatory responses through cannabinoid CB2 receptors. *British journal of pharmacology*, 165(8):2450–61, apr 2012.

[312] Bla Horváth, Lital Magid, Partha Mukhopadhyay, et al. A new cannabinoid CB2 receptor agonist HU-910 attenuates oxidative stress, inflammation and cell death associated with hepatic ischaemia/reperfusion injury. *British journal of pharmacology*, 165(8):2462–78, apr 2012.

[313] Ming Zhang, Billy R Martin, Martin W Adler, et al. Cannabinoid CB(2) receptor activation decreases cerebral infarction in a mouse focal ischemia/reperfusion model. *Journal of cerebral blood flow and metabolism : official journal of the International Society of Cerebral Blood Flow and Metabolism*, 27(7):1387–96, jul 2007.

[314] M Zhang, B R Martin, M W Adler, et al. Modulation of the balance between cannabinoid CB(1) and CB(2) receptor activation during cerebral ischemic/reperfusion injury. *Neuroscience*, 152(3):753–60, mar 2008.

[315] Ming Zhang, Martin W Adler, Mary E Abood, et al. CB2 receptor activation attenuates microcirculatory dysfunction during cerebral ischemic/reperfusion injury. *Microvascular research*, 78(1):86–94, jun 2009.

[316] S. Murikinati, E. Juttler, T. Keinert, et al. Activation of cannabinoid 2 receptors protects against cerebral ischemia by inhibiting neutrophil recruitment. *The FASEB Journal*, 24(3):788–798, mar 2010.

[317] C. Di Filippo, Francesco Rossi, Settimio Rossi, and Michele D'Amico. Cannabinoid CB2 receptor activation reduces mouse myocardial ischemia-reperfusion injury: involvement of cytokine/chemokines and PMN. *Journal of Leukocyte Biology*, 75(3):453–459, nov 2003.

[318] Fabrizio Montecucco, Sébastien Lenglet, Vincent Braunersreuther, et al. CB2 cannabinoid receptor activation is cardioprotective in a mouse model of ischemia/reperfusion. *Journal of Molecular and Cellular Cardiology*, 46(5):612–620, 2009.

[319] N. Defer, J. Wan, R. Souktani, et al. The cannabinoid receptor type 2 promotes cardiac myocyte and fibroblast survival and protects against ischemia/reperfusion-induced cardiomyopathy. *The FASEB Journal*, 23(7):2120–2130, jul 2009.

[320] Cristina González, Esperanza Herradón, Raquel Abalo, et al. Cannabinoid/agonist WIN 55,212-2 reduces cardiac ischaemiareperfusion injury in Zucker diabetic fatty rats: role of CB2 receptors and iNOS/eNOS. *Diabetes/metabolism research and reviews*, 27(4):331–40, may 2011.

[321] Peng-Fei Wang, Li-Sheng Jiang, Jun Bu, et al. Cannabinoid-2 receptor activation protects against infarct and ischemia-reperfusion heart injury. *Journal of cardiovascular pharmacology*, 59(4):301–7, apr 2012.

[322] Qian Li, Feng Wang, Yan-Min Zhang, Jing-Jing Zhou, and Yi Zhang. Activation of cannabinoid type 2 receptor by JWH133 protects heart against ischemia/reperfusion-induced apoptosis. *Cellular physiology and biochemistry : international journal of experimental cellular physiology, biochemistry, and pharmacology*, 31(4-5):693–702, 2013.

[323] Qian Li, Hui-cai Guo, Leonid N Maslov, et al. Mitochondrial permeability transition pore plays a role in the cardioprotection of CB2 receptor against ischemia-reperfusion injury. *Canadian journal of physiology and pharmacology*, 92(3):205–14, mar 2014.

[324] Georg D Duerr, Jan C Heinemann, Christopher Gestrich, et al. Impaired border zone formation and adverse remodeling after reperfused myocardial infarction in cannabinoid CB2 receptor deficient mice. *Life sciences*, 138:8–17, oct 2015.

[325] Georg D Duerr, Jan C Heinemann, Georg Suchan, et al. The endocannabinoid-CB2 receptor axis protects the ischemic heart at the early stage of cardiomyopathy. *Basic research in cardiology*, 109(4):425, jul 2014.

[326] S Cavanagh, M.J. Gough, and S. Homer-Vanniasinkam. The role of the neutrophil in ischaemia-reperfusion injury: potential therapeutic interventions. *Cardiovascular Surgery*, 6(2):112–118, apr 1998.

[327] Kathryn J Moore and Ira Tabas. Macrophages in the pathogenesis of atherosclerosis. *Cell*, 145(3):341–55, apr 2011.

[328] Ira Tabas, Kevin Jon Williams, and Jan Borén. Subendothelial lipoprotein retention as the initiating process in atherosclerosis: update and therapeutic implications. *Circulation*, 116(16):1832–44, oct 2007.

[329] Javier Mestas and Klaus Ley. Monocyte-endothelial cell interactions in the development of atherosclerosis. *Trends in cardiovascular medicine*, 18(6):228–32, aug 2008.

[330] K J Moore, F J Sheedy, and E A Fisher. Macrophages in atherosclerosis: a dynamic balance. *Nature reviews Immunology*, 13(10):709–721, 2013.

[331] F K Swirski, M Nahrendorf, M G School, F K Swirski, and M Nahrendorf. Leukocyte Behavior in Atherosclerosis, Myocardial Infarction, and Heart Failure. *Science*, 339(6116):161–166, 2013.

[332] Elizabeth G. Nabel and Eugene Braunwald. A Tale of Coronary Artery Disease and Myocardial Infarction. *New England Journal of Medicine*, 366(1):54–63, jan 2012.

[333] Donald Lloyd-Jones, Robert J Adams, Todd M Brown, et al. Executive summary: heart disease and stroke statistics–2010 update: a report from the American Heart Association. *Circulation*, 121(7):948–54, feb 2010.

[334] Sabine Steffens, Niels R Veillard, Claire Arnaud, et al. Low dose oral cannabinoid therapy reduces progression of atherosclerosis in mice. *Nature*, 434(7034):782–6, apr 2005.

[335] Yan Zhao, Zuyi Yuan, Yan Liu, et al. Activation of cannabinoid CB2 receptor ameliorates atherosclerosis associated with suppression of adhesion molecules. *Journal of cardiovascular pharmacology*, 55(3):292–8, mar 2010.

[336] Yan Zhao, Yan Liu, Weiping Zhang, et al. WIN55212-2 ameliorates atherosclerosis associated with suppression of pro-inflammatory responses in ApoE-knockout mice. *European Journal of Pharmacology*, 649(1-3):285–292, 2010.

[337] Courtney D Netherland, Theresa G Pickle, Alicia Bales, and Douglas P Thewke. Cannabinoid receptor type 2 (CB2) deficiency alters atherosclerotic lesion formation in hyperlipidemic Ldlr-null mice. *Atherosclerosis*, 213(1):102–8, nov 2010.

[338] Florian Willecke, Katharina Zeschky, Alexandra Ortiz Rodriguez, et al. Cannabinoid receptor 2 signaling does not modulate atherogenesis in mice. *PloS one*, 6(4):e19405, jan 2011.

[339] Friedrich Felix Hoyer, Martin Steinmetz, Sebastian Zimmer, et al. Atheroprotection via cannabinoid receptor-2 is mediated by circulating and vascular cells in vivo. *Journal of molecular and cellular cardiology*, 51(6):1007–14, dec 2011.

[340] Courtney Netherland-Van Dyke, Ward Rodgers, Makenzie Fulmer, Zachary Lahr, and Douglas Thewke. Cannabinoid Receptor Type 2 (CB2) Dependent and Independent Effects of WIN55,212-2 on Atherosclerosis in Ldlr-null Mice. *Journal of cardiology and therapeutics*, 3(2):53–63, jul 2015.

[341] Dianne J M Delsing, Frank P Leijten, Karin Arts, et al. Cannabinoid Receptor 2 Deficiency in Haematopoietic cells Aggravates Early Atherosclerosis in LDL Receptor Deficient Mice. *The open cardiovascular medicine journal*, 5:15–21, 2011.

[342] Mohanraj Rajesh, Partha Mukhopadhyay, S Batkai, et al. CB2-receptor stimulation attenuates TNF-alpha-induced human endothelial cell activation, transendothelial migration of monocytes, and monocyte-endothelial adhesion. *American journal of physiology. Heart and circulatory physiology*, 293(4):H2210–8, oct 2007.

[343] A J Iqbal, D Regan-Komito, I Christou, et al. A real time chemotaxis assay unveils unique migratory profiles amongst different primary murine macrophages. *PLoS One*, 8(3):e58744, 2013.

[344] Muthulekha Swamydas and Michail S Lionakis. Isolation, purification and labeling of mouse bone marrow neutrophils for functional studies and adoptive transfer experiments. *J Vis Exp*, (77):e50586, 2013.

[345] J J Tyson and J D Murray. Cyclic AMP waves during aggregation of Dictyostelium amoebae. *Development (Cambridge, England)*, 106(3):421–426, jul 1989.

[346] Len Stephens, Laura Milne, and Phillip Hawkins. Moving towards a better understanding of chemotaxis. *Current biology : CB*, 18(11):R485–94, jun 2008.

[347] Fei Wang. The signaling mechanisms underlying cell polarity and chemotaxis. *Cold Spring Harb Perspect Biol*, 1(4):a002980, oct 2009.

[348] E R Neptune, T Iiri, and H R Bourne. Galphai is not required for chemotaxis mediated by Gi-coupled receptors. *The Journal of biological chemistry*, 274(5):2824–8, jan 1999.

[349] Hongyan Li, Lei Yang, Hui Fu, et al. Association between Gαi2 and ELMO1/Dock180 connects chemokine signalling with Rac activation and metastasis. *Nature communications*, 4:1706, 2013.

[350] Julie Wu, Anne Pipathsouk, A Keizer-Gunnink, et al. Homer3 regulates the establishment of neutrophil polarity. *Molecular biology of the cell*, 26(9):1629–39, may 2015.

[351] Alexander Zarbock, Tracy L. Deem, Tracy L. Burcin, and Klaus Ley. Galphai2 is required for chemokine-induced neutrophil arrest. *Blood*, 110(10):3773–3779, nov 2007.

[352] Jingsong Xu, Fei Wang, Alexandra Van Keymeulen, et al. Divergent signals and cytoskeletal assemblies regulate self-organizing polarity in neutrophils. *Cell*, 114(2):201–214, 2003.

[353] D. M. Lehmann, A M P B Seneviratne, and A. V. Smrcka. Small molecule disruption of G protein beta gamma subunit signaling inhibits neutrophil chemotaxis and inflammation. *Mol Pharmacol*, 73(2):410–418, nov 2008.

[354] Sabine Suire, Alison M Condliffe, G John Ferguson, et al. Gbetagammas and the Ras binding domain of p110gamma are both important regulators of PI(3)Kgamma signalling in neutrophils. *Nature cell biology*, 8(11):1303–9, nov 2006.

[355] A V Vorotnikov. Chemotaxis: movement, direction, control. *Biochemistry. Biokhimiia*, 76(13):1528–55, dec 2011.

[356] Pablo A Iglesias. Spatial regulation of PI3K signaling during chemotaxis. *Wiley interdisciplinary reviews. Systems biology and medicine*, 1(2):247–53, 2009.

[357] Sylvain Merlot and Richard A Firtel. Leading the way: Directional sensing through phosphatidylinositol 3-kinase and other signaling pathways. *Journal of cell science*, 116(Pt 17):3471–8, sep 2003.

[358] Carsten Brock, Michael Schaefer, H. Peter Reusch, et al. Roles of G$\beta\gamma$ in membrane recruitment and activation of p110γ/p101 phosphoinositide 3-kinase γ. *Journal of Cell Biology*, 160(1):89–99, jan 2003.

[359] Emilio Hirsch, Vladimir L Katanaev, Cecilia Garlanda, et al. Central role for G protein-coupled phosphoinositide 3-kinase γ in inflammation. *Science*, 287(5455):1049–1053, feb 2000.

[360] Z Li, H Jiang, W Xie, et al. Roles of PLC-beta2 and -beta3 and PI3Kgamma in chemoattractant-mediated signal transduction. *Science (New York, N.Y.)*, 287(5455):1046–1049, feb 2000.

[361] T Sasaki. Function of PI3K in Thymocyte Development, T Cell Activation, and Neutrophil Migration. *Science*, 287(5455):1040–1046, feb 2000.

[362] Chanchal Sadhu, Boris Masinovsky, Ken Dick, C Gregory Sowell, and Donald E Staunton. Essential role of phosphoinositide 3-kinase delta in neutrophil directional movement. *Journal of Immunology (Baltimore, Md.: 1950)*, 170(5):2647–2654, mar 2003.

[363] Bart Vanhaesebroeck, Gareth E Jones, William E Allen, et al. Distinct PI(3)Ks mediate mitogenic signalling and cell migration in macrophages. *Nature cell biology*, 1(1):69–71, may 1999.

[364] C. Y. Wu, M. W. Lin, D. C. Wu, et al. The role of phosphoinositide-regulated actin reorganization in chemotaxis and cell migration. *British Journal of Pharmacology*, 171(24):5541–5554, dec 2014.

[365] Miki Nishio, Ken-ichi Watanabe, Junko Sasaki, et al. Control of cell polarity and motility by the PtdIns(3,4,5)P3 phosphatase SHIP1. *Nature cell biology*, 9(1):36–44, jan 2007.

[366] G John Ferguson, Laura Milne, Suhasini Kulkarni, et al. PI(3)Kgamma has an important context-dependent role in neutrophil chemokinesis. *Nature cell biology*, 9(1):86–91, jan 2007.

[367] Brendan D Manning and Lewis C Cantley. AKT/PKB Signaling: Navigating Downstream, jun 2007.

[368] Baogang Zhang, Yongjie Ma, Hua Guo, et al. Akt2 is required for macrophage chemotaxis. *European journal of immunology*, 39(3):894–901, mar 2009.

[369] Silvia M Goicoechea, Sahezeel Awadia, and Rafael Garcia-Mata. I'm coming to GEF you: Regulation of RhoGEFs during cell migration, 2014.

[370] Yuya Kunisaki, Akihiko Nishikimi, Yoshihiko Tanaka, et al. DOCK2 is a Rac activator that regulates motility and polarity during neutrophil chemotaxis. *Journal of Cell Biology*, 174(5):647–652, aug 2006.

[371] Elisabeth M. Gardiner, Kersi N. Pestonjamasp, Benjamin P. Bohl, et al. Spatial and temporal analysis of Rac activation during live neutrophil chemotaxis. *Current Biology*, 12(23):2029–2034, 2002.

[372] Reina E Itoh, Kazuo Kurokawa, Yusuke Ohba, et al. Activation of rac and cdc42 video imaged by fluorescent resonance energy transfer-based single-molecule probes in the membrane of living cells. *Molecular and cellular biology*, 22(18):6582–6591, sep 2002.

[373] Robert H. Insall and Laura M. Machesky. Actin Dynamics at the Leading Edge: From Simple Machinery to Complex Networks, 2009.

[374] Thomas D. Pollard. Regulation of actin filament assembly by Arp2/3 complex and formins. *Annual review of biophysics and biomolecular structure*, 36:451–477, 2007.

[375] Supriya Srinivasan, Fei Wang, Suzana Glavas, et al. Rac and Cdc42 play distinct roles in regulating PI(3,4,5)P3 and polarity during neutrophil chemotaxis. *Journal of Cell Biology*, 160(3):375–385, feb 2003.

[376] Chun Xiang Sun, Gregory P Downey, Fei Zhu, et al. Rac1 is the small GTPase responsible for regulating the neutrophil chemotaxis compass. *Blood*, 104(12):3758–3765, dec 2004.

[377] Pascale G Charest and Richard A Firtel. Big roles for small GTPases in the control of directed cell movement. *The Biochemical journal*, 401(2):377–390, jan 2007.

[378] D. Zicha, W. E. Allen, P. M. Brickell, et al. Chemotaxis of macrophages is abolished in the Wiskott-Aldrich syndrome. *British Journal of Haematology*, 101(4):659–665, jun 1998.

[379] Sachin Kumar, Juying Xu, Charles Perkins, et al. Cdc42 regulates neutrophil migration via crosstalk between WASp, CD11b, and microtubules. *Blood*, 120(17):3563–3574, oct 2012.

[380] Kit Wong, Alexandra Van Keymeulen, and Henry R Bourne. PDZRhoGEF and myosin II localize RhoA activity to the back of polarizing neutrophil-like cells. *Journal of Cell Biology*, 179(6):1141–1148, dec 2007.

[381] Hee Won Yang, Sean R. Collins, and Tobias Meyer. Locally excitable Cdc42 signals steer cells during chemotaxis. *Nature Cell Biology*, 18(2):191–201, dec 2015.

[382] Kirsi Riento and Anne J. Ridley. Rocks: multifunctional kinases in cell behaviour. *Nature reviews. Molecular cell biology*, 4(6):446–56, jun 2003.

[383] Alexandra Van Keymeulen, Kit Wong, Zachary A Knight, et al. To stabilize neutrophil polarity, PIP3 and Cdc42 augment RhoA activity at the back as well as signals at the front. *Journal of Cell Biology*, 174(3):437–445, jul 2006.

[384] Ya Zhou, Katarzyna Falenta, and Giovanna Lalli. Endocannabinoid signalling in neuronal migration. *International Journal of Biochemistry and Cell Biology*, 47(1):104–108, 2014.

[385] Z H Song and M Zhong. CB1 cannabinoid receptor-mediated cell migration. *The Journal of pharmacology and experimental therapeutics*, 294(1):204–209, jul 2000.

[386] Prakash Nagarkatti, Rupal Pandey, Sadiye Amcaoglu Rieder, Venkatesh L Hegde, and Mitzi Nagarkatti. Cannabinoids as novel anti-inflammatory drugs. *Future medicinal chemistry*, 1(7):1333–1349, 2009.

[387] G A Cabral and L Griffin-Thomas. Emerging role of the cannabinoid receptor CB2 in immune regulation: therapeutic prospects for neuroinflammation. *Expert reviews in molecular medicine*, 11:e3, 2009.

[388] A M Miller and N Stella. CB2 receptor-mediated migration of immune cells: it can go either way. *British journal of pharmacology*, 153(2):299–308, jan 2008.

[389] Fabrizio Montecucco, Fabienne Burger, François Mach, and Sabine Steffens. CB2 cannabinoid receptor agonist JWH-015 modulates human monocyte migration through defined intracellular signaling pathways. *American journal of physiology. Heart and circulatory physiology*, 294(3):H1145–55, mar 2008.

[390] M A Jorda, S E Verbakel, P J Valk, et al. Hematopoietic cells expressing the peripheral cannabinoid receptor migrate in response to the endocannabinoid 2-arachidonoylglycerol. *Blood*, 99(8):2786–2793, apr 2002.

[391] S Kishimoto, M Muramatsu, M Gokoh, et al. Endogenous cannabinoid receptor ligand induces the migration of human natural killer cells. *Journal of biochemistry*, 137(2):217–223, 2005.

[392] Saori Oka, Shinobu Ikeda, Seishi Kishimoto, et al. 2-arachidonoylglycerol, an endogenous cannabinoid receptor ligand, induces the migration of EoL-1 human eosinophilic leukemia cells and human peripheral blood eosinophils. *Journal of Leukocyte Biology*, 76(5):1002–1009, 2004.

[393] Seishi Kishimoto, Maiko Gokoh, Saori Oka, et al. 2-arachidonoylglycerol induces the migration of HL-60 cells differentiated into macrophage-like cells and human peripheral blood monocytes through the cannabinoid CB2 receptor-dependent mechanism. *The Journal of biological chemistry*, 278(27):24469–75, jul 2003.

[394] Allyn Franklin and Nephi Stella. Arachidonylcyclopropylamide increases microglial cell migration through cannabinoid CB2 and abnormal-cannabidiol-sensitive receptors. *European Journal of Pharmacology*, 474(2-3):195–198, 2003.

[395] L Walter, A Franklin, A Witting, et al. Nonpsychotropic cannabinoid receptors regulate microglial cell migration. *J Neurosci*, 23(4):1398–1405, 2003.

[396] Charles A Lunn, Jay S Fine, Alberto Rojas-Triana, et al. A novel cannabinoid peripheral cannabinoid receptor-selective inverse agonist blocks leukocyte recruitment in vivo. *The Journal of pharmacology and experimental therapeutics*, 316(2):780–8, feb 2006.

[397] Meritxell Alberich Jordà, Nazik Rayman, Marjolein Tas, et al. The peripheral cannabinoid receptor Cb2, frequently expressed on AML blasts, either induces a neutrophilic differentiation block or confers abnormal migration properties in a ligand-dependent manner. *Blood*, 104(2):526–534, 2004.

[398] Terry Kenakin. Functional selectivity and biased receptor signaling. *The Journal of pharmacology and experimental therapeutics*, 336(2):296–302, feb 2011.

[399] Jennifer L Shoemaker, Michael B Ruckle, Philip R Mayeux, and Paul L Prather. Agonist-directed trafficking of response by endocannabinoids acting at CB2 receptors. *The Journal of pharmacology and experimental therapeutics*, 315(2):828–838, nov 2005.

[400] Takashi Tanikawa, Kohta Kurohane, and Yasuyuki Imai. Regulatory effect of cannabinoid receptor agonist on chemokine-induced lymphocyte chemotaxis. *Biological & pharmaceutical bulletin*, 34(7):1090–3, jan 2011.

[401] R Kurihara, Y Tohyama, S Matsusaka, et al. Effects of peripheral cannabinoid receptor ligands on motility and polarization in neutrophil-like HL60 cells and human neutrophils. *The Journal of biological chemistry*, 281(18):12908–12918, 2006.

[402] D McHugh, C Tanner, R Mechoulam, R G Pertwee, and R A Ross. Inhibition of human neutrophil chemotaxis by endogenous cannabinoids and phytocannabinoids: evidence for a site distinct from CB1 and CB2. *Mol Pharmacol*, 73(2):441–450, 2008.

[403] P Sacerdote, P Massi, A E Panerai, and D Parolaro. In vivo and in vitro treatment with the synthetic cannabinoid CP55, 940 decreases the in vitro migration of macrophages in the rat: involvement of both CB1 and CB2 receptors. *Journal of neuroimmunology*, 109(2):155–63, sep 2000.

[404] P Sacerdote, C Martucci, A Vaccani, et al. The nonpsychoactive component of marijuana cannabidiol modulates chemotaxis and IL-10 and IL-12 production of murine macrophages both in vivo and in vitro. *Journal of Neuroimmunology*, 159(1-2):97–105, 2005.

[405] Erinn S Raborn and Guy A Cabral. Cannabinoid inhibition of macrophage migration to the trans-activating (Tat) protein of HIV-1 is linked to the CB(2) cannabinoid receptor. *The Journal of pharmacology and experimental therapeutics*, 333(1):319–27, apr 2010.

[406] Daniel Fraga, Erinn S. Raborn, Gabriela A. Ferreira, and Guy A. Cabral. Cannabinoids inhibit migration of microglial-like cells to the HIV protein tat. *Journal of Neuroimmune Pharmacology*, 6(4):566–577, 2011.

[407] J Joseph, B Niggemann, K S Zaenker, and F Entschladen. Anandamide is an endogenous inhibitor for the migration of tumor cells and T lymphocytes. *Cancer immunology, immunotherapy : CII*, 53(8):723–728, 2004.

[408] Sharmistha Ghosh, Anju Preet, Jerome E Groopman, and Ramesh K Ganju. Cannabinoid receptor CB2 modulates the CXCL12/CXCR4-mediated chemotaxis of T lymphocytes. *Molecular immunology*, 43(14):2169–79, jul 2006.

[409] K Coopman, L D Smith, K L Wright, and S G Ward. Temporal variation in CB2R levels following T lymphocyte activation: evidence that cannabinoids modulate CXCL12-induced chemotaxis. *International immunopharmacology*, 7(3):360–371, 2007.

[410] Erinn S Raborn, Francine Marciano-Cabral, Nancy E Buckley, Billy R Martin, and Guy A Cabral. The cannabinoid delta-9-tetrahydrocannabinol mediates inhibition of macrophage chemotaxis to RANTES/CCL5: linkage to the CB2 receptor. *Journal of neuroimmune pharmacology : the official journal of the Society on NeuroImmune Pharmacology*, 3(2):117–129, jun 2008.

[411] Sabina Adhikary, Virginia P Kocieda, Jui-Hung Yen, Ronald F Tuma, and Doina Ganea. Signaling through cannabinoid receptor 2 suppresses murine dendritic cell migration by inhibiting matrix metalloproteinase 9 expression. *Blood*, 120(18):3741–9, nov 2012.

[412] E Deusch, B Kraft, G Nahlik, et al. No evidence for direct modulatory effects of delta 9-tetrahydrocannabinol on human polymorphonuclear leukocytes. *Journal of Neuroimmunology*, 141(1-2):99–103, 2003.

[413] I Tabas and C K Glass. Anti-inflammatory therapy in chronic disease: challenges and opportunities. *Science*, 339(6116):166–172, 2013.

[414] Lewis Taylor, Ivy Christou, Theodore S Kapellos, et al. Primary Macrophage Chemotaxis Induced by Cannabinoid Receptor 2 Agonists Occurs Independently of the CB2 Receptor. *Scientific reports*, 5:10682, 2015.

[415] Bx Stephen Boyden and D Ph. The chemotactic effect of mixtures of antibody and antigen on polymorphonuclear leucocytes. *Assessment*, 115:453–466, mar 1962.

[416] J Q Davies and S Gordon. Isolation and culture of murine macrophages. *Methods in molecular biology*, 290:91–103, 2005.

[417] Yasmine Belkaid, TimothyW. Hand, N.A. Abreu, et al. Role of the Microbiota in Immunity and Inflammation. *Cell*, 157(1):121–141, mar 2014.

[418] N Guan, J Deng, T Li, et al. Label-free monitoring of T cell activation by the impedance-based xCELLigence system. *Molecular bioSystems*, 9(5):1035–1043, 2013.

[419] S Scrace, E O'Neill, E M Hammond, and I M Pires. Use of the xCELLigence system for real-time analysis of changes in cellular motility and adhesion in physiological conditions. *Methods in molecular biology*, 1046:295–306, 2013.

[420] N Yu, J M Atienza, J Bernard, et al. Real-time monitoring of morphological changes in living cells by electronic cell sensor arrays: an approach to study G protein-coupled receptors. *Analytical chemistry*, 78(1):35–43, 2006.

[421] Peter J. M. Van Haastert and Peter N. Devreotes. Chemotaxis: signalling the way forward. *Nature reviews. Molecular cell biology*, 5(8):626–634, aug 2004.

[422] Jenna L Cash, Rosie Hart, Andreas Russ, et al. Synthetic chemerin-derived peptides suppress inflammation through ChemR23. *J Exp Med*, 205(4):767–775, apr 2008.

[423] R G Pertwee. The pharmacology of cannabinoid receptors and their ligands: an overview. *International Journal of Obesity*, 30 Suppl 1:S13–8, 2006.

[424] Patricia M Cano, Amandine Vargas, and Jean-Pierre Lavoie. A real-time assay for neutrophil chemotaxis. *BioTechniques*, 251(May):245–251, 2016.

[425] Mark A Johnson and Gerald M Maggiora. *Concepts and applications of molecular similarity*. Wiley New York, 1990.

[426] F Navarrete, J M Perez-Ortiz, and J Manzanares. Cannabinoid CB(2) receptor-mediated regulation of impulsive-like behaviour in DBA/2 mice. *British Journal of Pharmacology*, 165(1):260–273, 2012.

[427] J J Burston, D R Sagar, P Shao, et al. Cannabinoid CB2 receptors regulate central sensitization and pain responses associated with osteoarthritis of the knee joint. *PLoS One*, 8(11):e80440, 2013.

[428] H Xu, C L Cheng, M Chen, et al. Anti-inflammatory property of the cannabinoid receptor-2-selective agonist JWH-133 in a rodent model of autoimmune uveoretinitis. *Journal of Leukocyte Biology*, 82(3):532–541, 2007.

[429] E S Kimball, J M Palmer, M R D'Andrea, P J Hornby, and P R Wade. Acute colitis induction by oil of mustard results in later development of an IBS-like accelerated upper GI transit in mice. *Am J Physiol Gastrointest Liver Physiol*, 288(6):G1266–73, 2005.

[430] M Fujii, P Sherchan, Y Soejima, et al. Cannabinoid receptor type 2 agonist attenuates apoptosis by activation of phosphorylated CREB-Bcl-2 pathway after subarachnoid hemorrhage in rats. *Exp Neurol*, 261:396–403, 2014.

[431] R A Fraga-Silva, F P Costa-Fraga, F Montecucco, et al. Treatment with CB2 agonist JWH-133 reduces histological features associated with erectile dysfunction in hypercholesterolemic mice. *Clin Dev Immunol*, 2013:263846, 2013.

[432] C Lehmann, M Kianian, J Zhou, et al. Cannabinoid receptor 2 activation reduces intestinal leukocyte recruitment and systemic inflammatory mediator release in acute experimental sepsis. *Crit Care*, 16(2):R47, 2012.

[433] S Mukherjee, M Adams, K Whiteaker, et al. Species comparison and pharmacological characterization of rat and human CB2 cannabinoid receptors. *Eur J Pharmacol*, 505(1-3):1–9, 2004.

[434] B Bingham, P G Jones, A J Uveges, et al. Species-specific in vitro pharmacological effects of the cannabinoid receptor 2 (CB2) selective ligand AM1241 and its resolved enantiomers. *British Journal of Pharmacology*, 151(7):1061–1070, 2007.

[435] Pamela Zengel, Anna Nguyen-Hoang, Christoph Schildhammer, et al. μ-Slide Chemotaxis: a new chamber for long-term chemotaxis studies. *BMC cell biology*, 12(1):21, 2011.

[436] Essen-Bioscience. Visualize and quantify chemotactic cell migration in real time.

[437] Gaia V Paolini, Richard H B Shapland, Willem P van Hoorn, Jonathan S Mason, and Andrew L Hopkins. Global mapping of pharmacological space. *Nature biotechnology*, 24(7):805–815, jul 2006.

[438] Ye Hu and Jürgen Bajorath. How promiscuous are pharmaceutically relevant compounds? A data-driven assessment. *The AAPS journal*, 15(1):104–11, jan 2013.

[439] Jordi Mestres, Elisabet Gregori-Puigjané, Sergi Valverde, and Ricard V Solé. Data completenessthe Achilles heel of drug-target networks. *Nature Biotechnology*, 26(9):983–984, sep 2008.

[440] Ye Hu and Jürgen Bajorath. High-resolution view of compound promiscuity. *F1000Research*, 2, 2013.

[441] Xavier Jalencas and Jordi Mestres. On the origins of drug polypharmacology. *MedChemComm*, 4(1):80–87, 2012.

[442] Ye Hu and Jürgen Bajorath. Compound promiscuity: What can we learn from current data?, 2013.

[443] International Human Genome Sequencing Consortium. Finishing the euchromatic sequence of the human genome. *Nature*, 431(7011):931–945, oct 2004.

[444] Andrew L. Hopkins and Colin R. Groom. The druggable genome. *Nature reviews. Drug discovery*, 1(9):727–30, sep 2002.

[445] Andreas P. Russ and Stefan Lampel. The druggable genome: An update, 2005.

[446] Jason Lazarou, Bruce H. Pomeranz, and Paul N. Corey. Incidence of adverse drug reactions in hospitalized patients: a meta-analysis of prospective studies. *Jama*, 279(15):1200–1205, apr 1998.

[447] F O Ajayi, H Sun, and J Perry. Adverse drug reactions: a review of relevant factors. *Journal of clinical pharmacology*, 40(10):1093–101, oct 2000.

[448] Michael C. Sanguinetti and Martin Tristani-Firouzi. hERG potassium channels and cardiac arrhythmia. *Nature*, 440(7083):463–469, mar 2006.

[449] J K Woodward and N L Munro. Terfenadine, the first non-sedating antihistamine. *Arzneimittel-Forschung*, 32(9a):1154–6, 1982.

[450] B P Monahan, C L Ferguson, E S Killeavy, et al. Torsades de pointes occurring in association with terfenadine use. *JAMA : the journal of the American Medical Association*, 264(21):2788–2790, dec 1990.

[451] Kaichiro Kamiya, Ryoko Niwa, Mikio Morishima, Haruo Honjo, and Michael C Sanguinetti. Molecular determinants of hERG channel block by terfenadine and cisapride. *Journal of pharmacological sciences*, 108(3):301–7, nov 2008.

[452] R L Woosley, Y Chen, J P Freiman, and R A Gillis. Mechanism of the cardiotoxic actions of terfenadine. *JAMA : the journal of the American Medical Association*, 269(12):1532–1536, 1993.

[453] M.-L. Roy, R Dumaine, and A M Brown. HERG, a Primary Human Ventricular Target of the Nonsedating Antihistamine Terfenadine. *Circulation*, 94(4):817–823, aug 1996.

[454] Birgit T Priest, Ian M Bell, and Maria L Garcia. Role of hERG potassium channel assays in drug development, 2008.

[455] Curtis R. Chong and David J Sullivan Jr. New uses for old drugs. *Nature*, 448(7154):645–646, aug 2007.

[456] Janice M Reichert. Trends in development and approval times for new therapeutics in the United States. *Nature reviews. Drug discovery*, 2(9):695–702, sep 2003.

[457] Ted T. Ashburn and Karl B. Thor. Drug repositioning: identifying and developing new uses for existing drugs. *Nature reviews. Drug discovery*, 3(8):673–683, aug 2004.

[458] Joseph A. DiMasi, Henry G. Grabowski, and Ronald W. Hansen. Innovation in the pharmaceutical industry: New estimates of R&D costs. *Journal of Health Economics*, 47:20–33, 2016.

[459] Natalia Novac. Challenges and opportunities of drug repositioning, 2013.

[460] Hossein Ardeschir Ghofrani, Ian H. Osterloh, and Friedrich Grimminger. Sildenafil: from angina to erectile dysfunction to pulmonary hypertension and beyond. *Nature reviews. Drug discovery*, 5(8):689–702, aug 2006.

[461] Irwin Goldstein, Tom F Lue, Harin Padma-Nathan, et al. Oral sildenafil in the treatment of erectile dysfunction. Sildenafil Study Group. *The New England journal of medicine*, 338(20):1397–1404, may 1998.

[462] Neil Vargesson. Thalidomide-induced teratogenesis: History and mechanisms. *Birth Defects Research Part C: Embryo Today: Reviews*, 105(2):n/a–n/a, jun 2015.

[463] Matthew Strobeck. Multiple myeloma therapies. *Nature reviews. Drug discovery*, 6(3):181–2, mar 2007.

[464] Lewis Taylor, Sridhar R Vasudevan, Chris I Jones, et al. Discovery of novel GPVI receptor antagonists by structure-based repurposing. *PLoS ONE*, 9(6):e101209, 2014.

[465] Saori Oka, Keisuke Nakajima, Atsushi Yamashita, Seishi Kishimoto, and Takayuki Sugiura. Identification of GPR55 as a lysophosphatidylinositol receptor. *Biochemical and Biophysical Research Communications*, 362(4):928–934, 2007.

[466] Marek Sawzdargo, Tuan Nguyen, Dennis K Lee, et al. Identification and cloning of three novel human G protein-coupled receptor genes GPR52, GPR53 and GPR55: GPR55 is extensively expressed in human brain. *Molecular Brain Research*, 64(2):193–198, 1999.

[467] Christopher M. Henstridge. Off-target cannabinoid effects mediated by GPR55. *Pharmacology*, 89(3-4):179–187, 2012.

[468] John M. McPartland, Isabel Matias, Vincenzo Di Marzo, and Michelle Glass. Evolutionary origins of the endocannabinoid system. *Gene*, 370(1-2):64–74, 2006.

[469] Francois Petitet, Mary Donlan, and André Michel. GPR55 as a new cannabinoid receptor: Still a long way to prove it, mar 2006.

[470] Evangelia Kotsikorou, Karla E Madrigal, Dow P Hurst, et al. Identification of the GPR55 agonist binding site using a novel set of high-potency GPR55 selective ligands. *Biochemistry*, 50(25):5633–5647, jun 2011.

[471] E Ryberg, N Larsson, S Sjogren, et al. The orphan receptor GPR55 is a novel cannabinoid receptor. *British Journal of Pharmacology*, 152(7):1092–1101, 2007.

[472] Markus Waldeck-Weiermair, Cristina Zoratti, Karin Osibow, et al. Integrin clustering enables anandamide-induced Ca2+ signaling in endothelial cells via GPR55 by protection against CB1-receptor-triggered repression. *J Cell Sci*, 121(Pt 10):1704–1717, may 2008.

[473] Jane E Lauckner, Jill B Jensen, Huei-Ying Chen, et al. GPR55 is a cannabinoid receptor that increases intracellular calcium and inhibits M current. *Proceedings of the National Academy of Sciences of the United States of America*, 105(7):2699–704, feb 2008.

[474] Hong Yin, Alan Chu, Wei Li, et al. Lipid G protein-coupled receptor ligand identification using β-arrestin PathHunter assay. *Journal of Biological Chemistry*, 284(18):12328–12338, may 2009.

[475] Ankur Kapur, Pingwei Zhao, Haleli Sharir, et al. Atypical responsiveness of the orphan receptor GPR55 to cannabinoid ligands. *Journal of Biological Chemistry*, 284(43):29817–29827, oct 2009.

[476] Ira Gantz, Akira Muraoka, Y K Yang, et al. Cloning and chromosomal localization of a gene (GPR18) encoding a novel seven transmembrane receptor highly expressed in spleen and testis. *Genomics*, 42(3):462–6, 1997.

[477] Masashi Kohno, Hitoshi Hasegawa, Atsushi Inoue, et al. Identification of N-arachidonylglycine as the endogenous ligand for orphan G-protein-coupled receptor GPR18. *Biochemical and Biophysical Research Communications*, 347(3):827–832, 2006.

[478] Linda Console-Bram, Eugen Brailoiu, Gabriela Cristina Brailoiu, Haleli Sharir, and Mary E Abood. Activation of GPR18 by cannabinoid compounds: A tale of biased agonism. *British Journal of Pharmacology*, 171(16):3908–3917, aug 2014.

[479] Douglas McHugh, Sherry S J Hu, Neta Rimmerman, et al. N-arachidonoyl glycine, an abundant endogenous lipid, potently drives directed cellular migration through GPR18, the putative abnormal cannabidiol receptor. *BMC neuroscience*, 11:44, jan 2010.

[480] Douglas McHugh, James Wager-Miller, Jeremy Page, and Heather B Bradshaw. siRNA knockdown of GPR18 receptors in BV-2 microglia attenuates N-arachidonoyl glycine-induced cell migration. *Journal of molecular signaling*, 7(1):10, 2012.

[481] Douglas McHugh, Jeremy Page, Emily Dunn, and Heather B Bradshaw. Delta(9) - Tetrahydrocannabinol and N-arachidonyl glycine are full agonists at GPR18 receptors and induce migration in human endometrial HEC-1B cells. *British Journal of Pharmacology*, 165(8):2414–2424, apr 2012.

[482] Rina Takenouchi, Kazuhiko Inoue, Yuki Kambe, and Atsuro Miyata. N-arachidonoyl glycine induces macrophage apoptosis via GPR18. *Biochemical and Biophysical Research Communications*, 418(2):366–371, 2012.

[483] P J Vaysse, E L Gardner, and R S Zukin. Modulation of rat brain opioid receptors by cannabinoids. *J Pharmacol Exp Ther*, 241(2):534–539, may 1987.

[484] Markus Kathmann, Karsten Flau, Agnes Redmer, Christian Tränkle, and Eberhard Schlicker. Cannabidiol is an allosteric modulator at mu- and delta-opioid receptors. *Naunyn-Schmiedeberg's Archives of Pharmacology*, 372(5):354–361, feb 2006.

[485] Tung M. Fong, L. P. Shearman, D. S. Stribling, et al. Pharmacological efficacy and safety profile of taranabant in preclinical species. *Drug Development Research*, 70(5):349–362, aug 2009.

[486] Resat Cinar and Maria Szucs. CB1 receptor-independent actions of SR141716 on G-protein signaling: coapplication with the mu-opioid agonist Tyr-D-Ala-Gly-(NMe)Phe-Gly-ol unmasks novel, pertussis toxin-insensitive opioid signaling in mu-opioid receptor-Chinese hamster ovary cells. *The Journal of pharmacology and experimental therapeutics*, 330(2):567–574, aug 2009.

[487] S Lagalwar, E Z Bordayo, K L Hoffmann, J R Fawcett, and W H Frey. Anandamides inhibit binding to the muscarinic acetylcholine receptor. *Journal of molecular neuroscience : MN*, 13(1-2):55–61, 1999.

[488] Arthur Christopoulos and Kathryn Wilson. Interaction of anandamide with the M 1 and M 4 muscarinic acetylcholine receptors. *Brain Research*, 915(1):70–78, 2001.

[489] J. Robert Lane, Margot W. Beukers, Thea Mulder-Krieger, and Ad P. IJzerman. The endocannabinoid 2-arachidonylglycerol is a negative allosteric modulator of the human A3 adenosine receptor. *Biochemical Pharmacology*, 79(1):48–56, 2010.

[490] Z Járai, J A Wagner, K Varga, et al. Cannabinoid-induced mesenteric vasodilation through an endothelial site distinct from CB1 or CB2 receptors. *Proceedings of the National Academy of Sciences of the United States of America*, 96(24):14136–14141, nov 1999.

[491] Christopher Stanley and Saoirse E O'Sullivan. Vascular targets for cannabinoids: Animal and human studies, mar 2014.

[492] Ruth A. Ross. The enigmatic pharmacology of GPR55, 2009.

[493] D G Johns, D J Behm, D J Walker, et al. The novel endocannabinoid receptor GPR55 is activated by atypical cannabinoids but does not mediate their vasodilator effects. *British journal of pharmacology*, 152(5):825–31, nov 2007.

[494] Stephen PH Alexander, John A Cidlowski, Eamonn Kelly, et al. The Concise Guide to PHARMACOLOGY 2015/16: Nuclear hormone receptors, dec 2015.

[495] Saoirse Elizabeth O'Sullivan. Cannabinoid activation of peroxisome proliferator-activated receptors: An update and review of the physiological relevance. *Wiley Interdisciplinary Reviews: Membrane Transport and Signaling*, 2(1):17–25, jan 2013.

[496] Saoirse Elizabeth O'Sullivan. An update on peroxisome proliferator-activated receptor (PPAR) activation by cannabinoids. *British Journal of Pharmacology*, 173(12):1899–1910, jun 2016.

[497] Jie Zheng. Molecular mechanism of TRP channels. *Comprehensive Physiology*, 3(1):221–242, jan 2013.

[498] David E Clapham. TRP channels as cellular sensors. *Nature*, 426(6966):517–524, dec 2003.

[499] Michael J. Caterina, Mark A. Schumacher, Makoto Tominaga, et al. The capsaicin receptor: a heat-activated ion channel in the pain pathway. *Nature*, 389(6653):816–824, oct 1997.

[500] Ning Qin, Michael P Neeper, Yi Liu, et al. TRPV2 is activated by cannabidiol and mediates CGRP release in cultured rat dorsal root ganglion neurons. *J Neurosci*, 28(24):6231–6238, jun 2008.

[501] L. de Petrocellis, P. Orlando, A. Schiano Moriello, et al. Cannabinoid actions at TRPV channels: Effects on TRPV3 and TRPV4 and their potential relevance to gastrointestinal inflammation, feb 2012.

[502] Hiroyuki Watanabe, Joris Vriens, Jean Prenen, et al. Anandamide and arachidonic acid use epoxyeicosatrienoic acids to activate TRPV4 channels. *Nature*, 424(6947):434–8, jul 2003.

[503] Luciano De Petrocellis, Vittorio Vellani, Aniello Schiano-Moriello, et al. Plant-derived cannabinoids modulate the activity of transient receptor potential channels of ankyrin type-1 and melastatin type-8. *Journal of Pharmacology and Experimental Therapeutics*, 325(3):1007–1015, jun 2008.

[504] Armen N Akopian, Nikita B Ruparel, Amol Patwardhan, and Kenneth M Hargreaves. Cannabinoids desensitize capsaicin and mustard oil responses in sensory neurons via TRPA1 activation. *The Journal of neuroscience : the official journal of the Society for Neuroscience*, 28(5):1064–75, jan 2008.

[505] Sven-Eric Jordt, Diana M Bautista, Huai-Hu Chuang, et al. Mustard oils and cannabinoids excite sensory nerve fibres through the TRP channel ANKTM1. *Nature*, 427(6971):260–265, jan 2004.

[506] David D McKemy, Werner M Neuhausser, and David Julius. Identification of a cold receptor reveals a general role for TRP channels in thermosensation. *Nature*, 416(6876):52–58, mar 2002.

[507] Andrea M. Peier, Aziz Moqrich, Anne C. Hergarden, et al. A TRP channel that senses cold stimuli and menthol. *Cell*, 108(5):705–715, 2002.

[508] Luciano De Petrocellis, Katarzyna Starowicz, Aniello Schiano Moriello, et al. Regulation of transient receptor potential channels of melastatin type 8 (TRPM8): Effect of cAMP, cannabinoid CB1 receptors and endovanilloids. *Experimental Cell Research*, 313(9):1911–1920, 2007.

[509] Yukio Okada, Kotapola G Imendra, Toshihiro Miyazaki, et al. Biophysical properties of voltage-gated Na+ channels in frog parathyroid cells and their modulation by cannabinoids. *The Journal of experimental biology*, 208(Pt 24):4747–56, dec 2005.

[510] Yin Duan, Jian Zheng, and Russell A. Nicholson. Inhibition of [3H]batrachotoxinin A-20α-benzoate binding to sodium channels and sodium channel function by endocannabinoids. *Neurochemistry International*, 52(3):438–446, 2008.

[511] Yin Duan, Chengyong Liao, Saurabh Jain, and Russell A. Nicholson. The cannabinoid receptor agonist CP-55,940 and ethyl arachidonate interfere with [3H]batrachotoxinin A 20 α-benzoate binding to sodium channels and inhibit sodium channel function. *Comparative Biochemistry and Physiology - C Toxicology and Pharmacology*, 148(3):244–249, 2008.

[512] R. A. Nicholson, C. Liao, J. Zheng, et al. Sodium channel inhibition by anandamide and synthetic cannabimimetics in brain. *Brain Research*, 978(1-2):194–204, 2003.

[513] Hui Fu, Jian Min Xiao, Xue Hong Cao, Zhang Yin Ming, and Lie Ju Liu. Effects of WIN55,212-2 on voltage-gated sodium channels in trigeminal ganglion neurons of rats. *Neurological research*, 30(1):85–91, feb 2008.

[514] Hong Im Kim, Tae Hoon Kim, Yong Kyoo Shin, et al. Anandamide suppression of Na+ currents in rat dorsal root ganglion neurons. *Brain Research*, 1062(1-2):39–47, 2005.

[515] Lina T Al Kury, Oleg I Voitychuk, Keun-Hang Susan Yang, et al. Effects of the endogenous cannabinoid anandamide on voltage-dependent sodium and calcium channels in rat ventricular myocytes. *British journal of pharmacology*, 171(14):3485–98, jul 2014.

[516] Andrew J. Hill, Nicholas A. Jones, Imogen Smith, et al. Voltage-gated sodium (NaV) channel blockade by plant cannabinoids does not confer anticonvulsant effects per se. *Neuroscience Letters*, 566:269–274, 2014.

[517] Murat Oz, Keun-Hang Yang, Meral Dinc, and Toni S Shippenberg. The endogenous cannabinoid anandamide inhibits cromakalim-activated K+ currents in follicle-enclosed Xenopus oocytes. *The Journal of pharmacology and experimental therapeutics*, 323(2):547–54, nov 2007.

[518] Charles E Spivak, Wook Kim, Qing Rong Liu, Carl R Lupica, and M??ire E Doyle. Blockade of β-cell KATP channels by the endocannabinoid, 2-arachidonoylglycerol. *Biochemical and Biophysical Research Communications*, 423(1):13–18, jun 2012.

[519] Haiyan Liu, Judith A Enyeart, and John J Enyeart. Potent inhibition of native TREK-1 K+ channels by selected dihydropyridine Ca2+ channel antagonists. *The Journal of pharmacology and experimental therapeutics*, 323(1):39–48, oct 2007.

[520] J. S. Poling, M. A. Rogawski, N. Salem, and S. Vicini. Anandamide, an endogenous cannabinoid, inhibits Shaker-related voltage-gated K+ channels. *Neuropharmacology*, 35(7):983–991, 1996.

[521] Eloy G Moreno-Galindo, Gabriel F Barrio-Echavarría, José C Vásquez, et al. Molecular basis for a high-potency open-channel block of Kv1.5 channel by the endocannabinoid anandamide. *Molecular pharmacology*, 77(5):751–758, may 2010.

[522] Adriana Barana, Irene Amorós, Ricardo Caballero, et al. Endocannabinoids and cannabinoid analogues block cardiac hKv1.5 channels in a cannabinoid receptor-independent manner. *Cardiovascular Research*, 85(1):56–67, jan 2010.

[523] Dominik Oliver, C.C. Cheng-Chang Lien, Malle Soom, et al. Functional conversion between A-type and delayed rectifier K+ channels by membrane lipids. *Science (New York, N.Y.)*, 304(5668):265–70, apr 2004.

[524] Irene Amorós, Adriana Barana, Ricardo Caballero, et al. Endocannabinoids and cannabinoid analogues block human cardiac Kv4.3 channels in a receptor-independent manner. *Journal of Molecular and Cellular Cardiology*, 48(1):201–210, 2010.

[525] C. Q. Zhang, H. J. Wu, S. Y. Wang, et al. Suppression of outward K+ currents by WIN55212-2 in rat retinal ganglion cells is independent of CB1/CB2 receptors. *Neuroscience*, 253:183–193, 2013.

[526] I Van den Bossche and B Vanheel. Influence of cannabinoids on the delayed rectifier in freshly dissociated smooth muscle cells of the rat aorta. *Br J Pharmacol*, 131(1):85–93, sep 2000.

[527] Hamish Redmond Ross, Ian Napier, and Mark Connor. Inhibition of recombinant human T-type calcium channels by Delta9-tetrahydrocannabinol and cannabidiol. *The Journal of biological chemistry*, 283(23):16124–34, jun 2008.

[528] W. Yang, Q Li, S-Y Wang, et al. Cannabinoid receptor agonists modulate calcium channels in rat retinal müller cells. *Neuroscience*, 313:213–24, 2016.

[529] Maoxing Shen and Stanley A Thayer. The cannabinoid agonist Win55,212-2 inhibits calcium channels by receptor-mediated and direct pathways in cultured rat hippocampal neurons. *Brain Research*, 783(1):77–84, 1998.

[530] Juan Guo and Stephen R Ikeda. Endocannabinoids modulate N-type calcium channels and G-protein-coupled inwardly rectifying potassium channels via CB1 cannabinoid receptors heterologously expressed in mammalian neurons. *Molecular pharmacology*, 65(3):665–74, mar 2004.

[531] Alexander Fisyunov, Vera Tsintsadze, Rogier Min, Nail Burnashev, and Natalia Lozovaya. Cannabinoids modulate the P-type high-voltage-activated calcium currents in purkinje neurons. *Journal of neurophysiology*, 96(3):1267–77, sep 2006.

[532] Bo Shi, Rong Yang, Xiaohui Wang, et al. Inhibition of 5-HT3 receptors-activated currents by cannabinoids in rat trigeminal ganglion neurons. *Journal of Huazhong University of Science and Technology [Medical Sciences]*, 32(2):265–271, apr 2012.

[533] Murat Oz, Shelley N Jackson, Amina S Woods, Marisela Morales, and Li Zhang. Additive effects of endogenous cannabinoid anandamide and ethanol on alpha7-nicotinic acetylcholine receptor-mediated responses in Xenopus Oocytes. *The Journal of pharmacology and experimental therapeutics*, 313(3):1272–80, jun 2005.

[534] Murat Oz, Li Zhang, Arippa Ravindran, Marisela Morales, and Carl R Lupica. Differential effects of endogenous and synthetic cannabinoids on alpha7-nicotinic acetylcholine receptor-mediated responses in Xenopus Oocytes. *The Journal of pharmacology and experimental therapeutics*, 310(3):1152–60, sep 2004.

[535] M. Oz, Arippa Ravindran, Oscar Diaz-Ruiz, Li Zhang, and Marisela Morales. The Endogenous Cannabinoid Anandamide Inhibits 7 Nicotinic Acetylcholine Receptor-Mediated Responses in Xenopus Oocytes. *Journal of Pharmacology and Experimental Therapeutics*, 306(3):1003–1010, may 2003.

[536] Mohamed Mahgoub, Susan Yang Keun-Hang, Vadym Sydorenko, et al. Effects of cannabidiol on the function of α7-nicotinic acetylcholine receptors. *European Journal of Pharmacology*, 720(1):310–319, 2013.

[537] Yongli Lu, Changjin Liu, and Hongwei Yang. Inhibitory effects of synthetic cannabinoid WIN55, 212-2 on nicotine-activated currents in rat trigeminal ganglion neurons. 6(8):610–616, 2011.

[538] Charles E Spivak, Carl R Lupica, and Murat Oz. The endocannabinoid anandamide inhibits the function of alpha4beta2 nicotinic acetylcholine receptors. *Molecular pharmacology*, 72(4):1024–32, oct 2007.

[539] Christopher Butt, Alp Alptekin, Toni Shippenberg, and Murat Oz. Endogenous cannabinoid anandamide inhibits nicotinic acetylcholine receptor function in mouse thalamic synaptosomes. *Journal of neurochemistry*, 105(4):1235–43, may 2008.

[540] L A Ford, A J Roelofs, S Anavi-Goffer, et al. A role for L-alpha-lysophosphatidylinositol and GPR55 in the modulation of migration, orientation and polarization of human breast cancer cells. *British Journal of Pharmacology*, 160(3):762–771, 2010.

[541] Brian D Hudson, Terence E Hé bert, Melanie E M Kelly, and Ophthalmology Memk. Ligand-and Heterodimer-Directed Signaling of the CB 1 Cannabinoid Receptor.

[542] N A Balenga, E Martínez-Pinilla, J Kargl, et al. Heteromerization of GPR55 and cannabinoid CB2 receptors modulates signalling. *British journal of pharmacology*, 171(23):5387–406, dec 2014.

[543] Susan R George, Brian F O'Dowd, and Samuel P Lee. G-protein-coupled receptor oligomerization and its potential for drug discovery. *Nature reviews. Drug discovery*, 1(10):808–20, oct 2002.

[544] L i. Call e n, Estefanía i. Moreno, Pedro Barroso-Chinea, et al. Cannabinoid receptors CB1 and CB2 form functional heteromers in brain. *The Journal of biological chemistry*, 287(25):20851–20865, jun 2012.

[545] Hanna Eckert and J??rgen Bajorath. Molecular similarity analysis in virtual screening: foundations, limitations and novel approaches, 2007.

[546] Ian Collins Ewan Smith. Photoaffinity labeling in target- and binding-site identification. *Future medicinal chemistry*, 7(2):159, 2015.

[547] Amy Grunbeck and Thomas P. Sakmar. Probing G Protein-Coupled ReceptorLigand Interactions with Targeted Photoactivatable Cross-Linkers. *Biochemistry*, 52(48):8625–8632, dec 2013.

[548] Jane E Lattin, Kate Schroder, Andrew I Su, et al. Expression analysis of G Protein-Coupled Receptors in mouse macrophages. *Immunome research*, 4:5, 2008.

[549] Daniel M. Hohenhaus, Kolja Schaale, Kim-Anh A Le Cao, et al. An mRNA atlas of G protein-coupled receptor expression during primary human monocyte/macrophage differentiation and lipopolysaccharide-mediated activation identifies targetable candidate regulators of inflammation. *Immunobiology*, 218(11):1345–1353, 2013.

[550] Paul J Groot-Kormelink, Lindsay Fawcett, Paul D Wright, Martin Gosling, and Toby C Kent. Quantitative GPCR and ion channel transcriptomics in primary alveolar macrophages and macrophage surrogates. *BMC immunology*, 13:57, 2012.

[551] Martin Guilliams, Ismé De Kleer, Sandrine Henri, et al. Alveolar macrophages develop from fetal monocytes that differentiate into long-lived cells in the first week of life via GM-CSF. *The Journal of Experimental Medicine*, 210(10):1977–1992, sep 2013.

[552] Yuta Murai, Katsuyoshi Masuda, Yui Ogasawara, et al. Synthesis of Photoreactive 2-Phenethylamine Derivatives - Synthesis of Adenosine Derivatives Enabling Functional Analysis of Adenosine Receptors by Photoaffinity Labeling. *European Journal of Organic Chemistry*, 2013(12):2428–2433, apr 2013.

[553] Alain Couvineau, Yossan-Var Tan, Emilie Ceraudo, and Marc Laburthe. Chapter Ten Strategies for Studying the Ligand Binding Site of GPCRs: Photoaffinity Labeling of the VPAC1 Receptor, a Prototype of Class B GPCRs. In *Methods in Enzymology*, volume 520, pages 219–237. 2013.

[554] Karen J Gregory, Ranganadh Velagaleti, David M Thal, et al. Clickable Photoaffinity Ligands for Metabotropic Glutamate Receptor 5 Based on Select Acetylenic Negative Allosteric Modulators. *ACS chemical biology*, 11(7):1870–9, jul 2016.

[555] Stephen PH Alexander, Anthony P Davenport, Eamonn Kelly, et al. The Concise Guide to PHARMACOLOGY 2015/16: G protein-coupled receptors. *British Journal of Pharmacology*, 172(24):5744–5869, dec 2015.

[556] Hans Selye, H. Selye, H. Selye, et al. on the Mechanism Through Which Hydrocortisone Affects the Resistance of Tissues To Injury. *Journal of the American Medical Association*, 152(13):1207, jul 1953.

[557] S W Martin, A J Stevens, B S Brennan, et al. The six-day-old rat air pouch model of inflammation: characterization of the inflammatory response to carrageenan. *Journal of pharmacological and toxicological methods*, 32(3):139–47, nov 1994.

[558] Y M Sin, A D Sedgwick, E P Chea, and D A Willoughby3. Mast cells in newly formed lining tissue during acute inflammation: a six day air pouch model in the mouse. *Annals of the Rheumatic Diseases*, 45:873–877, 1986.

[559] Chandan A S Alam, P G Winyard, and D A Willoughby. Murine Chronic Granulomatous Air Pouch Quantitative Analysis of Angiogenesis Using the Murine Chronic Granulomatous Air Pouch. *Inflammation Protocols*, 2003.

[560] J Dawson, A D Sedgwick, J C Edwards, and P Lees. A comparative study of the cellular, exudative and histological responses to carrageenan, dextran and zymosan in the mouse. *International journal of tissue reactions*, 13(4):171–85, 1991.

[561] Zhongdong Huang, Chunmei Zhao, Yanling Chen, et al. Recombinant human hyaluronidase PH20 does not stimulate an acute inflammatory response and inhibits lipopolysaccharide-induced neutrophil recruitment in the air pouch model of inflammation. *Journal of immunology (Baltimore, Md. : 1950)*, 192(11):5285–95, jun 2014.

[562] Carle Ryckman, Shaun R McColl, Karen Vandal, et al. Role of S100A8 and S100A9 in neutrophil recruitment in response to monosodium urate monohydrate crystals in the air-pouch model of acute gouty arthritis. *Arthritis and rheumatism*, 48(8):2310–20, aug 2003.

[563] P M Brooks, D Burton, and M J Forrest. Crystal-induced inflammation in the rat subcutaneous air-pouch. *British journal of pharmacology*, 90(2):413–9, feb 1987.

[564] M Perretti, J G Harris, and R J Flower. A role for endogenous histamine in interleukin-8-induced neutrophil infiltration into mouse air-pouch: investigation of the modulatory action of systemic and local dexamethasone. *Br J Pharmacol*, 112(3):801–808, jul 1994.

[565] A A Ahluwalia, C De Felipe, J O'Brien, S P Hunt, and M Perretti. Impaired IL-1 beta-induced neutrophil accumulation in tachykinin NK1 receptor knockout mice. *British Journal of Pharmacology*, 124(6):1013–1015, jul 1998.

[566] Gerben Bouma, Tatjana Nikolic, Jojanneke?M.?C. Coppens, et al. NOD mice have a severly impaired ability to recruit leukocytes into sites of inflammation. *European Journal of Immunology*, 35(1):225–235, jan 2005.

[567] Julia I Ellyard, Ljubov Simson, Anna Bezos, et al. Eotaxin selectively binds heparin: An interaction that protects eotaxin from proteolysis and potentiates chemotactic activity in vivo. *Journal of Biological Chemistry*, 282(20):15238–15247, may 2007.

[568] A.M. Das, R.J. Flower, and M Perretti. Resident mast cells are important for eotaxin-induced eosinophil accumulation in vivo. *J. Leukocyte Biol.*, 64(2):156–162, aug 1998.

[569] Simon McArthur, Thomas Gobbetti, Dennis H M Kusters, et al. Definition of a Novel Pathway Centered on Lysophosphatidic Acid To Recruit Monocytes during the Resolution Phase of Tissue Inflammation. *Journal of immunology (Baltimore, Md. : 1950)*, 195(3):1139–51, aug 2015.

[570] L.-P. Laurin, M.-J. Brissette, S. Lepage, and J.F. Cailhier. Regulation of Experimental Peritonitis: A Complex Orchestration. *Nephron Experimental Nephrology*, 120(1):e41–e46, 2012.

[571] Avijit Ray and Bonnie N Dittel. Isolation of mouse peritoneal cavity cells. *Journal of visualized experiments : JoVE*, (35), 2010.

[572] Rosa Barreira da Silva, Melissa E Laird, Nader Yatim, et al. Dipeptidylpeptidase 4 inhibition enhances lymphocyte trafficking, improving both naturally occurring tumor immunity and immunotherapy. *Nature Immunology*, 16(8):850–858, jun 2015.

[573] Luke C. Davies, Marcela Rosas, Stephen J. Jenkins, et al. Distinct bone marrow-derived and tissue-resident macrophage lineages proliferate at key stages during inflammation. *Nature Communications*, 4:1886, may 2013.

[574] Xiangyang Qin, Xinru Jiang, Xin Jiang, et al. Micheliolide inhibits LPS-induced inflammatory response and protects mice from LPS challenge. *Scientific reports*, 6:23240, 2016.

[575] M-H Hung, Y-R Jian, C-C Tsao, S-W Lin, and Y-H Chuang. Enhanced LPS-induced peritonitis in mice deficiency of cullin 4B in macrophages. *Genes and Immunity*, 15(6):404–412, sep 2014.

[576] William John Martin, Odette Shaw, Xiao Liu, Stefanie Steiger, and Jacquie L Harper. Monosodium urate monohydrate crystal-recruited noninflammatory monocytes differentiate into M1-like proinflammatory macrophages in a peritoneal murine model of gout. *Arthritis and rheumatism*, 63(5):1322–32, may 2011.

[577] Jenna L. Cash, Gemma E. White, and David R. Greaves. Chapter 17 ZymosanInduced Peritonitis as a Simple Experimental System for the Study of Inflammation. *Methods in Enzymology*, 461:379–396, 2009.

[578] M Perretti, S J Getting, E Solito, P M Murphy, and J L Gao. Involvement of the receptor for formylated peptides in the in vivo anti-migratory actions of annexin 1 and its mimetics. *The American journal of pathology*, 158(6):1969–73, jun 2001.

[579] Landin Boring, Jennifa Gosling, Stephen W Chensue, et al. Impaired Monocyte Migration and Reduced Type 1 (Th1) Cytokine Responses in C-C Chemokine Receptor 2 Knockout Mice. *The Journal of Clinical Investigation*, 100(10):2552–2561, 1997.

[580] Liping Liu, MeiZhang Li, Lisa C Spangler, et al. Functional defect of peripheral neutrophils in mice with induced deletion of CXCR2. *Genesis (New York, N.Y. : 2000)*, 51(8):587–95, aug 2013.

[581] Konrad Buscher, Huiyu Wang, Xueli Zhang, et al. Protection from septic peritonitis by rapid neutrophil recruitment through omental high endothelial venules. *Nature Communications*, 7:10828, mar 2016.

[582] F. L. Craciun, E. R. Schuller, and D. G. Remick. Early Enhanced Local Neutrophil Recruitment in Peritonitis-Induced Sepsis Improves Bacterial Clearance and Survival. *The Journal of Immunology*, 185(11):6930–6938, dec 2010.

[583] Liudmila Pietrovna Vlasenko and Alirio J Melendez. A critical role for sphingosine kinase in anaphylatoxin-induced neutropenia, peritonitis, and cytokine production in vivo. *Journal of immunology (Baltimore, Md. : 1950)*, 174(10):6456–61, may 2005.

[584] R A Ribeiro, M V Souza-Filho, M H Souza, et al. Role of resident mast cells and macrophages in the neutrophil migration induced by LTB4, fMLP and C5a des arg. *International archives of allergy and immunology*, 112(1):27–35, jan 1997.

[585] Christopher J Morris. Carrageenan-induced paw edema in the rat and mouse. *Methods in molecular biology (Clifton, N.J.)*, 225:115–21, 2003.

[586] Inmaculada Posadas, Mariarosaria Bucci, Fiorentina Roviezzo, et al. Carrageenan-induced mouse paw oedema is biphasic, age-weight dependent and displays differential nitric oxide cyclooxygenase-2 expression. *British journal of pharmacology*, 142(2):331–8, may 2004.

[587] M G Henriques, P M Silva, M A Martins, et al. Mouse paw edema. A new model for inflammation? *Brazilian journal of medical and biological research = Revista brasileira de pesquisas medicas e biologicas / Sociedade Brasileira de Biofisica ... [et al.]*, 20(2):243–9, 1987.

[588] E Sugishita, S Amagaya, and Y Ogihara. Anti-inflammatory testing methods: comparative evaluation of mice and rats. *Journal of pharmacobio-dynamics*, 4(8):565–75, aug 1981.

[589] Zekai Halici, Gunnur Ozbakis Dengiz, Fehmi Odabasoglu, et al. Amiodarone has anti-inflammatory and anti-oxidative properties: An experimental study in rats with carrageenan-induced paw edema. *European Journal of Pharmacology*, 566(1):215–221, 2007.

[590] Valiollah Hajhashemi, Mohsen Minaiyan, Hamid Reza Banafshe, Azam Mesdaghinia, and Alireza Abed. The anti-inflammatory effects of venlafaxine in the rat model of carrageenan-induced paw edema. *Iranian journal of basic medical sciences*, 18(7):654–8, jul 2015.

[591] Hossein Sadeghi, Valiolla Hajhashemi, Mohsen Minaiyan, Ahmad Movahedian, and Ardeshir Talebi. A study on the mechanisms involving the anti-inflammatory effect of amitriptyline in carrageenan-induced paw edema in rats. *European journal of pharmacology*, 667(1-3):396–401, sep 2011.

[592] Miklós Gábor. Models of acute inflammation in the ear. *Methods in molecular biology (Clifton, N.J.)*, 225:129–37, 2003.

[593] Vanesa Ivetic Tkalcevic, Boska Hrvacic, Martina Bosnar, et al. Cantharidin-induced inflammation in mouse ear model for translational research of novel anti-inflammatories. *Translational Research*, 160(2):137–145, 2012.

[594] Eve E Bralley, Phillip Greenspan, James L Hargrove, Louise Wicker, and Diane K Hartle. Topical anti-inflammatory activity of Polygonum cuspidatum extract in the TPA model of mouse ear inflammation. *Journal of inflammation (London, England)*, 5:1, 2008.

[595] Patricia Kiesler, Ivan J. Fuss, and Warren Strober. Experimental Models of Inflammatory Bowel Diseases. *CMGH Cellular and Molecular Gastroenterology and Hepatology*, 1(2):154–170, 2015.

[596] Puneet Kaur Randhawa, Kavinder Singh, Nirmal Singh, and Amteshwar Singh Jaggi. A review on chemical-induced inflammatory bowel disease models in rodents. *The Korean journal of physiology & pharmacology : official journal of the Korean Physiological Society and the Korean Society of Pharmacology*, 18(4):279–88, aug 2014.

[597] Janelle A. Jiminez, Trina C. Uwiera, G. Douglas Inglis, et al. Animal models to study acute and chronic intestinal inflammation in mammals. *Gut Pathogens*, 7(1):29, dec 2015.

[598] Stefan Wirtz, Clemens Neufert, Benno Weigmann, and Markus F Neurath. Chemically induced mouse models of intestinal inflammation. *Nature Protocols*, 2(3):541–546, mar 2007.

[599] David L. Delano, M. Carmen Montesinos, Peter D'Eustachio, Tim Wiltshire, and Bruce N. Cronstein. An Interaction Between Genetic Factors and Gender Determines the Magnitude of the Inflammatory Response in the Mouse Air Pouch Model of Acute Inflammation. *Inflammation*, 29(1):1–7, feb 2005.

[600] Melanie R. Gubbels Bupp. Sex, the aging immune system, and chronic disease. *Cellular Immunology*, 294(2):102–110, 2015.

[601] E. Kay, L. Gomez-Garcia, A. Woodfin, R. S. Scotland, and J. R. Whiteford. Sexual dimorphisms in leukocyte trafficking in a mouse peritonitis model. *Journal of Leukocyte Biology*, 98(5):805–817, nov 2015.

[602] DeLisa Fairweather. Sex differences in inflammation during atherosclerosis. *Clinical Medicine Insights. Cardiology*, 8(Suppl 3):49–59, 2014.

[603] JoAnn E Manson. Pain: sex differences and implications for treatment. *Metabolism: clinical and experimental*, 59 Suppl 1:S16–20, oct 2010.

[604] Martin K Angele, Sebastian Pratschke, William J Hubbard, and Irshad H Chaudry. Gender differences in sepsis: cardiovascular and immunological aspects. *Virulence*, 5(1):12–9, jan 2014.

[605] Ramona S Scotland, Melanie J Stables, Shimona Madalli, et al. Sex differences in resident immune cell phenotype underlie more efficient acute inflammatory responses in female mice. *Blood*, 118(22):5918–27, nov 2011.

[606] Catherine de Coupade, Adrienne S Brown, Paul F Dazin, Jon D Levine, and Paul G Green. beta(2)-Adrenergic receptor-dependent sexual dimorphism for murine leukocyte migration. *Journal of neuroimmunology*, 186(1-2):54–62, may 2007.

[607] Laura A Barker, Paul F Dazin, Jon D Levine, and Paul G Green. Sympathoadrenal-dependent sexually dimorphic effect of nonhabituating stress on in vivo neutrophil recruitment in the rat. *British journal of pharmacology*, 145(7):872–9, aug 2005.

[608] Fabio Martinon, Virginie Pétrilli, Annick Mayor, Aubry Tardivel, and Jürg Tschopp. Gout-associated uric acid crystals activate the NALP3 inflammasome. *Nature*, 440(7081):237–241, mar 2006.

[609] J. C. W. Edwards, A. D. Sedgwick, and D. A. Willoughby. The formation of a structure with the features of synovial lining by subcutaneous injection of air: an in vivo tissue culture system. *J Pathol*, 134(2):147–156, jun 1981.

[610] Lisette Bevaart, Margriet J. Vervoordeldonk, and Paul P. Tak. Evaluation of therapeutic targets in animal models of arthritis: How does it relate to rheumatoid arthritis? *Arthritis & Rheumatism*, 62(8):2192–2205, apr 2010.

[611] Valerio Chiurchiù, Mirko Lanuti, Giuseppina Catanzaro, et al. Detailed characterization of the endocannabinoid system in human macrophages and foam cells, and anti-inflammatory role of type-2 cannabinoid receptor. *Atherosclerosis*, 233(1):55–63, 2014.

[612] María Salomé Gachet, Peter Rhyn, Oliver G. Bosch, Boris B. Quednow, and Jürg Gertsch. A quantitiative LC-MS/MS method for the measurement of arachidonic acid, prostanoids, endocannabinoids, N-acylethanolamines and steroids in human plasma. *Journal of Chromatography B*, 976:6–18, 2015.

[613] Raissa Lerner, Beat Lutz, Laura Bindila, et al. Tricks and Tracks in the Identification and Quantification of Endocannabinoids. In *eLS*. John Wiley & Sons, Ltd, Chichester, UK, sep 2013.

[614] Matthew W Buczynski and Loren H Parsons. Quantification of brain endocannabinoid levels: methods, interpretations and pitfalls. *Br J Pharmacol*, 160(3):423–42, jun 2010.

[615] Hui Yang, Haoyi Wang, Chikdu S Shivalila, et al. One-step generation of mice carrying reporter and conditional alleles by CRISPR/Cas-mediated genome engineering. *Cell*, 154(6):1370–9, sep 2013.